ECE 505 Nanostructures: Fundamentals and Applications

Carmen S. Menoni
Prof. Electrical & Computer Engineering
Colorado State University

Nano-imaging

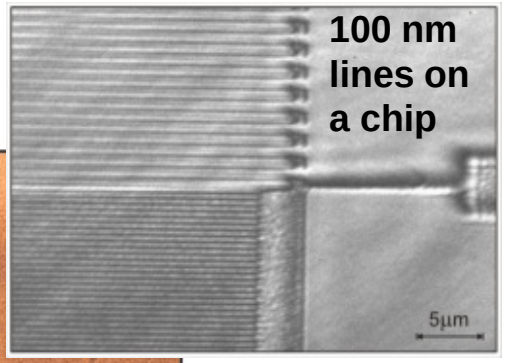

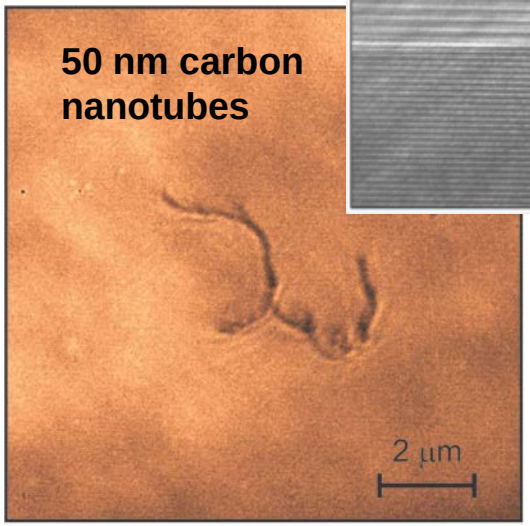

Nano-machining

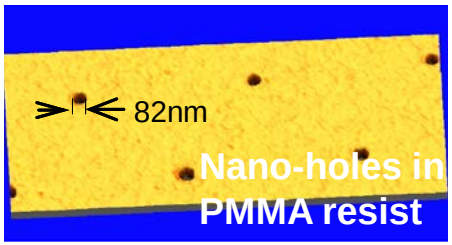

Nano-patterning

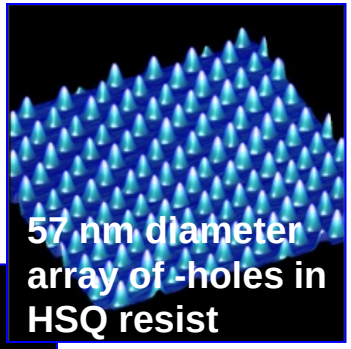

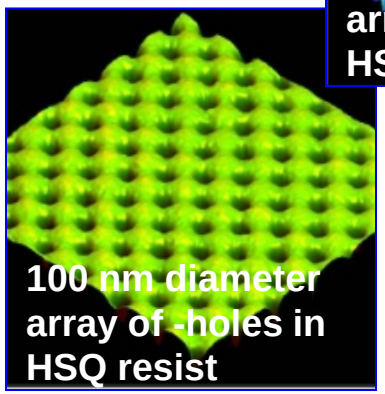

ECE 505 - Nanostructures: Fundamentals and Application Syllabus

Chapter 1 – The Basics and Electrons in Nanostructures Chps 1 and 7 of textbook (2 weeks)	**What is nanoscience The physics of quantum confinement, Quantum confined materials: quantum wells, wires, dots and rings. Electrons in nanostructures Quantum effects**
Chapter 2 Statistical Mechanics and chemical kinetics (2 weeks)	**Microscopic description of systems of many particles Chemical Kinetics Nanothermodynamics**
Chapter 3 - Making nanostructures top down (1 weeks)	**Projection lithography Epitaxy Nano-imprint**
Chapter 3 – Making nanostructures: bottom up (1 weeks)	**Nano-chemistry Self assembled systems DNA nanotechnology**
Chapter 4 – Nanostructured molecular architectures (2 weeks)	**Noncovalent interactions, Polymer nanostructures, Self-assembly, carbon nanotubes.**
Chapter 5 – Microscopy and manipulation tools (1 week)	**Optical microscopy Atomic force microscopy Electron Beam microscopy Other microscopies**
Chapter 6 – Nano-electronics and nanomagnetics (1 week)	**Logic devices based on quantized structures, Quantum transport devices. Magneto-resistive memory devices**
Chapter 7 – Nanostructured materials (1 week)	**Photonic Nanostructures Magnetic Nanostructures**
Nanobiology (1 week)	**Introduction to molecular biology Biology and nanostructures**
Review (1 week) Exam Week	

Syllabus –cont.

Grading: Homework – 30 %; 1 Midterm: 25% ; Final: 25% ; Project: 20%

Homework will consist of a combination of critique of papers; calculations and conceptual problems and laboratory practices.
An important component of this course will be a **research project** where students will investigate synthesis and characterization of nanostructures. Simple modeling will be required. At the end of the semester students will be expected to defend their work in a **10 min presentation**. Student will also be expected to give presentations during the semester on related topics to class contents.

Other reference material: The CSU library catalog list a number of electronic books that fit the contents of the class. For example, Introduction to Nanoscience and Nanotechnology by Chris Binns. Search by Nanoscience and nanotechnology

Fundamentals: Scales

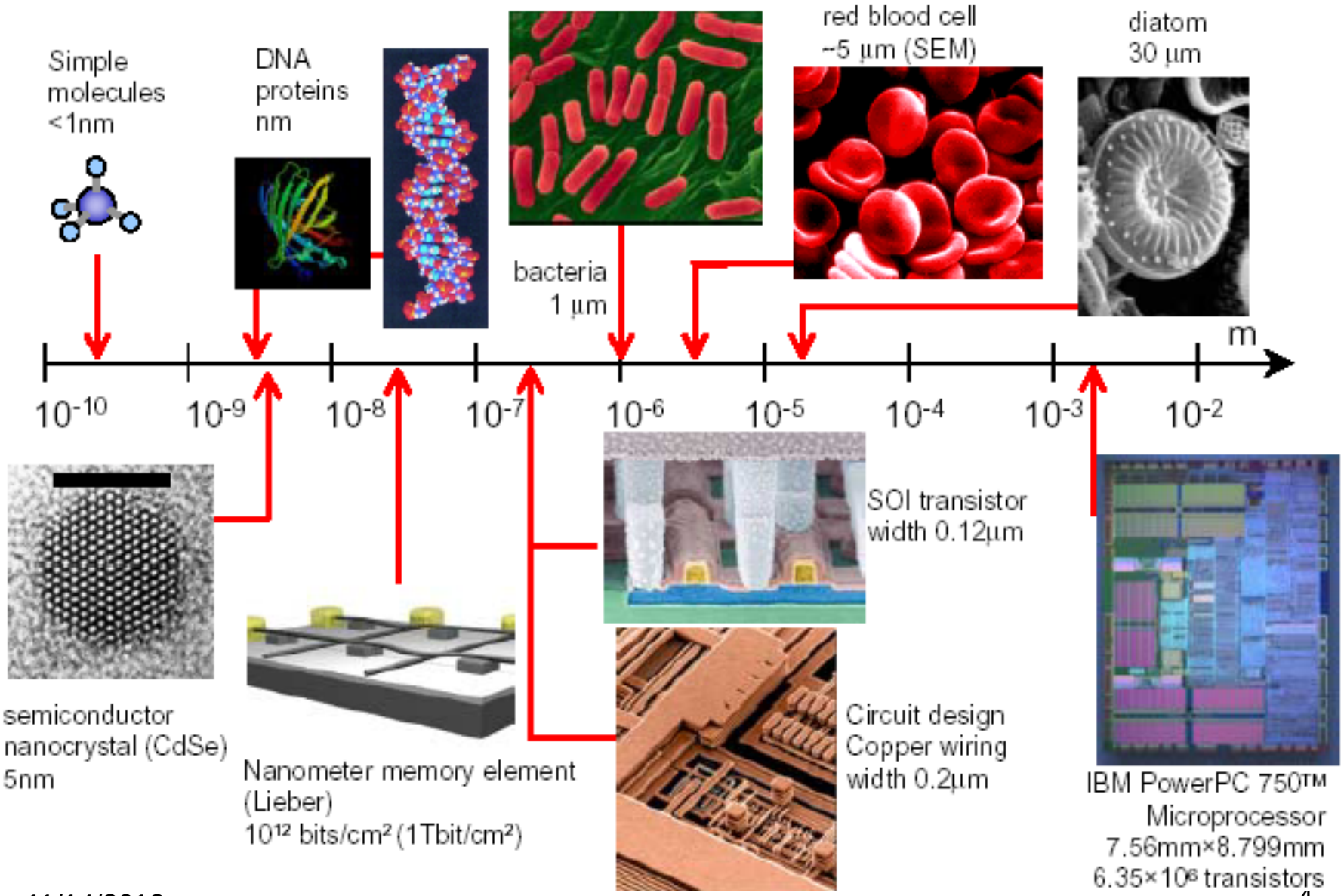

DRIVERS OF NANOSCIENCE AND TECHNOLOGY

TOOLS THAT ALLOW TO 'MAKE' NANOSTRUCTURES

- Epitaxy: Molecular beam, atomic layer deposition, …. (top down)
- Lithography (top down).
- Chemical methods, self assembly (bottom up)

TOOLS THAT ALLOW TO 'SEE' NANOSTRUCTURES

- Microscopes
- Spectroscopies

'ASSEMBLING' NANOSTRUCTURES INTO FUNCTIONAL DEVICES

THE NANOWORLD FOLLOWS THE LAWS OF QUANTUM MECHANICS

Fundamentals: EM waves and photons

Classical theory (Newton): light composed by particles

1900- Blackbody radiation: quantization of energy Planck

1905- Einstein proposed the existence of photons. Photoelectric effect

1924- Experimental demonstration of the existence of photons: Compton effect.

$$\begin{cases} E = h\nu = \hbar\omega \\ \boldsymbol{p} = \hbar\,\boldsymbol{k} \end{cases} \longrightarrow \quad \hbar = h/2\pi$$

$$h = 6.62\ 10^{-34}\ J\ s$$

Young's double slit experiment

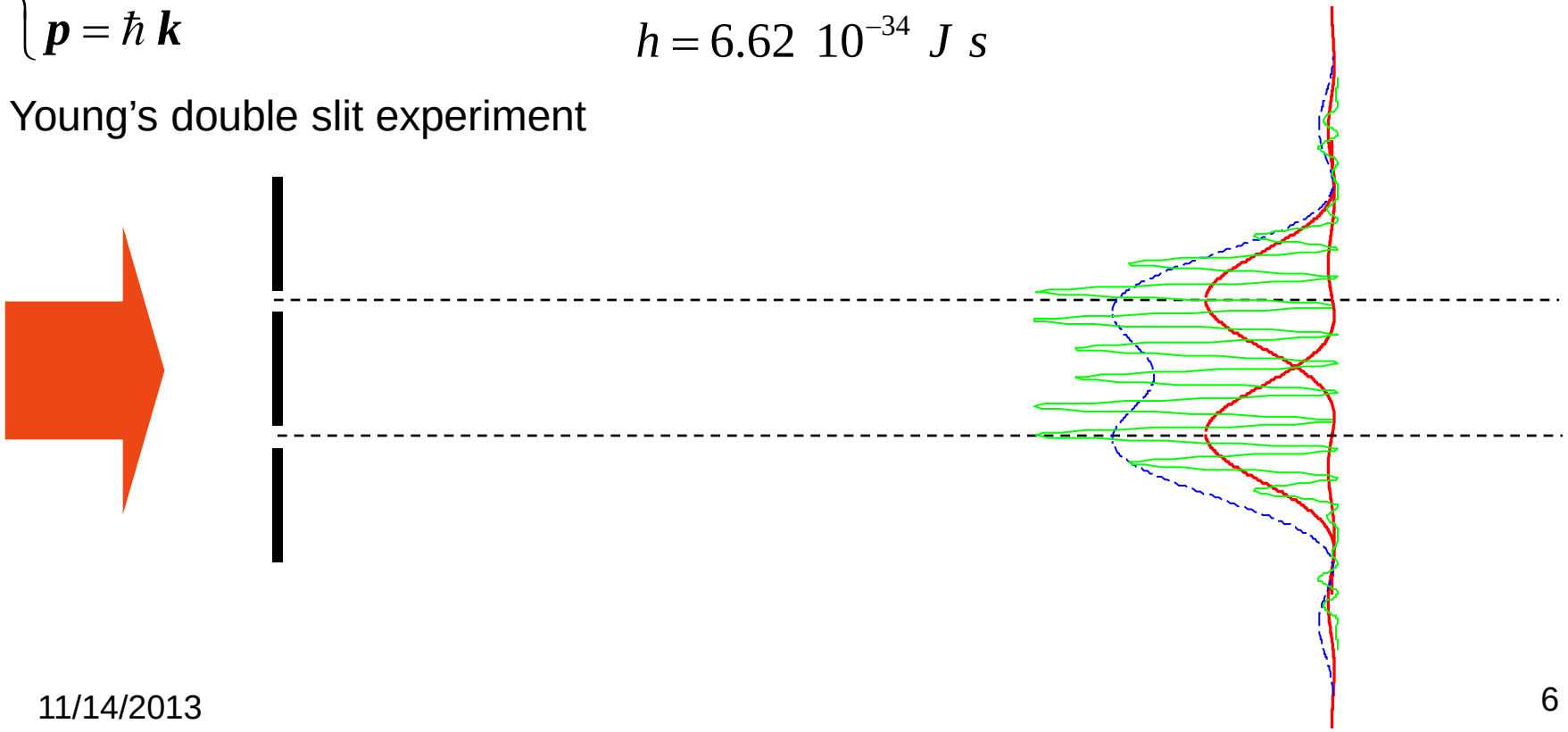

Fundamentals: Young's experiment

What happens when photons impinge the screen one by one?

a- if a photographic plate (screen) records the total intensity we will observe that the fringes do not disappear

→ NOT a purely corpuscular interpretation

b- if the photographic plate is exposed during a period so short to receive only few photons we will observe "localized" impacts in the film

→ NOT a purely wave interpretation

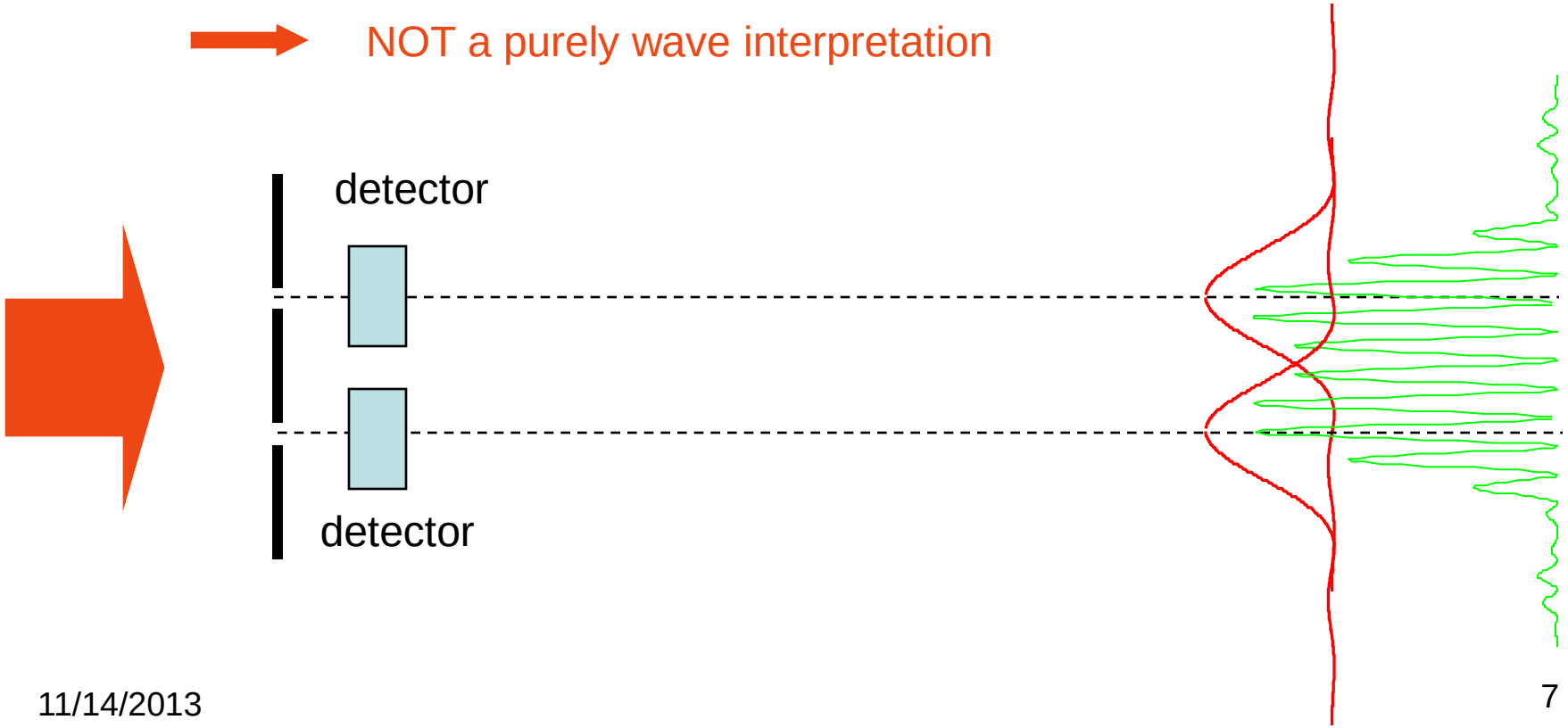

Fundamentals: The de Broglie relations

Parallel to the discovery of photons, atomic emission and absorption were observed to occur in narrow lines such that

$$E_j - E_i = h\nu_{ij}$$

In 1923 de Broglie put forth the following hypothesis: "*material particles just like photons can have a wavelike aspect*"

$$\begin{cases} E = h\nu = \hbar\omega \\ \boldsymbol{p} = \hbar\,\boldsymbol{k} \end{cases} \Rightarrow \quad \lambda = \frac{2\pi}{|\boldsymbol{k}|} = \frac{h}{|\boldsymbol{p}|}$$

He derived the quantization rules as a consequence of this hypothesis. The various permitted energy levels appears as analogs of the normal modes of a vibrating string

Two examples

a) A particle of dust

$$m \cong 10^{-15}\ kg$$
$$\mathrm{v} \cong 1\ \mathrm{mm/s}$$

$$\lambda = \frac{h}{|\boldsymbol{p}|} = \frac{6.6\,10^{-34}\ Js}{10^{-15}kg\ \ 10^{-3}\ m/s} = 6.6\ \ 10^{-6}\,A$$

b) A thermal neutron

$$m \cong 1.67\ \ 10^{-27}\ kg$$
$$\mathrm{v} \cong \sqrt{3m_n kT}$$

$$\lambda \cong 1.4A$$

Fundamentals: spectral decomposition

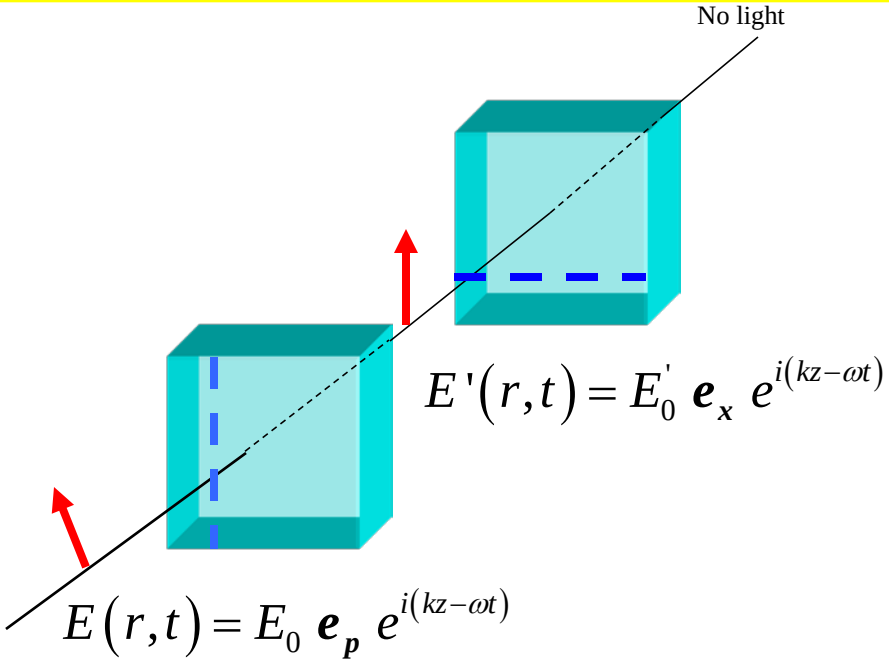

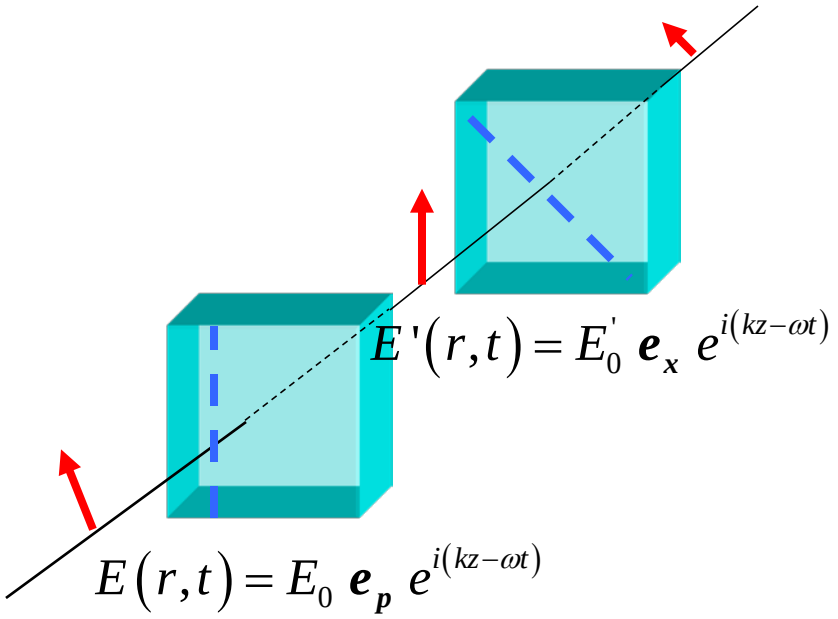

1- If we send the photons one by one, the analyzer can either transmit or stop the photon: there is a quantization of the result in *eigen* (proper) *result*

2- Each of these results (pass or stop) corresponds to an eigenstate (polarization x or y)

3- If the initial state is an eigenstate, the measurement gives an eigenvalue with probability 1 (certain result)

4- If the initial state is unknown, we can only evaluate the *probability* to obtain one of the eigenvalues

Fundamentals: Postulates of Quantum Mechanics

Macroscopic world ⟺ "Classical" mechanics

Particles obey Newtonian Mechanics – Waves obey Maxwell's equations

$$x = x_0 + v_0 t + \frac{1}{2} a\, t^2$$

Position variable – for a with a along the x-direction and initial velocity v_o

$$p = m\, v$$

Linear momentum variable – v is the velocity, m the mass of the particle

$$E = \frac{1}{2} m v^2$$

Kinetic energy

$$W = mgh$$

Potential energy

$$H = W + E$$

Total energy

Microscopic world ⟺ "Quantum" mechanics

Particles are indivisible, have mass, charge or in the case of the photons, energy. Their propagation is wave-like

Postulates of Quantum Mechanics

1- The state of a system with n position variables q_1, q_2, q_n is specified by a state (or wave) function $\Psi(q_1, q_2, \ldots q_n)$

2- To every observable (physical magnitude) there corresponds an Hermitian operator ($H = H^{*\dagger}$) given by the following rules:

a) The operator corresponding to the Cartesian position coordinate x is x. Similarly for y and z

b) The operator corresponding to the x component of the linear momentum p_x is $\left(\frac{h}{i}\right)\left(\frac{\partial}{\partial x}\right)$

c) the operator corresponding to any other observable is obtained by first writing down the classical expression of the observable in terms of x, y, z, p_x, p_y, p_z and then replacing each quantity by its corresponding operator according rules 1 and 2.

Ref.: Quantum Mechanics for engineering, material science and applied physics, Herbert Kroemer, Prentice Hall

Fundamentals: Postulates of QM

3- The only possible result which can be obtained when a measurement is made of an observable whose operator is A is an eigenvalue of A.

4- Let α be an observable whose operator A has a set of eigenfunctions Φ_j with corresponding eigenvalues a_i. If a large number of measurements of α are made on a system in the state Ψ the value obtained is given by

$$\langle A \rangle = \int \Psi^* A \ \Psi \ d\tau \qquad d\tau = d^3 r$$

where the integral is taken over all space.

5- If the result of a measurement of α is a_r, corresponding to the eigenfunction Φ_r, then the state function after the measurement is Φ_r

6- The time variation of the state function of a system is given by:

$$\frac{\partial \Psi}{\partial t} = \frac{1}{i\hbar} H \Psi$$

Where H is the Hamiltonian of the system

Fundamentals: state (or wave) function

- The wave function is the mathematical description used in QM for any physical system. It is expressed as a superposition of all the possible states of the system. In its simplest form it is givenby

$$\Psi(x) = A\exp\left[i\left(kx-\omega t\right)\right]$$

Wave function of a free particle traveling in one dimension

- The temporal evolution of the wave functions is described by the Schrodinger equation.

$$\frac{\partial\Psi\left(x,t\right)}{\partial t} = \frac{1}{i\hbar}H\Psi\left(x,t\right)$$

- The expectation values of the wave function are probability amplitudes: complex numbers.

- The squares of the absolute values gives the probability distribution that the system has in any of the possible states.

Fundamentals: Hermitian operator, eigenvalues and eigenfunctions

One of the QM postulates is $\langle A \rangle = \int \Psi^*(r) A \ \Psi(r) \ d\tau$

All physical observables are represented by such expectation values, so they must be real:

$$\Rightarrow \langle A \rangle = \langle A \rangle^* \qquad \int \Psi^*(r) A \ \Psi(r) \ d\tau = \int \Psi(r) \left[A \ \Psi(r) \right]^* \ d\tau$$

Operators which satisfy this condition are called *Hermitian or self-adjoint*. [$H=H^{\dagger *}$]

The eigenfunctions of a linear operator A are the set of functions f that fulfills the following relation

$$A \ f = \lambda \ f$$

In this relation the scalars λ, are the eigenvalues of the operator A

For example $f(x) = e^{\alpha x}$ is an eigenfunction for the operator $A = \frac{d^2}{dx^2} - \frac{d}{dx}$

With eigenvalue $\alpha^2 - \alpha$

Fundamentals: Probability of result of measurement

Eigenvalues a_j of an operator A are *discrete*, and the state function Ψ and all the eigenfunctions Φj are normalized. To find the probability p_r that the result of the measurement of an observable α is a particular value a_r we expand the wavefunction in terms of the eigenfunctions:

$$\Psi = \sum_j c_j \, \Phi_j$$

Then the probability will be $p_r = \left| c_j \right|^2$

$$c_r = \int \Phi_r^* \, \Psi \, d\tau$$

If the coefficients c_j are known, an expression for the expectation value is

$$\langle A \rangle = \sum_j p_j \, a_j = \sum_j \left| c_j \right|^2 a_j$$

Continuous eigenvalues. Let γ be an observable whose operator G has eigenvalues k which form a continuous spectrum. Assume only the one dimensional case for single particle. If Φ(k,x) are the eigenfunctions of G the wavefunction Ψ can be written as

$$\Psi(x) = \int g(k) \, \Phi(k, x) \, dk$$

$\left| g(k) \right|^2 dk$ is the probability that γ is measured in the range $k \to k + dk$

Fundamentals: Linear momentum

An example of an observable with continuous eigenvalues is the linear momentum. The eigenfunctions of the operator p_x are $\Phi(k,x) = c\, e^{ikx}$ with eigenvalues $\hbar k$

For the linear momentum the wave function can be expressed as

$$\Psi(x) = c\int_{-\infty}^{\infty} g(k)\; e^{ikx}\; dk$$

The functions $g(k)$ $\Psi(x)$ are related through the Fourier transform.

$$g(k) \propto \int_{-\infty}^{\infty} \Psi(x)\, e^{-ikx}\; dx$$

With the condition

$$\int_{-\infty}^{\infty} |g(k)|^2\; dk = 1$$

Fundamentals: time variation of the wave function and expected value

A system with a time independent Hamiltonian. If $\Psi(t=0)$ is known then

$$\Psi(t) = \sum_j c_j \, u_j \, \exp\left(-{iE_j t}/{\hbar}\right)$$

where u_j is the eigenvalue of H with energy E_j . The coefficients c_j are given by

$$c_j = \int_{-\infty}^{\infty} u_j^* \, \Psi(0) \, dx$$

If the eigenvalues of the Hammiltonian are a continuous spectrum with eigenfunctions u_k , the wavefunction is expressed as

$$\Psi(x,t) = \int_{-\infty}^{\infty} g(k) \, u_k \, \exp\left(-{iE_k t}/{\hbar}\right) dk$$

where $g(k) = \int_{-\infty}^{\infty} u_k^* \; \Psi(x,0) \; dx$

The time variation of the expectation value of an observable with operator A for a system with a wavefunction Ψ is

$$\frac{\partial}{\partial t}\langle A \rangle = \frac{1}{i\hbar}\int \Psi^* \; (AH - HA) \; \Psi \; d\tau = \frac{1}{i\hbar}\langle AH - HA \rangle$$

ELECTROMAGNETICS

Wave-like

$\nabla^2 \mathbf{E} - k^2 \boldsymbol{E} = 0$

$\boldsymbol{E} = \boldsymbol{E}_o exp^{j\omega t} exp^{j\boldsymbol{k}.\boldsymbol{r}}$ vector

k: wave-vector
r: vector position

Particle-like

$$\begin{cases} E = h\nu = \hbar\omega \\ \boldsymbol{p} = \hbar\,\boldsymbol{k} \end{cases}$$

QUANTUM MECHANICS

Particle-like

$$E = \frac{1}{2}mv^2$$

$$W = mgh$$

$H = W+E$

Wave-like

$$\begin{cases} E = h\nu = \hbar\omega \\ \boldsymbol{p} = \hbar\,\boldsymbol{k} \end{cases} \qquad \lambda = \frac{2\pi}{|\boldsymbol{k}|} = \frac{h}{|\boldsymbol{p}|}$$

$$\Psi(x) = A\exp\left[i\left(kx - \omega t\right)\right]$$

$$\frac{\partial\Psi(x,t)}{\partial t} = \frac{1}{i\hbar}H\Psi(x,t)$$

$$\Psi(x) = A\exp\left[i\left(kx - \omega t\right)\right]$$

$$\langle A\rangle = \int \Psi^* A\ \Psi\ d\tau$$

Fundamentals: Example

A particle moving in one dimension has a wavefunction $\Psi(x) = \frac{1}{(2\pi\,\Delta^2)^{\frac{1}{4}}} \exp\left(-x^2 \big/ 4\Delta^2\right)$

Where Δ is a constant. Show the following:

a) The wavefunction is normalized

$$\int_{-\infty}^{\infty} \Psi(x)\,\Psi^*(x)\,dx = \frac{1}{(2\pi\,\Delta^2)^{\frac{1}{2}}} \int_{-\infty}^{\infty} \exp\left(-x^2 \big/ 2\Delta^2\right) = \frac{1}{(2\pi\,\Delta^2)^{\frac{1}{2}}} \sqrt{2\pi}\Delta^2 = 1$$

b) The probability that the particle has a linear momentum in the range $p \rightarrow p + dp$

$|g(k)|^2\,dk$ is the probability that takes values in the range $p \rightarrow p + dp$

$$g(k) \propto \int_{-\infty}^{\infty} \Psi(x)\,e^{-ikx}\,dx = \int_{-\infty}^{\infty} \exp\left(-x^2 \big/ 4\,\Delta^2\right) e^{-ikx}\,dx \propto \exp\left(-k^2\,\Delta^2\right)$$

We set $g(k) = c\exp\left(-k^2\,\Delta^2\right)$ Using condition of normalization

$$\int_{-\infty}^{\infty} |g(k)|^2\,dk = 1 = c^2 \int_{-\infty}^{\infty} \exp\left(-2k^2\Delta^2\right) dk = c^2\,\sqrt{2\pi}\,\frac{1}{2\,\Delta}$$

Fundamentals: Example

From this result $g(k) = \frac{1}{(2\pi)^{\frac{1}{4}}} \sqrt{2\,\Delta}\, \exp\left(-k^2\,\Delta^2\right)$

The linear momentum is related to k by $p = \hbar\, k$ thus

$$P(p) = \left|g(k)\right|^2 \frac{dk}{dp} = \sqrt{\frac{2}{\pi}}\,\frac{\Delta}{\hbar}\exp\left(-2\,p^2\,\Delta^2/\hbar^2\right)$$

Uncertainty in position and momentum

$$\left|\Psi(x)\right|^2 = \frac{1}{\sqrt{2\pi}\;\;\Delta}\exp\left(-x^2/2\Delta^2\right) \qquad \left|g(k)\right|^2 = \frac{1}{\sqrt{2\pi}}\,2\,\Delta\exp\left(-2\,k^2\,\Delta^2\right)$$

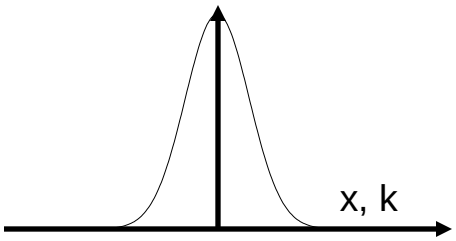

$$\Delta x = \Delta \qquad \Delta k = \frac{1}{2\Delta}$$

$$\Delta p = \Delta k\,\hbar \;\Rightarrow\; \Delta p\,\Delta x = \frac{\hbar}{2\Delta}\,\Delta = \frac{\hbar}{2}$$

Fundamentals: Schrodinger equation

From the classical to the quantum domain

One particle in one dimension moving in a potential V(x) has a Hamiltonian:

$$H = E_k + V(x) = \frac{p_x^2}{2m} + V(x)$$

kinetic energy ↗ ↖ potential energy

To find the expression of the Hamiltonian replace the impulse by $\left(\hbar/i\right) d/dx$

$$H = -\frac{\hbar^2}{2m}\frac{d^2}{dx^2} + V$$

If u(x) is an eigen-function of the Hamiltonian with eigen-value E, we can write

$$H\,u(x) = E\,u(x) \quad \Rightarrow \quad \left(-\frac{\hbar^2}{2m}\frac{d^2}{dx^2} + V\right)u(x) = E\,u(x)$$

Thus $$\frac{d^2\,u(x)}{dx^2} + \frac{2m}{\hbar^2}(E - V)u(x) = 0$$

In three dimensions $$H = \frac{\left(p_x^2 + p_y^2 + p_z^2\right)}{2m} + V(x, y, z)$$

and $$\nabla^2 u(x, y, z) + \frac{2m}{\hbar^2}(E - V)u(x, y, z) = 0$$

Fundamentals: Schrodinger equation

$$\nabla^2 u(x,y,z) + \frac{2m}{\hbar^2}(E - V)u(x,y,z) = 0$$

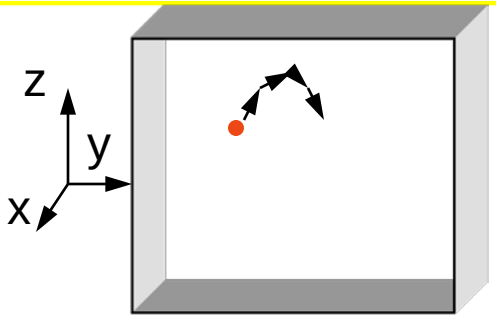

Free electrons –(electrons in metals) - V(r) =0

Wave-like behavior in all 3-directions

Electrons confined in one dimension – (quantum wells) - V(z) = constant in one direction.

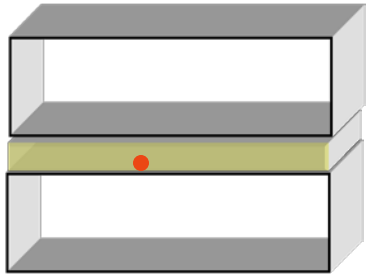

Bound states in z -Wave-like behavior in two directions

Electrons confined in two dimensions –(quantum wires) - V(x,z) = constant

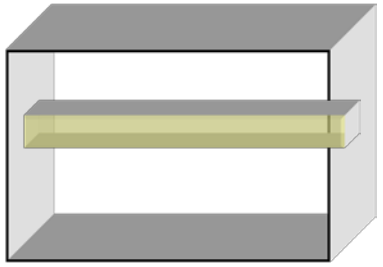

Bound states in z, x -Wave-like behavior in one directions only

Electrons confined in three dimensions –(quantum dots) - V(x,y,z) = constant -

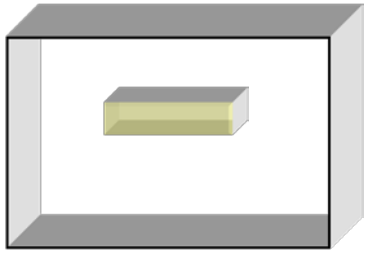

Bound states in x,y.z - These materials are like macro-atoms or molecules

Parity

Let us consider a one dimensional function f(x). If $f(x) = f(-x)$ the function is said to have *even* parity. If $f(x) = -f(-x)$ the function has *odd* parity. A function that does not satisfy either of these two conditions is said to have *mixed* parity. A mixed parity function can always be expressed as a sum of two functions, one with even parity and the other with odd parity.

$\sin(2\pi x)\, e^{-x^2/1000}$ $\cos(2\pi x)\, e^{-x^2/1000}$ $(2\pi x)^3\, e^{-x^2/1000} + (2\pi x)^2\, e^{-x^2/1000}$

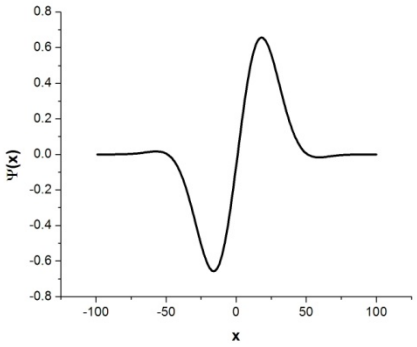

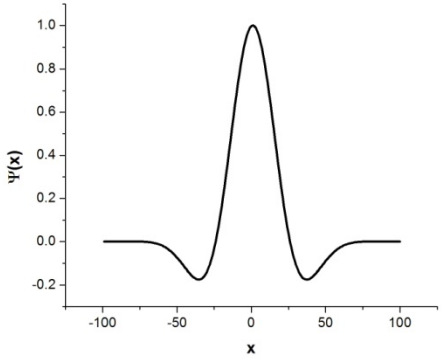

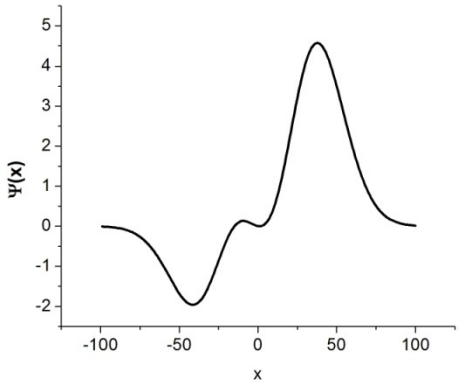

Continuity

The eigenfunction u is continuous everywhere. The derivatives of u are also continuous everywhere, except where the potential function has an infinite discontinuity (only possible in theory, cannot happen in an actual physical situation)

Fundamentals: Orbital angular momentum

The operator for the components of the orbital momentum are $L_x \quad L_y \quad L_z$

For the square of this magnitude the operator is $L^2 = L_x^2 + L_y^2 + L_z^2$

The operator L^2 commutes with L_x, L_y, L_z . The component operators do not commute with each other. The commutation rule for the angular momentum operators is $\left[L_x, L_y \right] = i\hbar \, L_z$ and cyclic permutations.

The common eigenfunctions of L^2 and L_z are the spherical harmonics Y_{lm}. The eigenvalues of L^2 and L_z are given by:

$$L_z \, Y_{lm} = m \;\; \hbar \, Y_{lm}$$

L is quantized

Where $l \geq 0$ and $-l \leq m \leq l$

The spherical harmonics are orthogonal and normalized $L^2 \, Y_{lm} = l\left(l+1\right) \;\; \hbar^2 \, Y_{lm}$

$$\int_0^{\pi} \int_0^{2\pi} Y^*_{l'm'} \, Y_{lm} \sin\theta \;\; d\theta \;\; d\phi = 1 \qquad \left(l' = l \;\; and \;\; m' = m \right)$$

$$\int_0^{\pi} \int_0^{2\pi} Y^*_{l'm'} \, Y_{lm} \sin\theta \;\; d\theta \;\; d\phi = 0 \qquad \left(otherwise \right)$$

Fundamentals: Examples

Do x and p_x commute?

$$\left[x, p_x\right] f\left(x\right) = -i\hbar\left[x\frac{df}{dx} - \frac{d\left(xf\right)}{dx}\right] = -i\hbar\left[x\frac{df}{dx} - x\frac{d\left(f\right)}{dx} - f\right] = i\hbar f\left(x\right)$$

Because $\left[x, p_x\right] \neq 0$, can't know momentum and position simultaneously and exactly.

Consider free particle for which momentum exactly known.

Do p_x and H commute?

$$\left[p_x, H\right] f\left(x\right) = -i\hbar\frac{d}{dx}\left[-\frac{\hbar^2}{2m}\frac{d^2}{dx^2} + V\left(x\right)\right] f\left(x\right) - \left[-\frac{\hbar^2}{2m}\frac{d^2}{dx^2} + V\left(x\right)\right]\left[-i\hbar\frac{d}{dx}\right] f\left(x\right)$$

$$= -i\hbar\frac{d}{dx}\left[V\left(x\right) f\left(x\right)\right] - \left[-V\left(x\right) i\hbar\frac{d}{dx}\right] f\left(x\right) = -i\hbar\frac{dV\left(x\right)}{dx} f\left(x\right)$$

They commute only for a free particle (V(x) = 0)

Fundamentals: Example Schrodinger equation

A particle of mass m moves in one dimensional potential as shown in the figure.

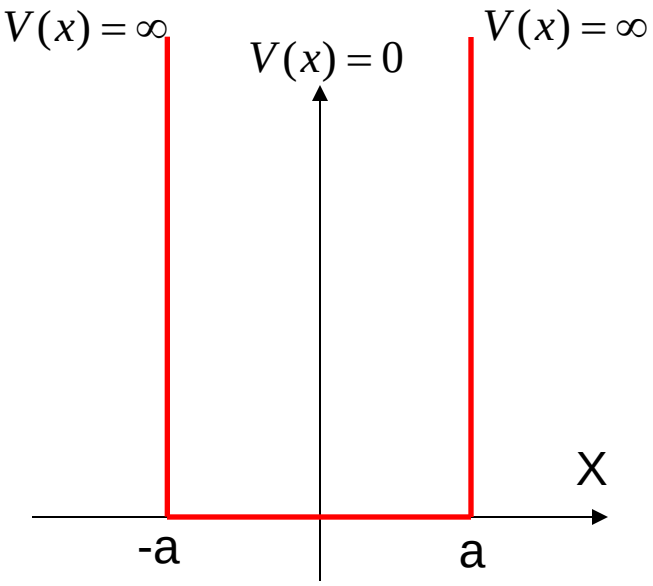

a) Derive the expressions of the normalized solutions of the Schrodinger equation and the corresponding energies

b) Sketch the wavefunctions

c) Indicate the parity of the wavefunctions

In the interval –a<x<a the Schrodinger eq is

$$\frac{d^2u}{dx^2}+k^2u=0 \qquad \left(\frac{2mE}{\hbar^2}=k^2\right)$$

Solutions $u(x)=A\cos(kx)+B\sin(kx)$

Boundary conditions $u(a)=u(-a)=0$

The boundary conditions impose $\begin{cases} B=0 & \cos(ka)=0 \\ A=0 & \sin(ka)=0 \end{cases}$

The solutions are $\begin{cases} u(x)=\cos(kx) \\ u(x)=\sin(kx) \end{cases}$

Fundamentals: Example Schrodinger equation

The boundary condition is fulfilled if $k = n\frac{\pi}{2a}$ With odd n for cos and even n for sin

Let $u(x) = A\ \cos\left(\frac{n\pi}{2a}x\right)$

Using the normalization condition:

$$\int_{-\infty}^{\infty} |u(x)|^2\ dx = A^2 \int_{-a}^{a} \cos^2\left(\frac{n\pi}{2a}x\right) dx = A^2\ \frac{2a}{n\pi} \int_{-n\pi/2}^{n\pi/2} \cos^2\theta\, d\theta = A^2\ a = 1$$

Similarly for the sin solution. The wavefunctions are:

$$|x| < a \quad u(x) = \frac{1}{\sqrt{a}}\ \cos\left(\frac{n\pi}{2a}x\right) \qquad [n \quad odd]$$

$$u(x) = \frac{1}{\sqrt{a}}\ \sin\left(\frac{n\pi}{2a}x\right) \qquad [n \quad even]$$

$$|x| > a \quad u(x) = 0$$

The energy is given by

$$\frac{2mE}{\hbar^2} = k^2 \rightarrow E = \frac{k^2\hbar^2}{2m} = n^2\ \frac{\pi^2\hbar^2}{8ma^2}$$

Fundamentals: Example Schrodinger equation

The first 4 wavefunctions are

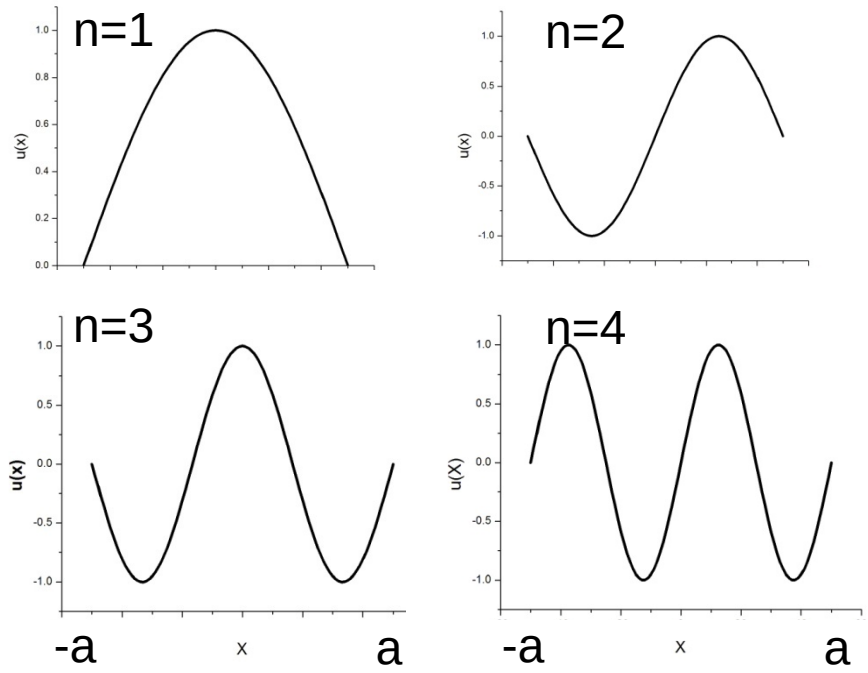

Even functions

Odd functions

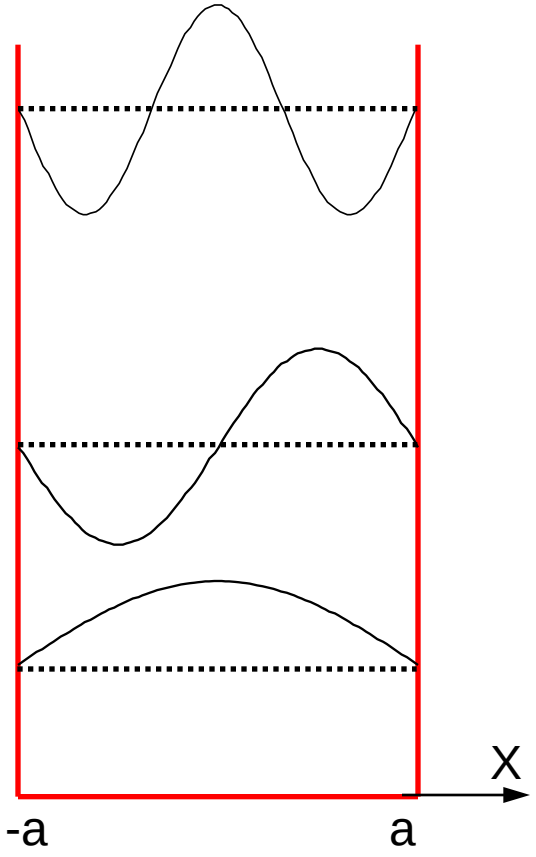

Class exercise

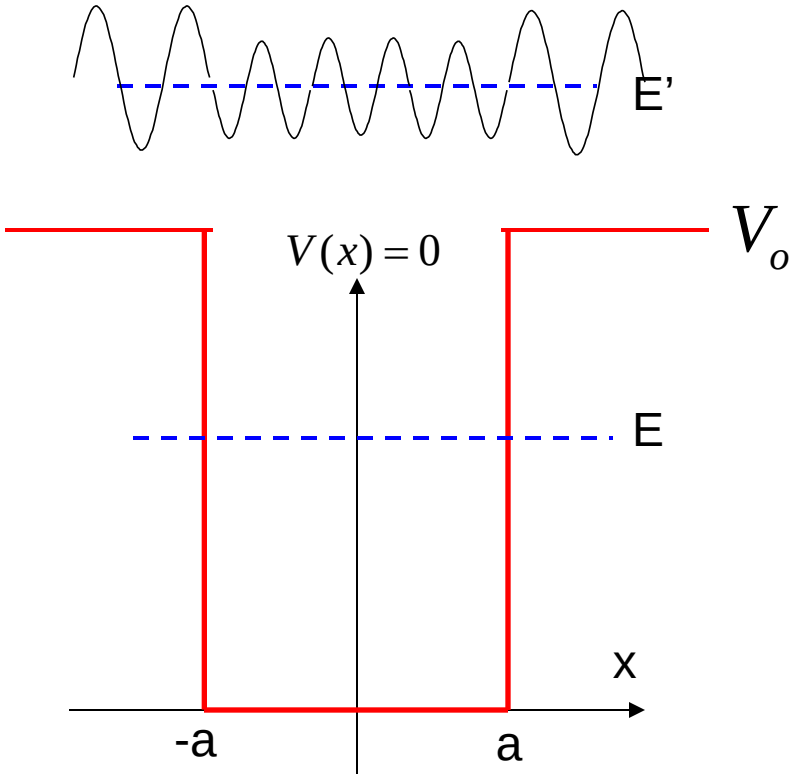

Solve Schroedinger's equation to determine the eigenergies and eigenfunctions for a particle within the box (E) and one outside (E')

-a<x<a

$$\frac{d^2u}{dx^2}+k^2u=0 \qquad \left(\frac{2mE}{\hbar^2}=k^2\right)$$

Solutions $u(x)=A\cos(kx)+B\sin(kx)$

-a>x and x>a

$$\frac{d^2u}{dx^2}+\frac{2m}{\hbar^2}(-V_o+E)u=0 \qquad k_2=\sqrt{\frac{2m}{\hbar^2}(E-V_o)}$$

Solutions $$u(x)=\begin{cases} C\exp(-k_2x) & x>a \\ D\exp(k_2x) & x<-a \end{cases}$$

Class exercise

For E’ -a<x<a

$$\frac{d^2u}{dx^2}+\frac{2m}{\hbar^2}(E')u=0 \qquad k=\sqrt{\frac{2m}{\hbar^2}E'}$$

$$u(x)=A\exp(ikx)+B\exp(-ikx)$$

-a>x x>a

$$\frac{d^2u}{dx^2}+\frac{2m}{\hbar^2}(E'-V_o)u=0 \qquad k_2=\sqrt{\frac{2m}{\hbar^2}(E'-V_o)}$$

$$u(x)=C\exp(ik_2x)+B\exp(-ik_2x)$$

Boundary conditions

$u(x=-a) \quad u(x=a) \quad continuous$

$\left.\frac{du}{dx}\right|_{x=-a} \quad \left.\frac{du}{dx}\right|_{x=a} \quad continuous$

Class exercise

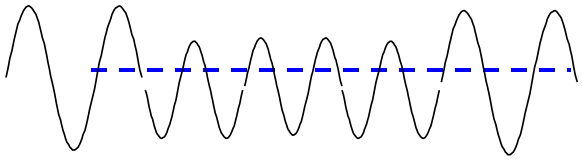

Free electron behavior

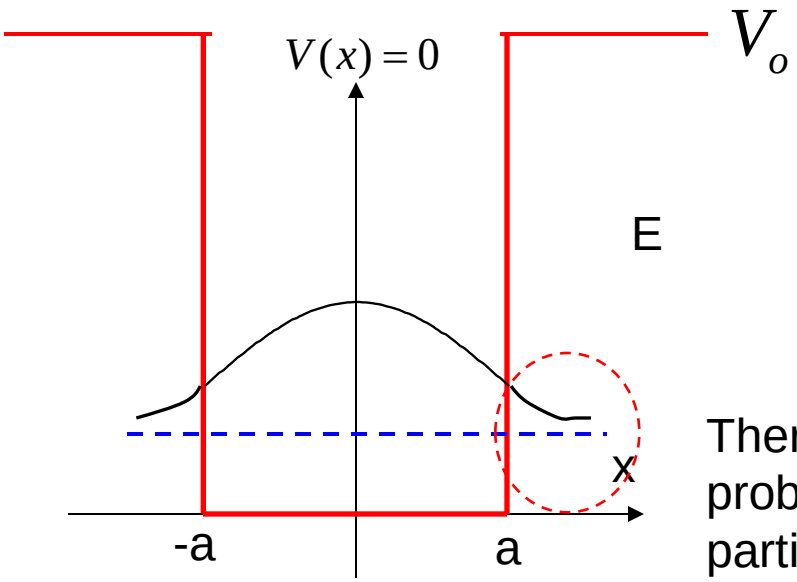

There is a small but finite probability of finding the particle outside the potential box

States of a set energy, described by a wavefunction u(x), small but not zero probability of finding the particle outside the region defined by the potential walls are what defines quantum behavior

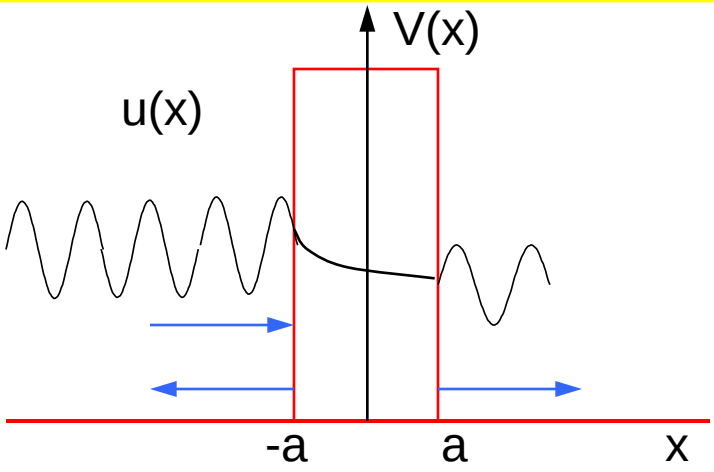

A particle described by a wavefunction u(x) has a finite probability of tunneling a thin potential barrier

Oscillatory behavior on the left is the superposition of a traveling wave in +x direction and one (reflected) traveling in –x direction (like in electro-magnetics)

Three dimensional well

Let's assume that a particle is confined to a 3-dimensional cube-shaped square well.

$$V(x,y,z)=\begin{cases}0 & for \quad 0<x,y,z<L\\ \infty & elsewhere\end{cases}$$

At the surface of the cube the wavefunctions vanish for all x, y, z.

$$\psi(0,y,z)=\psi(x,0,z)=\psi(x,y,0)=0$$
$$\psi(L,y,z)=\psi(x,L,z)=\psi(x,y,L)=0$$

To meet the boundary conditions, the wavefunctions Inside the well the wavefunctions are superposition of plane waves

$$\psi(x,y,z)=A(\vec{k})\sin(k_x x)\sin(k_y y)\sin(k_z z)$$

Where the vector **k** satisfies $k^2=k_x^2+k_y^2+k_z^2$

The corresponding energies are:

$$E_k = \frac{\hbar^2 k^2}{2M} = \frac{\hbar^2}{2M}(k_x^2 + k_y^2 + k_z^2)$$

Where the k components take values of

$$k_x L = n_x \pi \quad k_y L = n_y \pi \quad k_z L = n_z \pi$$

n_x, n_y, n_z are independent positive integers that vary in steps of 1. The corresponding energy eigenvalues are

$$E_n = \frac{\hbar^2}{2ML^2}(n_x^2 + n_y^2 + n_z^2) = E_1 n^2$$

E_1 is the ground state energy

Three dimensional well

Notice that there 3! Possible combinations for the n-indices that will have the same eigenenergy E_1

$(n_x, n_y, n_z) = (1,2,3); (1,3,2)\ldots\ldots \cong E = 14\ E_1$ This indicates that this energy level is degenerate.

This symmetry arises from the symmetry in the potential of interaction.

If we now consider that each n-state occupies a volume of 1 (this is increment for each of the n- values and that only positive values of n correspond to additional states, we can calculate the number of states contained within a quadrant of a sphere of radius n and volume $V = \frac{4\pi n^3}{3}$

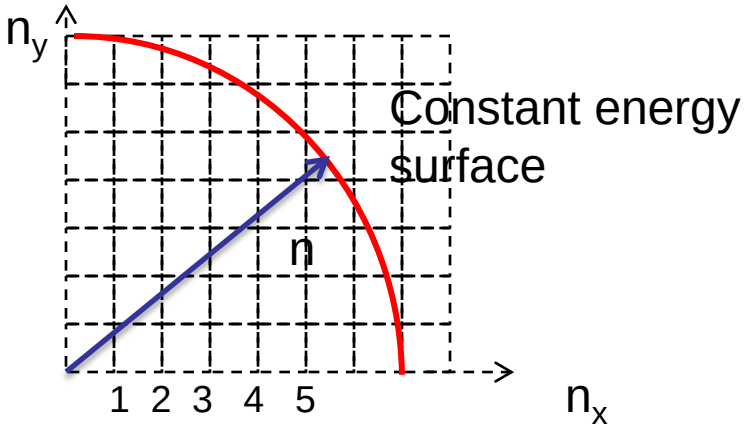

The total number of states in the octant is

$$N = \frac{1}{8}\frac{4\pi}{3}n^3 = \frac{\pi}{6}\left(\frac{E}{E_1}\right)^{3/2}$$

The number of states per unit energy is

$$\Delta N = \frac{d}{dE}\left[\frac{\pi}{6}\left(\frac{E}{E_1}\right)^{3/2}\right] = \frac{\pi}{4}\left(\frac{E}{E_1}\right)^{1/2} = \frac{\pi}{4}n$$

The number of states per unit energy in the vicinity of E and per unit volume is

$$D(E) = \frac{1}{L^3}\frac{dN}{dE} = \frac{\pi}{4L^3}\left(\frac{E}{E_1}\right)^{1/2} = \frac{\pi}{4L^2}\left(\frac{2M}{\hbar^2}\right)^{1/2}E^{1/2} \qquad E_1 = \frac{\hbar^2}{2ML^2}$$

The density of states plays an important role in the quantum mechanics of gasses and of free electrons in metals and semiconductors

REVIEW FROM LAST CLASS

Wavefunction of an a sub-atomic particle is obtained by solving Schroedinger's equation
H= E+V

This is a second order differential equation, therefore to find a unique solution we also need to boundary conditions.

- U(x) continuous; dU(x)/dx must be continuous;
- Normalization condition which relates to the probability density of finding the particle in space.
- We discussed the problem of the a particle in a one dimensional box – with infinite potential wall.
- We extended this case to a 3D box and used the concept to obtain the density of energy states per unit volume accessible to the particle.
- Particles could have one, two or three degrees of confinement, or conversely, 2, 1 and 0 degrees of 'free' motion.

Nanomaterials in preventive dentistry

Matthias Hannigmatthias.hannig@uks.eu & Christian Hannig

Journal name: Nature Nanotechnology, Volume: 5 ,Pages: 565–569
Year published: (2010), DOI: doi:10.1038/nnano.2010.83
Published online: 27 June 2010

Abstract
The prevention of tooth decay and the treatment of lesions and cavities are ongoing challenges in dentistry. In recent years, biomimetic approaches have been used to develop nanomaterials for inclusion in a variety of oral health-care products. Examples include liquids and pastes that contain nano-apatites for biofilm management at the tooth surface, and products that contain nanomaterials for the remineralization of early submicrometre-sized enamel lesions. However, the treatment of larger visible cavities with nanomaterials is still at the research stage. Here, we review progress in the development of nanomaterials for different applications in preventive dentistry and research, including clinical trials.

Nanomaterials in preventive dentistry

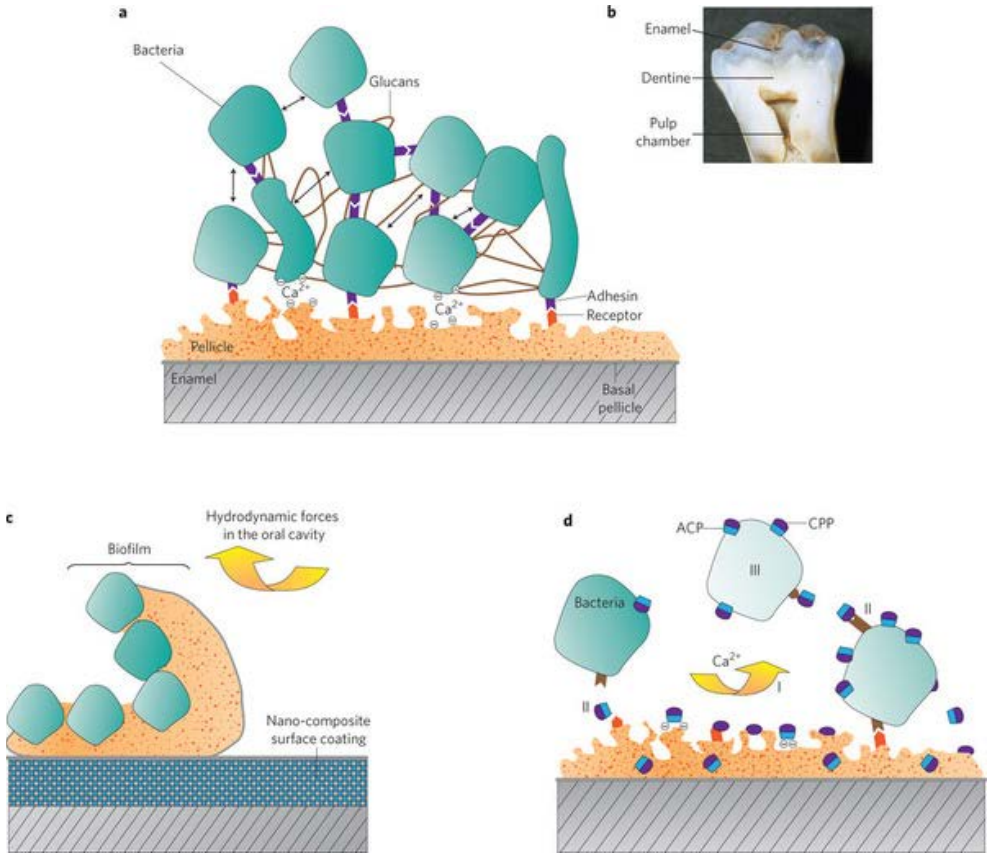

Figure 1: Bioadhesion and biofilm management in the oral cavity.

a, Bioadhesion in the oral cavity. Proteins interact with the enamel surface to form a proteinaceous pellicle layer. Bacteria adhere to this conditioning film through calcium bridges and specific adhesin–receptor interactions (purple and red). Bacteria are surrounded by an extracellular matrix of water-insoluble glucans, and they communicate through quorum sensing (arrows). **b,** Cross-section of a human molar tooth showing the enamel, dentine and pulp chamber. **c,** Easy-to-clean nanocomposite surface coating. The **low-surface-free-energy** coating (blue) causes poor protein–protein binding. Shear forces in the mouth (yellow arrow) can easily detach the outer layer of the pellicle and bacterial biofilm from the surface**. d**, CPP–ACP inhibits bacterial adhesion and oral biofilm formation. CPP attaches to the pellicle and limits bacterial adhesion. It competes with calcium for plaque–calcium binding sites (I), and decreases the amount of calcium bridging the pellicle and bacteria, and between the bacterial cells. Specific receptor molecules (red) in the pellicle layer and on the bacterial surfaces (brown) are blocked, further reducing adhesion and co-adhesion (II). This affects the viability of the bacteria (III).

Nanomaterials in preventive dentistry

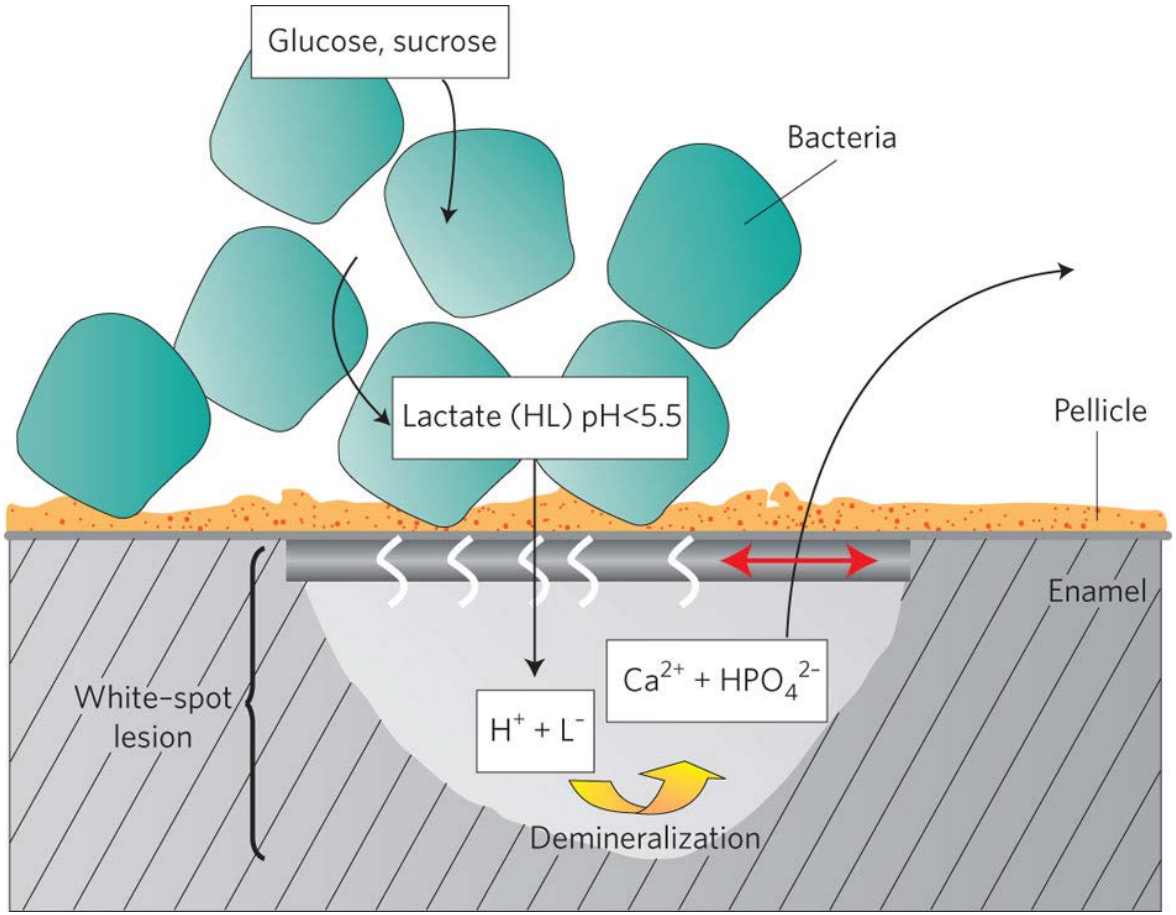

Figure 2: Early stages of tooth decay caused by bacterial biofilm.
Bacteria metabolize sugar and other carbohydrates to produce lactate (HL) and other acids that, in turn, dissociate to form H+ ions that demineralize the enamel beneath the surface of the tooth; calcium and phosphate are dissolved in the process. This is known as a white-spot lesion. Owing to reprecipitation, a pseudo-intact surface layer (red arrow) is observed on top of the body of the carious lesion in this early stage of tooth decay. This pseudo-intact layer is permeable to ions (indicated by white chevrons).

Nanomaterials in preventive dentistry

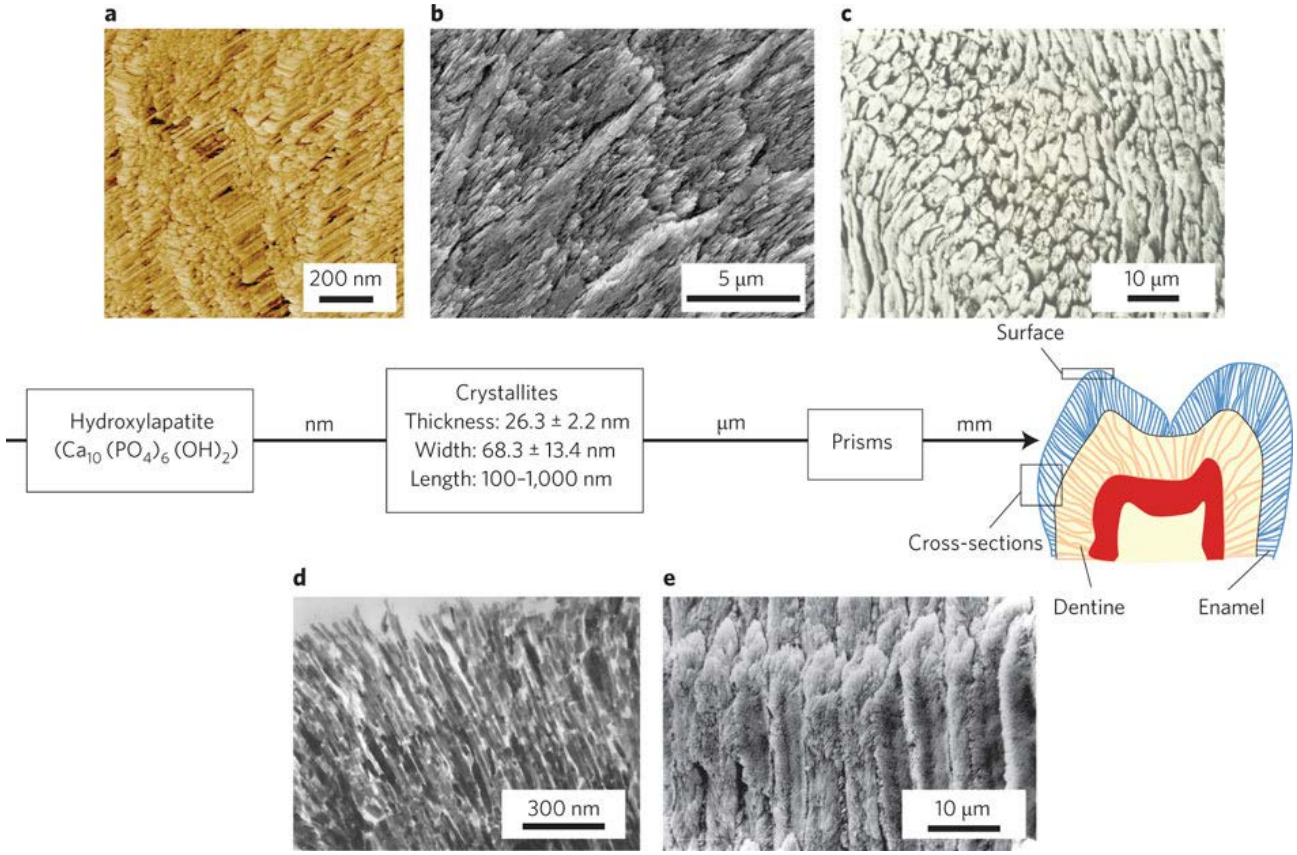

Figure 3: Hierarchical structure of the dental enamel.
Dental enamel is a masterpiece of bioceramics, containing structures at different hierarchical levels from the microscale down to the nanoscale. The enamel is composed of three-dimensionally organized nanosized hydroxyl apatite crystallites (a,b,d) that are arranged into micrometre-sized prisms (c,e). a, Atomic force microscope and b,c, scanning electron microscope images of the enamel surface. d, Transmission electron microscope and e, scanning electron microscope images of a cross-section of the enamel.

Nanomaterials in preventive dentistry

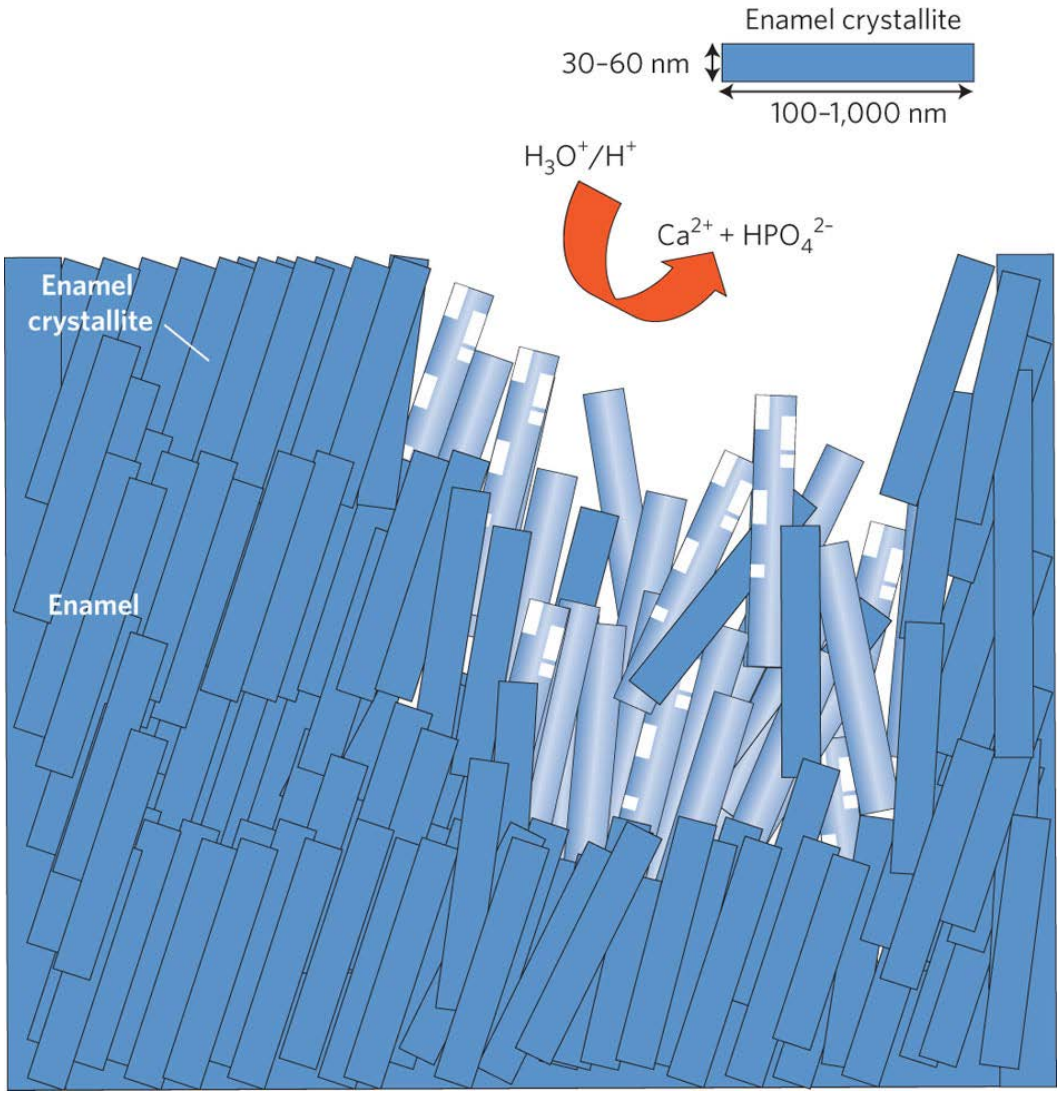

Figure 4: Dental erosion caused by acidic beverages or food in the oral cavity.
Low pH, caused by acidic beverages or gastric juices (pH 1–4), destroys the enamel surface by partial and complete dissolution of the enamel crystallites, resulting in the release of Ca2+ and HPO42− ions. This loosens the microstructure of the enamel and hydroxyl apatite crystallites (pale blue) become demineralized, or are lost.

Nanostructures to the rescue

Anti-adhesive surfaces- ultrahydrophobic – self-cleaning have been tried but not suitable for application in oral cavity due to surface wear and chemical incompatibility with pellicle layer

Easy-to-clean surface -properties are achieved by integrating nanometre-sized inorganic particles into a fluoropolymer matrix. These biocompatible surface coatings have a surface free-energy of 20–25 mJ m^{-2} — known as theta surfaces — and therefore can facilitate the detachment of adsorbed salivary proteins and adherent bacteria under the influence of physiological shearing forces in the mouth

Nanomaterials in preventive dentistry

Other nano-enabled approaches for biofilm management are **oral health-care products that contain bioinspired apatite nanoparticles**, either alone or in combination with proteinaceous additives such as casein phosphopeptides. Casein phosphopeptide (CPP)-stabilized amorphous calcium phosphate (ACP) nanocomplexes with a diameter of 2.12 nm seem to play a pronounced role in biomimetic strategies for biofilm management. There is in vivo evidence indicating that CPP–ACP complexes reduce bacterial adherence by binding to the surfaces of bacterial cells, the components of the intercellular plaque matrix and to adsorbed macromolecules on the tooth surface (Fig. 1d). CPP–ACP-treated germanium surfaces that are applied in the oral cavity for up to one week have been shown to significantly delay the formation of biofilms. (Ge is not biocompatible material)

Hydroxyl apatite has been adopted for years in preventive dentistry (um size particles are included in toothpaste); however, effective interaction of the biomineral with the bacteria is only possible if nano-sized particles that are smaller than the microorganisms are used (Fig. 1d).

Nanomaterials in preventive dentistry

Fluoride is an effective remineralizing agent, and has therefore been widely applied for the prevention of mineral loss. CPP–ACP has also been shown to promote remineralization of initial enamel lesions and to prevent demineralization in laboratory, animal and human experiments – (added to chewing gum)

Other biomimetic approaches, not yet in clinical trials, for remineralization of initial submicrometre enamel erosions are based on nano-sized **hydroxyl apatite particles**. In vitro data indicate that repair at the enamel surface can be greatly improved if the dimensions of the apatite particles are adapted to the scale of the submicrometre- and nano-sized defects caused by erosive demineralization of the natural apatite crystallites (Fig. 4). Hydroxyl apatite with a size of 20 nm fits well with the dimensions of the nanodefects caused at the enamel surface during acidic erosion. These particles adsorb strongly to the etched enamel surface under in vitro conditions and, interestingly, retard further erosive demineralization.

In vitro study of re-mineralization have been conducted using nano hydroxyl apatite toothpaste with either spheroidal or needle-like particles – regrowth has been observed but in a long time scale.
Formation of enamel and dentine –in vitro- has also been demonstrated –but in-vivo studies are yet far away.

The hydrogen atom: an electron orbiting a nucleous with an equal and positive charge. How do we determine allowed energy states of the electron?

The electron experiences a potential $V(r) \prec -1/r$

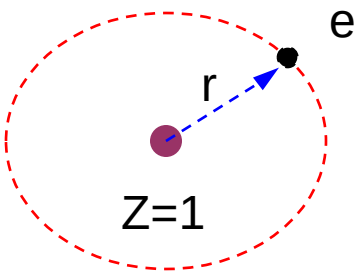

We solve Schroedinger's equation – in this case expressed in spherical coordinates. The problem is solved using separation of variables

$$\nabla^2 = \frac{\partial^2}{\partial r^2} + \frac{2}{r}\frac{\partial}{\partial r} - \frac{1}{r^2}\hat{\Lambda} \qquad (1)$$

$$\hat{\Lambda} = -[\frac{1}{\sin\theta}\frac{\partial}{\partial\theta}(\sin\theta\frac{\partial}{\partial\theta}) + \frac{1}{\sin^2\theta}\frac{\partial^2}{\partial\phi^2}] \qquad (2)$$

Spherical coordinates

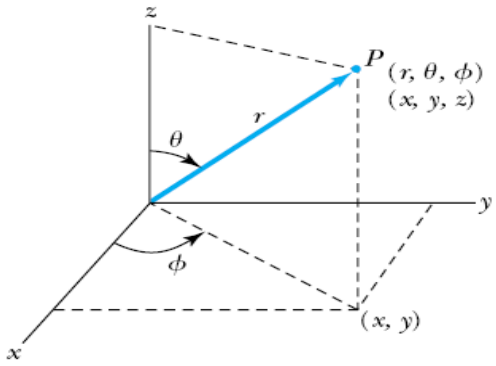

The wavefunction solution of SE is set in this case:

$$\psi(r,\theta,\phi) = \frac{1}{\sqrt{2\pi}} R(r) f(\theta)\Theta(\phi) \qquad (3)$$

Substituting (3) into (1) and (2) we get the following equations

$$\frac{1}{\Theta(\phi)}\frac{\partial^2\Theta(\phi)}{\partial\phi} = -m^2 \quad \rightarrow \Theta(\phi) = e^{im\phi}$$

$$-[\frac{1}{\sin\theta}\frac{\partial}{\partial\theta}(\sin\theta\frac{\partial}{\partial\theta}) - \frac{m^2}{\sin^2\theta}]f(\theta) = \Lambda f(\theta) \qquad (4)$$

$$(-\frac{\hbar^2}{2m_o}\frac{\partial^2}{\partial r^2} + \frac{2}{r}\frac{\partial}{\partial r} - \frac{1}{r^2}\Lambda)R(r) + V(r)R(r) = ER(r) \qquad (5)$$

Where Λ is an eigenvalue, resulting from the separation of angular and radial variables, m_o is the electron mass at rest and E are the eigen-energies that we need to solve for.

The eigenvalue Λ is independent of the shape of V(r) and is normally set equal to:

$\Lambda = l(l\_1)$ where

$l \geq |m|$

The solutions to the angular part of SE are the spherical harmonics

$$Y_l^m(\theta,\phi) = \frac{1}{\sqrt{2\pi}} f(\theta) e^{im\phi}$$

Which satisfy normalization conditions

$$\int_0^{2\pi} d\phi \int_0^{\pi} \left|Y_l^m(\theta,\phi)\right|^2 \sin\theta d\theta = 1$$

Examples of these functions are combinations of sinθ and cosθ :

$$l = 0 \quad Y_0^0 = \frac{1}{2}\sqrt{\frac{1}{\pi}}$$

$$l = 1: \quad Y_1^0 = \cos\theta \frac{1}{2}\sqrt{\frac{3}{\pi}}$$

$$Y_1^{\pm 1} = \mp e^{\pm i\phi} \sin\theta \frac{1}{2}\sqrt{\frac{3}{2\pi}}$$

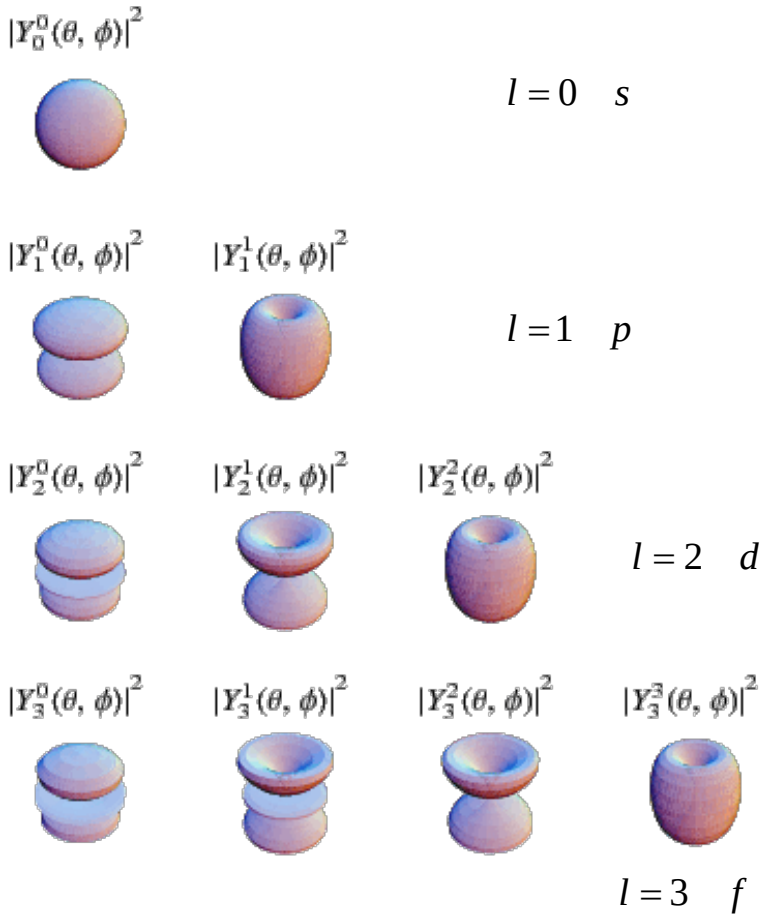

http://mathworld.wolfram.com/SphericalHarmonic.html

The solution of the radial part of SE is obtained by making the substitution

$$rR(r) = \chi(r)$$

$$-\frac{\hbar^2}{2m_o}\frac{\partial^2\chi(r)}{\partial r^2} + [\frac{\hbar^2 l(l+1)}{2m_o r^2} + V(r)]\chi(r) = E\chi(r)$$

The term $\frac{\hbar^2 l(l+1)}{2m_o r^2}$ can be interpreted as follows if one assumes it represents a classical potential. Then the potential is associated with a force,

$$F_l = -\frac{d}{dr}\frac{L^2}{2m_o r^2} = \frac{L^2}{m_o r^3} \qquad L^2 = \hbar^2 l(l+1)$$

Using that the angular momentum L of a particle moving in a circular trajectory with velocity *v* is $L = m_o v r$

$$F_l = \frac{L^2}{m_o r^3} = \frac{m_o v^2}{r}$$ Centripetal force

Using the expression for the Coulomb potential for an electron in free space, where ε_o is the permittivity of free space, the radial part of SE is expressed as

$$-\frac{\hbar^2}{2m_o}\frac{\partial^2\chi(r)}{\partial r^2}+[\frac{\hbar^2 l(l+1)}{2m_o r^2}-\frac{e^2}{4\pi\varepsilon_o r}]\chi(r)=E\chi(r)$$

The radial equation is called the associated Laguerre equation and the solutions are called associated Laguerre functions. There are infinitely many of them, for values of n = 1, 2, 3, …

Let's take the case of *l* =0

$$\frac{\hbar^2}{2m_o}\frac{\partial^2\chi(r)}{\partial r^2}+\frac{e^2}{4\pi\varepsilon_o r}\chi(r)-E\chi(r)=0$$

And a assume a solution of the form $\chi(r)=Cr\exp(-r/a_o)$

$$\frac{\hbar^2}{2m_o a_0^2}\left[-\frac{2a_o}{r}-1\right]\chi(r)+\frac{e^2}{4\pi\varepsilon_o r}\chi(r)-E\chi(r)=0$$

To satisfy this expression for any value of r, we equate the terms independent of r and those varying as 1/r

$$E=-\frac{\hbar^2}{2m_o a_o^2} \qquad a_o=\frac{4\pi\varepsilon_o\hbar^2}{e^2 m_o}$$

These results equal the values obtained in the Bohr's model

Bohr radius a_0=5.29 10^{-11} m

$$E=-\frac{\hbar^2}{2m_o a_o^2}=-13.6eV=-R_\infty \quad \textit{Rydberg Energy}$$

The solution to

$$-\frac{\hbar^2}{2m_o}\frac{\partial^2\chi(r)}{\partial r^2}+[\frac{\hbar^2 l(l+1)}{2m_o r^2}-\frac{e^2}{4\pi\varepsilon_o r}]\chi(r)=E\chi(r)$$

For *l* not equal to zero yields eigen-energies

$$E_n=-\frac{R_\infty}{n^2}$$

n is the principal quantum number

The three quantum numbers are

- n: Principal quantum number
- ℓ: Orbital angular momentum quantum number
- m_ℓ: Magnetic (azimuthal) quantum number

The restrictions for the quantum numbers:

$n = 1, 2, 3, 4, \ldots$

$\ell = 0, 1, 2, 3, \ldots, n-1$

$m\ell = -\ell, -\ell+1, \ldots, 0, 1, \ldots, \ell-1, \ell$

Table 7.1 Hydrogen Atom Radial Wave Functions

n	ℓ	$R_{n\ell}(r)$
1	0	$\frac{2}{(a_0)^{3/2}} e^{-r/a_0}$
2	0	$\left(2 - \frac{r}{a_0}\right) \frac{e^{-r/2a_0}}{(2a_0)^{3/2}}$
2	1	$\frac{r}{a_0} \frac{e^{-r/2a_0}}{\sqrt{3}(2a_0)^{3/2}}$
3	0	$\frac{1}{(a_0)^{3/2}} \frac{2}{81\sqrt{3}} \left(27 - 18\frac{r}{a_0} + 2\frac{r^2}{a_0^2}\right) e^{-r/3a_0}$
3	1	$\frac{1}{(a_0)^{3/2}} \frac{4}{81\sqrt{6}} \left(6 - \frac{r}{a_0}\right) \frac{r}{a_0} e^{-r/3a_0}$
3	2	$\frac{1}{(a_0)^{3/2}} \frac{4}{81\sqrt{30}} \frac{r^2}{a_0^2} e^{-r/3a_0}$

Visual representation of wavefunctions

http://webphysics.davidson.edu/physletprob/ch10_modern/radial.html

The Periodic table

Electron donors ← Decreasing ionization potential

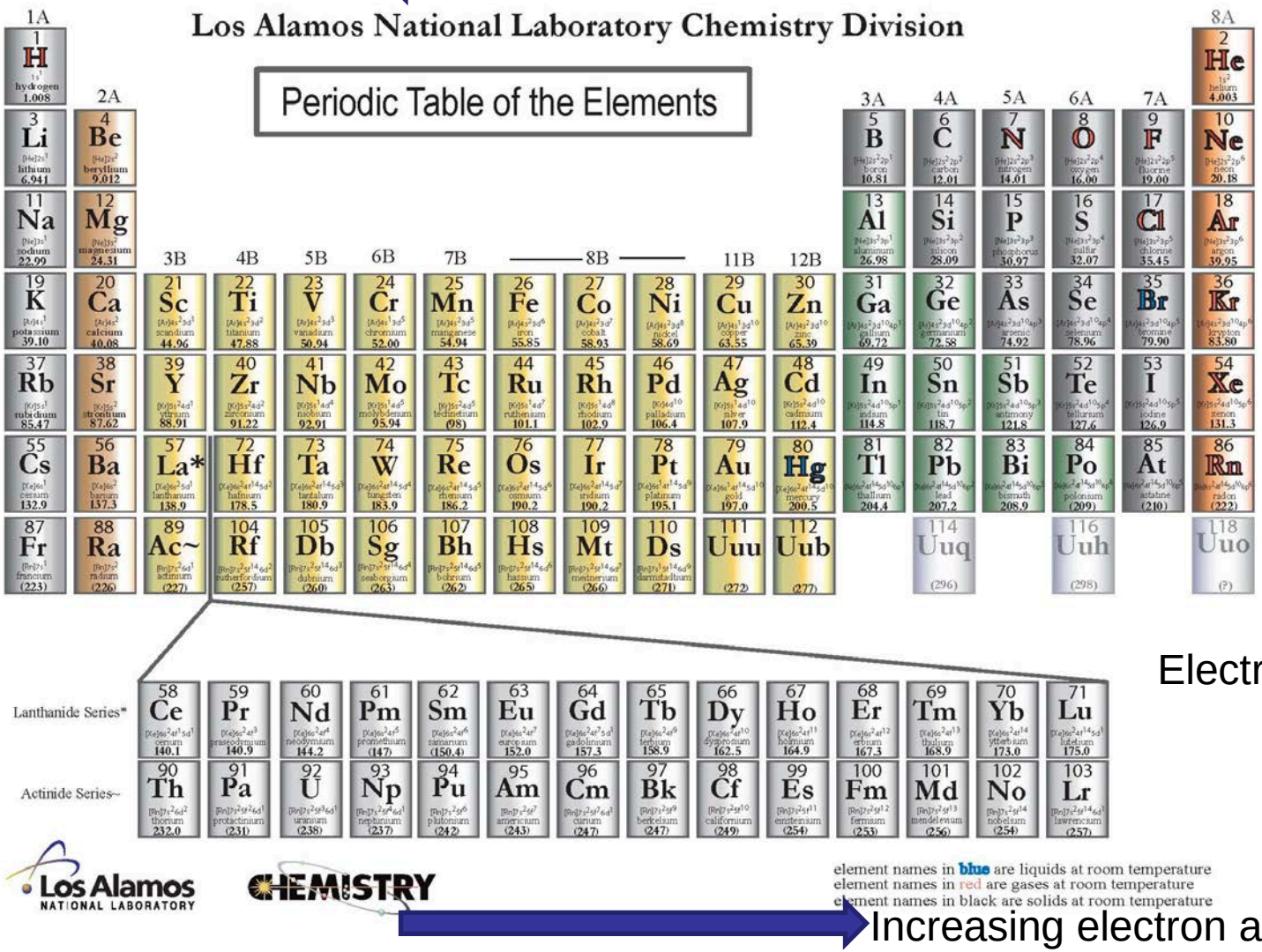

Electron acceptors

Increasing electron afinity

http://periodic.lanl.gov/downloads/periodictable.pdf

Multiple electron atoms

Valence electrons dominate in bonding
Multiple electron atoms are modeled as if they experience a potential that is ‘ Coulomb-like

$$V(r) = \frac{\kappa Z_{eff} e^2}{r}$$

Zeff is the effective charge the valence electron sees.

MOLECULAR BONDING

IONIC BONDS

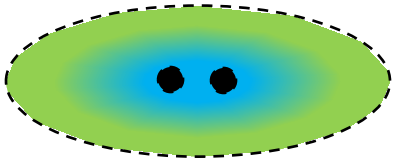

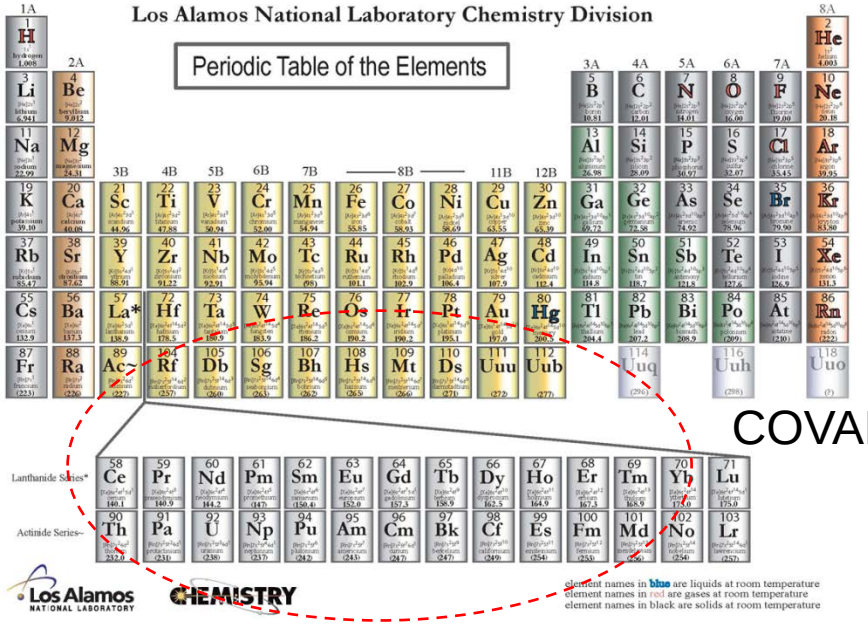

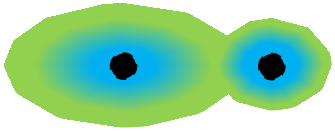

MORE COMPLEX BONDING, D AND F ELECTRONS PARTICIPATE

COVALENT BONDS

MOLECULAR BONDING

Bonding of atoms results in a molecule with lower energy than that of the atoms in isolation

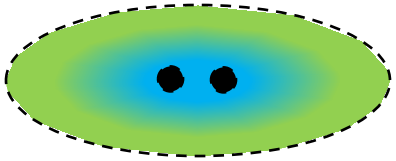

IONIC BONDS

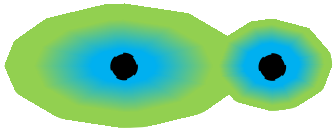

COVALENT BONDS

How do we model multiple electron atoms?

1. Reduce the atom to H-like
2. Consider the interaction of valence electrons among themselves
3. Consider the interaction among cores

Textbook example $H2^+$

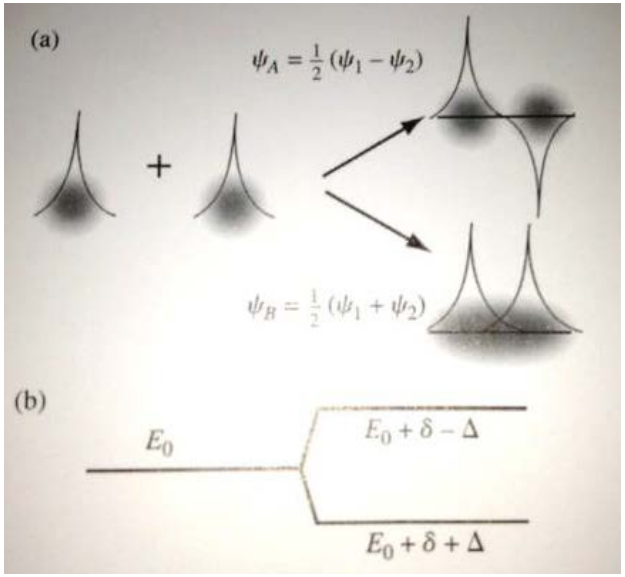

Problems that deal with many interacting electrons are treated with density functional theory (DFT)
It consists of finding a functional (function of a function) of the electron density n(r), E(n (r)] that satisfies the condition

$$\frac{\delta E[n(r)]}{\delta(n(r))} = 0$$

The correct electron density is the one that minimizes the ground state energy of the system. The output is the ground state energy and the equilibrium electron density

Electrons in solids

Solids consist of a geometrical arrangement of of atoms with valence electrons that feel a periodic potential of the lattice

The behavior of electrons in a solid is also described by quantum mechanics. In this case, the system has translational symmetry.

This is expresses as using the time-independent Schroedinger equation as:

$$H(\vec{r}+\vec{T}) = H(\vec{r})$$

r is a position vector and ***T*** is a vector of the form:

$$\vec{T} = u_1\hat{a}_1 + u_2\hat{a}_2 + u_3\hat{a}_3$$

Any vector ***T*** can describe the whole lattice arrangement

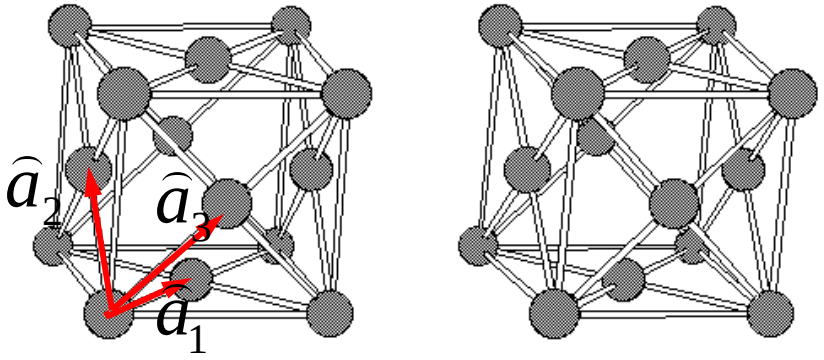

Face center cubic lattice

Therefore to model the interaction of electrons with the crystal it is only necessary to account for electrons within a unit cell.

The electron wavefunctions are also periodic

$$\psi(\vec{r}+T)=\psi(\vec{r})$$

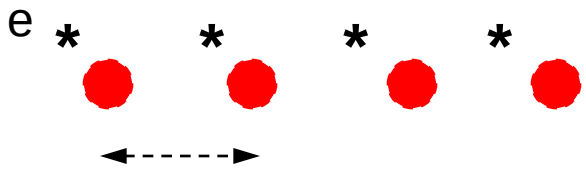

a=0.5 nm

a: lattice constant

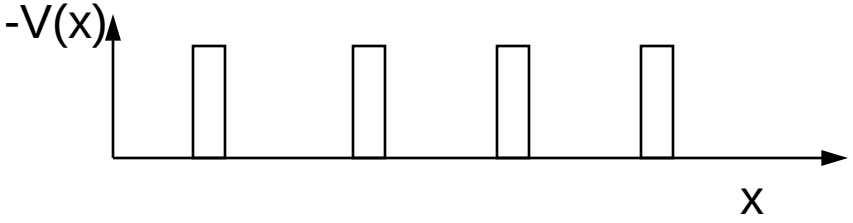

The periodic potential gives rise to two different states for the electrons

Electrons that are quasi-free and can participate in conduction

Electrons that are strongly attached to core

The wavefunction of the quasi-free electrons is expressed as:

$$\psi(x)=u(x)e^{ikx}$$

Electrons in solids

$$\psi(x) = u(x)e^{ikx}$$

Wave-like character

Amplitude depends on position reflects potential interaction

Consider that each atom contains several valence electrons, each characterized by a wavefunction and corresponding eigen-energy. The collective effect of these valence electrons is such that gives rise to the formation of a collection of energy states that are called bands.

The striking behavior is that these bands are separated by energy gaps, that indicates that the electrons can not access these energy states

Electrons in solids

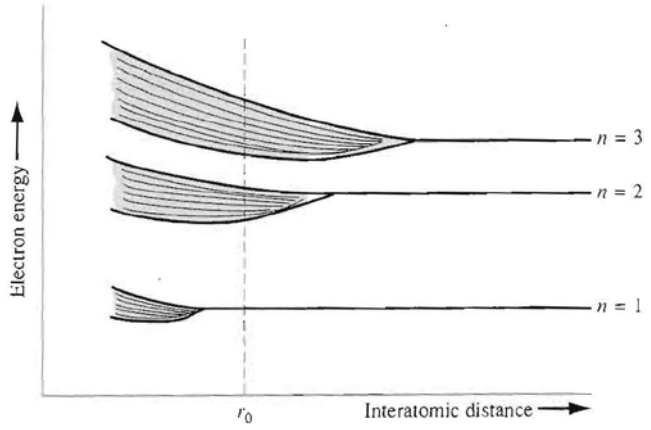

Schematic of origin of bands when atoms are brought closer together

Si - Z=14

Valence electrons: 4- [2 in 3s and 2 in 3p

Covalent bonding

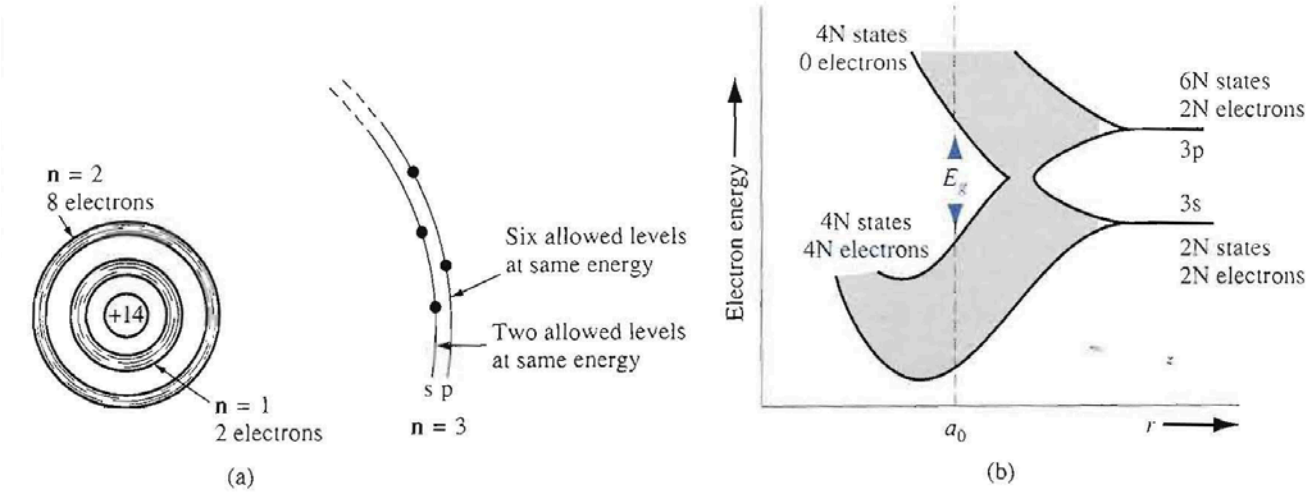

Schematic of an isolated Si- atom; b) the splitting of the 3s and 3p states of silicon into allowed and forbidden energy bands

Fig. 2.13 –D. Neamen –Semiconductor Physics and Devices.

Electrons in solids

The bands that are of interest from the stand point of optical and electrical activity are the top most full and the next higher empty bands called VALENCE and CONDUCTION bands respectively. These two bands are separated by an energy gap Eg

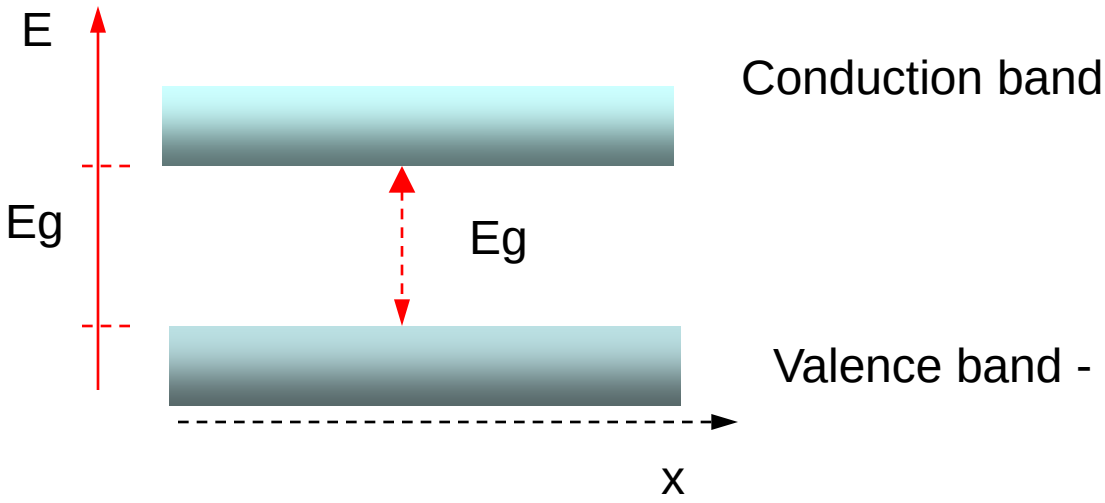

Shadowing indicates band is partially filled

Conduction band is partially filled for T>0, else is empty

Valence band is partially empty for T>0, else is full

It is these electrons that give nanoscale materials their unique behavior

Electrons in solids

Let's consider a quasi-bound electron in the conduction band represented by

$$\psi(x) = u(x)e^{ikx}$$ k is an index – here associated with momemtun

The electron has a momentum and energy represented by

$$p = \hbar k$$

$$E = \frac{p^2}{2m} = \frac{\hbar^2 k^2}{2m}$$

k values are discrete but separated by small quantity. There is finite probability of finding an electron with a momentum between k and k+Δk

For small values of k, the E-k relationship is parabolic.

We can define a density of states, i.e. the number of energy states per unit volume in which the electrons have energy between E, and E+ΔE, g(E)

Electrons in solids

In this E-k picture of electrons in a solid, the curvature of the E-k relationship is related to the 'mass' of the electron in the band, or effective mass

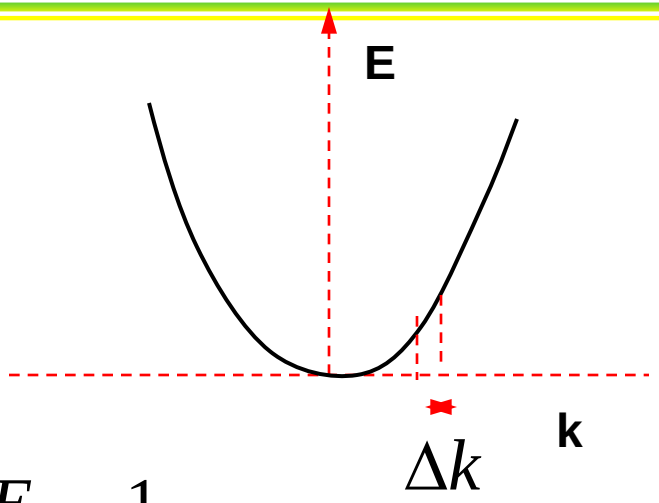

$$E = \frac{\hbar^2 k^2}{2m} \quad \rightarrow \frac{1}{\hbar^2}\frac{d^2E}{dk^2} = \frac{1}{m}$$

m is called the electron effective mass and symbolized by m*, as it is different whether the electron occupies a state in the conduction band (CB) or valence band (VB)

In Si, the conduction band electron effective mass is $m^* = 1.2\ m_o$ where m_o is the free electron mass

The E-k diagram also contains information about the velocity of the electrons in the band

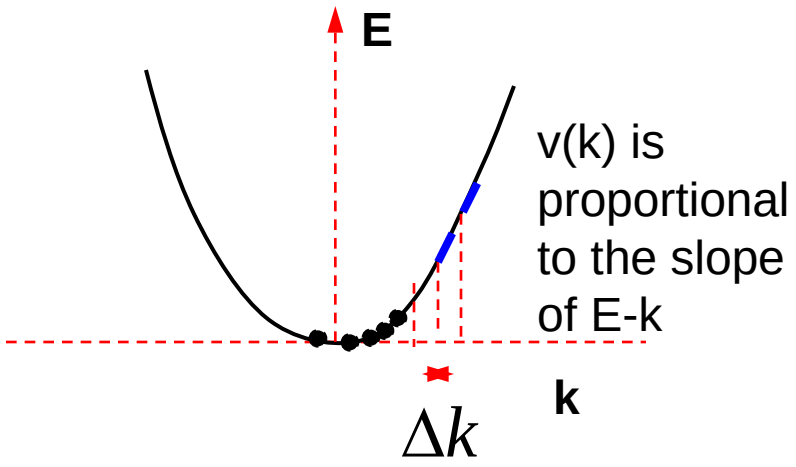

v(k) is proportional to the slope of E-k

$$p = \hbar k \qquad p = mv$$

$$E = \frac{p^2}{2m} = \frac{\hbar^2 k^2}{2m}$$

$$\frac{dE}{dk} = \frac{\hbar^2 k}{m} = \frac{\hbar\ mv}{m} = \hbar v$$

This parabolic band model holds for values of k near k=0. At higher k, the parabolic relationship deviates and becomes cos k like. This means that the velocity of the electrons near a band edge can be zero. Of importance is the value of the effective mass near k=0.

CONCEPT OF A HOLE

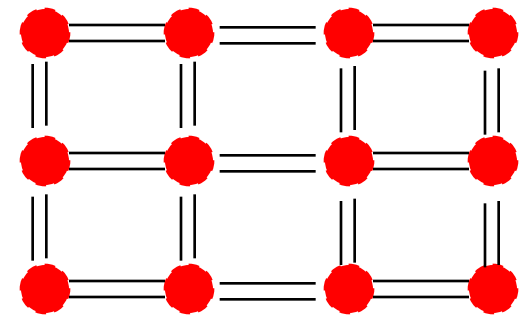

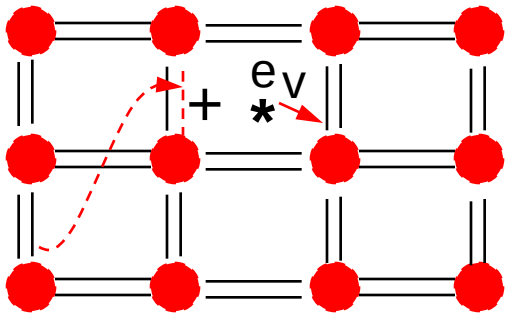

Cores

2 valence electron bonds

When a bond is broken, the electron can now participate in conduction –i.e. can access a state in the conduction band. In this process the electron leaves an 'empty' bond that behaves as a positive charge.

This empty bond, can also be filled by an electron originating from another bond or by a free electron. So in essence, it is as if this +e also contributes to carrier conduction. This +e is called a 'hole'

The dispersion E-k characteristics of holes that dominate conduction in the valence band is given by

$$E = -\frac{\hbar^2 k^2}{2m}$$

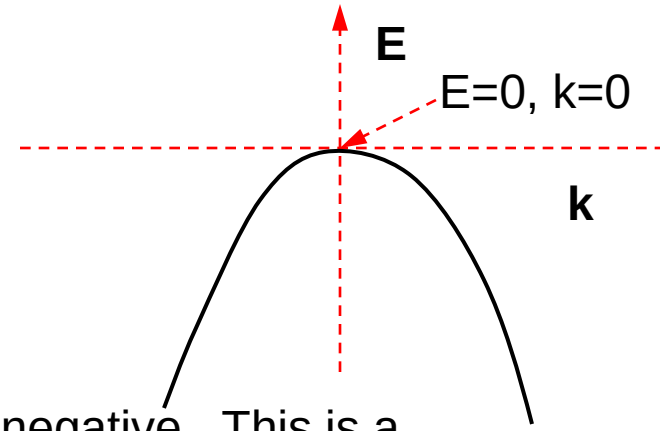

Notice that the hole effective mass is negative. This is a concept only possible in quantum mechanics.

If we consider an electron moving near the top of the band in the presence of an electric field E_a, it experiences a force

$$F = m^* a = -e\mathrm{E}_a$$

$$a = \frac{-e\mathrm{E}_a}{-|m^*|} = \frac{e\mathrm{E}_a}{|m^*|}$$

An electron moving near the top of the valence band moves in the same direction as the applied electric field. This is the behavior of a positive charge

METALS, SEMICONDUCTORS AND INSULATORS

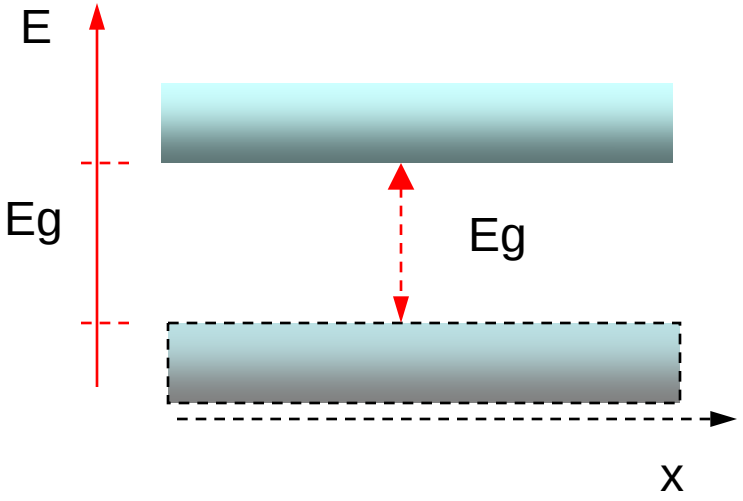

Eg from 0.5 to 3 eV

SEMICONDUCTOR

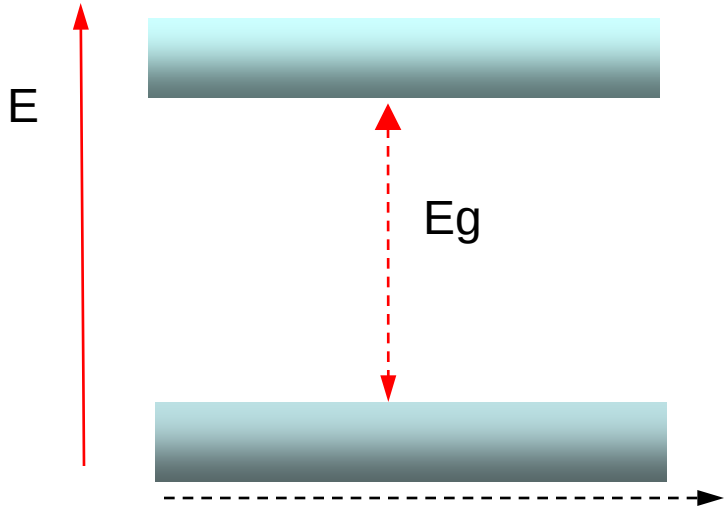

Eg greater than 3 eV

INSULATOR

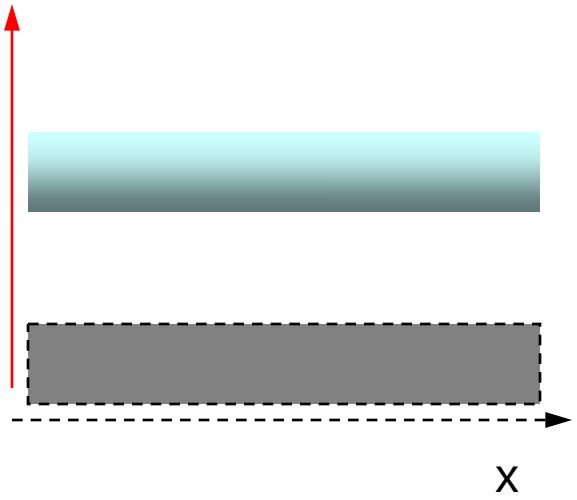

Partially field band

Full band

METALS

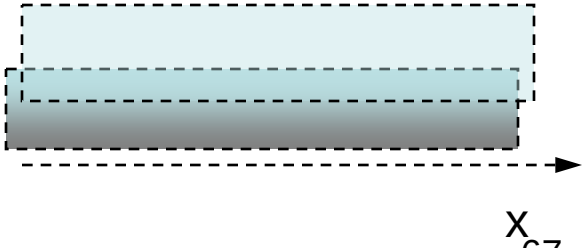

ELECTRONS IN SOLIDS

In the band picture, the allowed energy states electrons can occupy in the conduction band are expressed by

$$E_c = E_g + \frac{\hbar^2 k^2}{2m_e^*}$$ And in the valence band $$E_c = -\frac{\hbar^2 k^2}{2m_h^*}$$

m_e^*, m_h^* Are the electron and hole effective mass respectively. They are different because the effective mass represents the potential of interaction

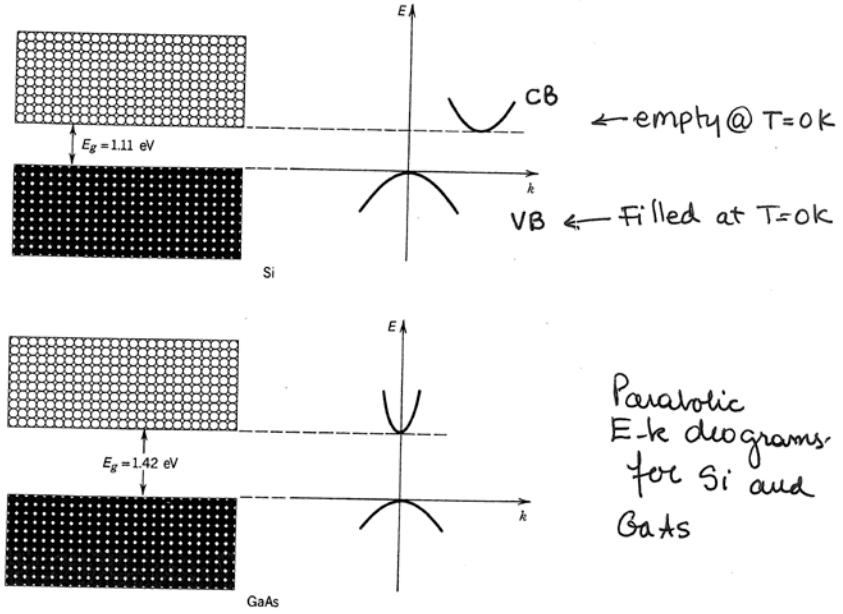

Figures from Fundamentals of Photonics, Saleh and Feich

Characteristics parameters for common semiconductor materials

Name	Symbol	Germanium	Silicon	Gallium Arsenide
Band minimum at $k = 0$				
Minimum energy	$E_{g,direct}$ (eV)	0.8	3.2	1.424
Effective mass	m_e^*/m_0	0.041	0.2	0.067
Band minimum *not* at $k = 0$				
Minimum energy	$E_{g,indirect}$ (eV)	0.66	1.12	1.734
Longitudinal effective mass	$m_{e,l}^*/m_0$	1.64	0.98	1.98
Transverse effective mass	$m_{e,t}^*/m_0$	0.082	0.19	0.37
Longitudinal direction		-111	-100	-111
Heavy hole valence band maximum at $E = k = 0$				
Effective mass	m_{hh}^*/m_0	0.28	0.49	0.45
Light hole valence band maximum at $k = 0$				
Effective mass	m_{lh}^*/m_0	0.044	0.16	0.082
Split-off hole valence band maximum at $k = 0$				
Split-off band valence band energy	$E_{v,so}$ (eV)	-0.028	-0.044	-0.34
Effective mass	$m_{h,so}^*/m_0$	0.084	0.29	0.154

http://ece-www.colorado.edu/~bart/book/book/chapter2/ch2_3.htm#tab2_3_3

Electron and hole concentrations

For a free electron cloud, the density of states is given by

$$g(E) = \frac{(2m)^{3/2}}{2\pi\hbar^3} E^{1/2}$$

For electrons in the conduction band

$$g_c(E) = \frac{(2m_e^*)^{3/2}}{2\pi\hbar^3} (E - E_c)^{1/2}$$

For holes in the valence band

$$g_v(E) = \frac{(2m_h^*)^{3/2}}{2\pi\hbar^3} (E)^{1/2}$$

The states in the bands are filled in a form that is determined by the fact that electrons are 'fermions', and hence must satisfy Pauli's Exclusion Principle: there can not be two electrons with identical quantum numbers.

The probability of occupancy of a state of energy E :

$$f(E) = \frac{1}{1 + \exp\left(\frac{E - E_F}{k_B T}\right)}$$

k_B: Boltzman's constant (0.026 eV at T=300K)

E_F: Fermi Energy – in a semiconductor or insulator in equilibrium, E_F is near the midgap energy

1-f(E) is the probability of occupancy by a hole

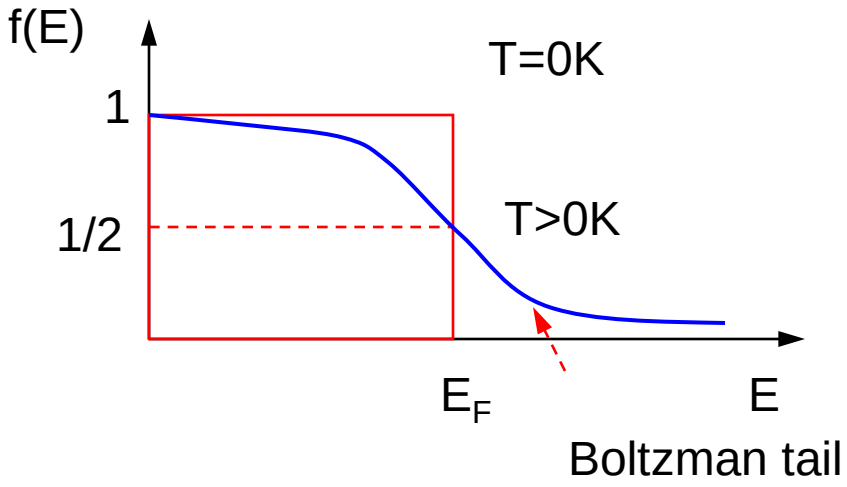

Knowing the density of states and the probability of occupancy of the states one can calculate the number of electrons in the conduction and valence band respectively.

$$n = \int_{E_C}^{\infty} g_c(E) f(E) dE \qquad p = \int_{-\infty}^{E_v} g_v(E)(1 - f(E)) dE$$

Number of electrons Number of holes

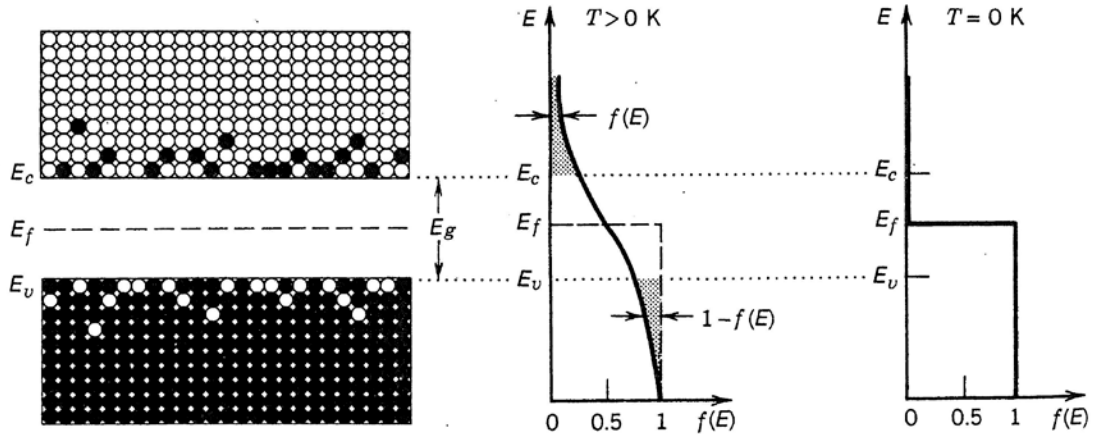

Figure 15.1-8 The Fermi function $f(E)$ is the probability that an energy level E is filled with an electron; $1 - f(E)$ is the probability that it is empty. In the valence band, $1 - f(E)$ is the probability that energy level E is occupied by a hole. At $T = 0$ K, $f(E) = 1$ for $E < E_f$, and $f(E) = 0$ for $E > E_f$; i.e., there are no electrons in the conduction band and no holes in the valence band.

Quantum confined materials

Quantum confinement is mainly observed in semiconductor materials. Quantum wells and superlattices are fabricated by depositing thin (10 nm) layers of alternating materials of different bandagps.

The selection of the materials also requires that their lattice constants be similar so they could be grown epitaxially within the limits of the elastic strain of the materials. The selection fo the materials is made with the help of the semiconductor roadmap

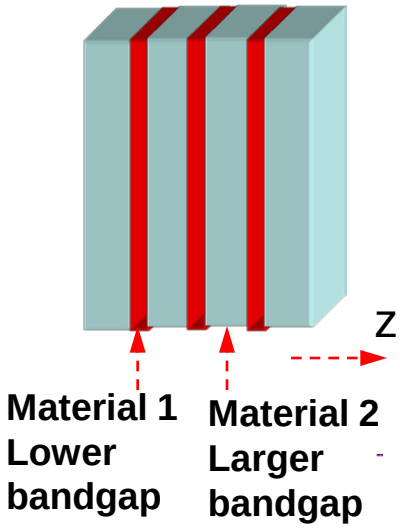

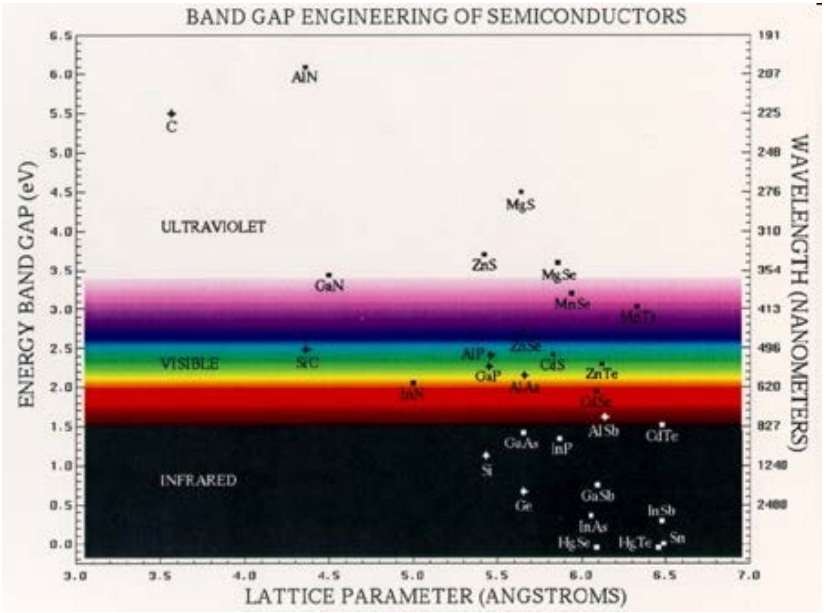

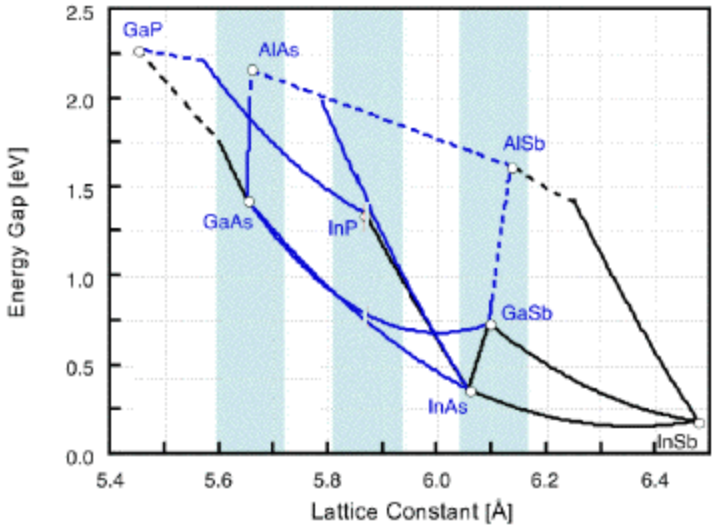

http://people.seas.harvard.edu/~jones/ap216/images/bandgap_engineering/rosette_global.jpg

http://people.seas.harvard.edu/~jones/ap216/images/bandgap_engineering/bandgap_engineering.html

The Ga-In-Al-N

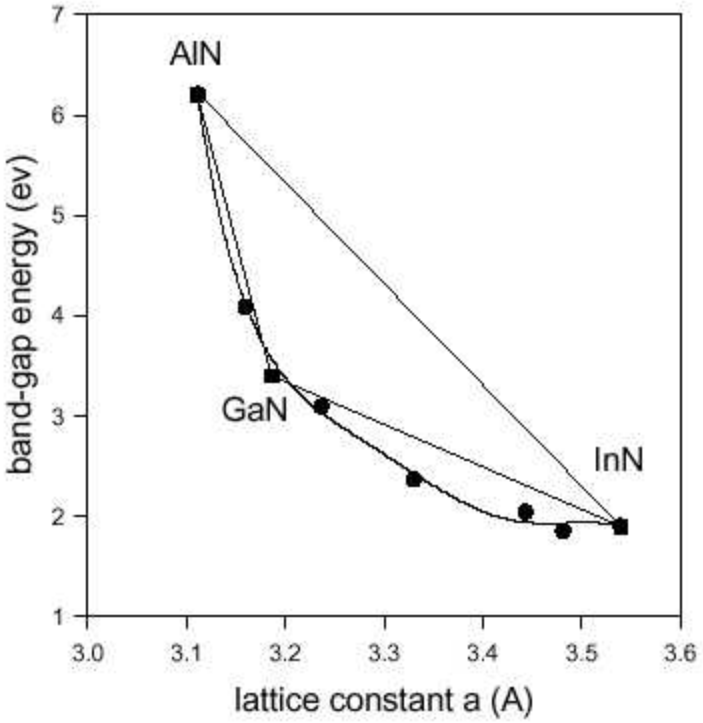

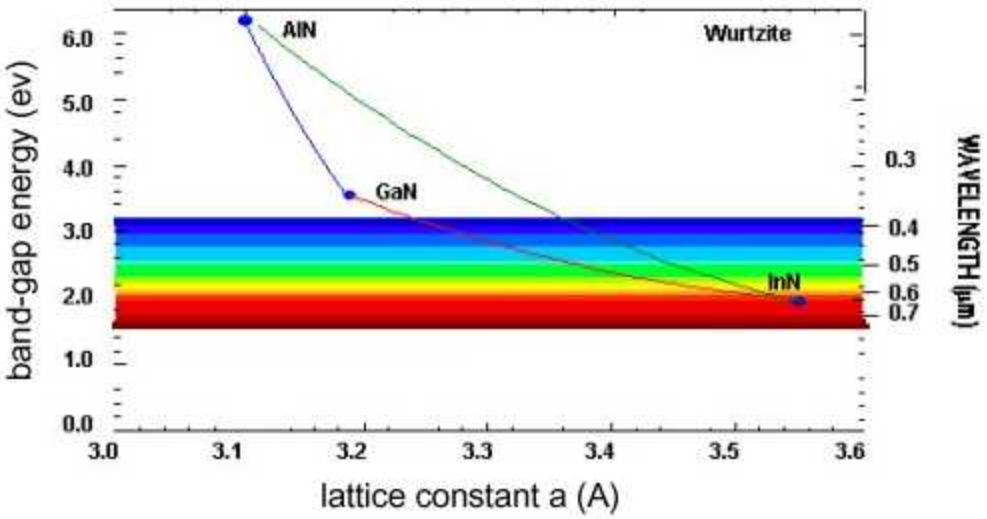

These are the alloys used to make light emitting diodes

http://people.seas.harvard.edu/~jones/ap216/images/bandgap_engineering/rosette_gan.jpg

Quantum confined materials are modeled assuming the electrons are confined in one or more directions. For quantum wells this is the growth direction. The confined energy levels are calculated from solving Schroedinger's equation for a square potential.

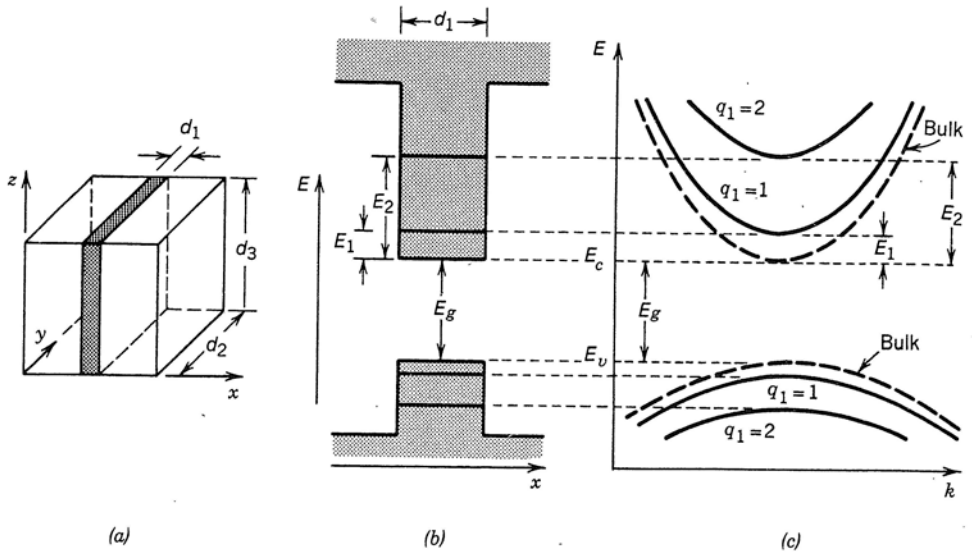

Figure 15.1-21 (*a*) Geometry of the quantum-well structure. (*b*) Energy-level diagram for electrons and holes in a quantum well. (*c*) Cross section of the E–k relation in the direction of k_2 or k_3. The energy subbands are labeled by their quantum number $q_1 = 1, 2, \ldots$. The E–k relation for bulk semiconductor is indicated by the dashed curves.

The E-k relationship for the conduction band is given by:

$$E = E_g + E_q + \frac{\hbar^2}{2m_c^*}(k_x^2 + k_y^2)$$ Conduction band

$$E_q = \frac{\hbar^2}{2m_c^*}(k_x^2 + k_y^2)$$

$$E = -E_{qv} - \frac{\hbar^2}{2m_v^*}(k_x^2 + k_y^2)$$ Valence band

$$E_q = \frac{\hbar^2}{2m_c^*}\left(\frac{q\pi}{d_1}\right)^2$$

Notice that as q increases the confined states get closer together. Also, Eq increases with the well thickness decreases

Unique to quantum confined materials is that the density of states, obtained from the two dimensional wavectors k_x, k_y is constant.

$$g_c(E) = \begin{cases} \dfrac{m_c^*}{\pi\hbar^2 d_1} & E > E_g + E_q \quad q = 1,2,3... \\ 0 & otherwise \end{cases}$$

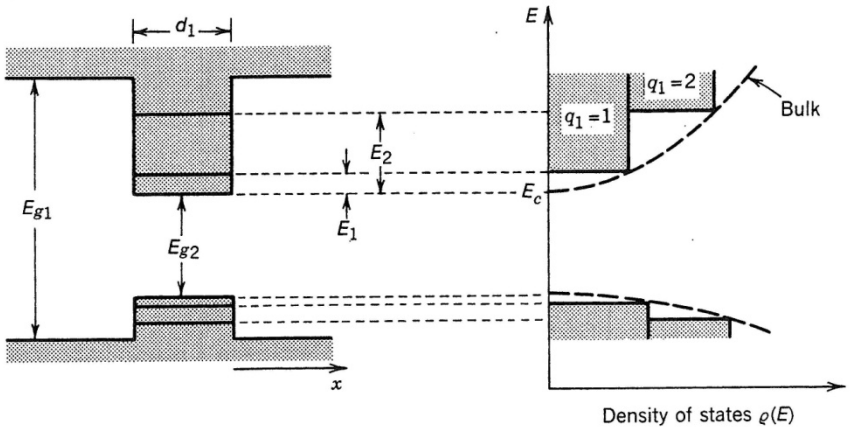

Figure 15.1-22 Density of states for a quantum-well structure (solid) and for a bulk semiconductor (dashed).

Quantum wells are grown by molecular beam epitaxy. Typical structures contain 4-8 wells, ~5-8 nm thick, separated by barriers 15-20 nm thick.

The reduced number of states have important consequences when quantum wells are used in the fabrication of laser diodes. This results in a lower injection current to achieve threshold for lasing

Quantum wires

Following the analysis, one can infer that as the confinement increases to other dimensions, the density of states in the conduction and valence bands would decrease.

Quantum wire

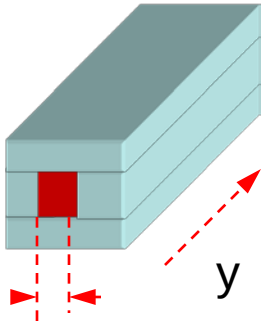

5-10 nm

Quantum rods (ZnO) have 100 nm diameter typically

Electrons have only one degree of freedom

$$E = E_g + E_{q1} + E_{q2} + \frac{\hbar^2}{2m_c^*}(k_y^2)$$

$$E_{qn} = \frac{\hbar^2}{2m_c^*}\left(\frac{q_n \pi}{d_n}\right)$$

Each pair (q1,q2) is associated with an energy sub-band with density of states

$$g_{ck} = \frac{1}{\pi}$$

Per unit length of the wire

Quantum dots

Quantum dot

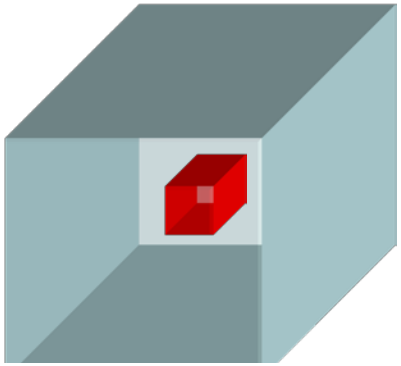

$$E = E_g + E_{q1} + E_{q2} + E_{q3}$$

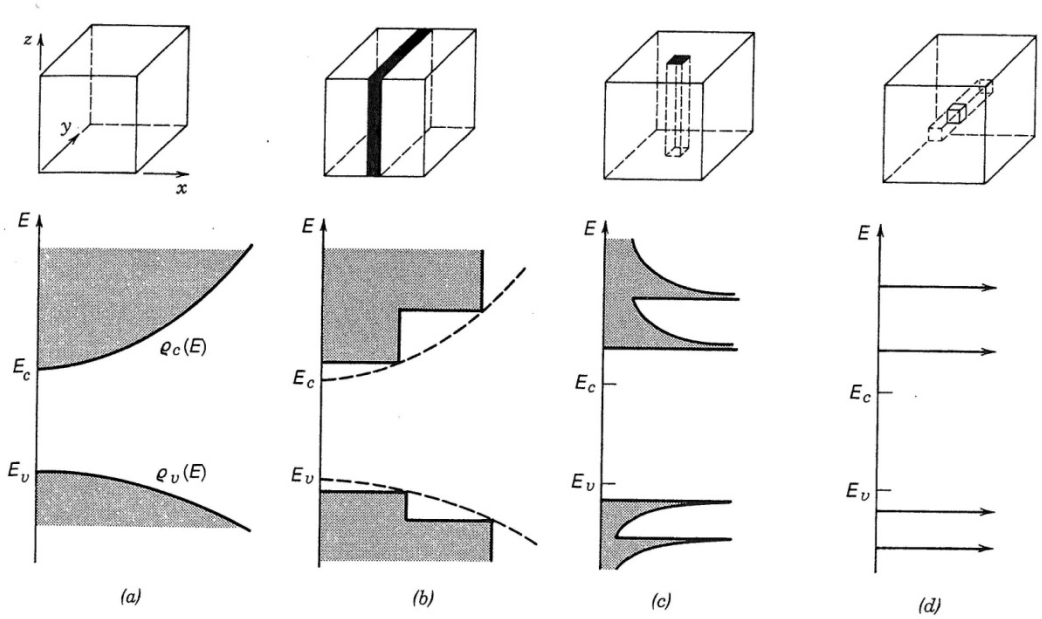

Figure 15.1-24 The density of states in different confinement configurations: (*a*) bulk; (*b*) quantum well; (*c*) quantum wire; (*d*) quantum dot. The conduction and valence bands split into overlapping subbands that become successively narrower as the electron motion is restricted in more dimensions.

Confluence of nanostructure materials with special optical properties and their interaction with light has given rise to the field of NANOPHOTONICS

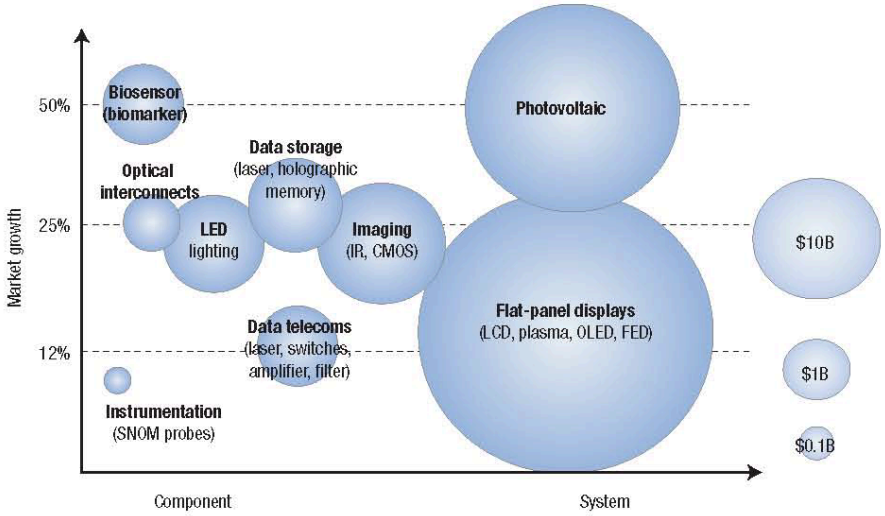

Figure 2 Market growth and size for applications targeted by nanophotonics. The size of the bubble corresponds to the market size in 2009. Sectors most likely to flourish in Europe include imaging, lighting and data telecoms. B: billion; SNOM: scanning near-field optical microscopy; IR: infrared; OLED: organic LED; FED: field-emission display.

Box 1 Hot topics in nanophotonics

Photonics–electronics convergence:

- Integrating photonic functions with electronics may aid progress in several application fields (for example datacoms and telecoms, imaging and displays, and sensors).
- A generic, high-volume fabrication process (for example, one that is CMOS-compatible) is mandatory for rapid progress in the field and competitive prices.

Semiconductor nanostructures for emission and detection of light:

- Compound semiconductor nanowires and quantum dots for lasers and LEDs (for example, III–V nanowire laser sources grown on silicon, quantum-dot lasers, II–VI or III–V nanowire-based LEDs and quantum-dot nanophosphors)
- All-silicon lasers
- Solar cells

Plasmonics and metamaterials:

- Nanostructured materials open up new possibilities (for example strong light confinement, and light filtering, guiding and extracting). Applications lie in sensing, optical interconnects, data storage, displays, lighting, imaging and photovoltaics.
- Left-handed metamaterials could potentially provide optical cloaking and superlensing, as well as other applications.

nature photonics | VOL 2 | MAY 2008 | www.nature.com/naturephotonics

Amber Jenkins, Nature Photonics, vol. 2, pg 258, 2008

COMMENTARY

Box 2 Key recommendations

Displays:
Strong European competencies exist in carbon nanotubes, glass substrates and display systems. Provide support services for displays, for example R&D and process equipment such as chemical vapour deposition for carbon nanotubes.

Photovoltaics:
Market growth is high. Develop quantum-dot technology for solar cells.

Sensing:
Maintain R&D on visible and infrared sensing for various application areas. Companies such as STV, e2v and Sofradir are strong players.

Lighting:
Intensify R&D. Two key players in this field (Osram & Philips) are a major asset.

Datacoms and telecoms:
Maintain R&D for this field, specifically for further integration of optical and electronic chips.

Sensing:
Maintain R&D into microstructured fibres, II–VI quantum dots and plasmonics for nanophotonics-based sensors (for example, surface-plasmon-resonance instruments, which have been successfully commercialized by Biacore in Sweden).

Optical interconnects:
Maintain R&D competence in this arena, to compete with the USA where government agencies, microelectronics companies (such as Intel and IBM) and start-ups (such as Luxtera and Kotura) are already highly active.

Amber Jenkins, Nature Photonics, vol. 2, pg 258, 2008

Ohm's Law survives to the atomic scale
B. Weber et al, Science, pp64-67, vol.335 (2012)

- As silicon electronics approaches the atomic scale, interconnects and circuitry become comparable in size to the active device components. Maintaining low electrical resistivity at this scale is challenging because of the presence of confining surfaces and interfaces. We report on the fabrication of wires in silicon—only one atom tall and four atoms wide—with exceptionally low resistivity (~0.3 milliohm-centimeters) and the current-carrying capabilities of copper. By embedding phosphorus atoms within a silicon crystal with an average spacing of less than 1 nanometer, we achieved a diameter-independent resistivity, which demonstrates ohmic scaling to the atomic limit. Atomistic tight-binding calculations confirm the metallicity of these atomic-scale wires, which pave the way for single-atom device architectures for both classical and quantum information processing.

Ohms Law

- From class notes:

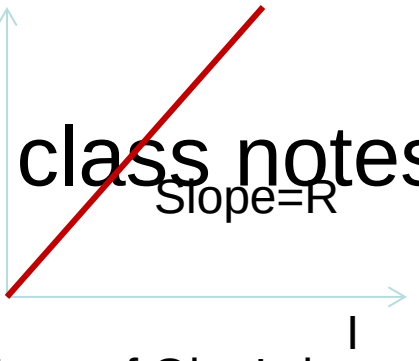

Point Form of Ohm's law

$$\boldsymbol{J} = \sigma \boldsymbol{E}$$

J= current density (A/m^2)
E: electric field

Conducting cylinder

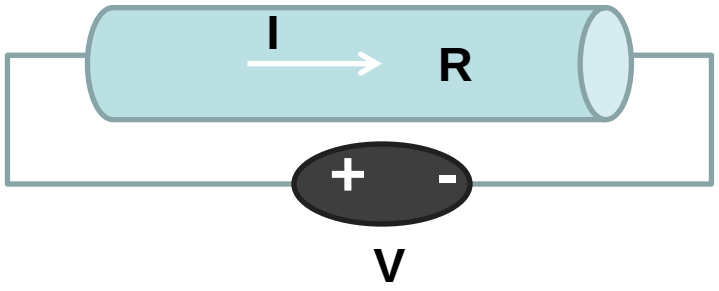

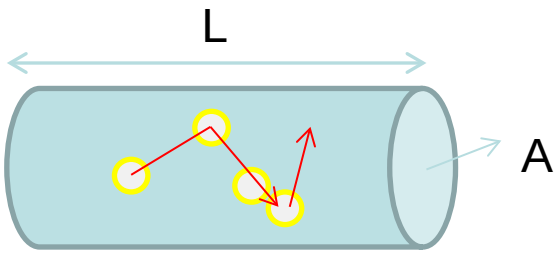

Electrons move short distances, and collide with other electrons, with ion cores. The effect of collisions is represented in the property RESISTANCE (CLASSICAL PICTURE)

$$R = \rho L/A$$

ρ; resistivity
L: length - A: cross sectional area

Resistivity
Cu: 1.68 10^{-8} Ω-m @ 20°C
Si: 4.6 10^{-2} Ω-m(with no doping) – 8.9$10^{-7}$ Ω-m (with 10^{21} P atoms)

P atoms separated by 1 nm (Nd=10^{21} cm^{-3})
Bias voltage: 500μV
Measure current

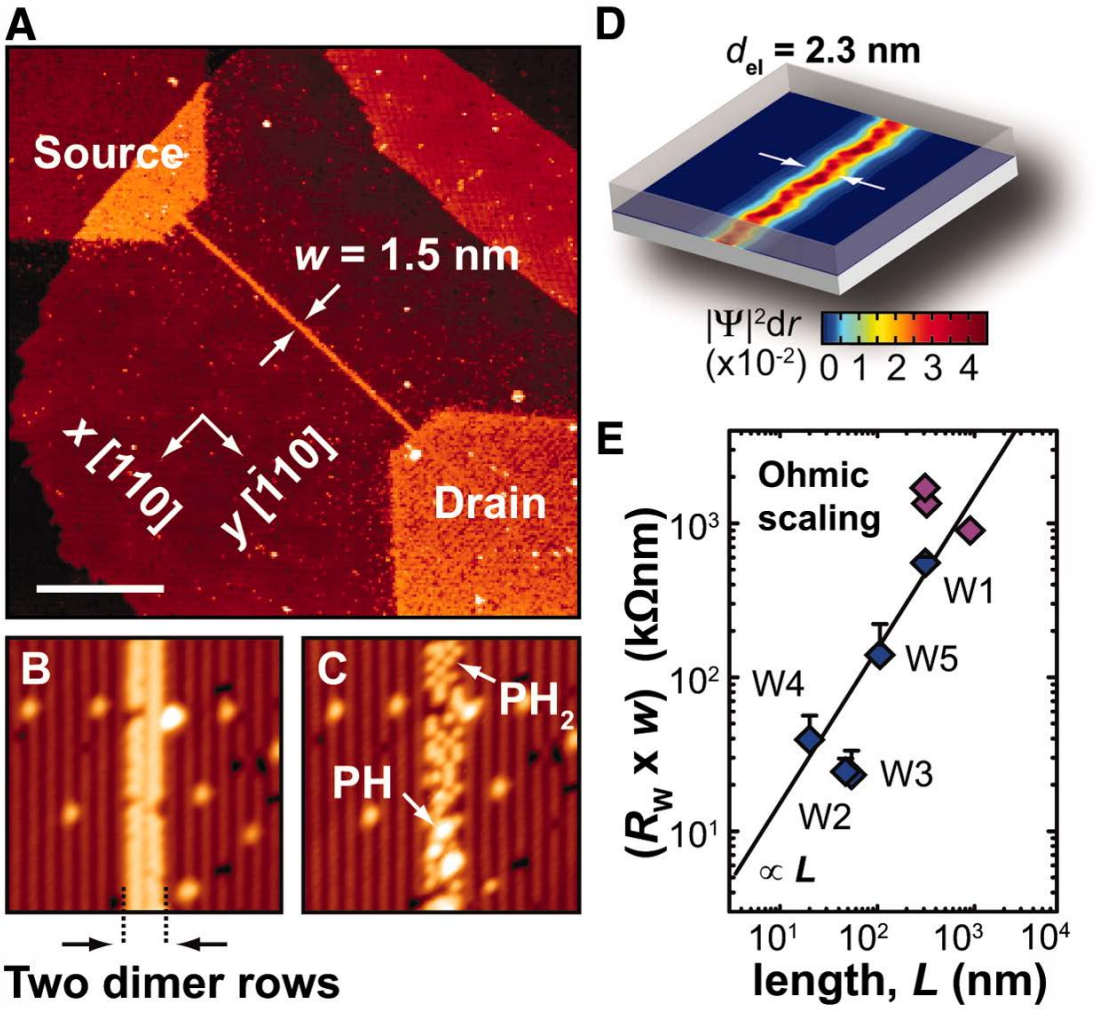

Fig. 1 Atomically abrupt dopant wires in silicon. (**A**) STM image of a 4-atom-wide (1.5 nm), one-atom-tall, and 106-nm-long wire template, patterned along the <110> direction and connected to source/drain leads. Scale bar, 50 nm. (**B** and **C**) Atomic resolution images of a two-dimer-row-wide wire, before (B) and after (C) PH_3 dosing. After PH_3 exposure, the wire shows a large number of PH_x (x = 1,2) fragments, strictly confined within the patterned regions. (**D**) Atomistic NEMO modeling of the electron distribution in a 1.5-nm dopant wire demonstrating tight charge confinement with a spread of the wave function outside the lithographic width. (**E**) Four-terminal resistances corrected for series resistances and normalized with the lithographic width ($R_W \times w$), plotted versus wire length L (blue and purple

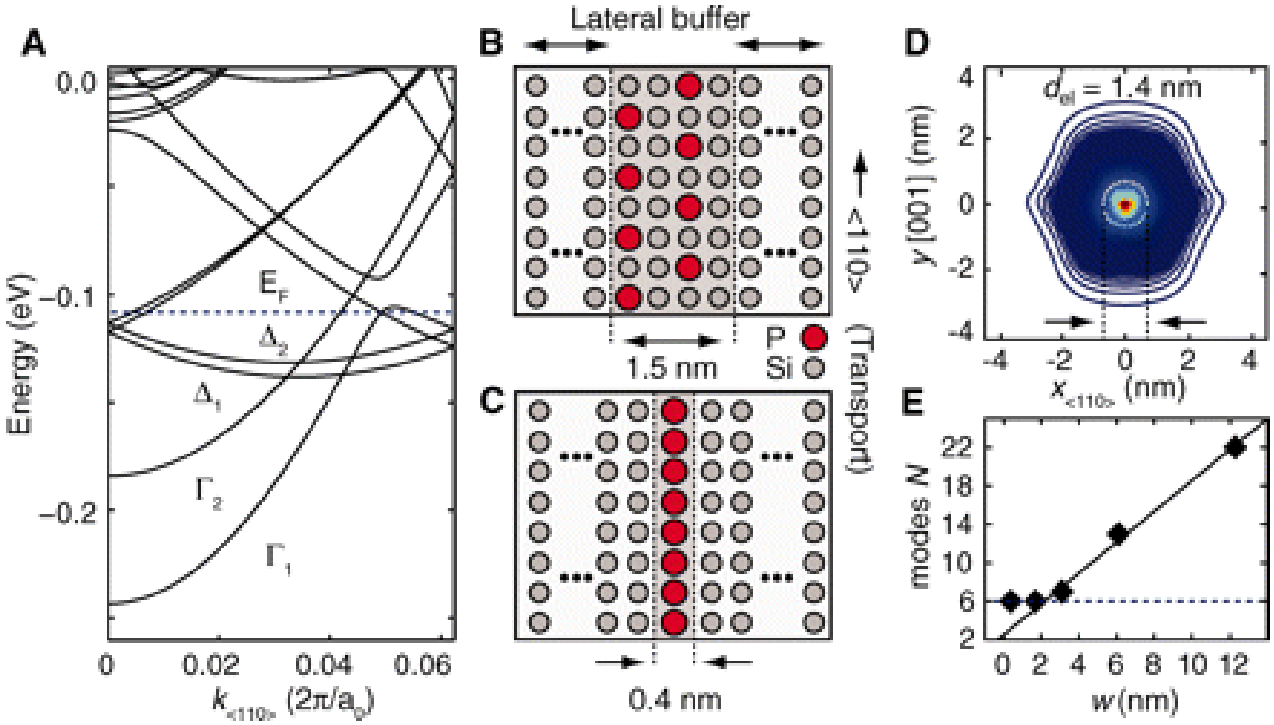
A
0.0
−0.1
−0.2
Energy (eV)
E_F
Δ_2
Δ_1
Γ_2
Γ_1
0
0.02
0.04
0.06
k_<110> (2π/a_0)
B
Lateral buffer
1.5 nm
P
Si
<110> (Transport)
C
0.4 nm
D
d_el = 1.4 nm
y [001] (nm)
x_<110> (nm)
E
modes N
w (nm)

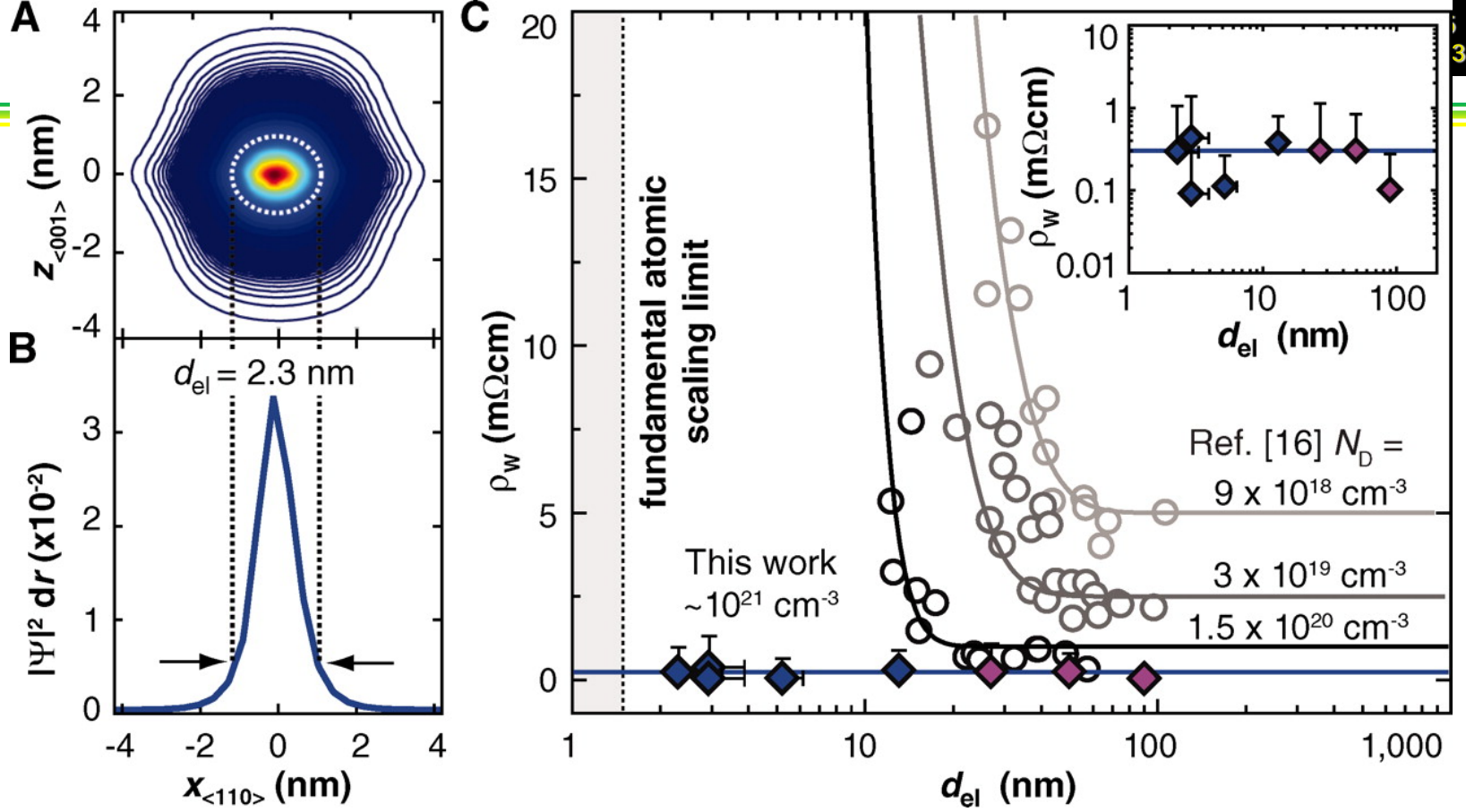

Diameter-independent bulk-like resistivity down to the atomic limit. (**A**) Radial charge density $|\psi|^2$ dr of the thinnest wire (W5) showing the effective cross-sectional area A_{el} (white dotted ellipse), used to calculate the wire resistivity ρ_W. (**B**) The corresponding effective wire diameter d_{el} (arrows) is determined from a cut through $|\psi|^2$ dr in the plane of the dopants. (**C**) Resistivity ρ_W (d_{el}) of the STM-patterned wires (blue and purple diamonds), showing that it remains constant down to the fundamental scaling limit. The average value is near that for the silicon bulk resistivity at equivalent doping density (blue line). This is in contrast to an exponential deviation from bulk values as found in VLS-grown nanowires. [Open circles, data graphically extracted from (*16*). The lines are guides to the eye.] (Inset) ρ_W (d_{el}) on a double-logarithmic scale.

B Weber et al. Science 2012;335:64-67

Table 1
Atomic dopant wires of different width. L and w denote the lithographic length and width of each wire studied. A_{el} and d_{el} are the effective electronic cross section and diameter of the wires as determined by atomistic calculations. Resistivities, ρ_W, were extracted from the wire resistance R_W using A_{el}. Measured wire resistances are compared to theoretically predictions R_{calc} based on the tight-binding calculations.

Sample	***w*** **(nm)**	***L*** **(nm)**	A_{el} **(nm^2)**	d_{el} **(nm)**	R_W **(kΩ**	ρ_W **(mΩ cm)**	R_{calc} **(kΩ)**
W1	11.0	312	27.5	13.1	48.6	0.43	30 ± 4
W2	4.6	47	9.8	5.2	5.3	0.11	7 ± 1
W3	2.3	54	5.0	2.9	10.1	0.10	15 ± 2
W4	2.3	20	5.0	2.9	17.1	0.42	6 ± 1
W5	1.5	106	3.8	2.3	82.3	0.26	31 ± 4

Classical vs quantum behavior

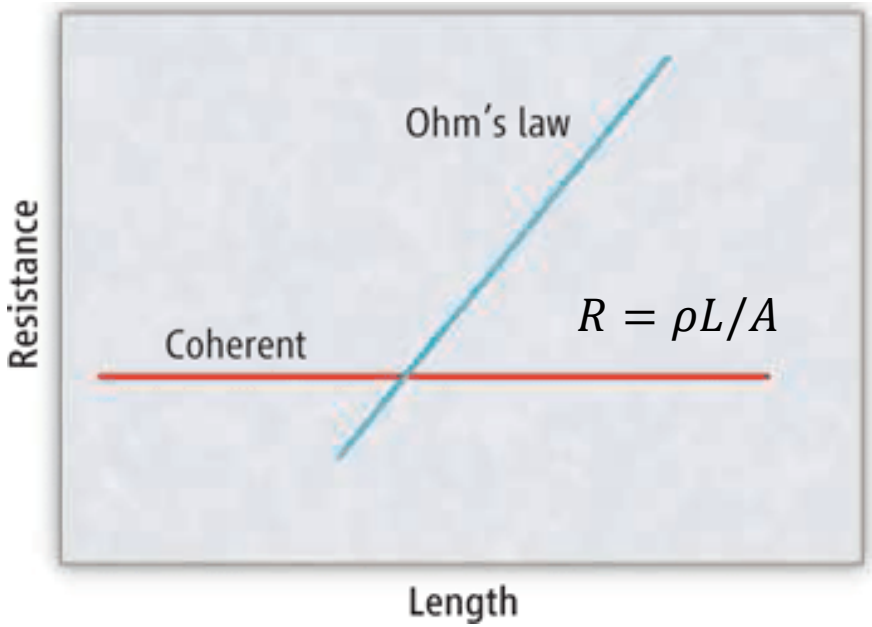

Ideal behavior. In systems where quantum coherence governs the transport, the resistance is independent of the length of the sample of material (red curve). Classical Ohm's law requires that the resistance be linearly proportional to the length (blue curve). Hence, for a given sample, a cross-over from quantum to classical behavior where the two curves meet is expected. The measured resistance would be a sum of these two curves. Weber *et al.* (2) report classical behavior under conditions where quantum effects would be expected.

How do confinement effects are manifested?

- Optical and electrical properties
- Characterization techniques
- Growth methods
- Examples

September 24 – HOMEWORK DISCUSSION

Participants
Tylor green
Brandon
Michael
Travis
Clayton
Drew
Michael

Missing: Chris and Stephan

ELECTRON'S IN NANOSTRUCTURES AND QUANTUM EFECTS

Electronic properties of materials are dominated by electron scattering effects. This is what makes electrons travel at a 'drift velocity'. The scattering event occur within the mean free path of the electron

Conducting cylinder

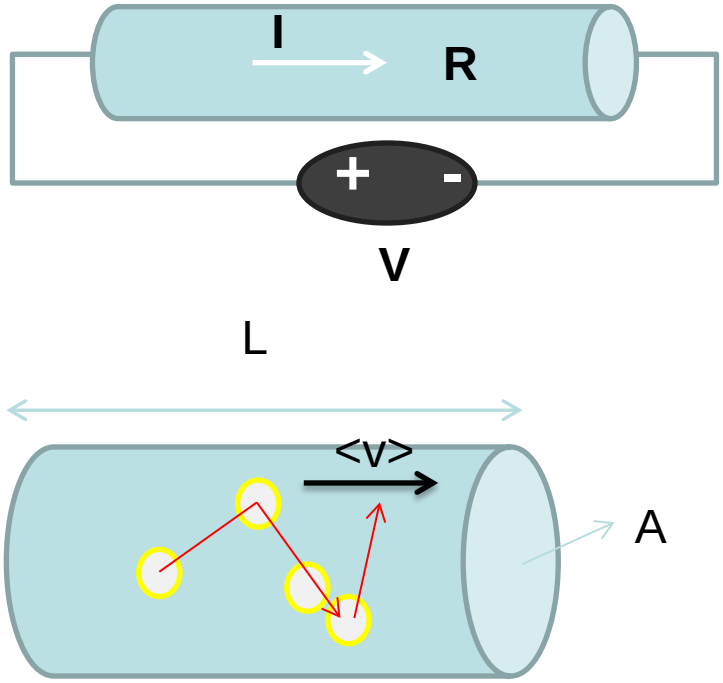

In a simple model of 'free electrons' (Drude model)
If **v** is the instantaneous electron velocity, and τ the scattering time

$$m\frac{< v >}{< \tau >} = -e\bar{E}$$

Point Form of Ohm's law

$$\boldsymbol{J} = \sigma\, \boldsymbol{E}$$

J= current density (A/m^2)
E: electric field

$$\boldsymbol{J} = \sigma \boldsymbol{E} = \text{ne<v>}$$

n: electron density

For Cu, the electron density is calculated from the number of atoms per unit volume in the crystal, considering that Cu only has one valence electron

$$\sigma = \frac{1}{\rho} = \frac{ne^2\langle\tau\rangle}{m}$$

Resistivity
Cu: 1.68 10^{-8} Ω-m @ 20°C

$<\tau>= 3\ 10^{-14}$ s (agrees with experiments)

$$l = < v >< \tau >$$

For E=10 V
<v>= (10*1.6e-19*3 e-14/9.1 e-31)=3.3 e-2 m/s
Compared to the thermal velocity: $(3k_BT/m)^{0.5}$= 1.6e10 m/s at T=300K

Free electron model has its limitations, as it does not consider quantum effects.
Electrons are Fermions, that obey Pauli exclusion principle.
Moreover, at room temperature not all valence electrons are participating in conduction

If we call f(n) the fraction of the carriers that participate in conduction, then we can write Ohm's law

$$\sigma = \frac{1}{\rho} = \frac{ne^2\langle\tau\rangle}{m}\frac{k_B T}{E_F}$$ f(n)

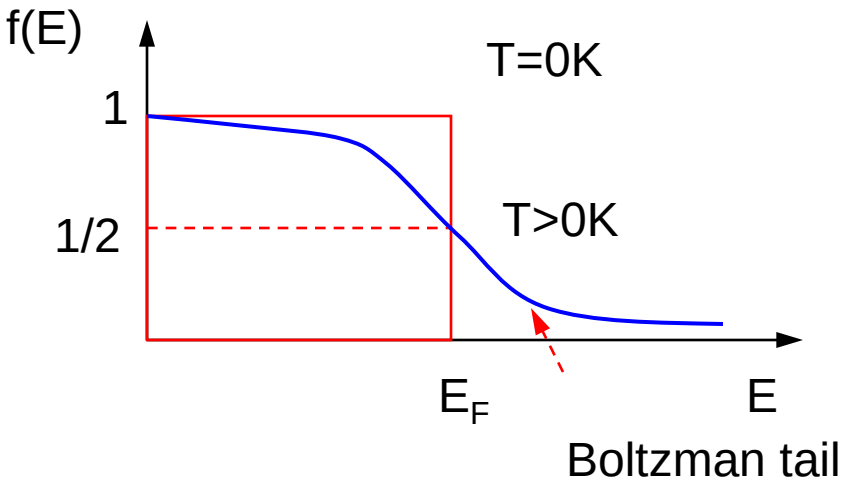

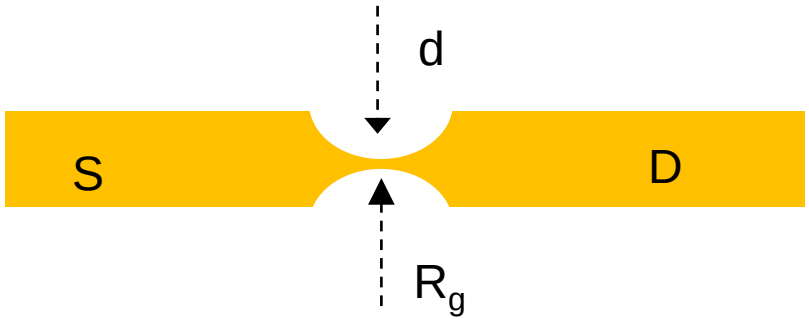

If d <τ then Ohm's law does not obey

To calculate an equivalent resistance, one needs to assume that there are N channels that connect the source and sink, or equivalently that there are N types of electronic wavefunctions that can occupy the gap d.

We can calculate the transition probability for an electron characterized by an eigenfunction ψ_k make a transition to a final state characterize by final state ψ_m

$$R_g = \frac{h}{2Ne^2} = \frac{1}{N} R_L$$

Where

R_L: Landauer resistance is approximately equal to 12.9 KΩ

Junction between an STM tip and a surface is R_L

The same result can be obtained with quantum mechanics using Fermi Golden Rule that allows one to calculate transition probabilities between initial (k) and final (m) states of the system.

Page 63

$$P(m,k) = \frac{2\pi}{\hbar}\left|\left\langle \psi_m \right| \hat{H}' \left| \psi_k \right\rangle\right|^2 \rho(E_k)$$

Where $\hat{H}'$ Represents a perturbation to the original system. The letters k and m identify initial and final states. $\rho(E_k)$ is the density of initial states.

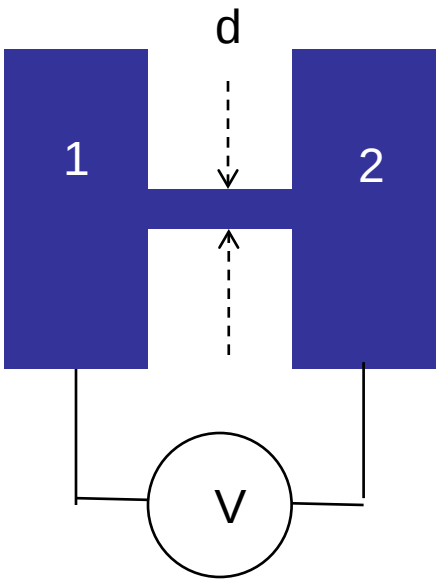

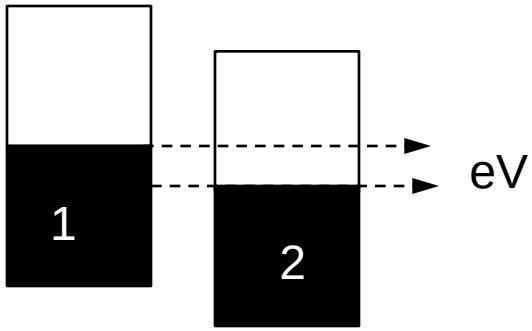

Shift in E_F with bias

$$v_g = \frac{1}{\hbar}\frac{dE_k}{dk}$$ Electron group velocity

For a one dimensional system the distance between allowed states is $\frac{2\pi}{d}$ and the density of states per unit length $\frac{dn}{dk} = \frac{1}{2\pi}$

One can calculate the current flowing through the channel of thickness d as:

$$i = nev_g = 2e\frac{dn}{dk}\frac{dk}{dE}eV\frac{1}{\hbar}\frac{dE_k}{dk} = 2eN\frac{1}{2\pi}\frac{1}{\hbar v_g}eV\,v_g$$

Accounts for spin

Allowed number of states in the channel

From this expression, the resistance per channel can be calculated as

$$R_o = \frac{V}{i} = \frac{\hbar}{2e^2} = 12.9\ k\Omega$$

This result is independent of material properties.

The Landauer resistance is a fundamental constant associated with quantum transport. There is no power dissipated in the quantum channel. It represents a probability of transmission changes when the bias is changed. The absence of dissipation makes it possible to achieve enormous current densities in a STM probe

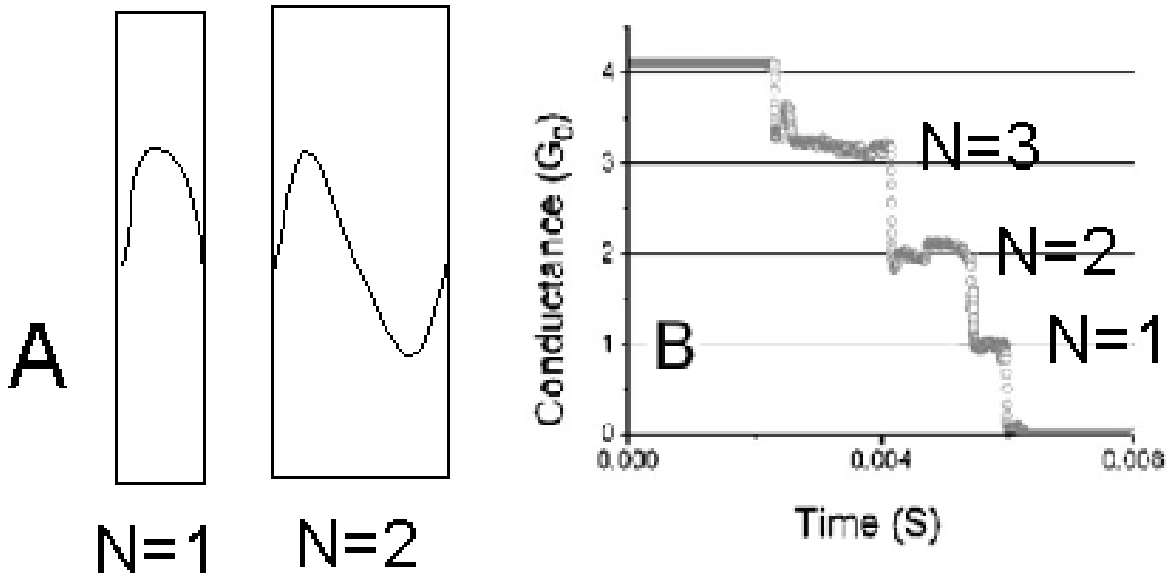

Fig. 7.6. (A) Illustration of a nanochannel in which just one (N=1) or two (N=2) quantum modes propagate. (B) Measured Landauer steps in conductance of a gold break junction

When do quantum processes start to dominate?

a. When the size (d) of the structure approaches mean free path for scattering, tens to hundreds of nanometers.(upper limit)
b. When only one mode is available in the channel, and the channel width is of the order of the Fermi wavelength (lower limit)

CHARGING NANOSTRUCTURES: COULOMB BLOCKADE (7.9)

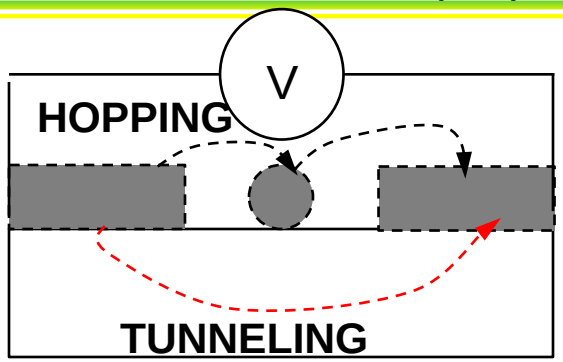

Electrons can tunnel from one electrode to the other efficiently

Or

Electrons hop to the center particle hop off to the second electrode

The hopping process is sensitive to the potential of the center island. Charging of the nanoparticle even with one electron can be significant

If the charging energy is greater than the thermal energy, electron hopping is inhibited, resulting in a region of suppressed current in the I-V curve. When the applied bias exceeds this value, conduction occurs again. This effect is termed “COULOMB BLOCKADE’.

We can estimate the value of the potential difference necessary to charge the nanoparticle

CHARGING NANOSTRUCTURES: COULOMB BLOCKADE (7.9)

Capacitance of a sphere of radius a is: $C = 4\pi\epsilon\epsilon_o a$

The energy to charge a capacitor with capacitance: $C\ is\ e^2/2C$

The voltage required to charge the island is given by:

$$\Delta V = \frac{e}{8\pi\varepsilon\epsilon_o a} \text{ volts}$$

For a=100 nm, ε=1, ε_o=8.85 10^{-12} F/m, ΔV= 7 mV

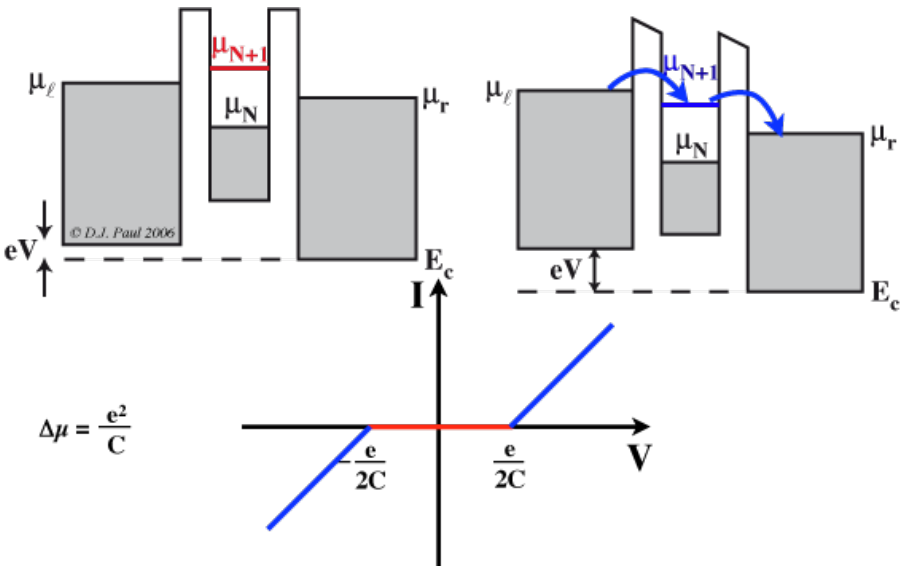

http://www.google.com/imgres?imgurl=http://www.sp.phy.cam.ac.uk/~SiGe/Images/SET1.png&imgrefurl=http://www.sp.phy.cam.ac.uk/~SiGe/Single%2520Electron%2520Transistors%2520%28SETs%29.html&h=351&w=564&sz=11&tbnid=_7IVsC3RXZCbQM:&tbnh=77&tbnw=124&zoom=1&usg=__ZhC4p-zXfndOkZ3LdmALEK88idk=&docid=vjwV2q3K97zwkM&sa=X&ei=PUBEUon5DIaMigL8x4H4DA&ved=0CD0Q9QEwAw

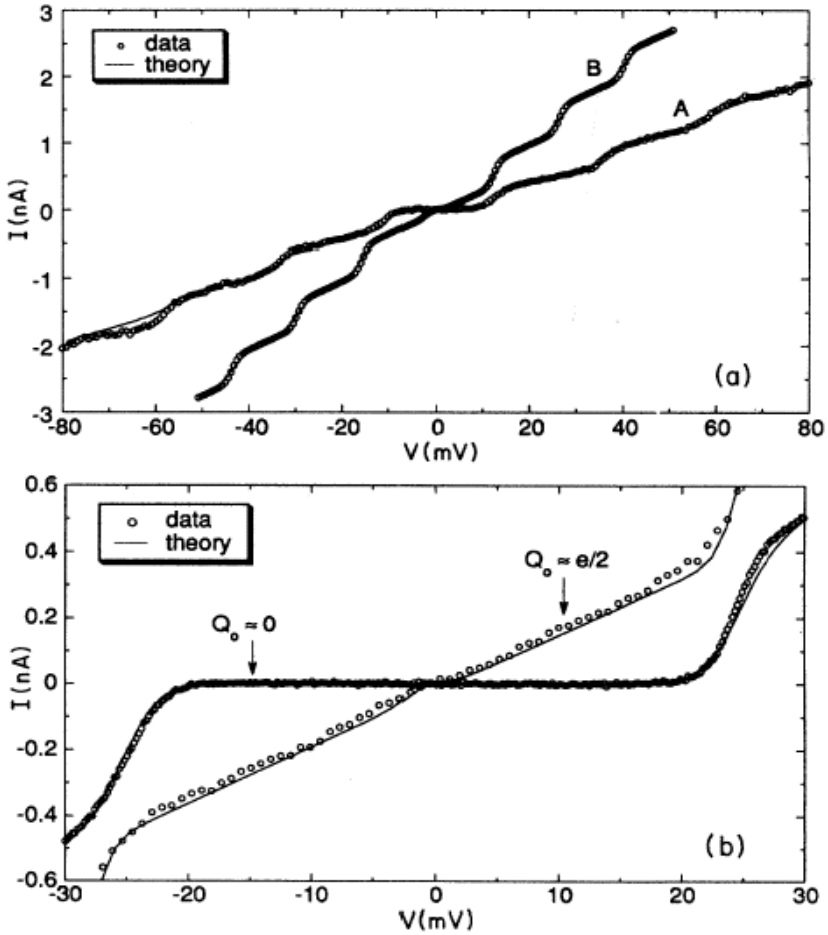

Figure 7.10 Experimental measurements of I-V curves from nanoscale double junctions (dots) fitted with Coulomb blockade theory (Hanna & Tinkham, PRB.

SINGLE ELECTRON TRANSISTOR

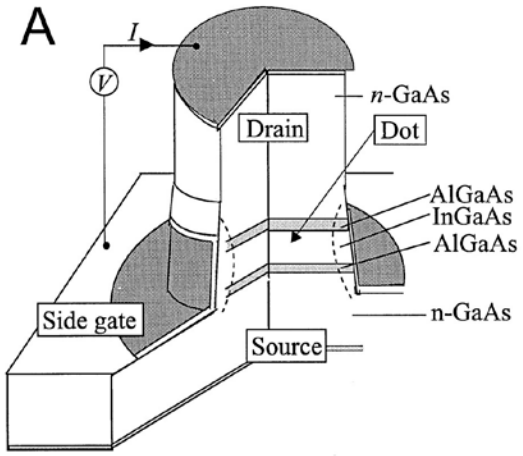

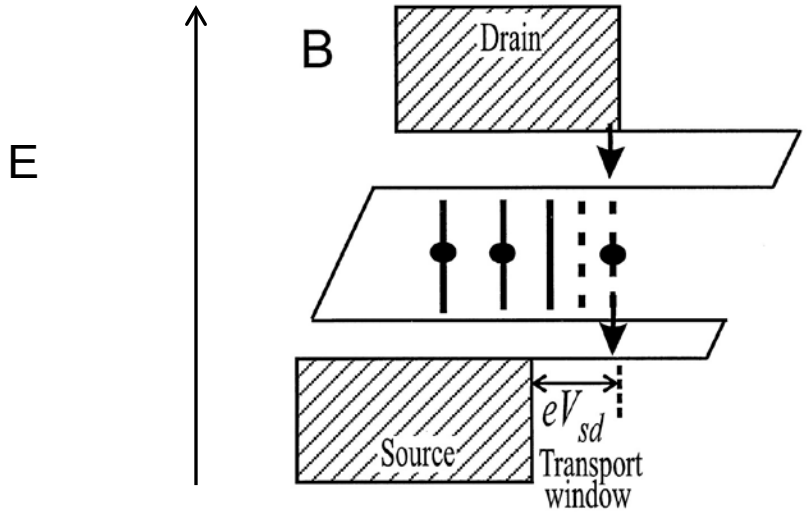

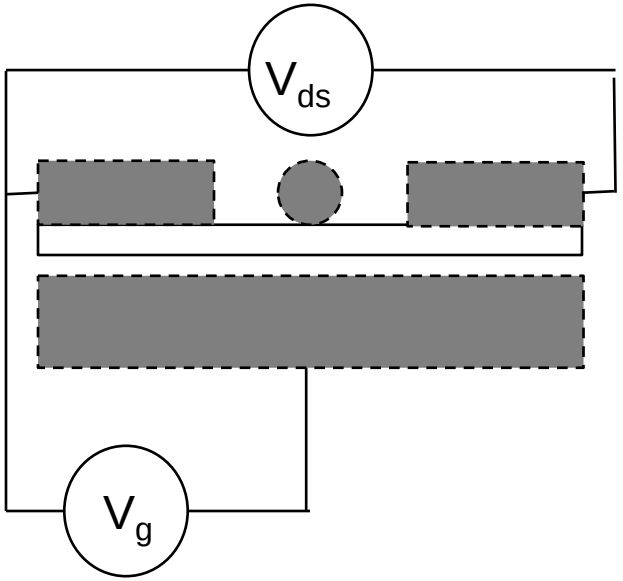

Nanostructure capacitively coupled to the gate electrode

Electrons can transport from drain to source over an energy window eV_{sd} coincides with dot quantum states. The energy of the dot states is controlled by V_g.

A. Structure of a quantum dot SET. InGaAs insulates the dot from gate electrode. (B) Energy diagram for the dot trapped between electrodes. Electron tunnel in an energy window determined by the source drain bias. States from the dot in this window empty into the drain

Fig. 7.12. Differential conductance, di/dV_{sd} plotted as a function of both source-drain voltage and gate voltage. Darker colors show SET is on. The white diamonds correspond to values of the differential conductance equal to zero.

White, di/dv = 0

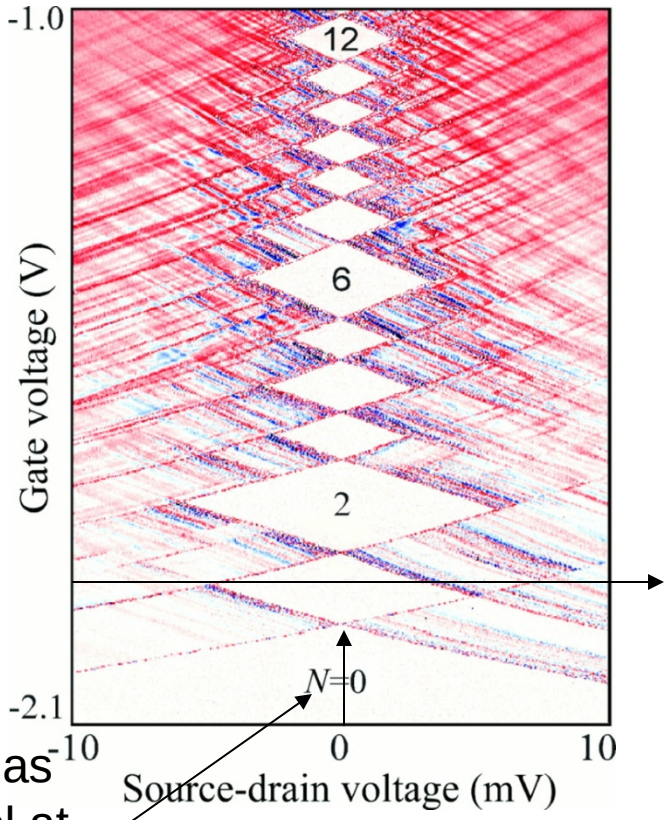

Coulomb Step = max di/dv

Gate bias for level at Vds = 0

SET as a micromechanical sensor

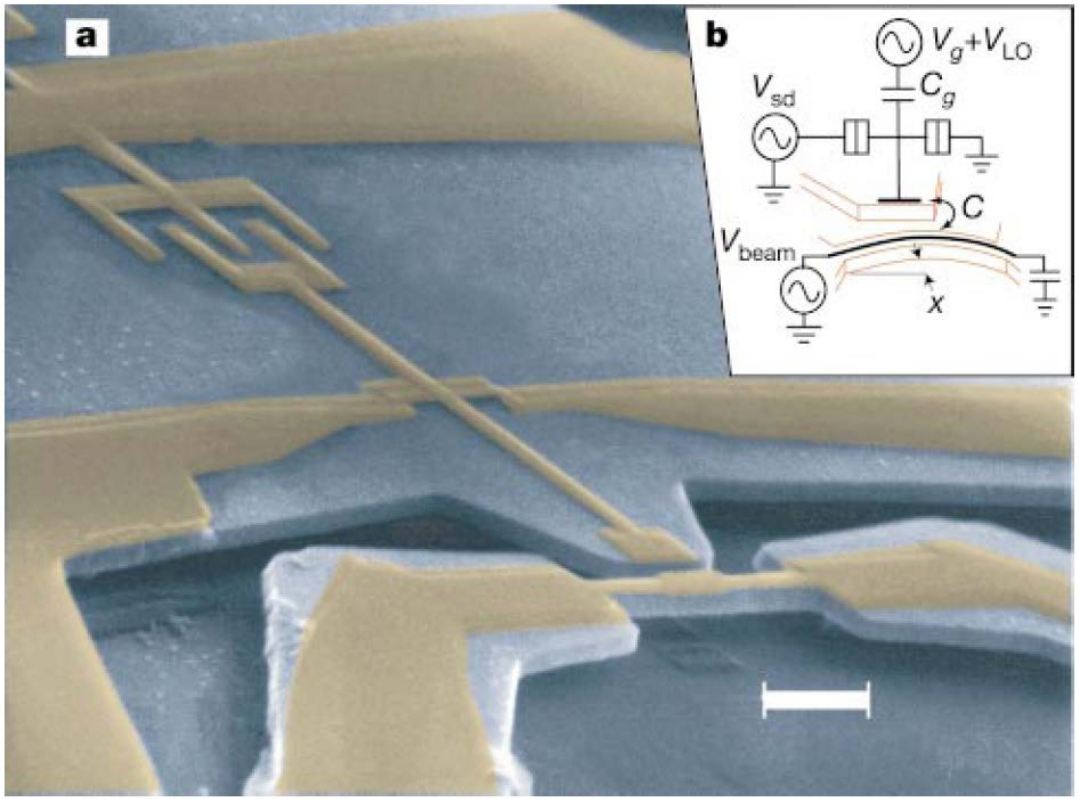

Fig. 7.13. A SET used as a nanomechanical sensor. (a) Shows a SEM image of the device shown schematically in (b). The scale bar is one micron. The vibrating beam at the bottom of is biased and alters the potential of the gate electrode in the SET (upper left) to a degree that depends on the capacitance C between the beam and gate electrode. (Nobel and Cleland, 2003).

EXPERIMENTAL MANIFESTATION OF QUANTUM CONFINEMENT

The most significant evidences of quantum confinement in different material systems are the changes observed in the optical and electronic properties. This is a consequence of the change in the density of states.

To model the optical response of a semiconductor material, including quantum dots or quantum wires, it is assumed that the quasi-free electrons in the crystal are subjected to a Lorentz force F, which is expressed as:

$$\overline{F} = -e(\overline{E} + \overline{v} \times \overline{B})$$

Where **E** is the electric field intensity, **B** is the magnetic flux density and v is the velocity of the electron

In the low intensity regime (linear regime) the hamiltonian for the electrons can be written as:

$$H = \frac{p^2}{2m_o} + V(r) - \frac{e}{m_o c}\overline{A} \cdot \overline{p}$$

$e_q \cdot d$

A is the vector potential associated with **B**

This problem is solved using perturbation theory to calculate the probability of transition between an initial and final state

DIPOLE MOMENT

In an absorption process, a photon is annihilated and an electron is promoted to a higher energy state. Optical transitions conserve energy and momentum.

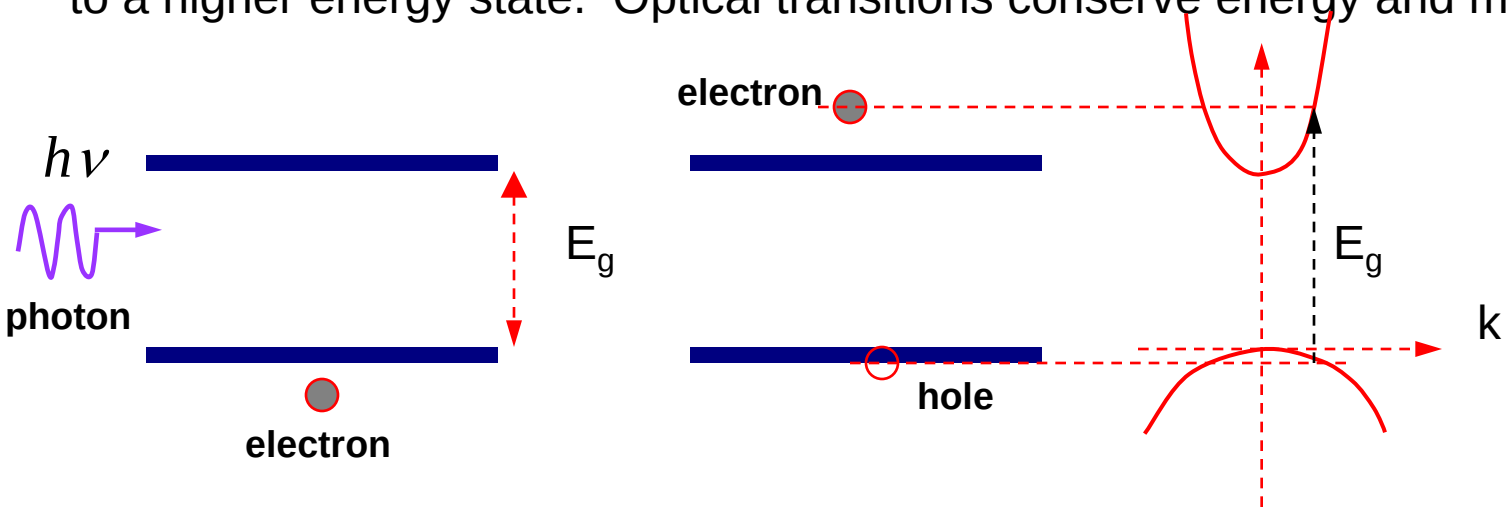

There is a threshold for absorption, the photon energy needs to be equal or larger than E_g

The transition rate for absorption is calculated from quantum mechanics by adding to the crystal potential, a potential of interaction between the electron and the photon that is of the form of a dipole field $e\vec{r}$

The strength of the optical transition depends on the material. Because photons carry polarization information, the electron-photon interaction obeys certain rules. This is significant in quantum confined systems.

The interaction of photons with carriers in a semiconductor material gives key information on confinement as it is a way to directly probe the density of states. This interaction gives rise to 'photon absorption and emission'.

Emission can be categorized as 'spontaneous' or 'stimulated'. These processes are modeled using quantum mechanics.

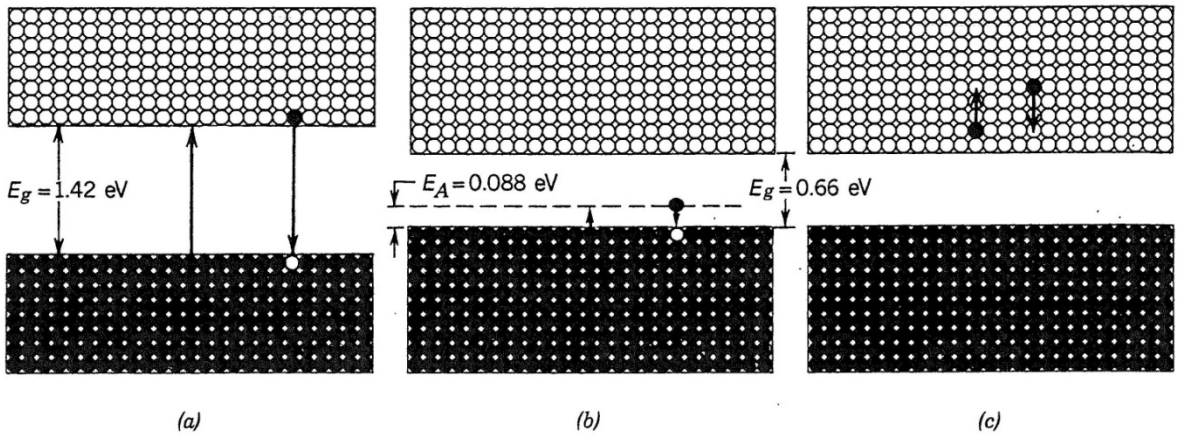

Figure 15.2-1 Examples of absorption and emission of photons in a semiconductor. (*a*) Band-to-band transitions in GaAs can result in the absorption or emission of photons of wavelength $< \lambda_g = hc_o/E_g = 0.87$ μm. (*b*) The absorption of a photon of wavelength $\lambda_A = hc_o/E_A = 14$ μm results in a valence-band to acceptor-level transition in Hg-doped Ge (Ge:Hg). (*c*) A free-carrier transition within the conduction band.

Schroedinger's equation is solved in the context of first order perturbation theory where the term ***A.p*** is considered a first order perturbation. Using this formalism, it is possible to calculate transition probability between conduction and valence band states. From the transition probability, one can obtain the absorption coefficient.

In this analysis, energy and momentum are conserved. Notice that the momentum of the photon is negligible with respect to the electron momentum

$$E_c = -E_v + h\nu$$

$$\bar{k}_c = \bar{k}_v$$

Where the momentum of the photon has been neglected as $\lambda_{photon} >> \lambda_{electron}$

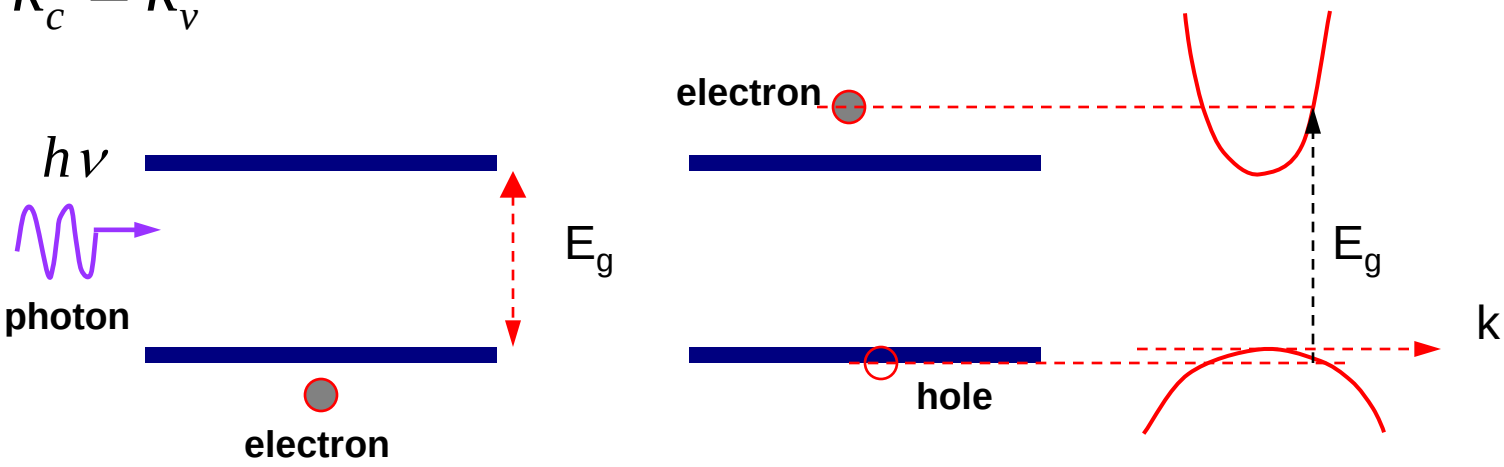

The results of this calculation are stricking, in that for direct gap materials, the absorption coefficient is found to be proportional to the density of states,

$$\alpha(E) \prec g(E) \left|d_{cv}\right|^2$$

$$\alpha(\nu) \prec (h\nu - E_g)^{1/2} \left|d_{cv}\right|^2 \qquad direct \quad gap\ 3D\ semiconductors$$

$$\left|d_{cv}\right|^2 = \left| \int d\bar{r}\, \psi_{ck}^{*}(r)[\bar{e}_q \cdot \bar{d}\,]\psi_{vk}(r) \right|$$

$\mathbf{e_q}$ is a unit vector specifying the direction of polarization

Transition matrix element calculated using the eigen-functions of the initial and final states

The transition matrix element carries information on the strength of the interaction, and the response of the material to the electric field polarization.

ABSORPTION IN SEMICONDUCTORS

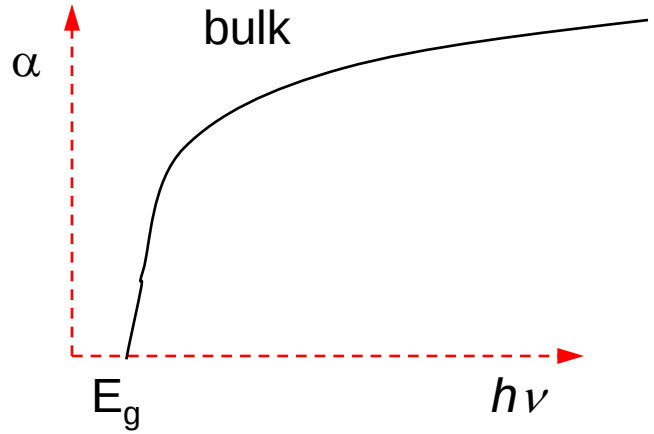

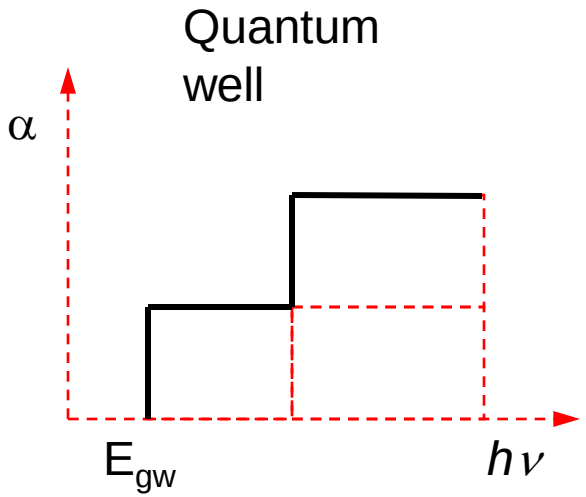

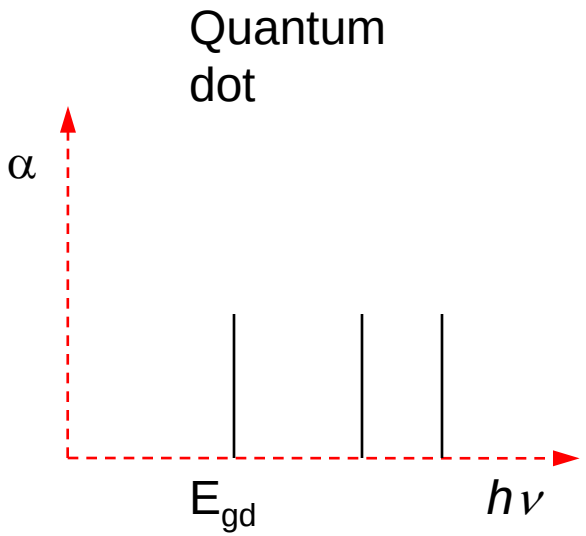

Absorption spectra of CdSe quantum dots

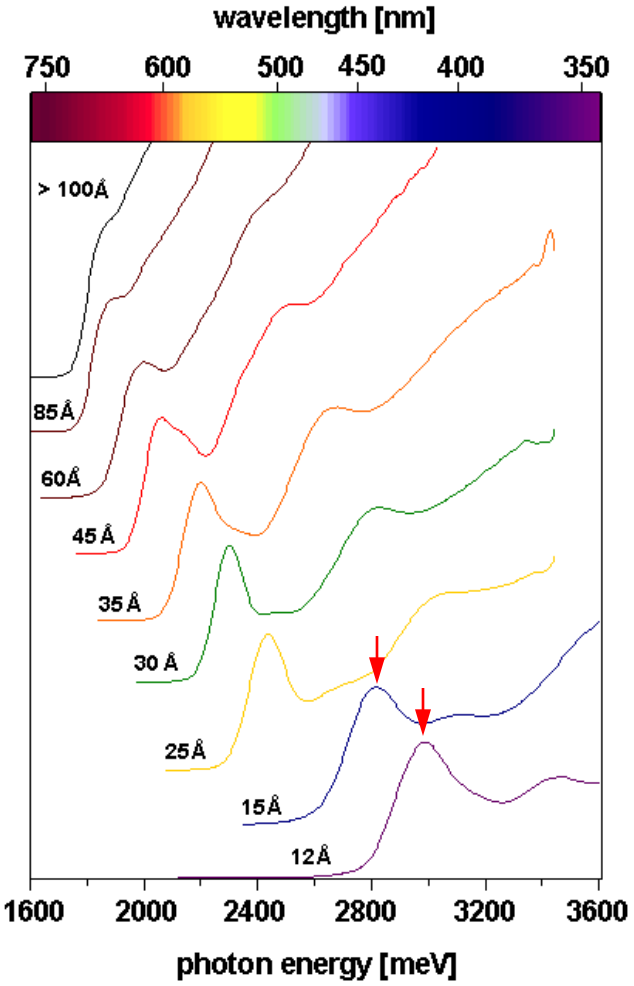

Nanocrystals have a 'bulk-like' core and are surrounded by a layer of a material that passivates the surface states.

Why if the density of states is like δ-functions is it that the absorption vs photon energy look more of step-like function?

Absorption vs photon energy for CdSe nanocrystals of different diameter

DJ Norris et al, PRB 1996

$$E = E_g + 3E_{q1}$$

$$E_{qn} = \frac{\hbar^2}{2m_c^*}\left(\frac{q\,\pi}{d_n}\right)^2 \quad q = 1,2,3$$

When an electron-hole pair is created via an absorption transition, it is also possible that the electron and the hole remain attracted via the Coulomb interaction. In this case, the electron and hole form an exciton, and the total ground state energy for the quantum dot is expressed as

$$E = E_g + 3E_{q1} - E_{Coul}$$

$$E_{q1} = \frac{\hbar^2}{2m_c^*}\left(\frac{\pi}{d}\right)^2$$

$$E_{Coul} = -\frac{1.8e^2}{2\pi\varepsilon d}$$ ← Dominates for large radii

ABSORPTION IN SEMICONDUCTORS

Exciton formation in semiconductor nanostructures is prevalent. Excitons are analogous to the hydrogen atom, and are modeled as such.

Excitons are paired electron and hole that move through the crystal as such. They can anchor to impurities or other defects. This is a bound exciton.

There are two types of excitons: Wannier and Frenkel. The first ones are characterized by a large (i.e. a few lattice constants) distance of interaction between the electron and hole. This is refered to as the 'Bohr radius'. This condition is met in most II-VI, III-V and group IV semiconductors.

Instead in wide-gap semiconductor/insulators and in some organic materials Frenkel excitons exist.

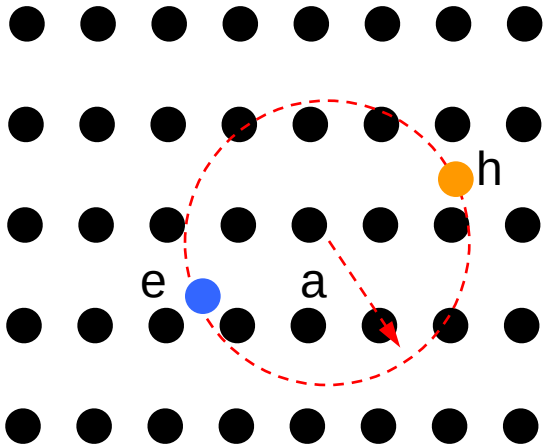

The presence of excitons modify the absorption spectra of semiconductors

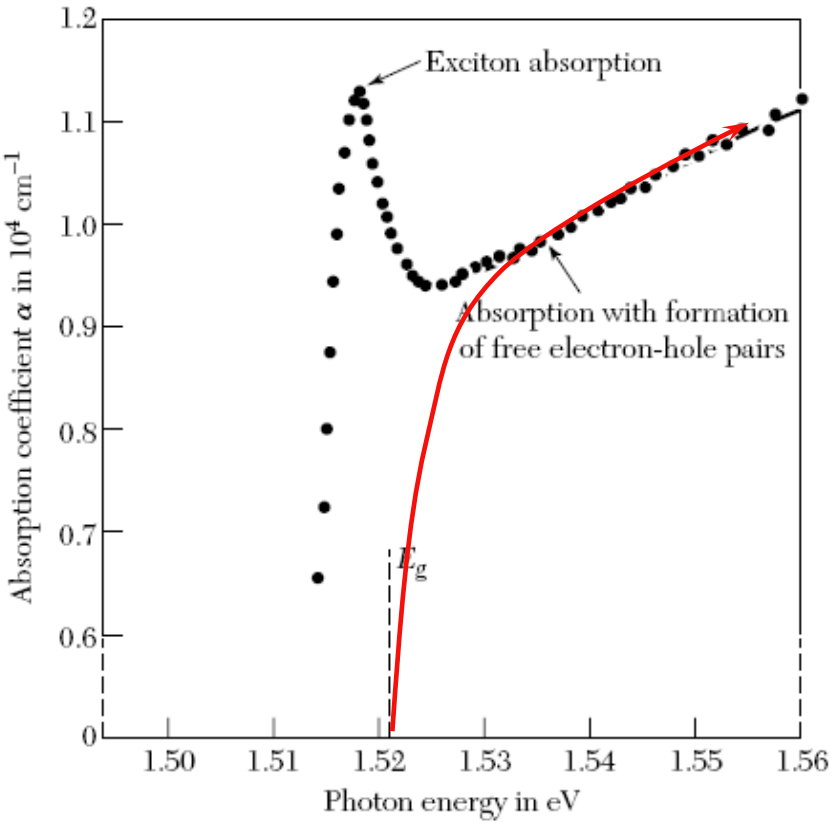

Figure 7 Effect of an exciton level on the optical absorption of a semiconductor for photons of energy near the band gap E_g in gallium arsenide at 21 K. The vertical scale is the intensity absorption coefficient α, as in $I(x) = I_0 \exp(-\alpha x)$. The energy gap and exciton binding energy are deduced from the shape of the absorption curve: the gap E_g is 1.521 eV and the exciton binding energy is 0.0034 eV. (After M. D. Sturge.)

In bulk materials, excitons can only be observed at low temperature.

In confined materials, they are readily observed at room temperature

To obtain allowed excitonic energy states, we consider that the e-h pair is a hydrogen atom immersed in a material of permittivity ε. In this case, Schroedinger's equation for the hydrogen atom is solved, with the consideration that the eigenfunctions are now linear combinations of the electron and hole wavefunctions. The eigen-energies are discrete states expressed by:

$$\varepsilon_{nlm} = -\frac{m_r e^4}{2\hbar^2 \varepsilon^2}\left[\frac{1}{n^2}\right] = -E_B\left[\frac{1}{n^2}\right]$$

Eigen-energies

$$n = 1,2,\ldots \quad E_B = \frac{\hbar^2}{2m_r a_B^2} \quad a_B = \frac{\varepsilon\hbar^2}{m_r e^2} \quad m_r^{-1} = \frac{1}{m_e} + \frac{1}{m_h}$$

Here ε is the permittivity of the material, E_B is the exciton binding energy, a_B is the Bohr's radius for the excitoin and m_r is the reduced mass of the electron and hole pair

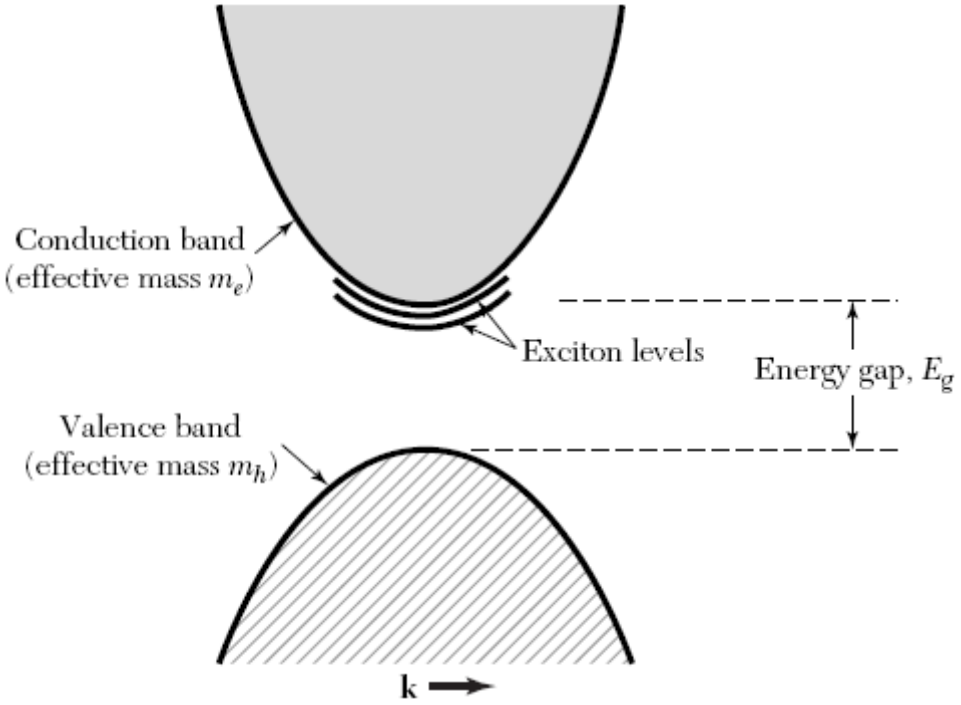

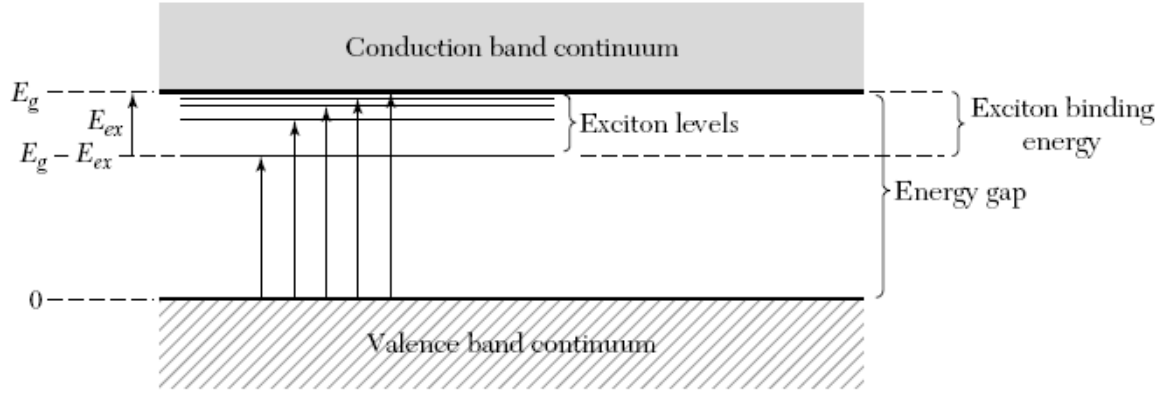

Because the Coulomb interaction is attractive, excitonic states have an energy slightly reduced with respect to a free electron hole pair. In the band diagram, these discrete states are close to the conduction band minima.

The exciton eigenfunctions are expressed as:

$$\Psi(r,R) = u_{co}u_{vo}\varphi(r)e^{iK_c \cdot R}$$

R: coordinate of the center of mass

r: coordinate around center of mass

$$\Psi(r,R) = u_{co}u_{vo}\varphi(r)e^{iK_c\cdot R}$$

Wave-like character of the exciton- expresses the translational symmetry of crystal

Conduction and valence band Bloch functions. Contain information on the character of the atomic orbitals forming the conduction and valence bands. The symmetry of these functions determines strength of the optical interband transition.

Exciton envelope function (hydrogen-like solution) that describes relative motion of the electron and hole on a large scale

Table 1 Binding energy of excitons, in meV

Si	14.7	BaO	56.	RbCl	440.
Ge	4.15	InP	4.0	LiF	(1000)
GaAs	4.2	InSb	(0.4)	AgBr	20.
GaP	3.5	KI	480.	AgCl	30.
CdS	29.	KCl	400.	TlCl	11.
CdSe	15.	KBr	400.	TlBr	6.

EXCITON ABSORPTION

Exciton absorption for the case of Wannier excitons can be calculated from the theory of optical absorption and was done by Elliott in 1957. There are conservation laws that apply on an absorption transition, i.e. energy, momentum, angular momentum, and parity need to be conserved.

Since the exciton is created via absorption of a photon, then it must have an energy

$$\varepsilon_n(K_c) = h\nu$$

Similarly, the center-of-mass momentum must be equal to the momentum of the absorbed photon

$$\hbar\overline{K}_c = \hbar\overline{q} \approx 0 \quad q \approx 0$$

q is the photon momentum

Angular momentum conservation

The photon carries an angular momentum *l* =1 in the dipole approximation. Since the angular momentum of the whole system must be unchanged before and after an optical transition, the following relationship must be satisfied:

$$\Delta l = \pm 1$$

$$\Delta l = \Delta l_{\text{int}} + \Delta l_{env} = \pm 1$$

Internal motion of the exciton represented by u_{co} and u_{vo}

Envelope wavefunction condition

This gives rise to the following possibilities

$$\Delta l_{\text{int}} = \pm 1 \quad \Delta l_{env} = 0 \quad (1)$$

p-valence band, s-conduction band, s-exciton envelope function – These are called: DIPOLE ALLOWED TRANSTIONS. Exciton series starts at n-1

$$\Delta l_{\text{int}} = 0, \mp 2 \quad \Delta l_{env} = \pm 1 \quad (2)$$

s or d-valence band, s-conduction band, p-exciton envelope function. These are second class transitions that are much weaker. Exciton series starts at n=2

The parity of the whole system must be conserved. A photon with *l*=1 carriers a parity of -1. Therefore the exciton overall must have a parity of -1 for a totally symmetric crystal ground state that has positive parity.

An exciton with negative parity can be constructed for example by p-like valence band Bloch function (u_{vo}), a s-like conduction band Bloch function (u_{co}) and a s-like exciton envelope function. (DIPOLE ALLOWED TRANSITION); or if all have negative parity or if u_{co}, u_{vo} have positive parity and the envelope wavefunction negative parity.

The exciton absorption for a first class dipole allowed transition can be computed for a direct bandgap semiconductor material conditioned to all of the conservation rules just discussed (Elliott, 1957)

$$\alpha(\omega) = \frac{8\pi^2 \omega \left| d_{cv} \right|^2}{n_b c} \sum_n \left| \phi_n(r=0) \right|^2 \delta(\hbar\omega - E_g + \frac{E_B}{n^2})$$

Momentum matrix element

Sommerfeld enhancement factor: specifies the probability of finding the electron at the same lattice site than the hole

Absorption characteristics in semiconductor bulk and nanostructured materials

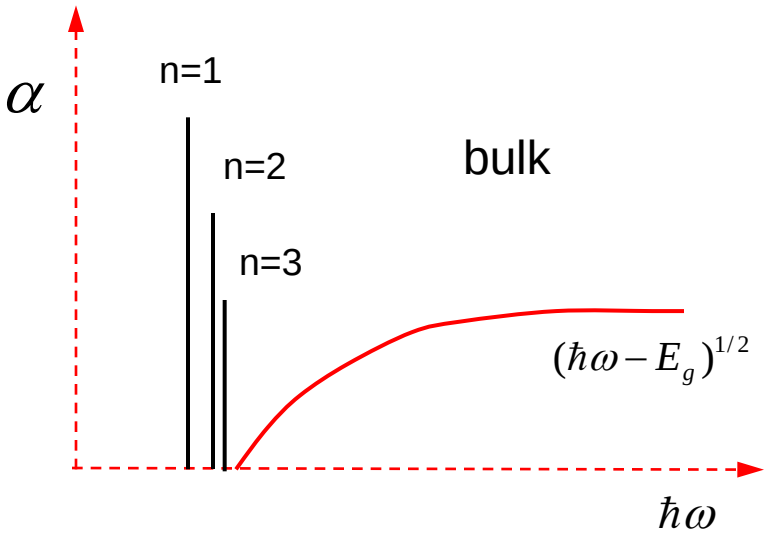

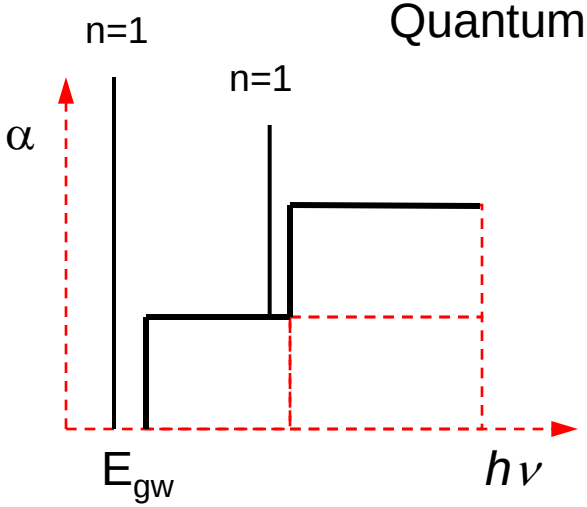

$$E_B^{2D} = \frac{E_B}{(n-1/2)^2}$$

$$n=1 \quad E_B^{2D} = 4E_B$$

Enhancement of exciton binding energy in quantum wells is used to make modulators

Absorption in GaAs quantum wells

Investigation of Optical Absorption Spectra of GaAs/AlAs Multiple Quantum Wells Fabricated on a GaAs Substrate Using Surface Photovoltage and Piezoelectric Photothermal Techniques

Ping Wang, Shingo Kurayama, Atsuhiko Fukuyama, Yoshito Akashi, and Tetsuo Ikari

Jpn. J. Appl. Phys., Vol. 46, No. 10A (2007)

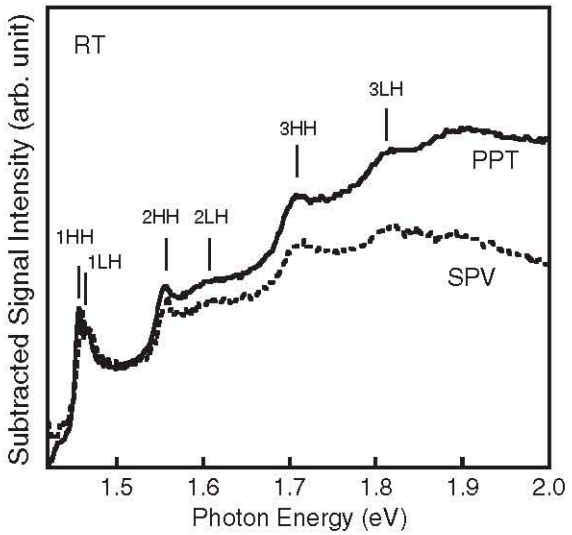

Fig. 3. Subtracted PPT and SPV spectra obtained by deducing background signal.

Absorption in quantum wires

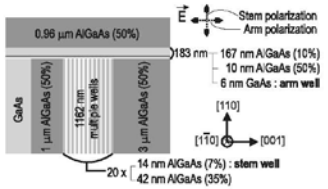

FIG. 1: Schematic view of 20-wire device, where 20 T-wires are embedded in T-waveguide. Cross-section of each T-wire is 14 nm (stem well)×6 nm (arm well). Percentages in parentheses represent Al content x of $Al_xGa_{1-x}As$.

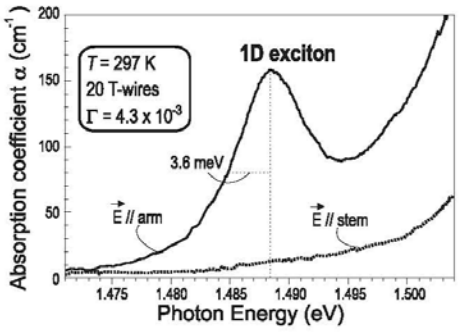

FIG. 2: Absorption spectra of 20 wires at 297 K. Solid curve and dotted curve represent absorption spectra for arm and stem polarizations, respectively. Room-temperature 1D excitonic absorption is observed at 1.4884 eV.

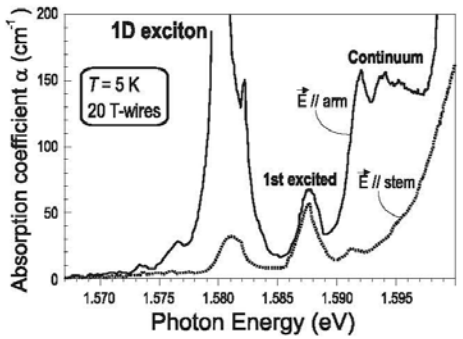

FIG. 3: Absorption spectra of 20 wires at 5 K. Solid curve and dotted curve show absorption spectrum for arm and stem polarizations, respectively.

Room-temperature excitonic absorption in quantum wires

Authors: Yasushi Takahashi, Yuhei Hayamizu, Hirotake Itoh, Masahiro Yoshita, Hidefumi Akiyama, Loren N. Pfeiffer, Ken W. West

Absorption in quantum dots

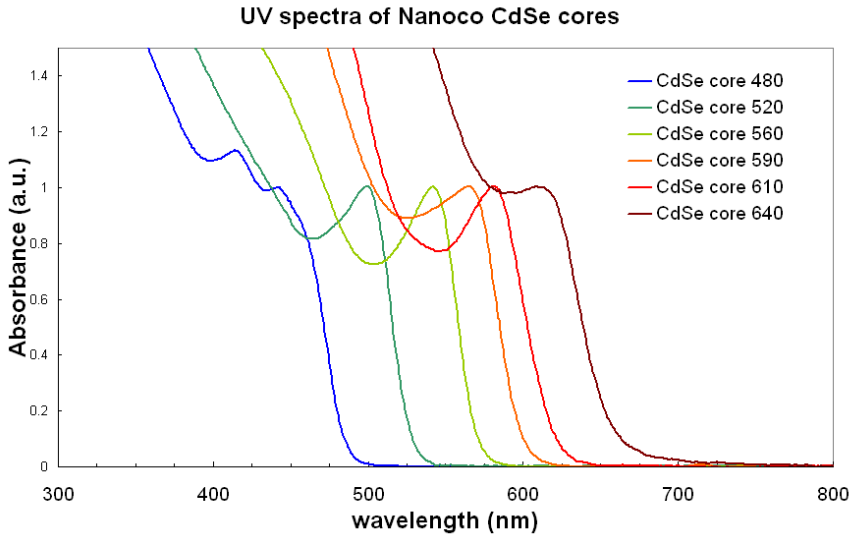

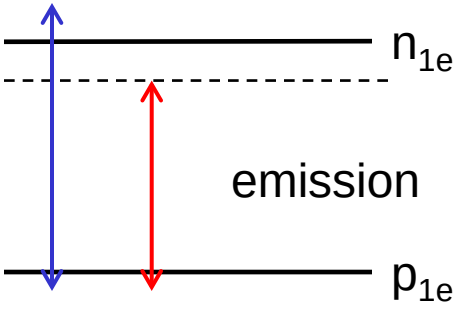

absorption

emission

Absorption and emission

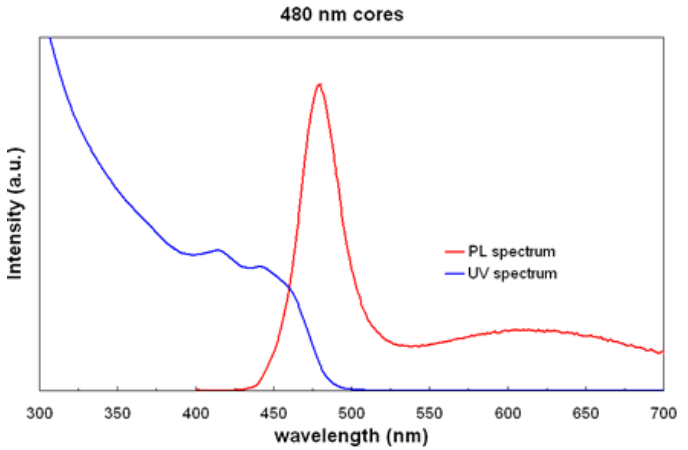

Absorption rate, spontaneous emission and stimulated emission rates are all related via Einstein Coefficients. Thus, if absorption is known, all of the other two rates can be calculated. The importance of knowing the absorption versus wavelength is exemplified in applications such as laser diodes whereby one can directly obtain the gain spectrum.

ABSORPTION

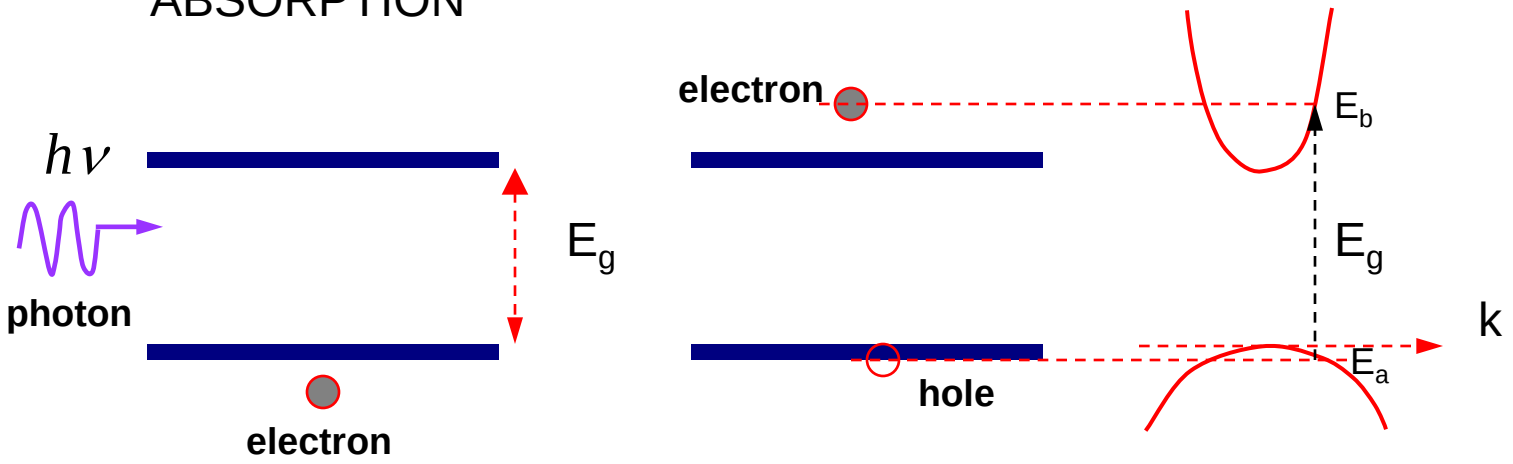

Since the absorption process links a state in the VB with one in the conduction band, the distribution of states that can participate in this process are described by a reduced density of states:

$$\rho_{red}(h\nu) = \frac{1}{4\pi^2}\left(\frac{2m_r}{\hbar^2}\right)^{3/2}(h\nu - E_g)^{1/2}$$

$$m_r = \left[\frac{1}{m_e} + \frac{1}{m_h}\right]^{-1}$$

SPONTANEOUS RECOMBINATION

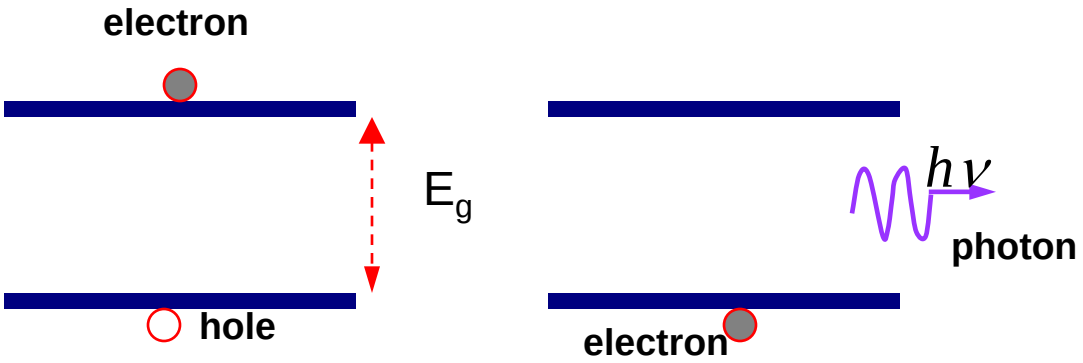

Energy and momentum are conserved

STIMULATED RECOMBINATION

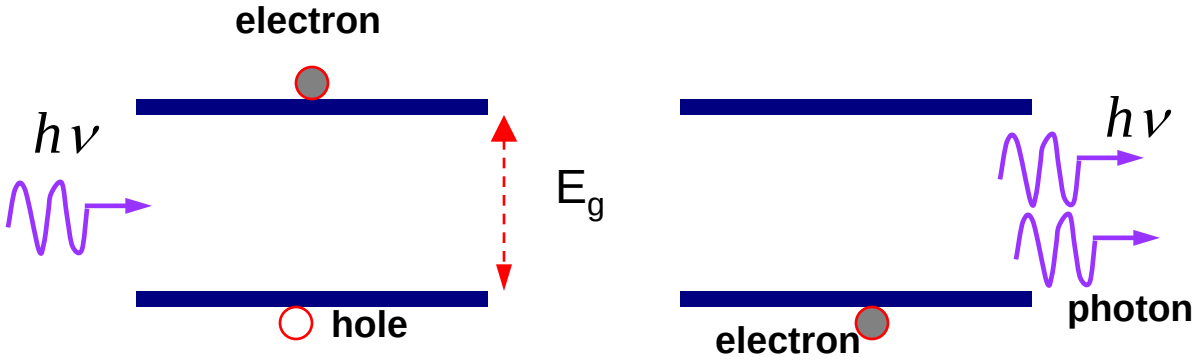

One can calculate the number of absorptive transitions $R_{a\to b}$ caused by the absorption of a photon with energy $E=h\nu$ as

$$R_{a\to b} = [B_{12}]\cdot[P(h\nu)d(h\nu)]\rho_{red}(h\nu)\{f_v(E_a)[1-f_c(E_b)]\}$$

For the stimulated transition rate $R_{b\to a}$

$$R_{a\to b} = [B_{21}]\cdot[P(h\nu)d(h\nu)]\rho_{red}(h\nu)\{f_c(E_b)[1-f_v(E_a)]\}$$

f's are Fermi-Dirac distribution functions, P is the blackbody distribution function which is the energy density of the electromagnetic field inside a cavity, and B_{21} and B_{12} are Einstein coefficients.

Subtracting the two expressions, one obtains the net stimulated rate, which using $B_{21}=B_{12}$ is expressed as:

$$R_{b\to a} - R_{a\to b} = [B_{21}]\cdot[P(h\nu)d(h\nu)]\rho_{red}(h\nu)\{f_c(E_b) - f_v(E_a)\} \qquad (**)$$

$$and \quad h\nu = E_b - E_a$$

$$P(\nu) = \frac{8\pi n_b \nu^2}{c^3}\frac{h\nu}{e^{h\nu/k_bT}-1}$$

n_b is the index of refraction of the material and k_b, Boltzman Constant

The gain coefficient can be calculated from (**) as

$$\gamma(h\nu) = \frac{1}{I(\nu)}\frac{dI(\nu)}{dz} = \frac{Power\ emitted\ \ per\ unit\ of\ \ volume}{Power\ \ per\ unit\ of\ \ area\ \ cross\sin g\ \ the\ volume}$$

$$\gamma(h\nu) = \frac{(R_{b\to a} - R_{a\to b})h\nu n_g}{h\nu P(h\nu)d(h\nu)c} = \underbrace{B_{21}\frac{n_g}{c}\rho_{red}(h\nu)}_{K\alpha(h\nu)}[\,f_c(E_b) - f_v(E_a)]$$

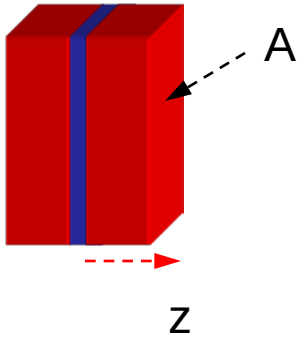

c/n_g is the group velocity

The spontaneous emission rate can also be calculated, as in thermodynamics equilibrium the rate of recombination of electron-hole pairs yielding a photon between ν and ν+d ν must exactly equal the absorption rate of photons in the same interval from the ambient (blackbody) background radiation.

$$R(\nu)d\nu = \alpha(\nu)\frac{c}{n_g}\left\{\frac{8\pi n_b^2 n_g \nu^2}{c^3}\left[\frac{d\nu}{\exp(h\nu/k_bT) - 1}\right]\right\}$$

Radiative transition

$$for\ h\nu/k_bT >> 1 \quad R(\nu) = \alpha(\nu)\frac{8\pi n_b^2\nu^2}{c^2}\exp[-h\nu/k_bT]$$

Generation processes

Energy-band visualization of generation processes

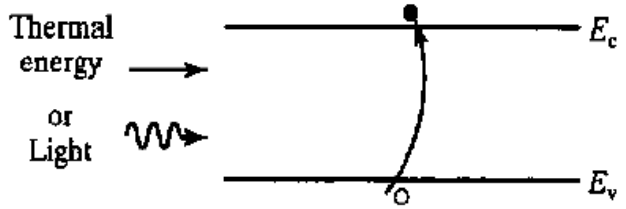

(a) Band-to-band generation

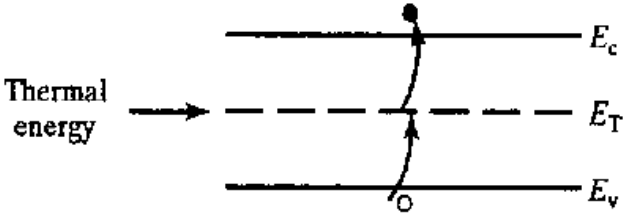

(b) R–G center generation

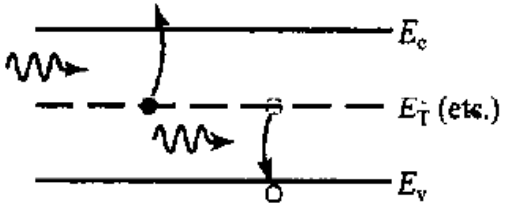

(c) Photoemission from band gap centers

Energy band visualization of Recombination processes

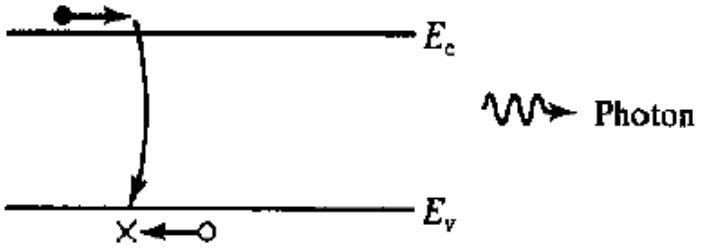

(a) Band-to-band recombination

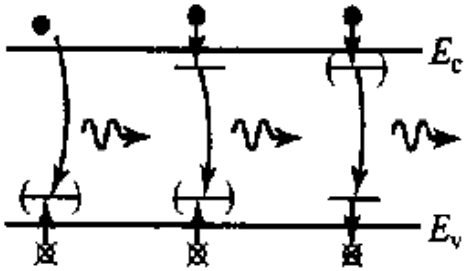

(d) Recombination involving excitons

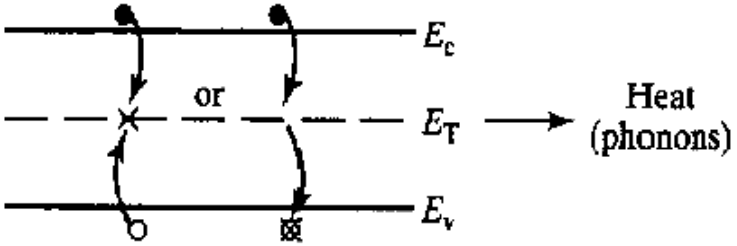

(b) R–G center recombination

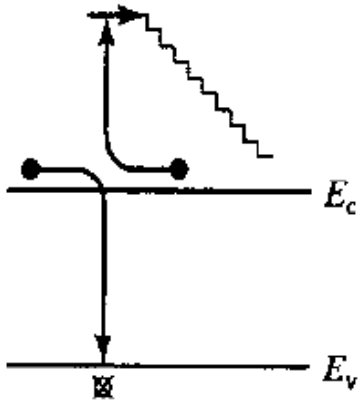

(Intrinsic)

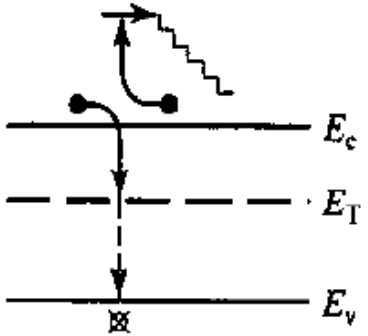

(Extrinsic)

(e) Auger recombination

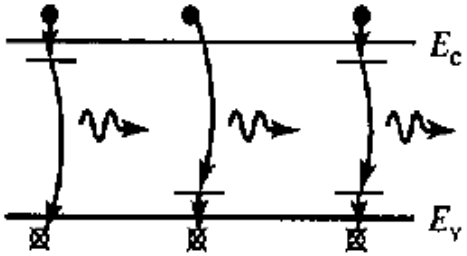

(c) Recombination via shallow levels

Energy released in the form of phonon generates heat in the lattice

Recombination processes in which there is a photon emitted are called RADIATIVE.

If no photon is emitted, the excess energy of the electron in the conduction band is dissipated in the form of heat. These processes are called NON-RADIATIVE

Emission occurs with conservation of energy and momentum

Carrier dynamics in materials can be studied via the use of external excitation. If light is used to generate excess carriers, the emission process is called PHOTOLUMINESCENCE.

If the excitation is via injection of electrons, it is called ELECTRO-LUMINESCENCE

Photoluminescence and absorption measurements –

Typical characterization of quantum confined semiconductor nanostructures

Absorption is measured with a spectrophotometer

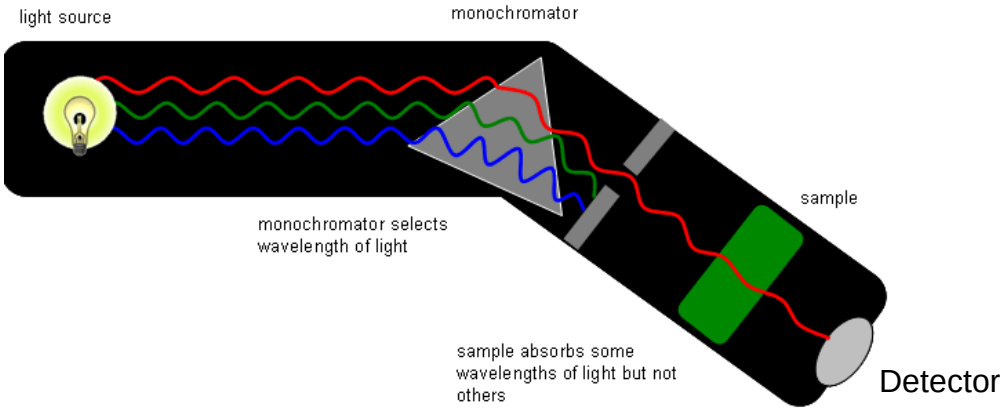

Simple schematic of the principle of operation of a spectrophotometer

Absorbance: sample is excited with white light and the absorption versus wavelength is monitored

RESULTS

GaN

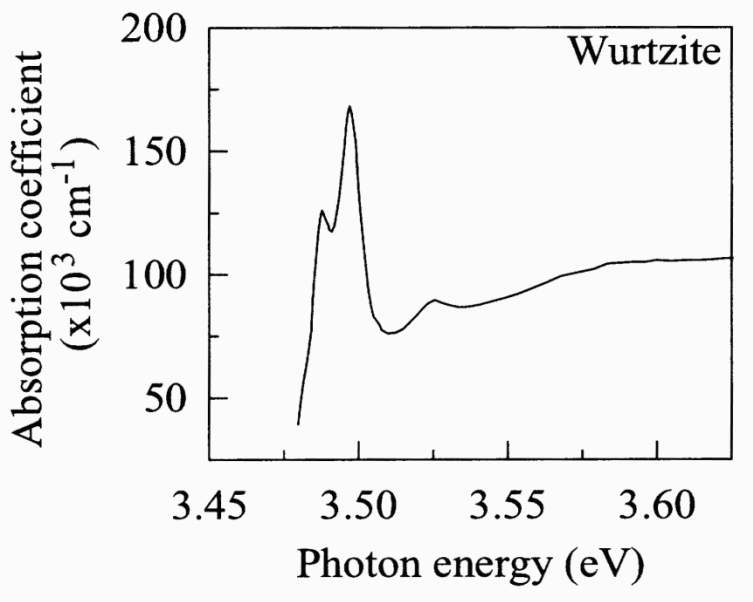

http://www.ioffe.ru/SVA/NSM/Semicond/GaN/figs/muth972.gif

GaN comparison between refractive index dispersion and absorption

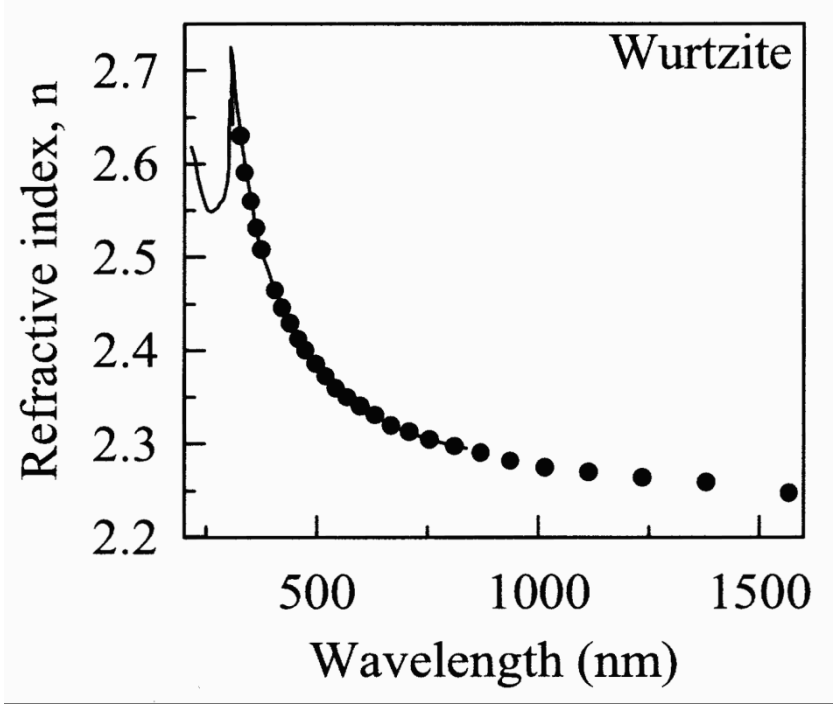

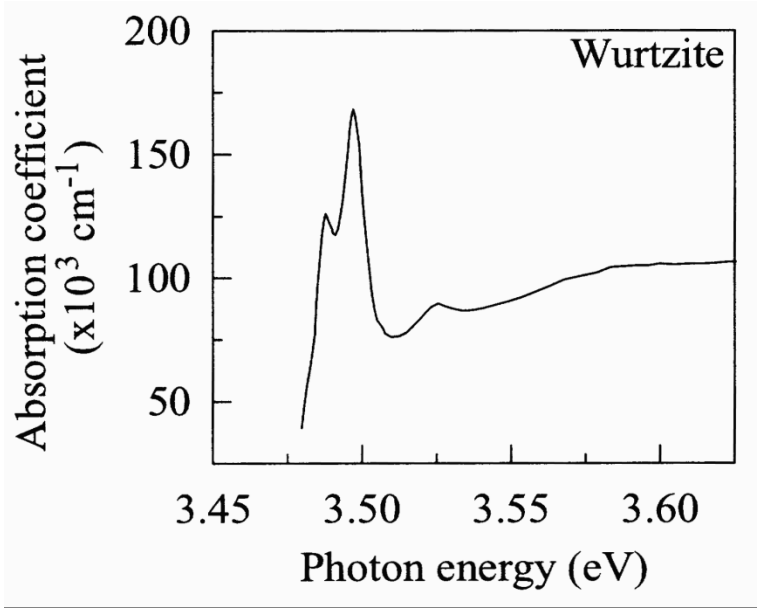

Real and imaginary parts of the dielectric function are related by Kramer-Kronig relationship.
Extinction includes scattering and absorption

Photoluminescence and absorption measurements –

Photoluminescence: sample is excited with photons of energy greater than the bandgap and the emission versus wavelength is monitored

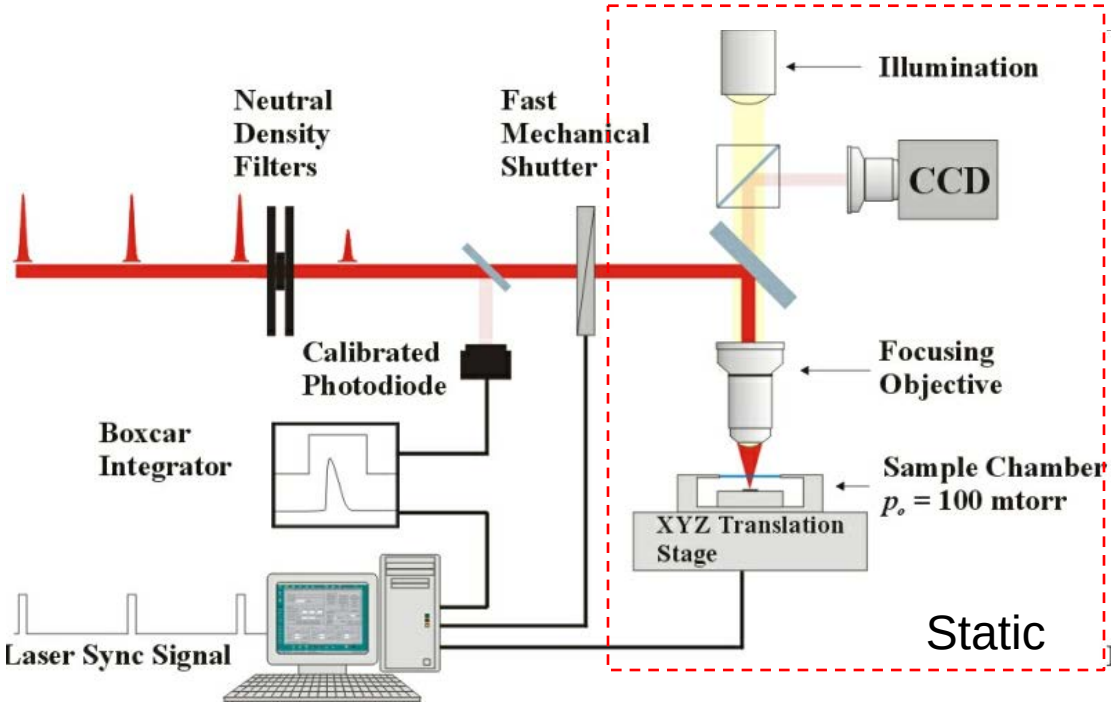

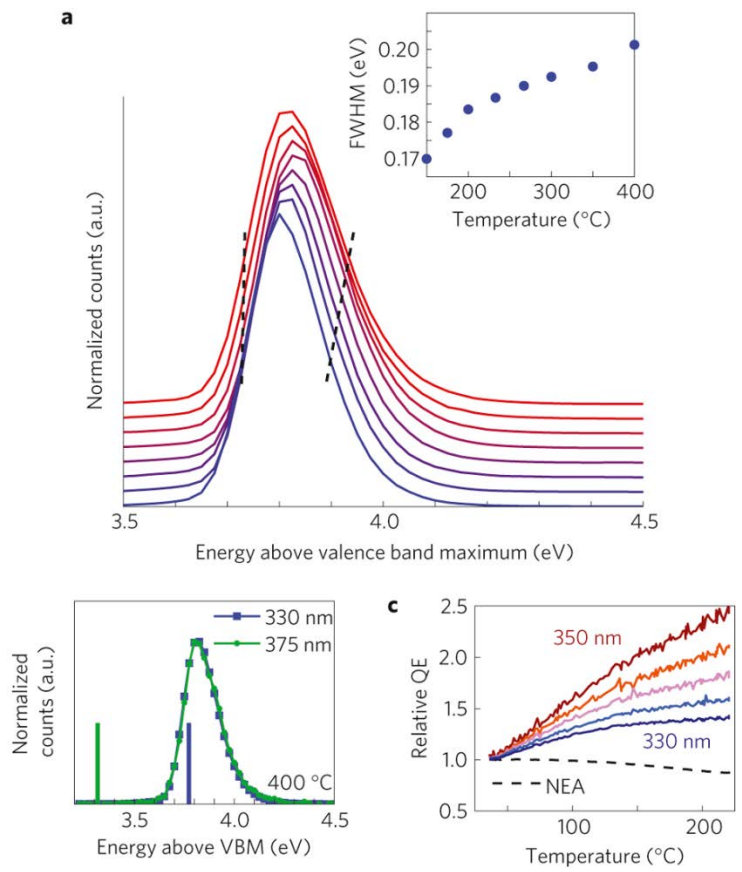

http://www.nature.com/nmat/journal/v9/n9/images/nmat2814-f3.jpg

EXAMPLE

Synthesis and Characterization of Colloidal InP Quantum Rods
S. P. Ahrenkiel, O. I. Mii, A. Miedaner, C. J. Curtis, J. M. Nedeljkovi, and A. J. Nozik
Nano Letters, 2003, 3 (6), 833-837• DOI: 10.1021/nl034152e • Publication Date (Web): 13 May 2003

ABSTRACT
InP nanorods and nanowires in the diameter range of 30-300 Å and 100-1000 Å in length were synthesized. For the preparation of nanorods, we used an organometallic precursor that decomposes thermally into InP and In metal particles. The latter serves as nucleation catalyst for the growth of the semiconductor. Quantum rods of zinc blende structure with a high degree of crystallinity are grown along the (111) crystallographic planes. The absorption spectrum of InP nanorods with diameter of about 30 Å and 100-300 Å in length is in the visible spectral regime, suggesting a substantial blue shift with respect to the bulk (band gap 1.35 eV) that is due to size confinement. Moreover, the Stokes shift of the emission band in the quantum rods is substantially larger than the shift in the corresponding quantum dots.

GROWTH METHOD
Air and water free conditions – use of organo-chemical precursor . Solution was stirred for a day and heated at temperatures of 120, 170 and 250ºC. Rods were highly reactive to Oxygen.

EXAMPLE

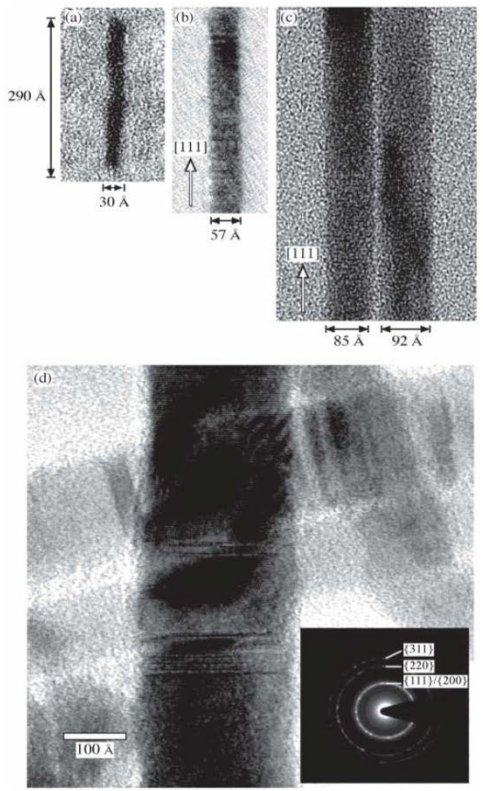

Figure 1. TEM images showing InP nanorods of various dimensions prepared in amine: (a) $[(t\text{-Bu})_2InP(SiMe_3)_2]_2$ and $[Cl_2InP(SiMe_3)_2]_2$ precursors in TOA/DDA heated at 250 °C for 3 h. The crystallinity of these very small nanorods is weak. (b, c) Prepared with $[Cl_2InP(SiMe_3)_2]_2$ precursor (without $[(t\text{-Bu})_2InP(SiMe_3)_2]_2$) on indium particles (diameter 60−110 Å) in TOA/ethylenediamine (0.1%) at 110 °C for 3 h. (d) $[(t\text{-Bu})_2InP(SiMe_3)_2]_2$ and $[Cl_2InP(SiMe_3)_2]_2$ precursors in TOP/TOPO heated at 250 °C for 24 h. The diameter distribution is broad (150−350 Å).

Transmission electron microscopy used to determine structure and composition of rods

Fringes along 111 direction are observed. These are perpendicular to growth axis. They are associated to planar defects

X-ray diffraction of a collection of large rods

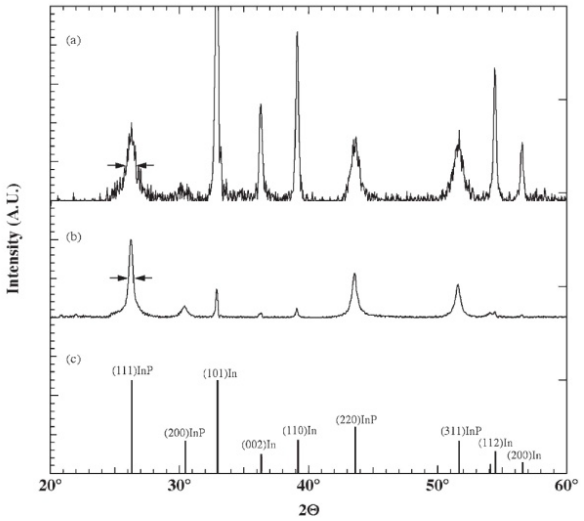

Figure 2. X-ray diffraction patterns from two ensembles of InP nanorods prepared with (a) $[Cl_2InP(SiMe_3)_2]_2$ on indium particles in TOA/ethylenediamine and (b) $[(t\text{-Bu})_2InP(SiMe_3)_2]_2$ and $[Cl_2InP(SiMe_3)_2]_2$ in TOP/TOPO. The pattern intensities were normalized to the (111) InP peaks. The arrows indicate the fwhm of the (111) InP peaks. (c) Powder diffraction lines for zinc blende InP and tetragonal indium.

Spectra shows cubic InP and tetragonal In metal.

EXAMPLE

TEM image of nanorods 3 nm in diameter grown with different precursors

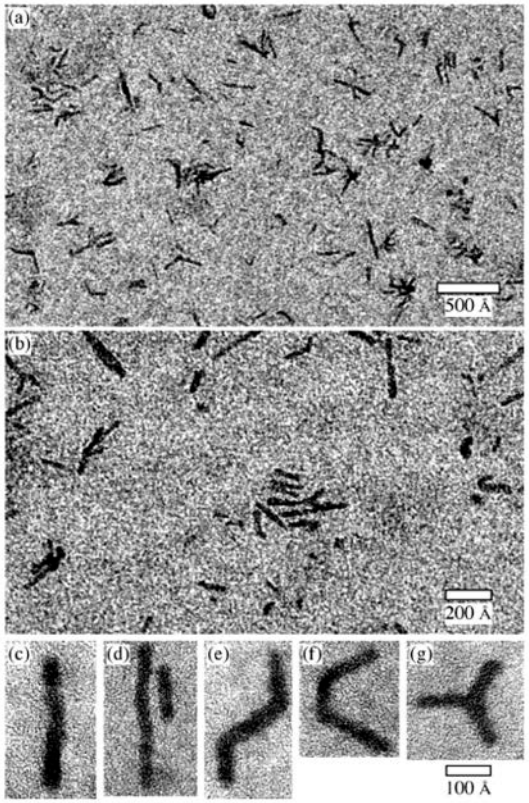

Figure 3. TEM images showing (a, b) ensemble of very small InP nanorods of about 30 Å diameter prepared from $[(t\text{-Bu})_2\text{InP}(\text{SiMe}_3)_2]_2$ and $[\text{Cl}_2\text{InP}(\text{SiMe}_3)_2]_2$ precursors in TOA/DDA heated at 250 °C for 3 h. Typical configurations and shapes of these very small nanorods are shown: (c) a single rod, (d) parallel rods, (e) zigzag rod, (f) "U"-shaped rod, and (g) three-armed rod.

Absorption and Emission Strong confinement is observed for rods 2.8 nm in diameter. Results compared with quantum dots 3 nm in diameter

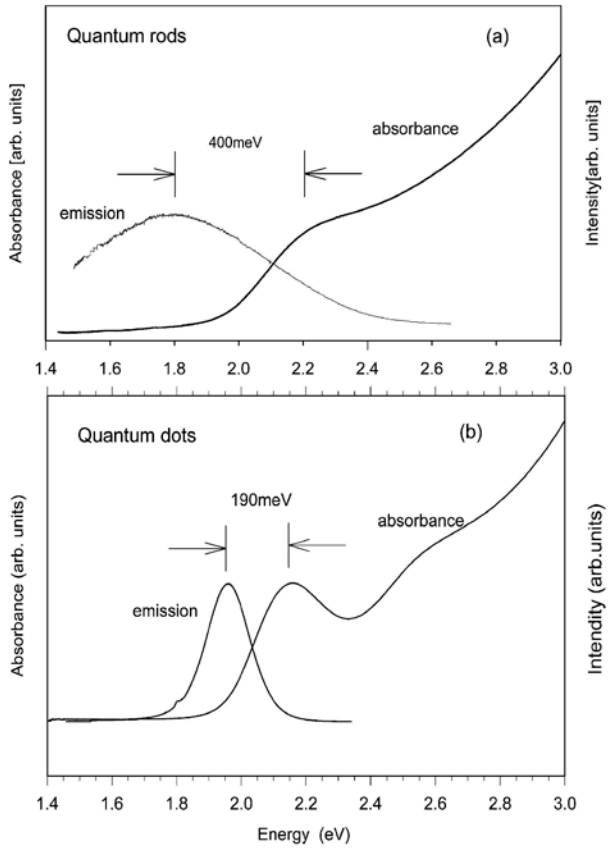

Figure 4. Absorption spectra for (a) InP quantum rods and (b) InP quantum dots (diameter ≈ 30 Å).

NANOSTRUCTURE FABRICATION/GROWTH

Making nanostructures top down (Chapter 5)

Talks by students – 10 min presentations at the end

Physical chemistry of surfaces: Chemical potential as a function of the surface curvature

Surface atoms or molecules properties are different from interior atoms. The chemical potential is also dependent on the curvature of the surface. Suppose we transfer *dn* atoms from an infinite flat surface to a spherical solid particle. The volume change of the spherical particle, dV, is equal to the atomic volume Ω times *dn*.

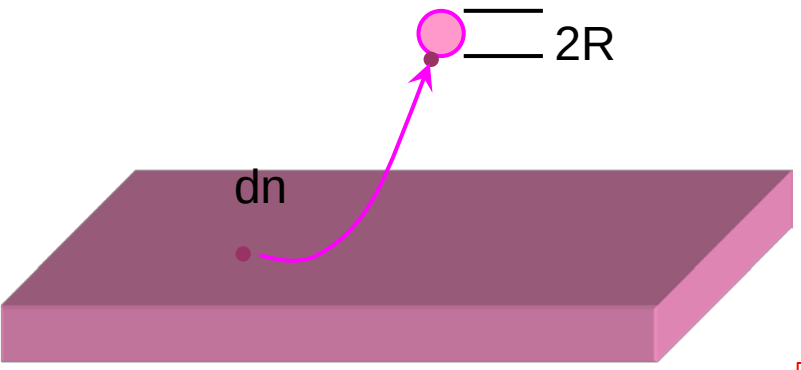

$$dV = 4\pi R^2\, dR = \Omega\, dn$$

Obtain dn/dV

$$dV = A dR \qquad \Delta A = 8\pi R dR$$

The work per atom transferred, Δμ, is the change of the chemical potential

$$\Delta\mu = \mu_c - \mu_\infty = \gamma \frac{dA}{dn} = \gamma\, 8\pi R\, dR \frac{\Omega}{dV}$$

Combining the two former equations

$$\Delta\mu = 2\gamma \frac{\Omega}{R}$$

Chemical potential of a convex surface (positive curvature) is higher than that on a flat surface

γ: surface energy

In general, this equation can be used to express the change in chemical potential of a curved surface characterized by radii R1 and R2

For an spherical particle the equilibrium vapor pressure is $\Delta\mu = kTln(P_c/P_\infty)$

$$\ln\left(\frac{P_c}{P_\infty}\right)=\frac{2\gamma\Omega}{kRT}$$

Similarly, the solubility of a curved solid surface is $$\ln\left(\frac{S_C}{S_\infty}\right) = \gamma\,\Omega\,\frac{R_1^{-1}+R_2^{-1}}{kT}$$

Where S_C is the solubility of the curved surface and S_∞ is the solubility of a flat surface

This is the Gibbs-Thompson relation

Solubility of SiO2 as a function of surface curvature Vapor pressure of the small particles is higher

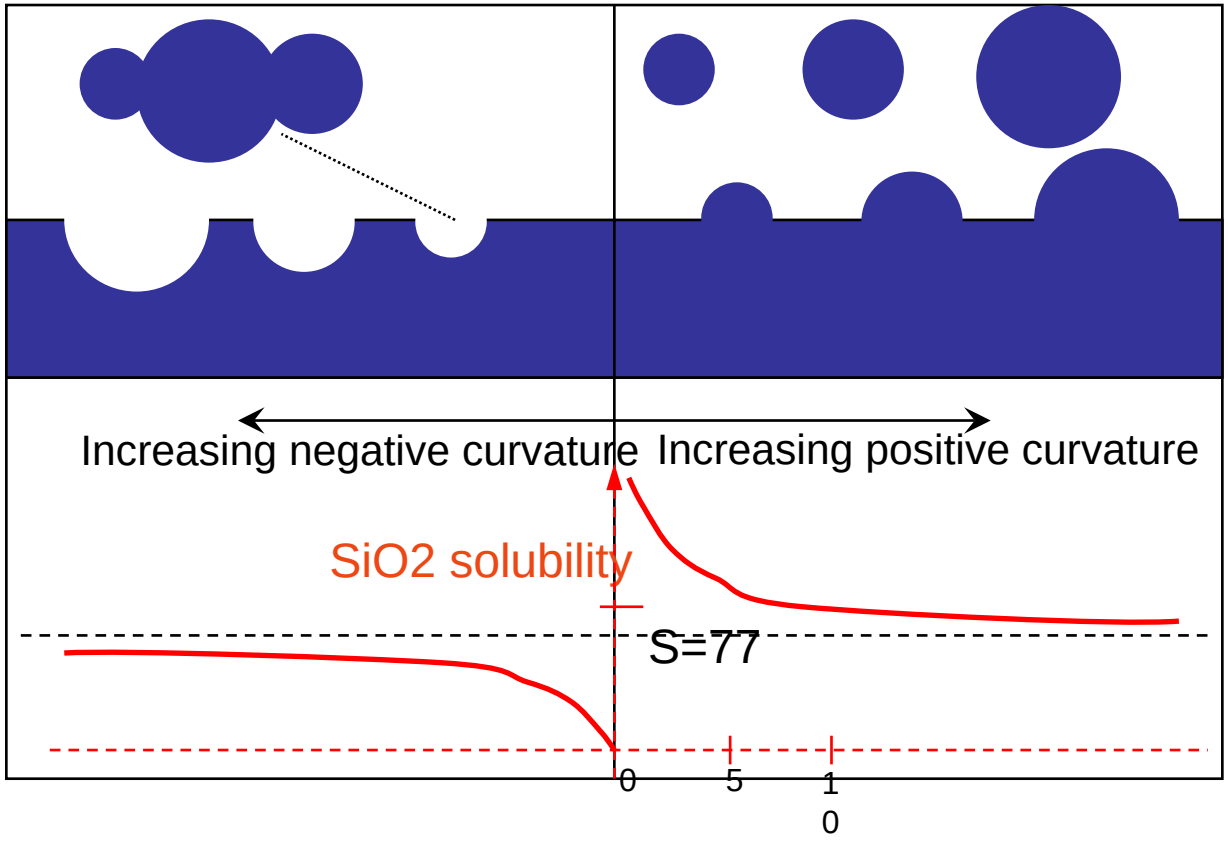

Physical chemistry of surfaces: Ostwald ripening

Occurs when two particles with different radii, assuming R1>>R2 are mixed into a solvent.

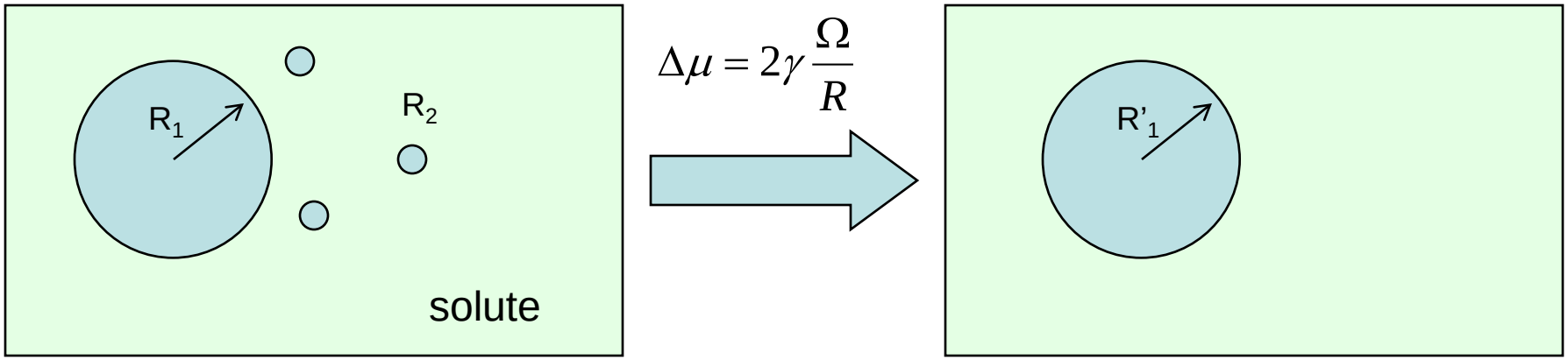

The solubility of the smaller particle is larger than that of the large particle. To maintain the equilibrium, solute deposits onto the surface of the larger particle while the small particle has to continue to dissolve to compensate for amount of solute diffused away. The result is that the small particle gets smaller and the large particle larger.

Ostwald ripening has been used to narrow the size distribution of nano-particles by eliminating small particles. Large particles grow at the expense of smaller particles. The result is the elimination of the smaller particles thus the size distribution of the particles becomes narrower.

Ostwald ripening is temperature sensitive and can be promoted by varying processing temperatures.

Physical chemistry of surfaces: Ostwald ripening

When two particles $R_1 >> R_2$ are in a solvent, each particle develops an equilibrium with the surrounding. The solubility of the smaller particle is larger. So there is a net diffusion of solute from the proximity of a smaller particle to the proximity of the larger particle.

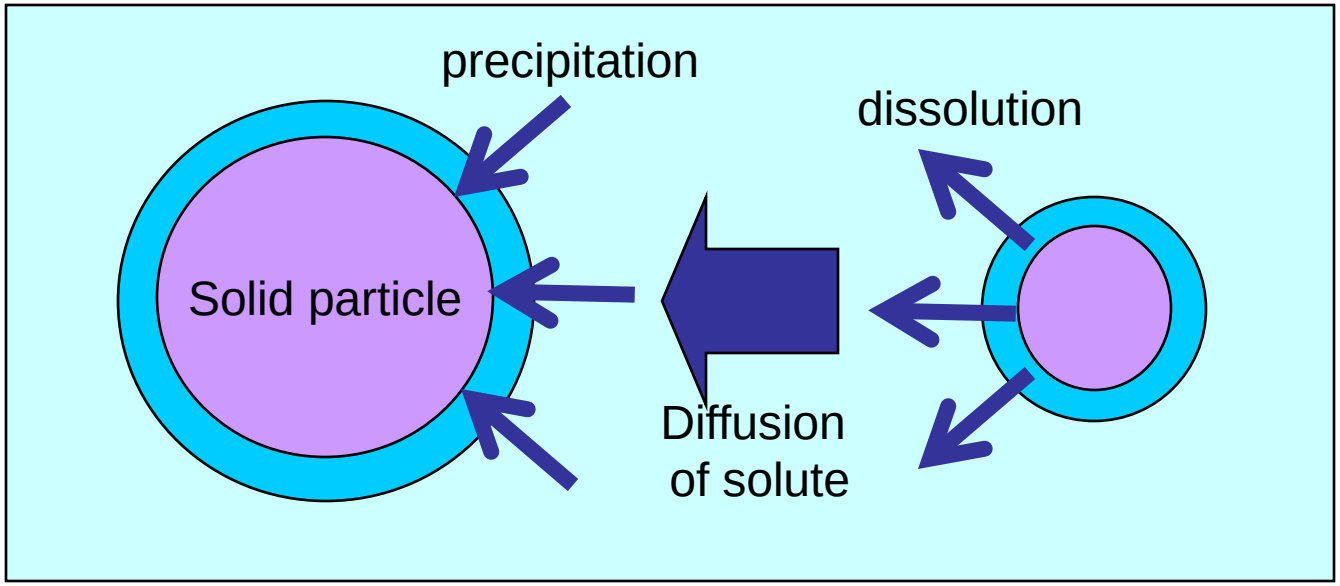

This phenomenon can be considered also as a solid state diffusion or a evaporation/condensation process

In nanostructure fabrication it is imperative to overcome huge surface energy

Fundamentals of homogeneous nucleation – Zero dimensionally confined nanoparticles

For the growth of nanoparticles by homogeneous nucleation, a supersaturation of the growth specie needs to be achieved. This can be achieved by decreasing temperature of an equilibrium mixture. Example: formation of metal dots in a glass matrix by annealing at moderate temperatures.

A supersaturated solution decreases its Gibbs energy by forming a solid phase and maintaining an equilibrium concentration in the rest of the solution. The change of the Gibbs free energy per unit volume depends on the concentration of the solute:

$$\Delta G_v = -\frac{kT}{\Omega}\ln\left(\frac{C}{C_0}\right) = \frac{kT}{\Omega}\ln\left(1+\sigma\right)$$

C_o: equilibrium concentration or solubility
σ: supersaturation $(C-C_o)/C_o$
Ω: atomic volume

When ΔG_v is negative, nucleation occurs spontaneously

Assuming an spherical nucleus with a radius r , the change of the volume energy is

$$\Delta\mu_v = \frac{4}{3}\pi r^3\ \Delta G_v$$

This energy reduction is counterbalanced by the surface energy. The increase in the surface energy is

$$\Delta\mu_s = 4\pi r^2\ \gamma$$

The total change in the Gibbs free energy is $\Delta G = \Delta\mu_v + \Delta\mu_s = \frac{4}{3}\pi r^3\Delta G_v + 4\pi r^2\gamma$

Fundamentals of homogeneous nucleation

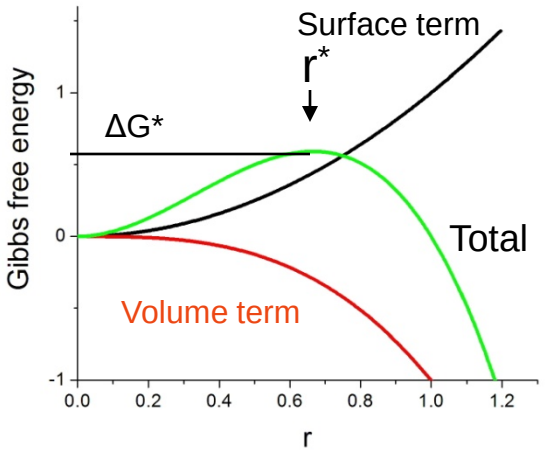

The newly formed nucleus is stable only if the radius exceeds a critical size r* . If r < r* the nucleus will dissolve into the solution to reduce the overall Gibbs free energy.

If r > r* the nucleous is stable and continuous to grow bigger. At the critical size r = r*

$$\frac{d}{dr}(\Delta G) = 0$$

and the critical size r* and critical energy ΔG* are defined by:

$$r^* = -2\frac{\gamma}{\Delta G_v} \qquad \Delta G^* = \frac{16\pi\gamma}{3(\Delta G_v)^2}$$

This is valid for a supersaturated solution, but all the concepts can be generalized for a supersaturated vapor and a supercooled gas or liquid.

In the synthesis of nanoparticles by nucleation this critical size represents a limit. To reduce this limit one needs to increase ΔG_v and reduce the surface energy of the new phase γ. The value of ΔG_v can be increased by increasing the supersaturation σ, which increases with decreasing the temperature.

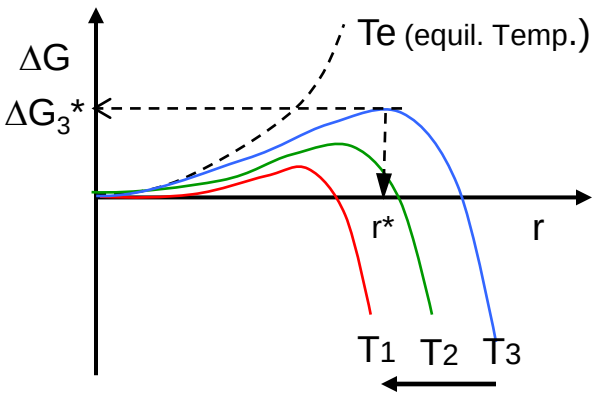

Fundamentals of homogeneous nucleation

The rate of nucleation per unit volume and per unit time R_N is proportional to:

* the probability of a thermodynamic fluctuation of the critical free energy ΔG*

$$P = \exp\left(-\Delta G^* / kT\right)$$

* the number of growth species per unit volume that can be used as nucleation centers (in homogeneous nucleation this is proportional to the concentration).

* the successful jump frequency of growth species from one site to another which is given by $\Gamma = kT / 3\pi\lambda^3\eta$

where λ is the diameter of the growth species and η is the viscosity of the solution.

So the rate of nucleation can be described by

$$R_N = nP\Gamma = \left\{\frac{C_0 kT}{3\pi\lambda^3\eta}\right\}\exp\left(-\frac{\Delta G^*}{kT}\right)$$

Fundamentals of homogeneous nucleation

$$R_N = nP\Gamma = \left\{\frac{C_0 kT}{3\pi\lambda^3\eta}\right\}\exp\left(-\frac{\Delta G^*}{kT}\right)$$

Large number of nuclei are obtained if: high initial concentration, low viscosity and low critical energy barrier

For a given concentration solute a large number of nuclei means smaller sized nuclei

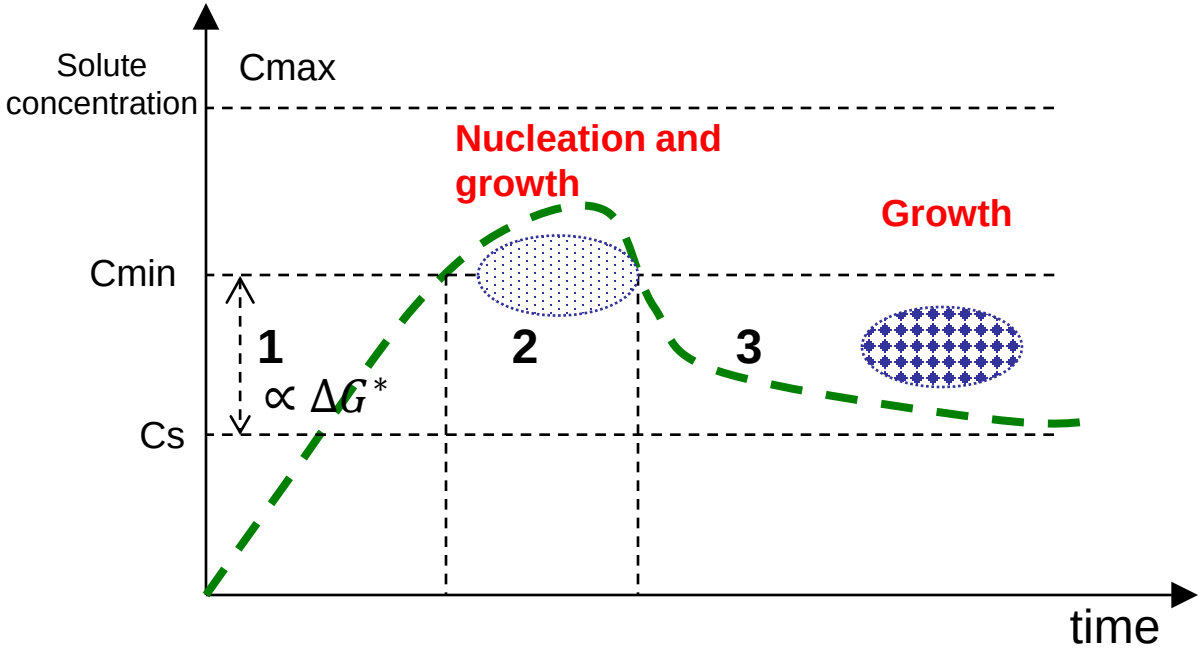

1: when C increases with time no nucleation occurs even above the equilibrium solubility (Cs)

2: when supersaturation reaches a value (Cmin) corresponding to the energy barrier nucleation starts

3: after nucleation the concentration decreases. When concentration decreases below the critical energy nucleation stops and only growth proceeds till the equilibrium concentration

Nuclei growth

The growth process of the nuclei involves several steps:

- generation of growth species
- diffusion of the growth species from the bulk solution to the surface of the growth nuclei
- adsorption of the growth species onto the growth surface
- surface growth due to irreversible incorporation of the growth species onto the solid surface.

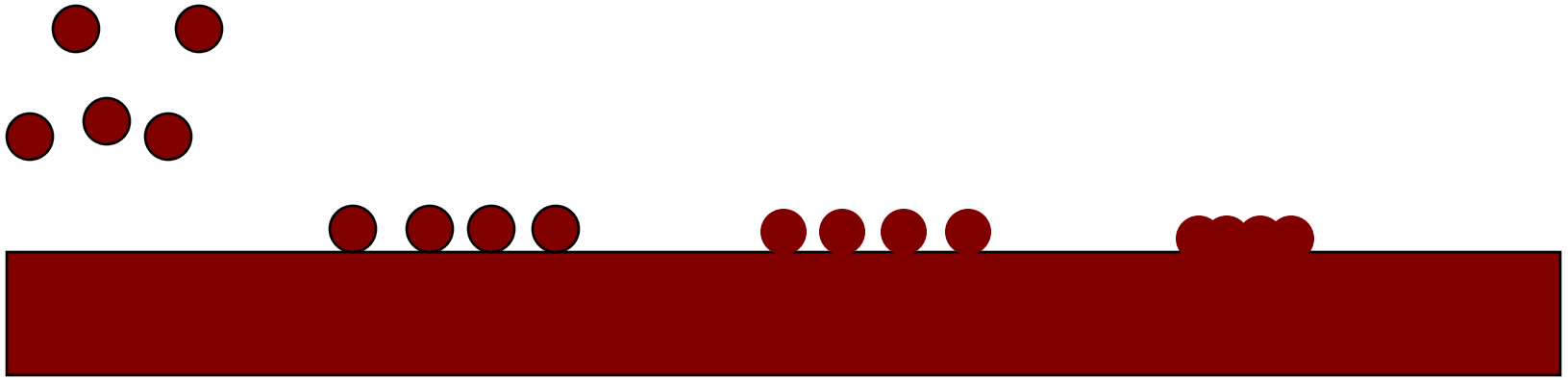

Growth controlled by diffusion

If the concentration of the growth species in the solution (or saturated vapor) reduces below the minimum concentration for nucleation, the nucleation stops however the growth continues.

If this growth is controlled by diffusion the growth rate is given by $dr/dt = D\left(C - C_s\right)\frac{V_m}{r}$

where r is the radius of the spherical nucleus, D is the diffusion coefficient of the growth species, C is the bulk concentration, C_s is the concentration in the surface, V_m the molar volume of the nuclei.

Solving the differential equation, assuming that the concentration in the bulk remains constant:

$$r^2 = 2D\left(C - C_s\right)V_m t + r_0^2 = k_D\, t + r_0^2$$

This indicates that the radius of the particles tends to be equal.

For two particles with an initial radius difference δr_0 the radius difference δr decreases as

$$\delta r = \frac{r_0\ \delta r_0}{r} = \frac{r_0\ \delta r_0}{\sqrt{k_D\, t + r_0^2}}$$

This is: the radius difference decreases with time. The diffusion controlled growth promotes the formation of uniformly sized particles.

Growth controlled by surface process

When the diffusion of the growth species from bulk is sufficiently fast, the concentration of the growth species at the surface is the same as the concentration in the bulk.
In this case the growth process is controlled by surface process. For the surface process there are two possible mechanisms:

1- mononuclear growth
2- polynuclear growth.

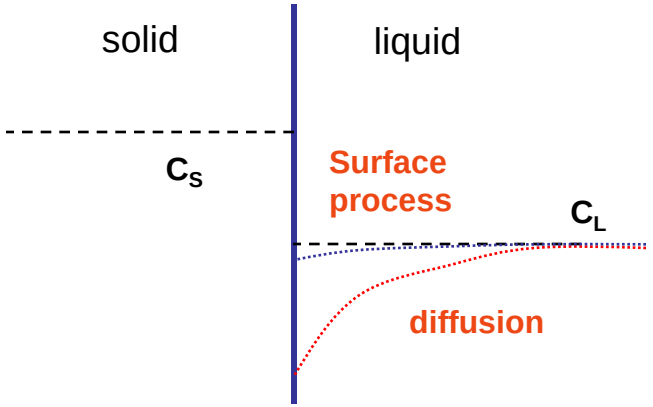

Mononuclear growth

The growth species are incorporated into the layer and proceed to form another layer only after the growth of the previous layer is completed. The growth rate is thus proportional to the area of the growth surface:

$$\frac{dr}{dt} = k_m\, r^2 \longrightarrow \text{Solving} \quad \frac{1}{r} = \frac{1}{r_0} - k_m t$$

The radius difference increases with an increasing radius $\delta r = r^2 \frac{\delta r_0}{r_0^2}$ or $\delta r = \frac{\delta r_0}{\left(1 - k_m r_0\, t\right)^2}$

$k_m r_o t < 1$

This mechanism does not favor the generation of monosized particles.

Growth controlled by surface process

Polynuclear growth

The surface concentration is so high that a second layer starts to grow before the first layer is complete. The growth rate is constant and independent of particle size or time

$$\frac{dr}{dt} = k_p$$

The particles grow linearly with time:

$$r = k_p t + r_0$$

The relative radius difference remains constant regardless of the growth time and the absolute particle size.

As the radius difference remains constant, the particle grows in size and the relative radius difference becomes smaller.

This process leads to the synthesis of monosized particles.

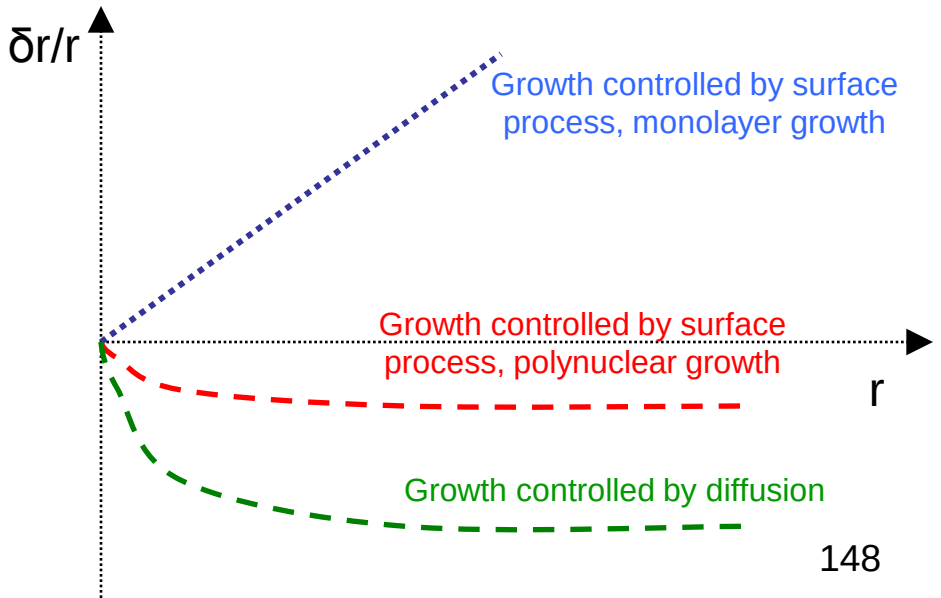

Summary

For the formation of monosized nanoparticles, diffusion-limited growth is desired. This can be achieved by:

A. Keeping the concentration of the growth specie low
B. Increasing the viscosity of solution
C. Introducing a diffusion barrier (monolayer on the surface).
D. Controlling rate of reaction, controls supply of growth species.

Synthesis of metallic nanoparticles

Metallic nanoparticles are synthesized by reduction of metal complexes in dilute solutions to generate colloids solutions. Size of the nanoparticles is controlled by use of low concentration solute and that of a polymeric monolayer that adheres to the surface thus hindering diffusion of growth specie from the solute to the growing particles. This is a diffusion limited process.

Different metallic colloidal dispersion, precursors, reactive agents and other chemicals are used in the growth of metallic nanoparticles.

PRECURSORS: elemental metals, inorganic salts, metal complexes, (Ni, Co, PdCl2)

REACTIVE AGENTS: Sodium Citrate, Hydrogen Peroxide, aqueous methanol, sodium citrate

POLYMERIC STABILIZERS: polyvinyl alcohol,

Gold nanoparticles

Gold nanoparticles are produced in a liquid ("liquid chemical methods") by reduction of chloroauric acid ($H[AuCl_4]$), although more advanced and precise methods do exist. After dissolving $H[AuCl_4]$, the solution is rapidly stirred while a reducing agent is added. This causes Au^{3+} ions to be reduced to neutral gold atoms. As more and more of these gold atoms form, the solution becomes supersaturated, and gold gradually starts to precipitate in the form of sub-nanometer particles. The rest of the gold atoms that form stick to the existing particles, and, if the solution is stirred vigorously enough, the particles will be fairly uniform in size. (Wikipedia)

Faraday in 1857 published a comprehensive study of the preparation of colloidal Au

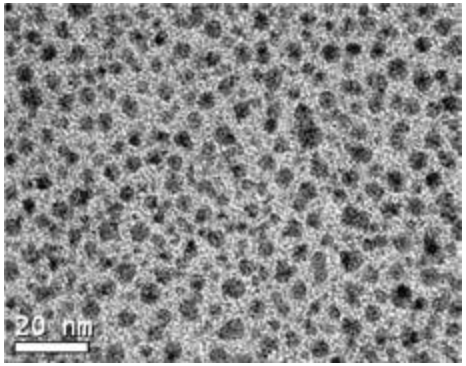

Other types of metal nanoparticles:
Pt, Pd, Ag,

Synthesis of nanoparticles: kinetically confined

Growth termination

This method uses a suitable element to stop or control the growth in size of the nanoparticels. For example particles of CdS can be controlled in size by terminating the growth by capping the surface of the crystallites with thiophenol. The thyophenol attaches to the surface of the growing CdS crystal covering the surface, quenching the chemical reaction and canceling the crystal growth. With this method and a control of the reactants concentrations it is possible to accurately control the size of the nanoparticles that can be as small a 3.5 nm. The characterization of these nanoparticles can be done studying the spectral composition of the photoluminescence.

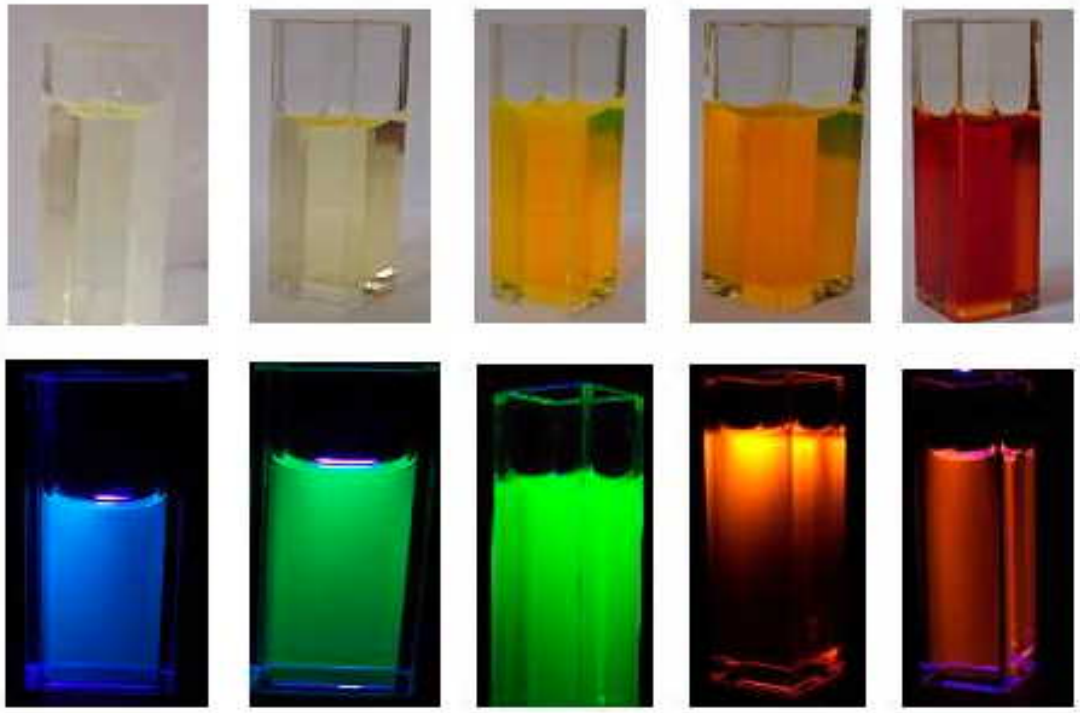

Heterogeneous nucleation

When a new phase is formed on the surface of another material, the process is called heterogeneous nucleation.
Assuming growth in the vapor phase, species impinge on the surface, diffuse and aggregate to form a nucleus.
The total change in the free energy ΔG associated with the formation of this nucleus is given by

$$\Delta G = a_3\, r^3\, \Delta\mu_v + a_1\, r^2\, \gamma_{vf} + a_2\, r^2\, \gamma_{fs} - a_2\, r^2\, \gamma_{sv}$$

r is the mean dimension of the nucleus , $\Delta\mu_v$ is the change in the Gibbs free energy per unit of volume, γ_{vf} , γ_{fs} , γ_{sv} are surface energies and the geometrical constants are

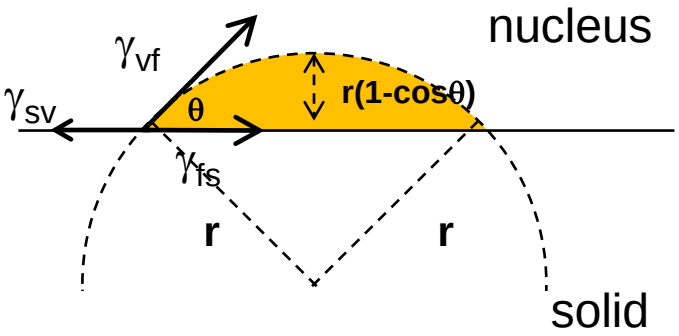

$$a_1 = 2\pi\left(1-\cos\theta\right)$$

$$a_2 = \pi \sin^2\theta$$

$$a_3 = 3\pi\left(2-3\cos\theta+\cos^2\theta\right)$$

The relation between these coefficients is defined by Young's equation $\gamma_{sv} = \gamma_{fs} + \gamma_{vf}\cos\theta$

s: solid, v: vapor, f: fluid or liquid

Heterogeneous nucleation

The formation of a new phase results in a reduction of the Gibbs free energy and an increase in the total surface energy. The nucleus will be stable only when its size is larger than the critical size r* :

$$r^* = -\frac{2\left(a_1\,\gamma_{vf} + a_2\,\gamma_{fs} - a_2\,\gamma_{sv}\right)}{3a_3\,\Delta G_v}$$

and the critical energy barrier ΔG* is given by $\Delta G^* = \frac{4\left(a_1\gamma_{vf} + a_2\gamma_{fs} - a_2\gamma_{sv}\right)^3}{27\,a_3^3\,\Delta G_v}$

Substituting the constants

$$r^* = -\frac{2\,\gamma_{vf}}{\Delta G_v}\left\{\frac{\sin^2\theta\cos\theta + 2\cos\theta - 2}{2 - 3\cos\theta + \cos^3\theta}\right\}$$

$$\Delta G^* = \left\{\frac{16\pi\,\gamma_{vf}}{3\left(\Delta G_v\right)^2}\right\}\left\{\frac{2 - 3\cos\theta + \cos^3\theta}{4}\right\}$$

Wetting factor

Homogeneous nucleation

$$r^* = -2\frac{\gamma}{\Delta G_v}$$

$$\Delta G^* = \frac{16\pi\,\gamma}{3\left(\Delta G_v\right)^2}$$

The first term represents the critical energy barrier while the second term is the wetting factor. When the contact angle θ is 180° the wetting factor equals 1 and the critical energy barrier equals the one obtained in homogeneous nucleation. New phase does not wet on the substrate.
For angles smaller than 180° the energy barrier for heterogeneous nucleation is always smaller than the energy barrier for homogeneous nucleation.
Heterogeneous nucleation is easier than homogeneous nucleation in most cases. When the contact angle is zero, the wetting factor is zero and there is no barrier for the formation of the new phase. This occurs for example when the deposit is the same as the substrate.

Synthesis of nanoparticles

For synthesis of nanoparticles we need nucleation centers. Evaporated metals as Ag and Au tend to form small metal nanoparticles associated with surface defects:

- When edges are the only defects the particles are concentrated only around the edges.
- Nanoparticles grow in other defects as pit holes over the substrate surface.

For example gold clusters were produced by condensing evaporated gold in nanometer-sized preformed pits on the surface of highly oriented pyrolytic graphite (HOPG). The height of the clusters was 6.7 -0.7 nm, the lateral width was 10.1 - 1.9 nm

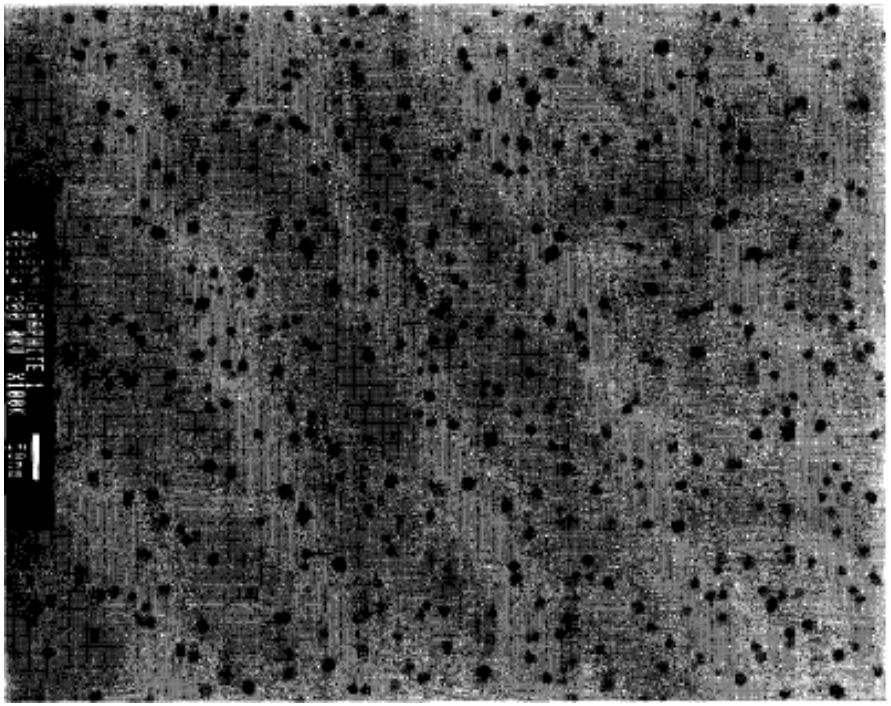

Nanowires and nanorods: Spontaneous Growth

Vapor-Liquid-Solid and Solution-Liquid-Solid growth (VLS and SLS)

In the VLS growth a second phase material, commonly referred as either impurity or catalyst is purposely introduced to direct and confine the crystal growth.
A catalyst forms a liquid droplet by itself or by alloying with growth material during the growth, which acts as a trap of growth species.
Enriched growth species in the catalyst droplets subsequently precipitates at the growth surface resulting in one-directional growth.
The requirements for VLS growth are:

* The catalyst must form a liquid solution with the crystalline material to be grown at the deposition temperature.
* The distribution coefficient of the catalyst must be less than unity at the deposition temperature
* The equilibrium vapor pressure of the catalyst over the liquid droplet must be very small
* The catalyst must be chemically inert
* The wetting characteristics influence the diameter of the nanowire. For a given volume of the droplet , a small wetting angle results in a large growth area and a large diameter nanowire
* For a compound nanowire growth, one of the constituents can serve as the catalyst.
* For a controlled unidirectional growth the solid-liquid interface must be well defined crystallographically.

Nanowires and nanorods: Spontaneous Growth

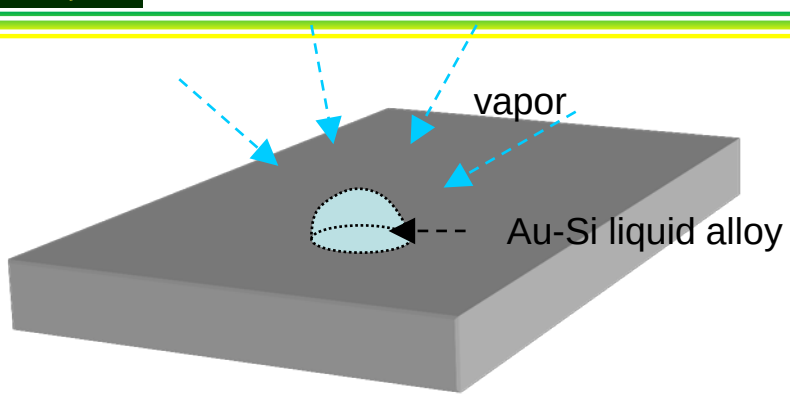

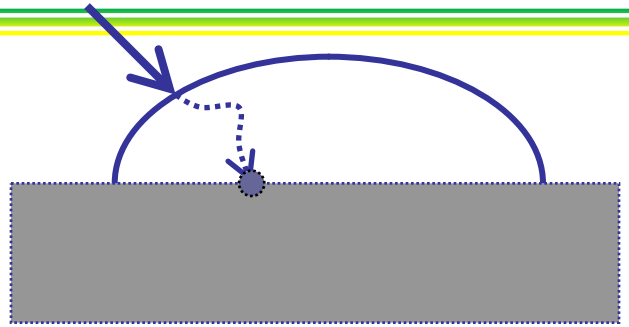

The growth species (Si) is adsorbed in the vapor-liquid interface, incorporated in the liquid, diffuse to the liquid-solid surface and finally incorporated in the solid phase. The material transport is diffusion controlled and occurs essentially under isothermal conditions.

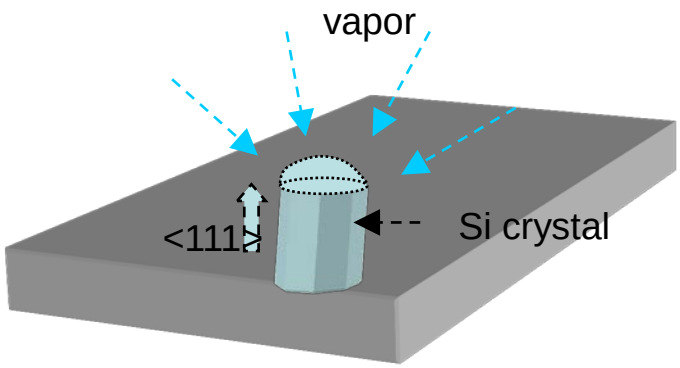

Growth occurs in a preferential crystal orientation

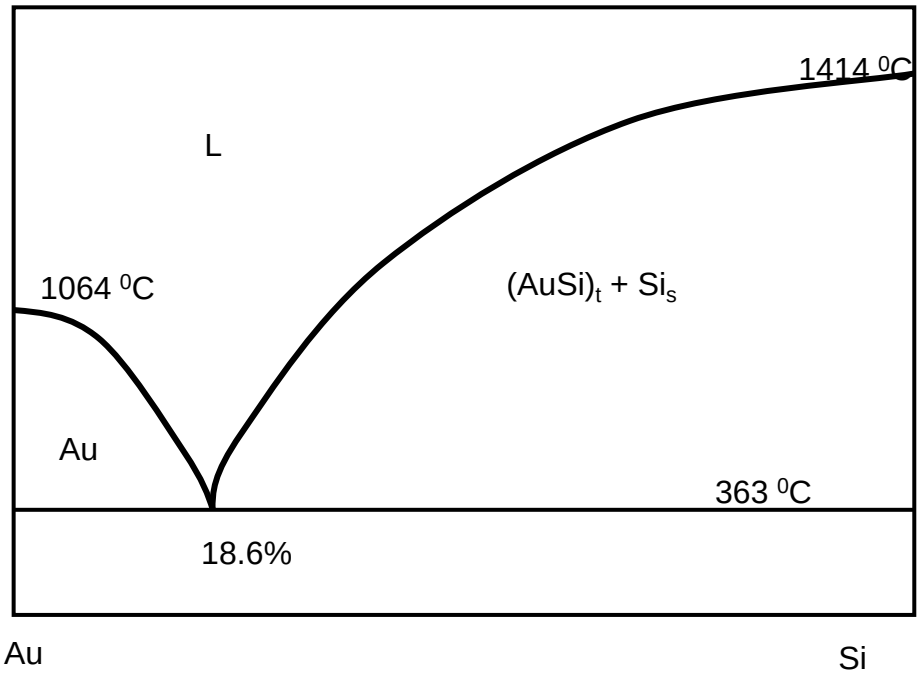

Nanowires and nanorods: Template based synthesis

This method can be used to grow nanorods and nanowires. Various templates with nanometer size channels have been explored for the template growth. The most commonly used are anodized alumina membranes, radiation track etched polymer membranes, nanochannel array glass, radiation track etched mica and mosoporous materials.

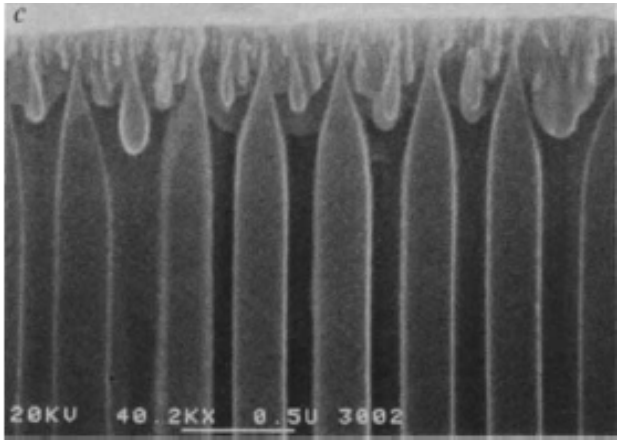

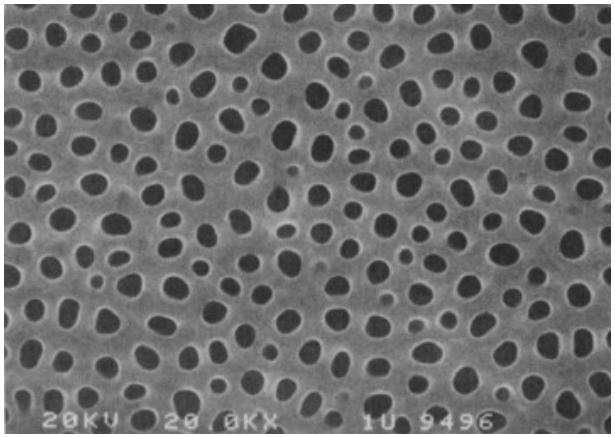

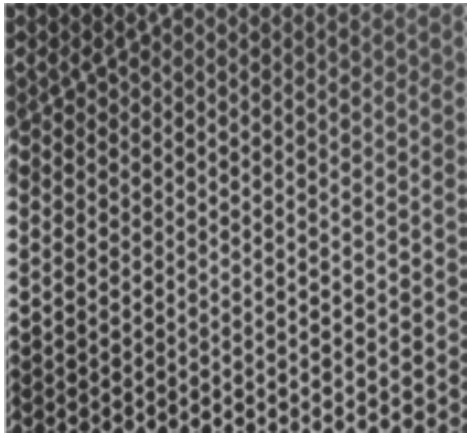

Anodized Al

Glass

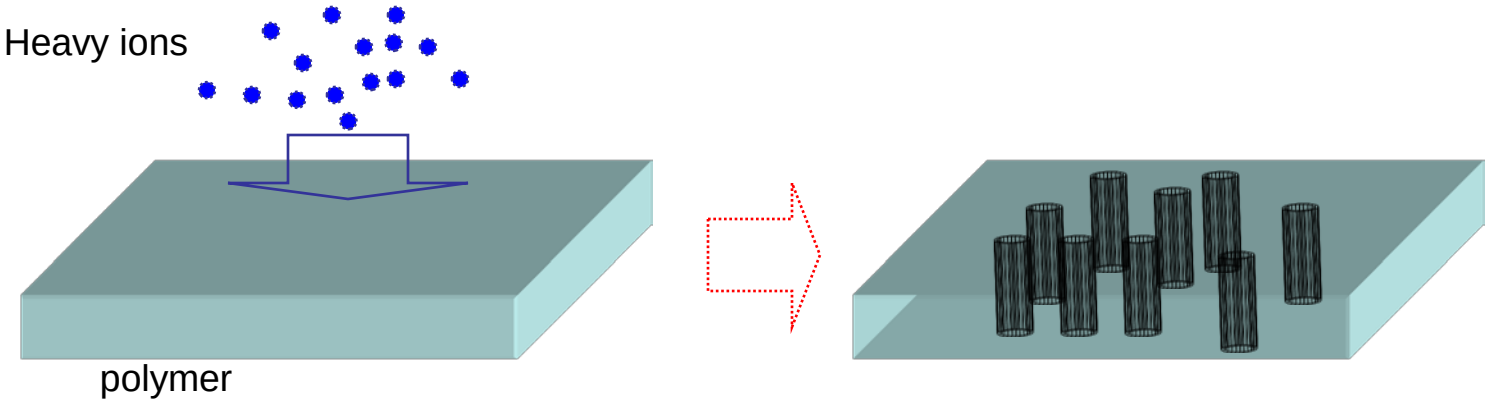

Quantum confined materials

A quantum well is fabricated by depositing very thin layers of different materials. The carriers (electrons or holes) located in the thin crystal will experience a potential well that will keep them confined in a plane allowing only free movement in two dimensions and forcing them to occupy a planar region. Quantum confinement take place when the quantum well thickness becomes comparable at the de Broglie wavelength of the carriers ($\lambda = h/p$)

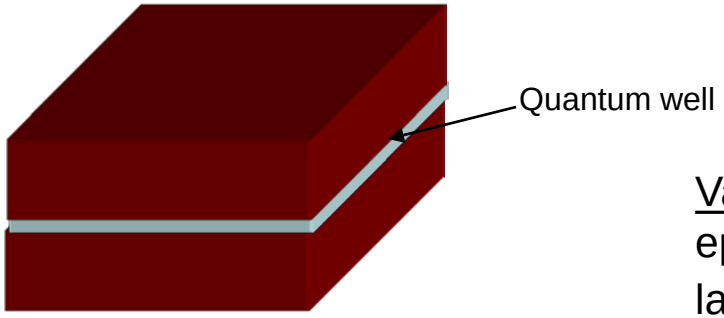

Thin film growth methods can be divided in two main groups:

Vapor-phase deposition: evaporation, molecular beam epitaxy, sputtering, chemical vapor deposition and atomic layer deposition.

Liquid-phase deposition: electrochemical deposition, chemical solution deposition, Langmiur-Blodgett films and self-assembled monolayers

Nucleation modes: Island, layer, island-layer.

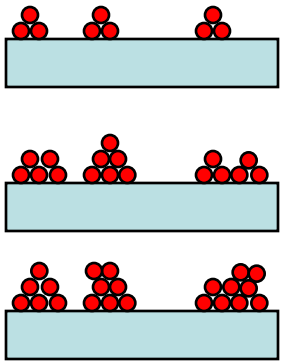

Island

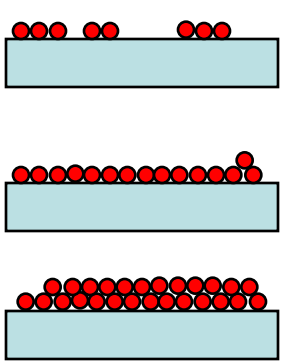

layer

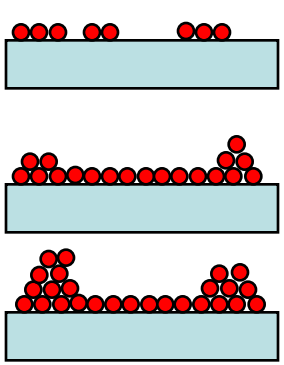

Island-layer

Two dimensional structures: thin films

Nucleation modes: Island, layer, island-layer.

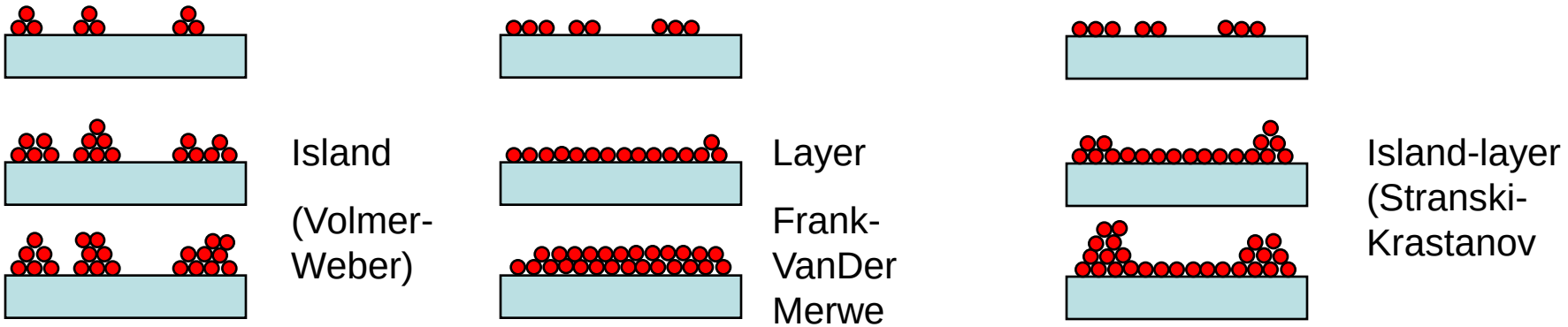

Island growth occurs when the growth species are more bounded to each other than to the substrate. Many metals on insulator substrates, alkali halides, graphite and mica substrates display this type of nucleation during the initial film deposition stages. Subsequent growth generates islands that coalescence to form a continuous film.
Layer growth is the opposite. The growth species are more likely to bound to the substrate than to each other. In this case a first monolayer is formed before the deposition of a second layer. The most important examples of this type of nucleation is the epitaxial growth of single crystal layers.
The island-layer growth is an intermediate situation. Such type of growth usually involves the stress which is developed during the formation of the nuclei or films

$$r^* = \frac{2\pi\,\gamma_{vf}}{\Delta G_v}\left\{\frac{\sin^2\theta\cos\theta + 2\cos\theta - 2}{2 - 3\cos\theta + \cos^3\theta}\right\} \qquad \Delta G^* = \left\{\frac{16\pi\,\gamma_{vf}}{3\left(\Delta G_v\right)^2}\right\}\left\{\frac{2 - 3\cos\theta + \cos^3\theta}{4}\right\}$$

Two dimensional structures: thin films

For island growth the contact angle must be greater than zero. If we look at the Young's equation,

$$\gamma_{sv} = \gamma_{fs} + \gamma_{vf} \cos\theta$$

That means $\gamma_{sv} < \gamma_{fs} + \gamma_{vf}$

If the deposit does not wet the substrate at all or θ = 180°, the nucleation is homogeneous. For layer growth, the deposit wets the substrate completely and the contact angle equals zero; the corresponding Young's equation becomes:

$$\gamma_{sv} = \gamma_{fs} + \gamma_{vf}$$

Single crystal films are grown either by *homoepitaxy* or *heteroepitaxy*
Homoepitaxy is like a simple extension of the substrate. The crystal structure in the deposit and the substrate has no difference and virtually there is no interface. This occurs when the lattice constants of the substrate and deposit are equal or very similar.
If the lattice constants are different, that commonly leads to stress in the deposit that originates the island-layer growth.
When the deposit is elastically strained due to for example lattice mismatch, strain energy is developed. In this case the Gibbs function includes the strain energy per unit volume ω.

$$\Delta G^* = \left\{ \frac{16\pi\ \gamma_{vf}}{3\left(\Delta G_v + \omega\right)^2} \right\} \left\{ \frac{2 - 3\cos\theta + \cos^3\theta}{4} \right\}$$

Since ΔG_v is negative and the sign of ω is positive, the overall barrier to nucleation increases. When the stress exceeds a critical point, and cannot be released, the strain energy per unit area of deposit is large with respect to γ_{vf} permitting nuclei to form above the initial layer deposit. In this case the surface energy of the substrate exceeds the combination of both the surface energy of the deposit and the interfacial energy between the substrate and the deposit.

$$\gamma_{sv} > \gamma_{fs} + \gamma_{vf}$$

Whether the deposit is single crystalline, polycrystalline or amorphous depends on the growth conditions and the substrate. The deposition temperature and the impinging rate of growth species are the two most important factors:

- Growth of single crystal layers requires i) a single crystal substrate, ii) a clean substrate to avoid secondary nucleations, iii) a high growth temperature to assure sufficient mobility of the growth species and iv) low impinging rate to assure a sufficient time for the surface diffusion and incorporation of growth species into the crystal structure and for the structural relaxation before arrival of next growth species.
- Deposition of amorphous films occurs when i) low growth temperature is applied and there is insufficient surface mobility and/or ii) when the influx of growing species is very high and the growth species does not have time to find growth sites.
- Polycrystalline films fall in between these two situations. In general the temperature is high to assure a good mobility and the influx of deposit is large.

Two dimensional structures: thin films

Epitaxy is a process that refers to the formation or growth of single crystals on top of single crystals substrates. Epitaxy growth can be divided into homoepitaxy and heteroepitaxy.

The lattice mismatch is also called misfit and it is given by $$f = \frac{a_s - a_f}{a_f}$$

If f > 0 the film is strained in tension whereas if f < 0 the film is strained in compression.

Strain energy develops in strained films

$$E_s = 2\,\mu_f \left(\frac{1+\nu}{1-\nu}\right) \varepsilon^2\, h\, A$$

μ_f: sheer modulus of film
ν: Poisson's ratio
ε: in-plane or lateral strain
h: film thickness
A: area

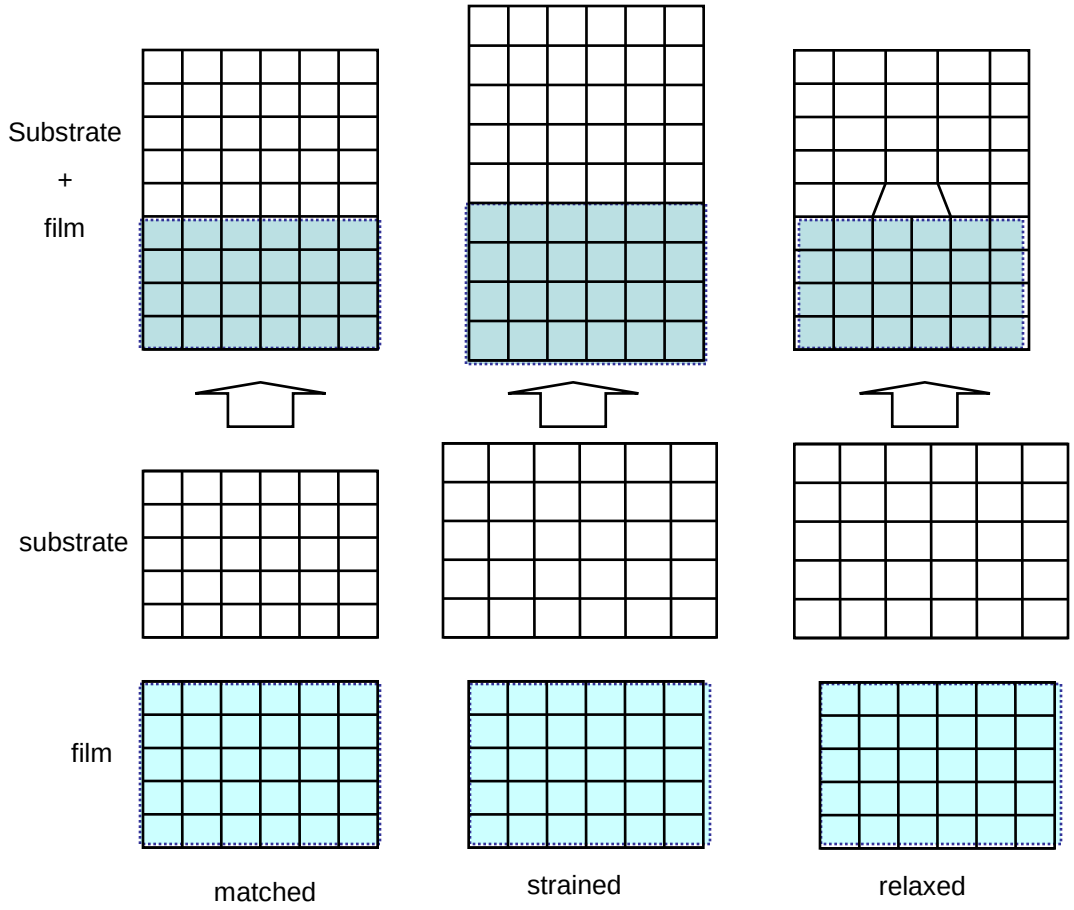

Two dimensional structures: Physical vapor deposition

Evaporation

Consists of an evaporation source that vaporizes the desired material and a substrate located at an appropriate distance. The concentration of the growth species can be controlled changing the source temperature (T) and the flux of the carrier gas. The equilibrium vapor pressure can be estimated as:

$$\ln P_e = -\frac{\Delta H_e}{R_g T} + C$$

ΔH_e: molar heat of evaporation

Evaporation of compounds is more complicated as they can undergo chemical reactions, such as pyrolysis, decomposition and association, and frequently the vapor composition differs from the composition of the source material. The rate of evaporation Φ_e depends on the material in question

$$\Phi_e = \alpha_e N_A (P_e - P_h) / \sqrt{2\pi m R_g T}$$

α_e: coefficient of evaporation
Pe: vapor pressure in Torr
Ph: hydrostatic pressure acting on the source
m: molecular weight

Different elements can evaporate differently and that will deplete the abundance of this element in the source. As a consequence that can change the vapor composition and change the composition of the film for different thickness.

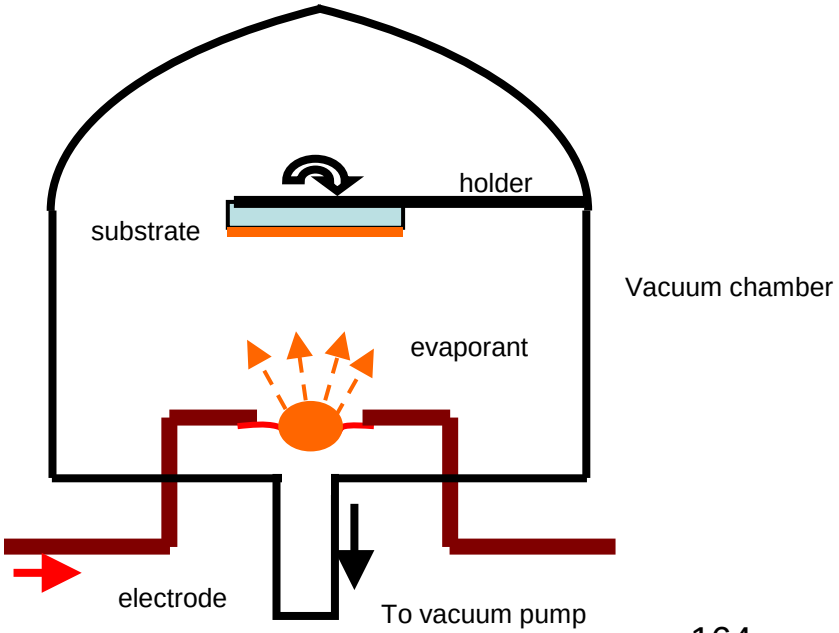

Two dimensional structures: Molecular beam epitaxy (MBE)

MBE can be considered as a special case of evaporation for single crystal film growth with highly controlled evaporation rates in ultra low vapor pressures, 10^{-10} to 10^{-11} torr.

The individual evaporation source allows a good control of the chemical composition of the film. The slow deposition rate allows a long diffusion time and minimizes crystal defects.

- A low growth temperature that limits the diffusion and maintain abrupt interfaces, which are important in the fabrication of quantum wells.
- A slow growth rate that ensures a well controlled two dimensional growth at a typical growth rate of 1 micron per hour
- A simple growth mechanism that ensures a better understanding of the layer, due to the individual control of the independent sources
- A variety of in situ analysis capabilities that gives valuable information of the growth process

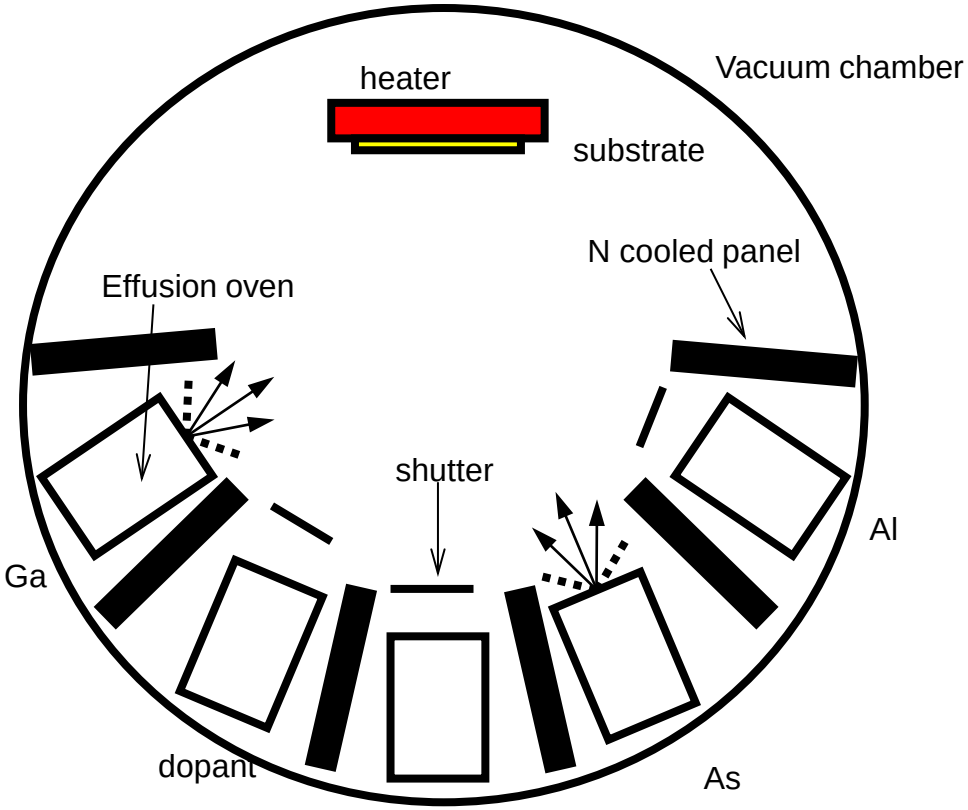

Two dimensional structures: Sputtering

Sputtering uses energetic ions to knock atoms or molecules out from a target that acts as one electrode and consequently deposit these atoms/molecules on the other electrode. The ions impinging the surface of the target are knock out the bulk material and deposited in a substrate located nearby. The target is the cathode of the discharge.

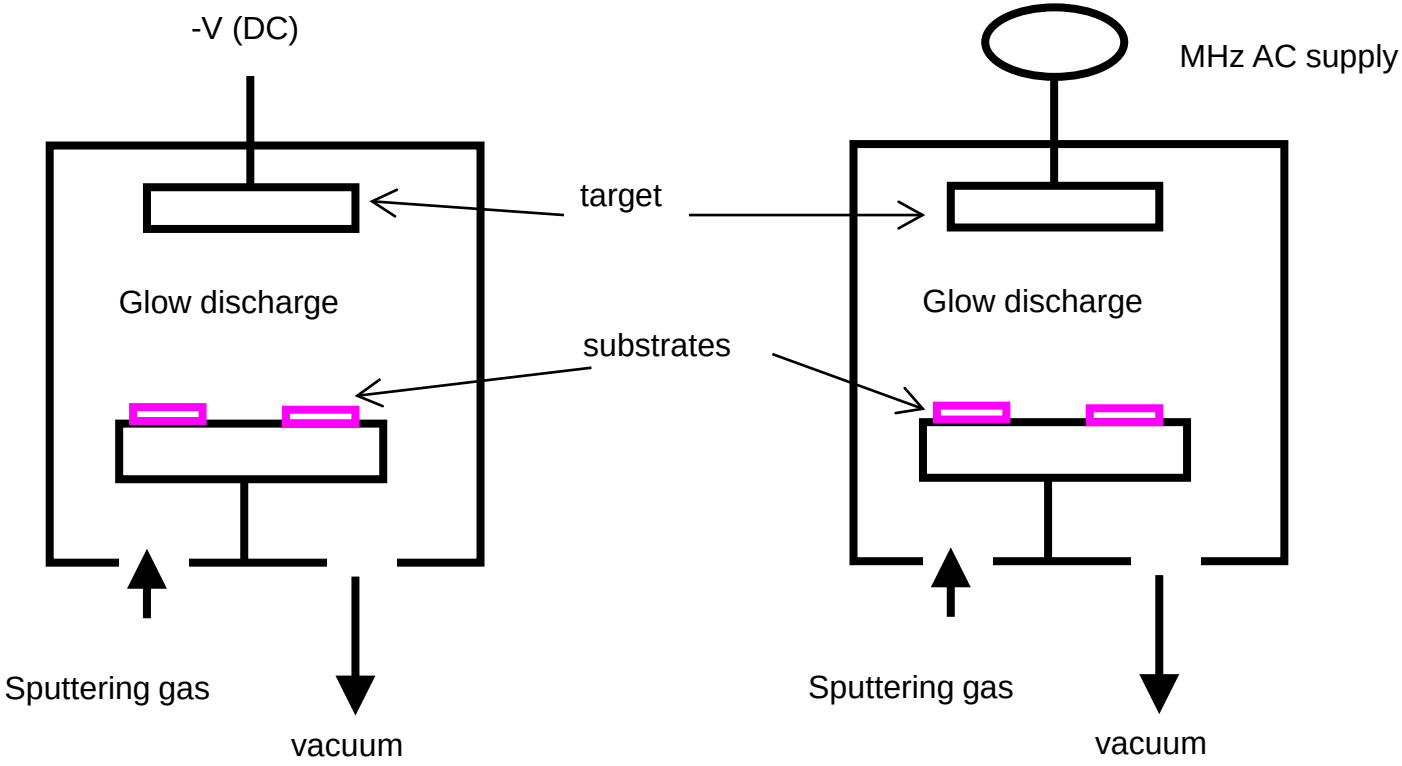

Dual Ion Beam Sputtering (DIBS) with gridded sources

- DIBS coatings have the highest density of all deposition methods
- Most robust in terms of temperature and environment stability

- **State-of-the art 2002 Veeco Ion Beam deposition system uses assist source to improve film morphology and minimize loss**
- **Additional RF reactive oxygen source**

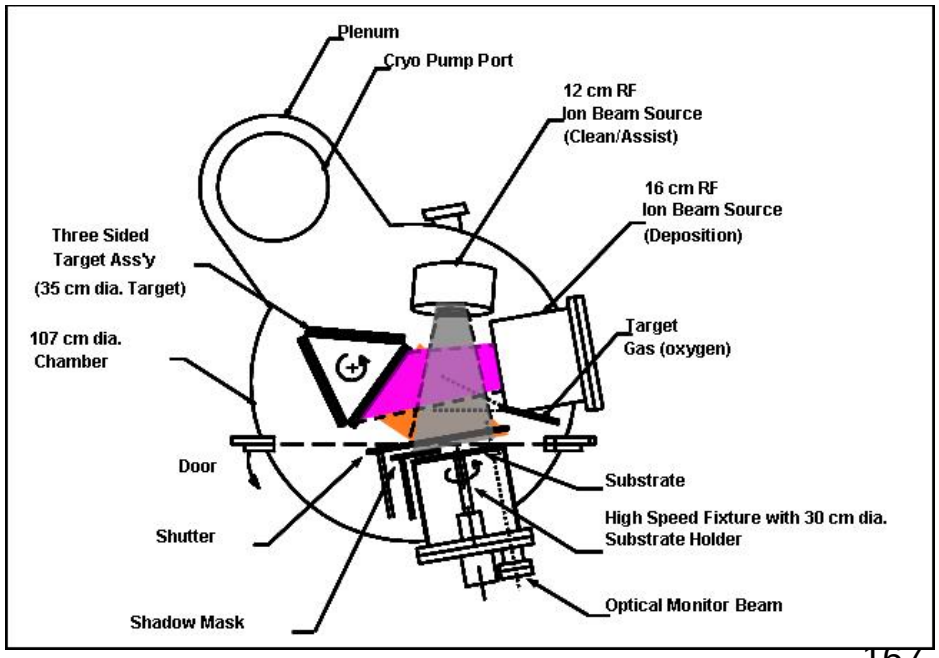

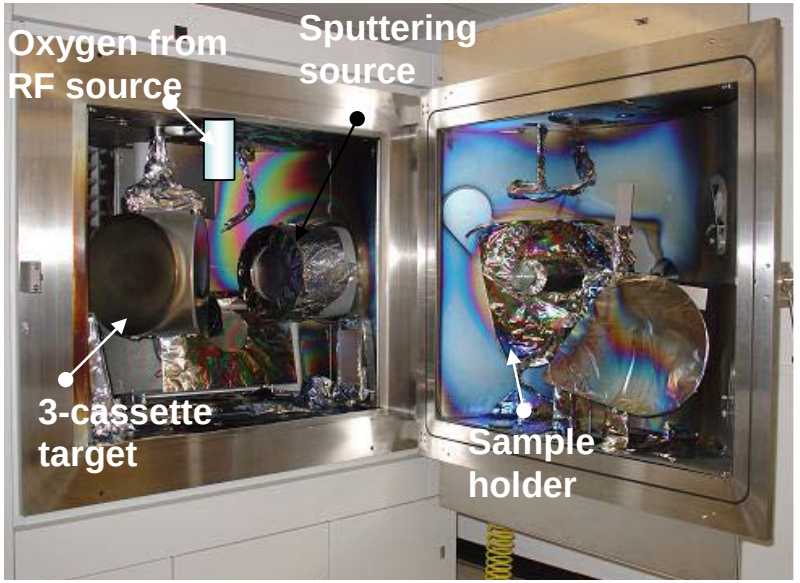

In all of these deposition methods, the mean free path (λ_{mfp}) of the atoms and molecules is a function of the pressure P of the deposition

$$\lambda_{mfp} = \frac{510^{-3}}{P}$$

At low pressures, collisions occur with the walls of the deposition chamber and there are no collisions among molecules

The number of gas molecules that strike a surface per unit area per unit time is:

$$\Phi = 3.513\ 10^{22}\ \frac{P}{(MT)^{1/2}}$$

P is the pressure in Torr, M is the molecular weight, T is the temperature

Two dimensional structures: Chemical vapor deposition (CVD)

CVD is the process that uses a chemically reacting volatile compound of a material to be deposit, mixed with other gases to produce a non-volatile solid that deposits atomistically on the surface of a substrate.

There are many possible reactions and the chemistry is the most important component of this method. Gas phase and surface reactions are intrinsically mixed in this method. The wide range of possible reactions can be grouped into pyrolysis, reduction, oxidation and compound formation

- Metal organic compounds are used as precursors: MOCVD
- Plasma is used to enhance the reaction is called PECVD
- Low pressure CVD (LPCVD)
- Laser enhanced CVD (LECVD)
- Aerosol assisted CVD (AACVD).

Pyrolysis or thermal decomposition

$$SiH_4(g) \rightarrow Si(s) + 2H_2(g) \qquad at\ \ 650^oC$$

$$Ni(CO)_4(g) \rightarrow Ni(s) + 4CO(g) \qquad at\ \ 180^oC$$

Reduction

$$SiCl_4(g) + 2H_2(g) \rightarrow Si(s) + 4HCl(g) \qquad at\ \ 1200^oC$$

$$WF_6 + 3H_2(g) \rightarrow W(s) + 6HF(g) \qquad at\ \ 300^oC$$

Two dimensional structures: Atomic layer deposition

Atomic layer deposition is self limited growth Atomic layer deposition (ALD) is also called atomic layer epitaxy (ALE), atomic layer growth (ALG) atomic layer CVD (ALCVD) and molecular layer epitaxy (MLE).

Can be considered as a modification of the CVD.

- The surface of the substrate is first activated by a chemical reaction.
- When precursor molecules are introduced into the deposition chamber they react only with the activated surface of the substrate and form chemical bonds in the surface.
- The precursors will not react with each other.
- In a second activation reaction, the newly formed surface is activated by other surface reaction and a new layer of equal or different precursor atoms can be added.

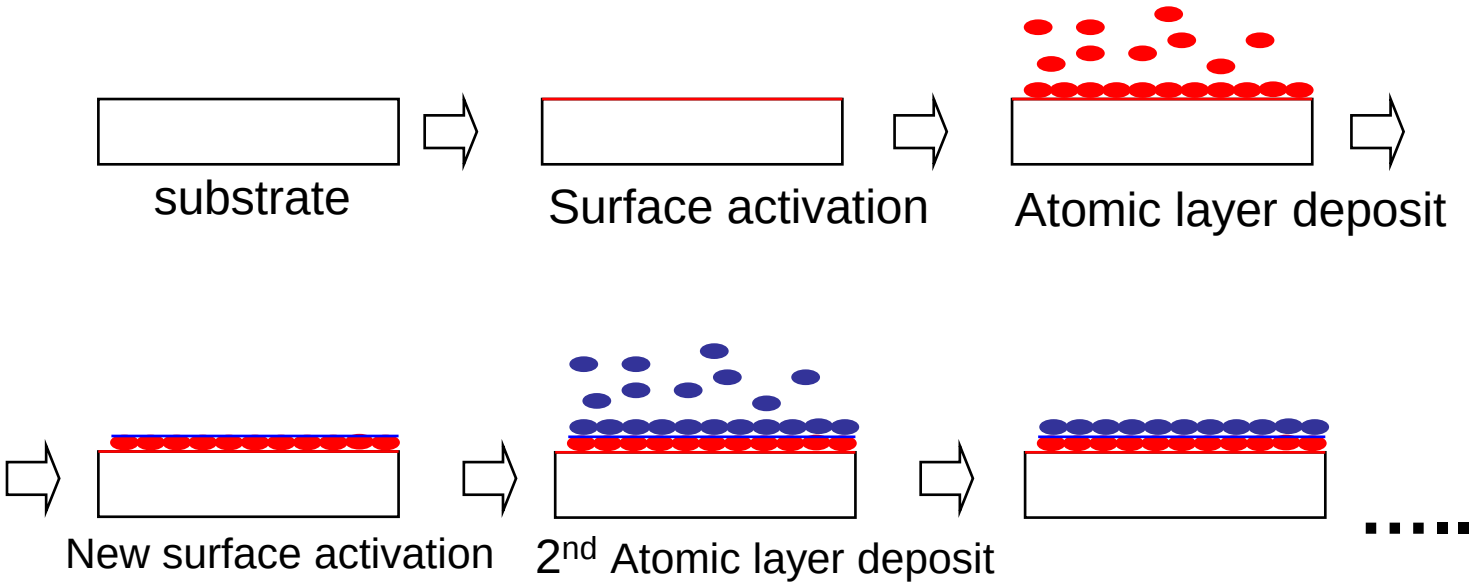

Nanolithography and nanopatterning

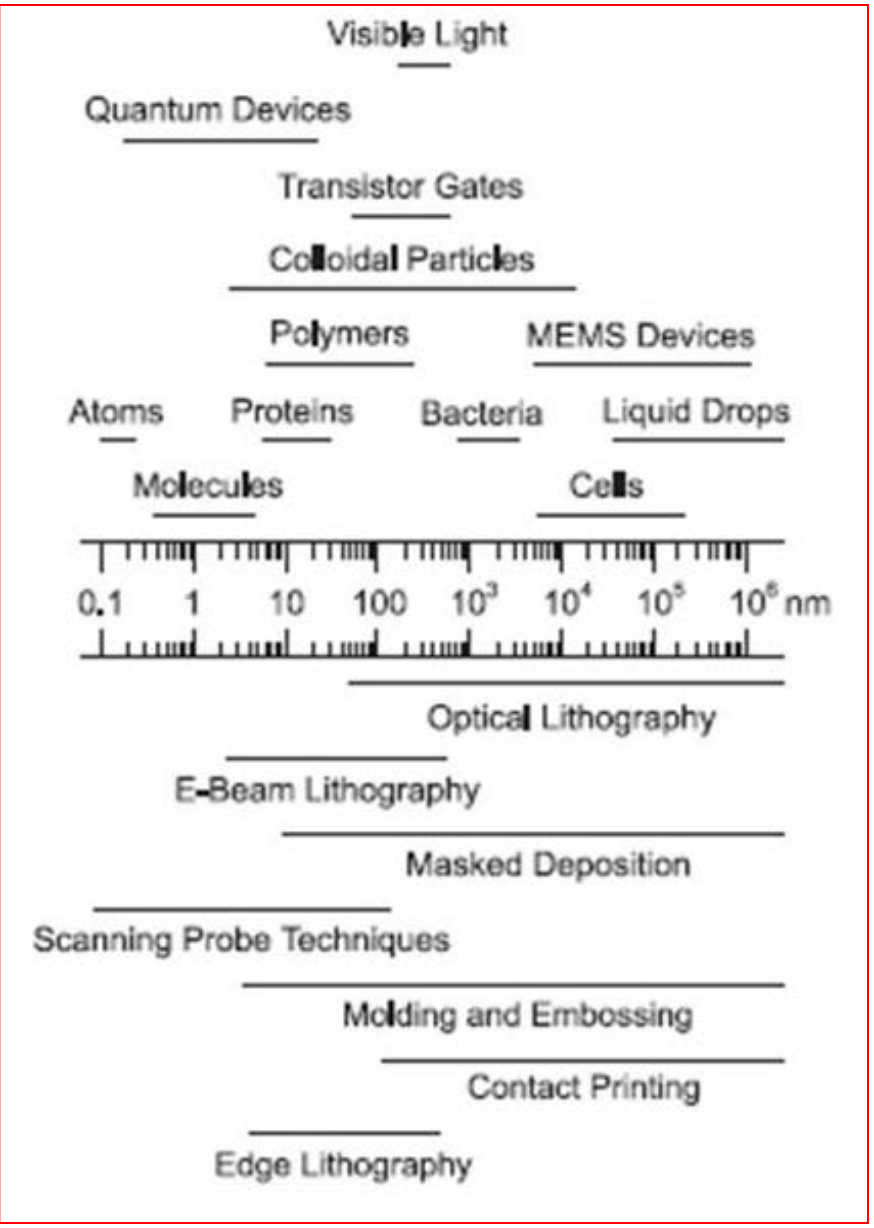

Modify the surface of a material by patterning the surface:

- in the fabrication of integrated circuits (IC),
- information storage devices
- fabrication of micro-electromechanical systems (MEMS)
- sensors
- nano and microfluidic devices
- biochips
- photonics

Depending on the application the nanopatterning technique can vary and many times different techniques must be applied in series to achieve the required final product.

One critical parameter is the **minimum feature size** that determines the particular capability of the chosen technique to print nanometer size devices.

Nanolithography and nanopatterning

Photolithography is probably the most well established technique. It is the main technology used by the microelectronics industry. Other approaches:

•“direct writing” on a surface (with or without the addition of material).

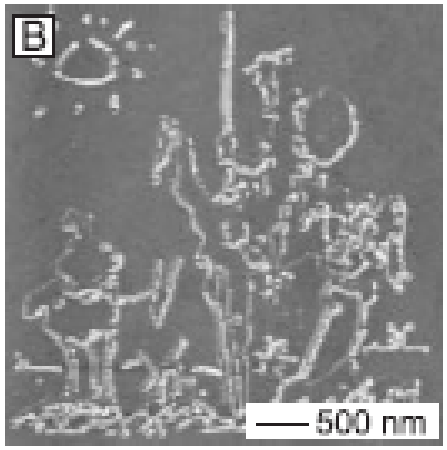

stylus

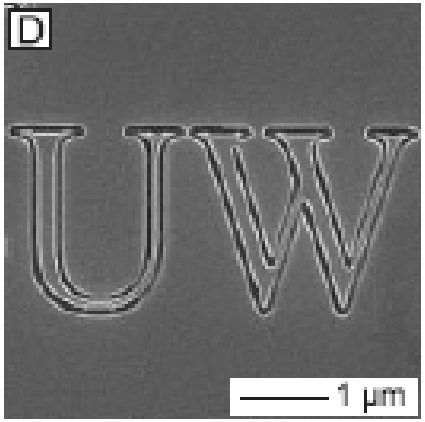

E beam writing

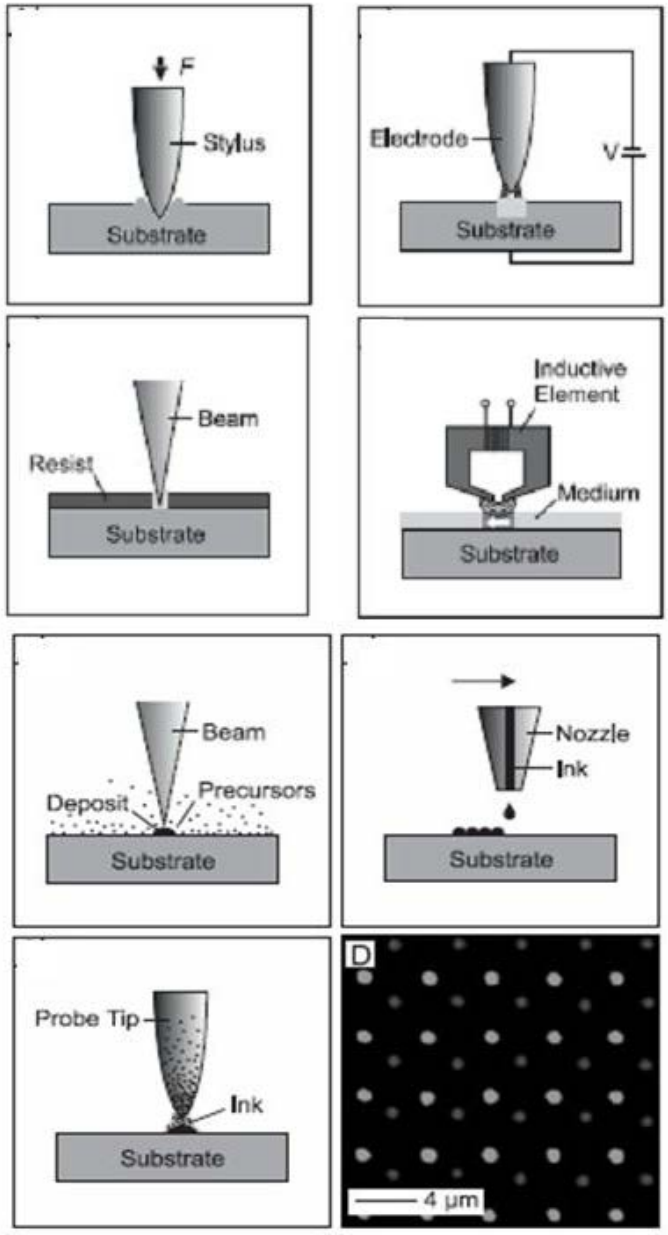

Photo-lithography was the driver in the microelectronics industry to maintain the Moore's Law. An empirical observation made in 1965 by Gordon E. Moore: "number of transistors on an integrated circuit doubles every 24 months."
Photo-lithography refers to the technique that allows to define patterns in a surface at ever decreasing length scales.

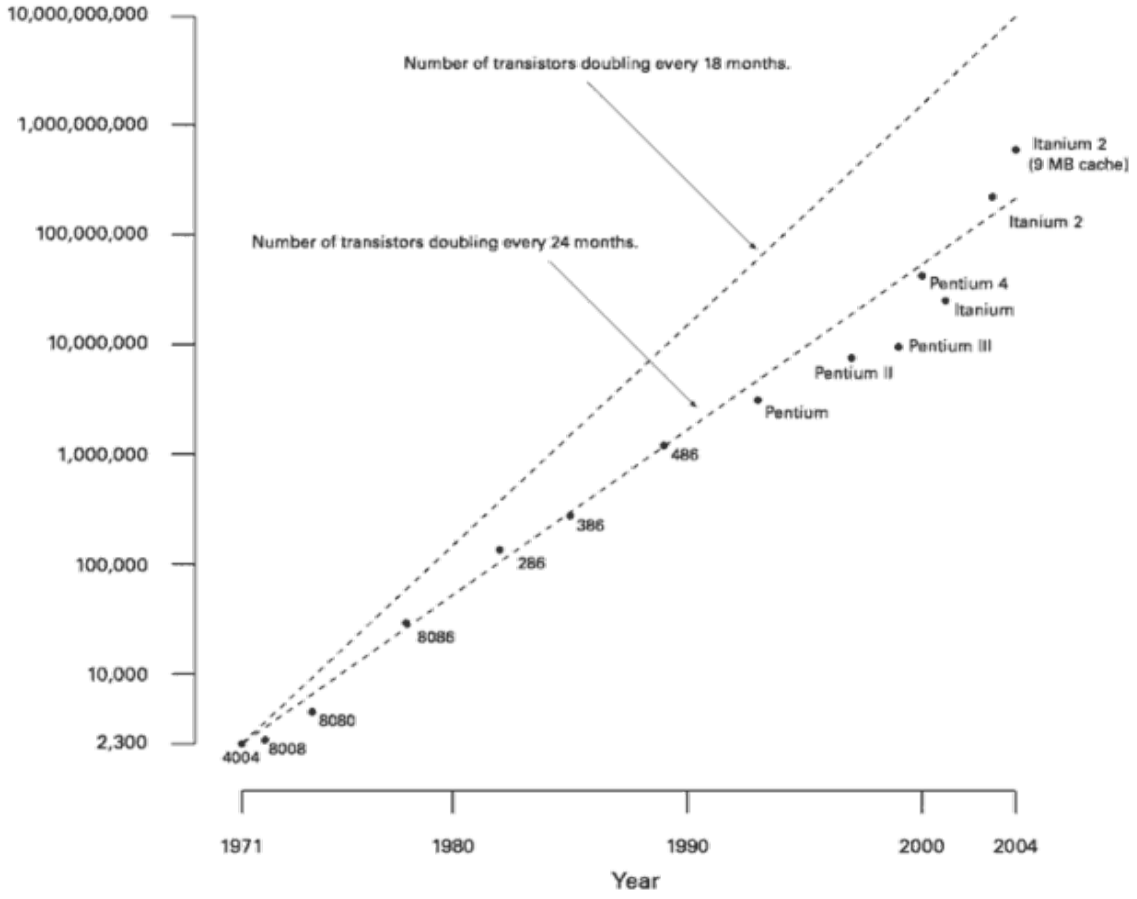

Nanolithography and nanopatterning

The most prevalent approach employs the exposure of resist materials which are most usually polymeric by energetic photons and particles. (Top Down)

The exposed areas undergo structural or chemical modification such that they will have a differential solubility in the “developing” solution with respect to the unexposed areas.

The exposed regions may reduce or increase the solubility and that is referred as “negative “ and “positive” resists.

This layer of resist applied on the surface of sample will cover specific regions that will be “protected” in the further processing of the sample for example by chemical etching, or other processing techniques to fabricate surface structures with the size determined by the initial lithographic step.

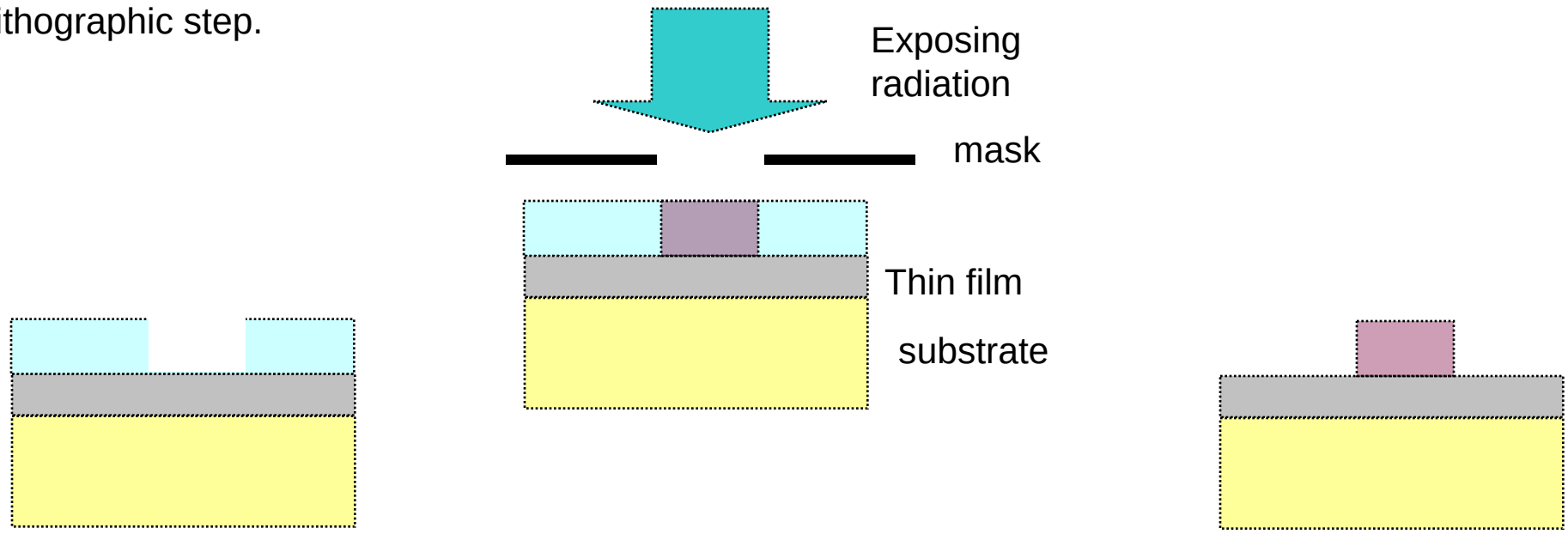

Nanolithography and nanopatterning

Resist materials for lithography must combine a number of optical, chemical, mechanical and process properties in order to be useful.

* They must be able to form high resolution images. This requires that the response of the resist to the exposed radiation/particle beam be highly non linear or that it has "high contrast". Typical contrast values ranges from γ =2 for old conventional resists as PMMA to γ = 15 for last generation resists as UV-6, commonly used in IC manufacturing.

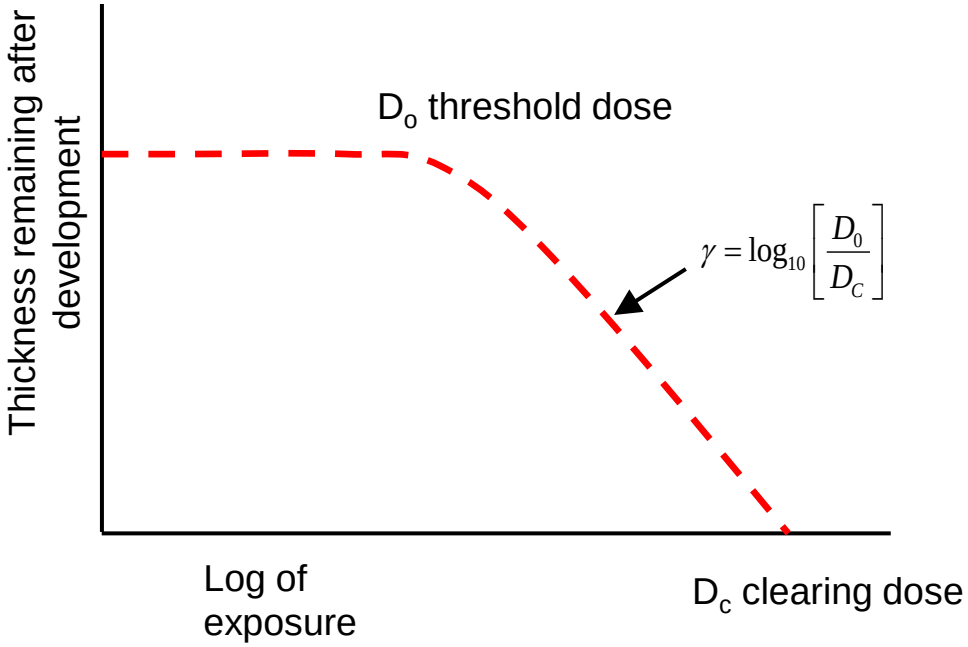

- Resists must have the necessary mechanical properties to be useful in the subsequent processing of the sample. Considering its chemical characteristics, resists can be characterized in two categories: conventional and chemically amplified.

Nanolithography and nanopatterning

Conventional photoresists: the energy of the radiation in the exposure directly converts into a chemical reaction in the resist.
Amplified: an intermediate catalytic process happens prior to development.

Polymethylmethacrylate (PMMA) is a positive tone resist that can be activated with UV light, X-rays, electrons or ions. Molecular weights form 500kDa to 1000 kDa with slightly different properties, has low contrast $\gamma < 3$.
In IC fabrication, the most common used resist is diazonapthoquinones (DNQ). It uses a resin mixed with a photoactive compound. Upon exposure the compound is converted to soluble acid allowing the exposed areas to be removed in the development. Typical exposure doses are in the range of 0.1 J cm^{-2}. This resist presents a moderate contrast $\gamma = 6$.

Chemical amplified resists also use a polymer backbone. A photo-acid compound added changes to an acid after irradiation. Also in the polymer a dissolution inhibitor is added. The acid generated in the exposure reacts with the dissolution inhibitors groups and makes the polymer soluble in the developing solution. The acid acts as a catalytic agent so that the polymer is rendered soluble and the acid is free to move to other locations in the polymer backbone rendering soluble other sites in the polymer chain. In this way the acid compound can react with many sites (up to 100) in the polymer chain and an amplified effect is obtained. Using these resists the dose can be reduced to 5 mJ cm^{-2}.

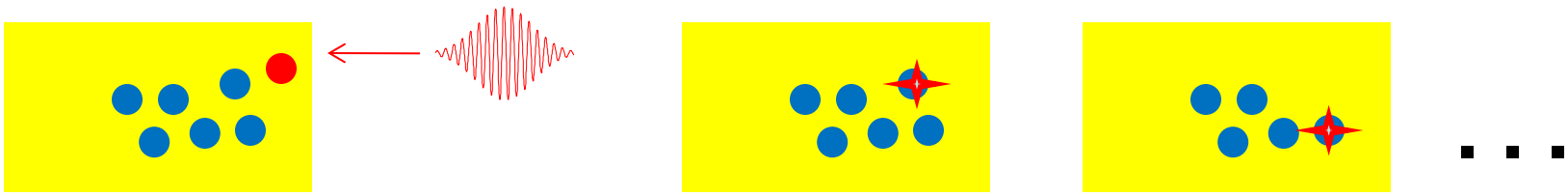

Contact and proximity photolithography

In contact photolithography the mask is located in contact with the photoresist. This method allows very good resolution but has few main complications.

•After exposure the mask should be separated from the photoresist and in this process defects can be produced in the printed pattern.

•Also part residues of the resist can remain in the surface of the mask that has to be cleaned after each exposure with the consequent probably degradation of the mask quality.

•These residues of dust particles can be attached to the mask surface not allowing a perfect contact between the mask and the photoresist and consequently degrading the printing.

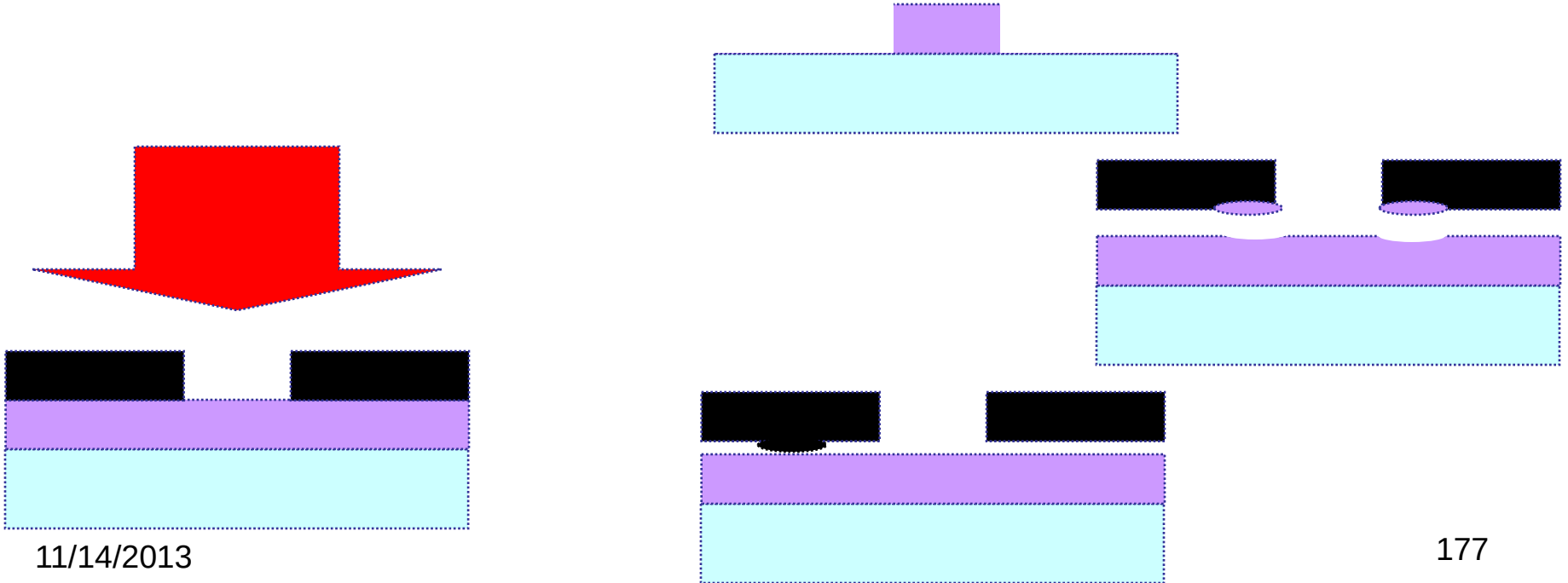

Photolithography

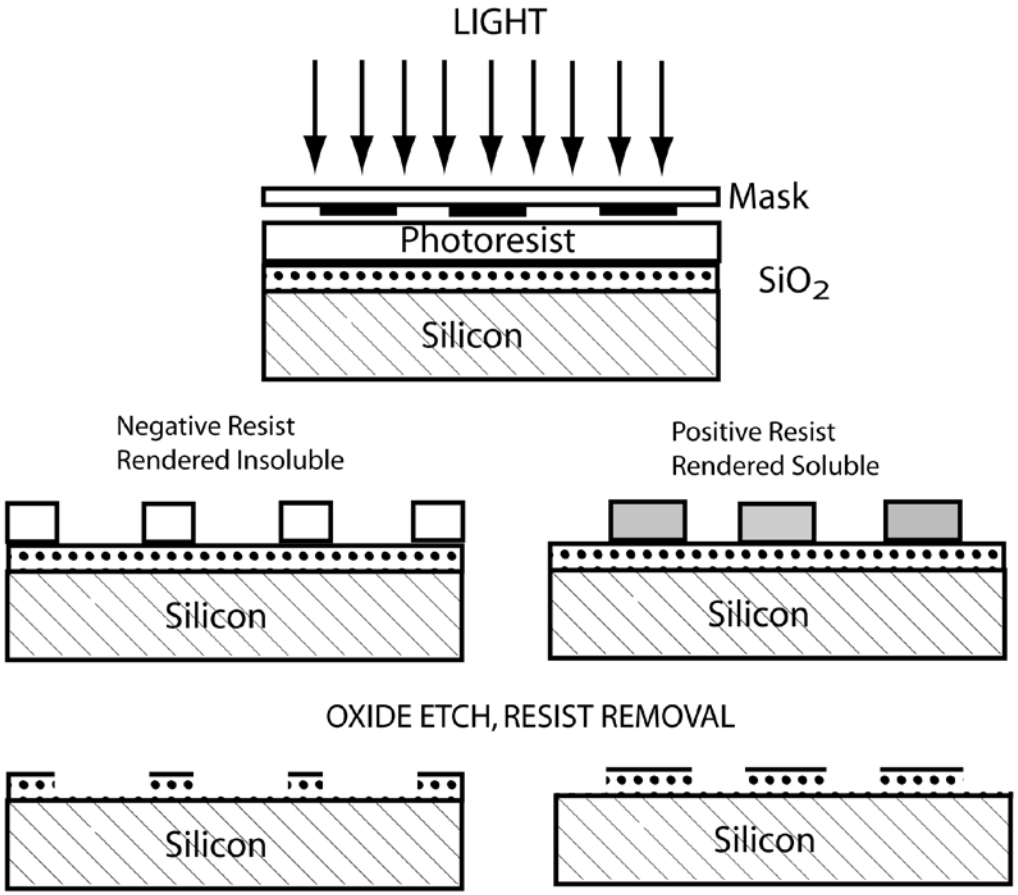

Steps in device fabrications

- Oxidation
- Masking
- Implantation
- Etching
- Metalization
- Lift-off

$$r = \frac{\lambda}{2NA}$$

Photon based nanolithography

Proximity printing: A small gap between the mask and the sample is left. This small gap reduces the problems that generate dust and contaminants in contact photolithography.

The resolution achievable is limited by diffraction of the light in the features of the mask. In this case diffraction patterns are considered as near field diffraction or Fresnel diffraction. The minimum printable feature size is

$$W_{\min} \approx \sqrt{\lambda\, g}$$

g: gap distance

Projection photolithography

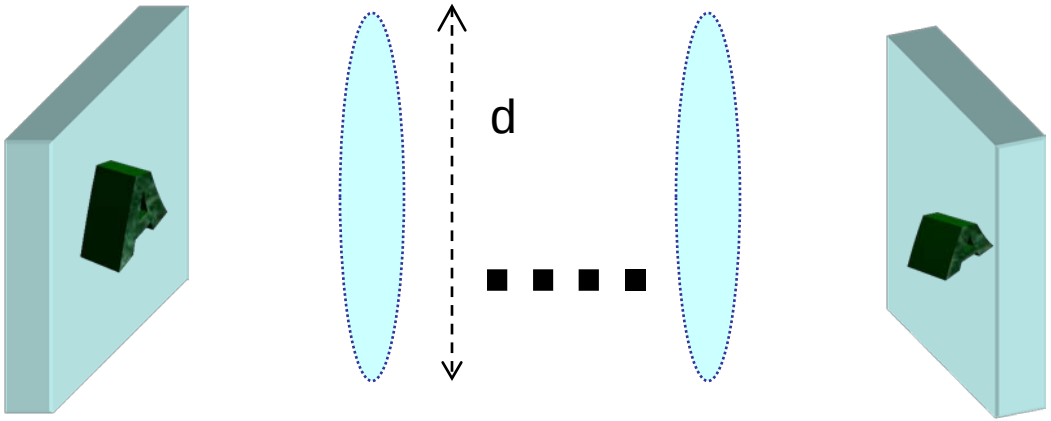

The image resolution is limited by diffraction but in this case the image plane is far away from the masks. The far field or Fraunhoffer diffraction models apply in this case. The resolution the simple analysis that is used is Rayleigh criterion is

$$D = 1.22\ \frac{\lambda f}{d}$$

$$R = 1.22\ \frac{\lambda f}{d} = 1.22\ \frac{\lambda f}{2 f \sin\alpha} = 0.61 \frac{\lambda}{\sin\alpha} = 0.61\ \frac{\lambda}{NA}$$

Photon based nanolithography

The resolution of the system however it is more common to write in terms of a constant k1

$$R = k_1 \frac{\lambda}{NA}$$

The equation above has three parameters that can be manipulated in order to increase the spatial resolution: decrease the empirical constant k1, illuminate with shorter wavelengths and increase the numerical aperture of the system.

The illumination wavelengths used have been picked based on the availability of efficient sources. Hg arc lamps spectrally filtered to narrow the bandwidth to optimize the optical system to a given wavelength and reach the diffraction limit.
Lenses can be compensated at determined wavelengths, this is compensated in the primary aberrations (spherical and chromatic). Hg arc lamps produce strong emission at 435 and 365 nm.

Laser based sources are now used. KrF excimer laser emits strongly at 248 nm. Changing the gas to ArF it is possible to produce light at 193 nm and with F_2 down to 157 nm.
At these wavelengths the materials used in the optical systems start to be a problem.

Photon based nanolithography

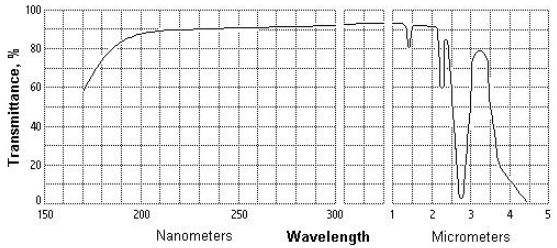

Synthetic quartz

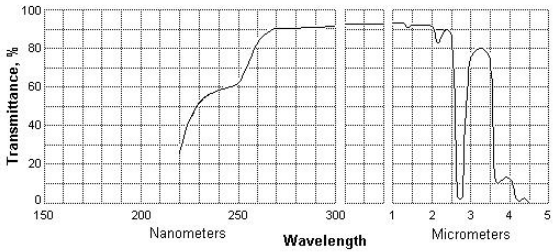

Fused quartz

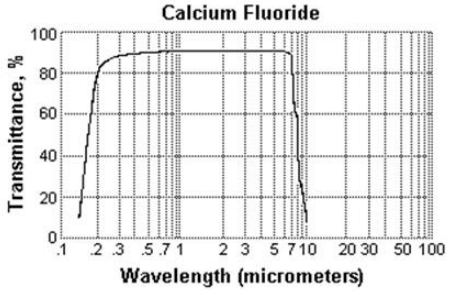

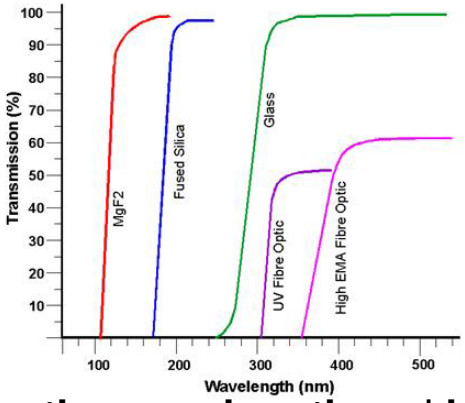

The main complication using crystalline materials as CaF2 is its birefringence, this is that exhibit a different refractive index depending on the polarization. This fact enormously complicate the optical design of the projection optics.

The general idea of **decreasing the wavelength** and **increasing the NA** has been proved to be effective but at the cost of decreased depth of focus (DOF) and consequently more stringent requirements in the planarity of the wafers and focusing accuracy. **The DOF** is modeled as the deviation on the focal plane position that would cause a <u>phase shift of λ/4 between the central ray and one ray at the edge of the lens</u>.

$$DOF = \pm 0.5 \frac{\lambda}{NA^2} = \pm k_2 \frac{\lambda}{NA^2}$$

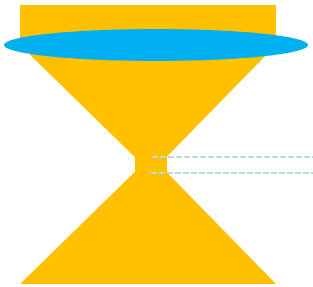

$DOF \geq$ Thickness of the photoresist

Photon based nanolithography

Excimer Laser Stepper

Lithography Handbook

Minimum feature size (resolution)

$MFS = k_1\lambda/NA$
$k_1 \approx 0.8$
(resist/enhancements)

Depth of Focus

$DOF = k_2\lambda/(NA)^2$
$k_1 \approx 1$
(enhancements)

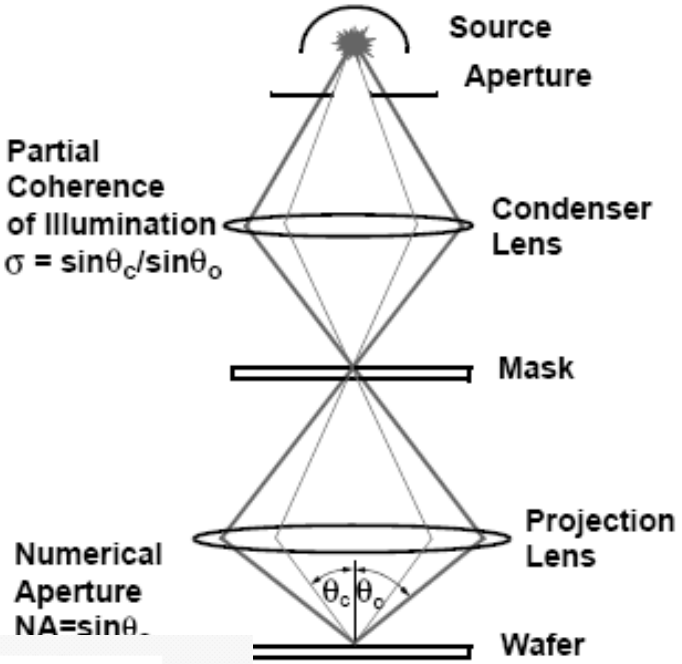

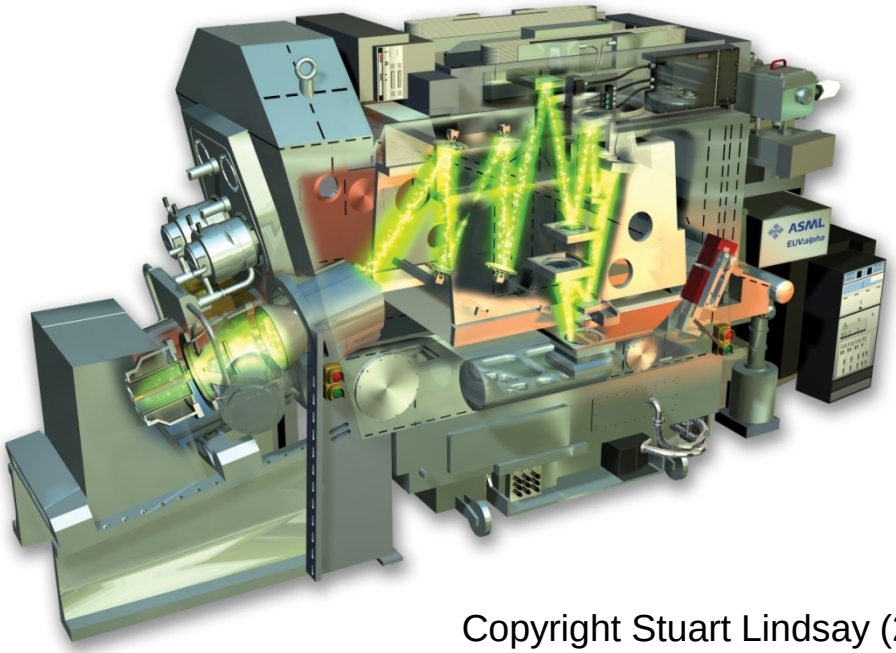

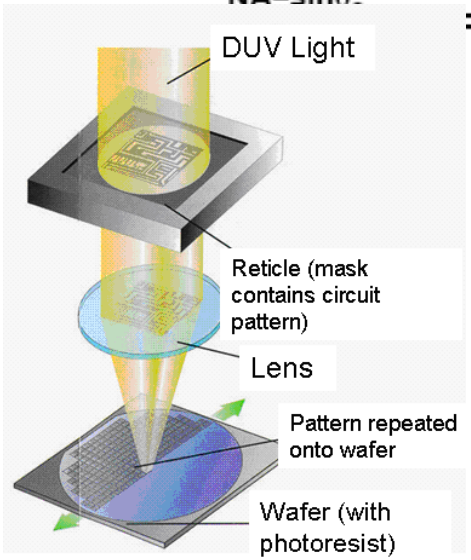

Photon based nanolithography

EUVL

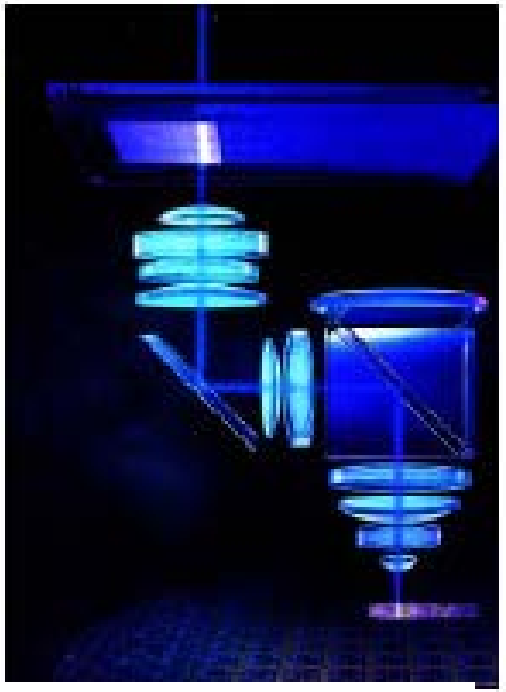

Lithography "Laws"

- CD = k_1*λ/NA
- DOF = 1.2*λ/NA^2

"k_1 factor"

Conventional: k_1 = 0.7

Strong PSM: k_1 = 0.3

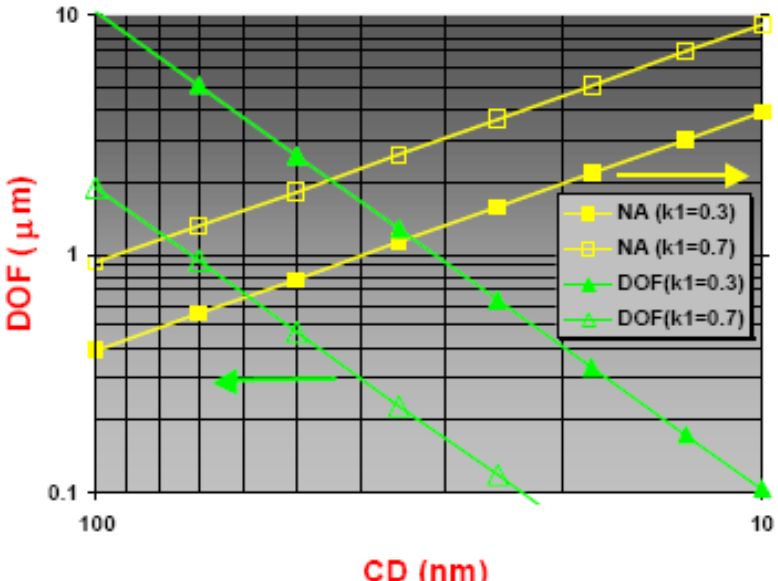

Photon based nanolithography: EUV lithography

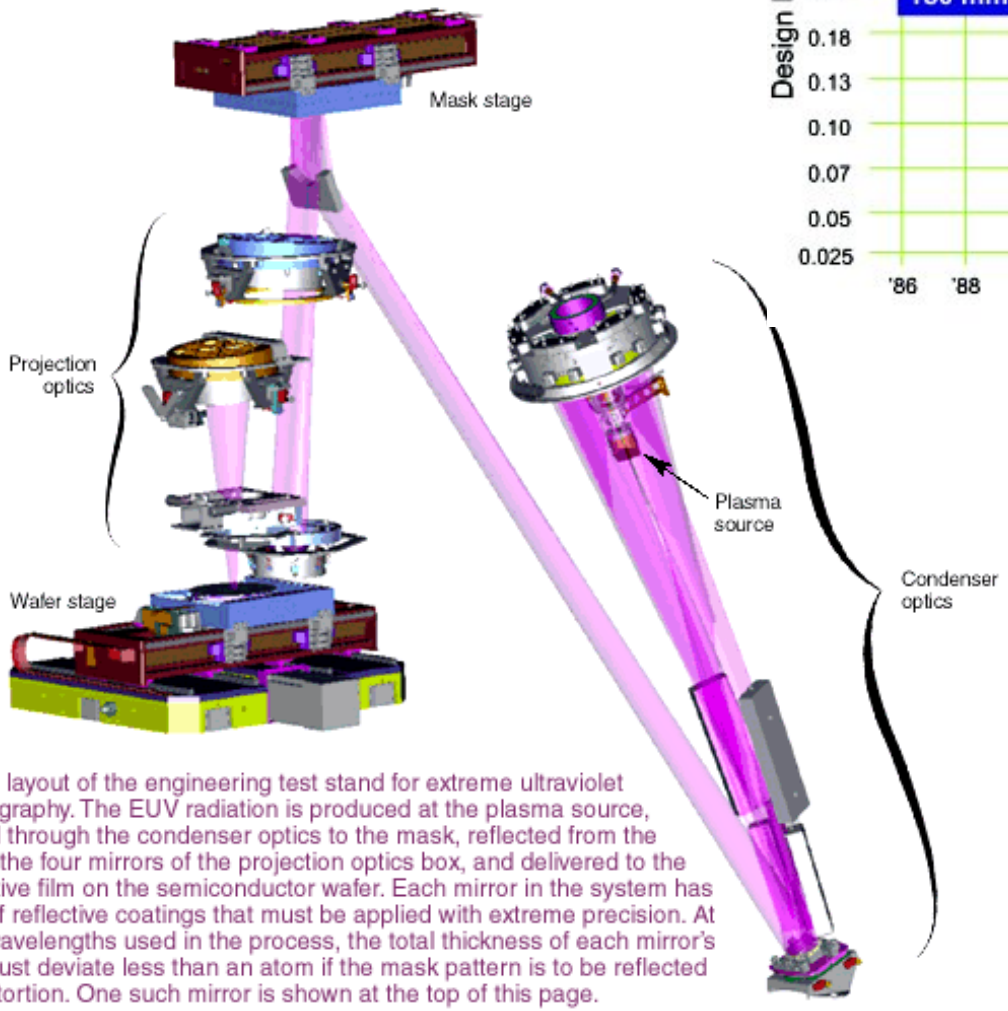

The optical layout of the engineering test stand for extreme ultraviolet (EUV) lithography. The EUV radiation is produced at the plasma source, transmitted through the condenser optics to the mask, reflected from the mask onto the four mirrors of the projection optics box, and delivered to the EUV-sensitive film on the semiconductor wafer. Each mirror in the system has 81 layers of reflective coatings that must be applied with extreme precision. At the short wavelengths used in the process, the total thickness of each mirror's coatings must deviate less than an atom if the mask pattern is to be reflected without distortion. One such mirror is shown at the top of this page.

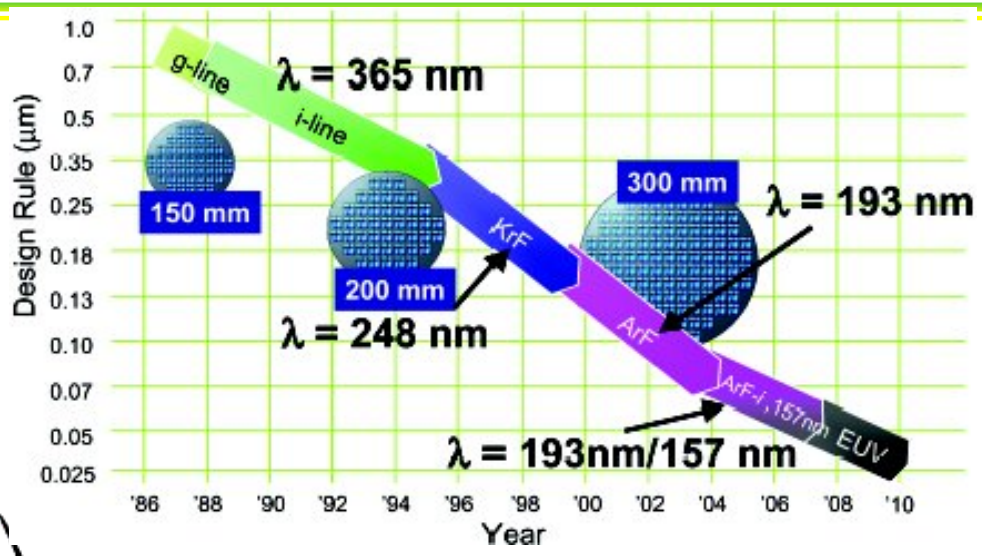

Smallest lines printed with EUV lithography: 20 nm

http://www.llnl.gov/str/Sween.html

Photon based nanolithography: EUV lithography

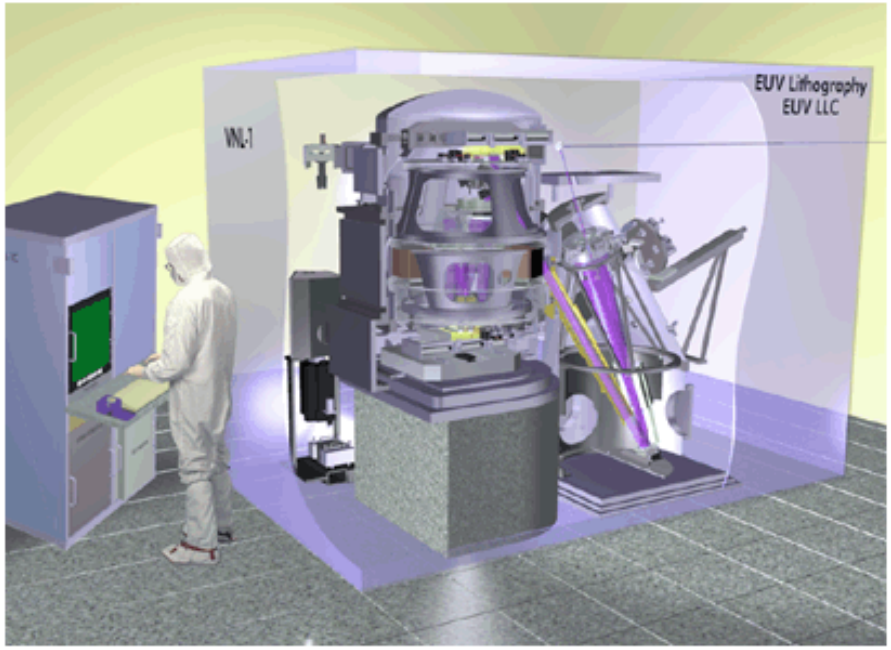

A conceptual drawing of the extreme ultraviolet engineering test stand. The goal of the ETS is to demonstrate how ultraviolet wavelengths can be used to print patterns on integrated circuits at production levels and sizes.

- Reflective optics
- High quality multilayers
- Printable defects
- At wavelength inspection

EUV sources

http://www.llnl.gov/str/Sween.html

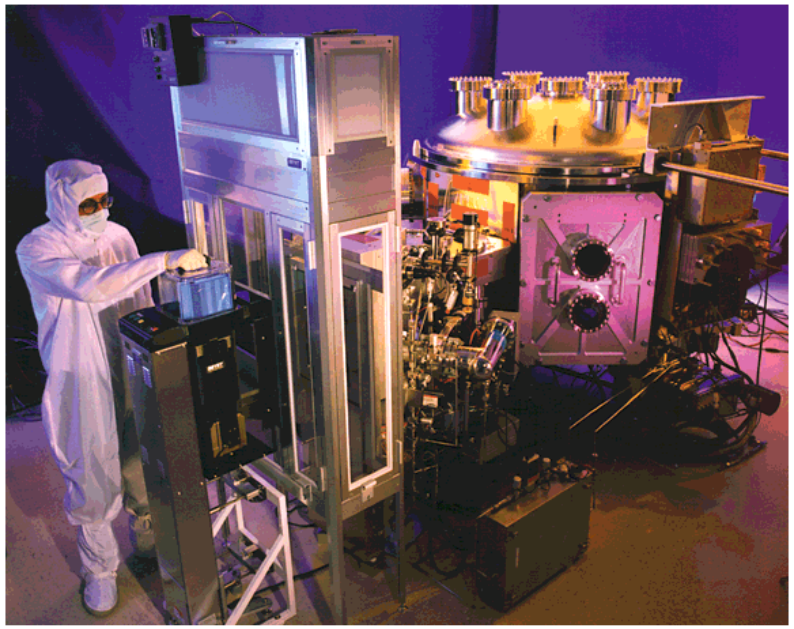

The Ultra Clean Ion Beam Sputter Deposition System, developed at Lawrence Livermore, is used to produce precise, uniform, highly reflective masks. A key requirement of the next-generation lithography system is that it produce virtually defect-free masks. The system contributes fewer than 0.1 defects per square centimeter to each mask. The ultimate goal for extreme ultraviolet lithography is to add no more than 0.001 defects per square centimeter to a finished wafer blank.

E-beam Lithography

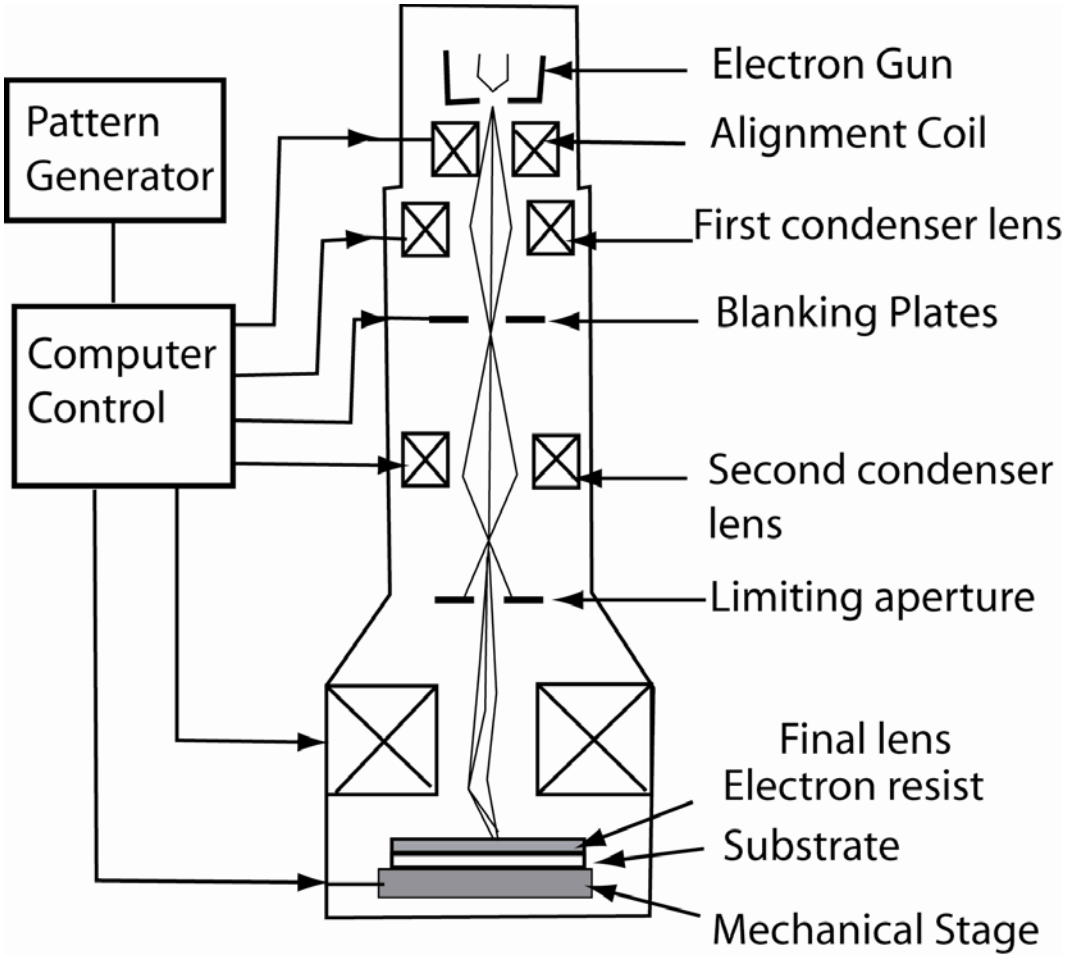

Mo/Si multilayers have high reflectance at 13.5 nm wavelength

6”×6” Mo/Si multilayer coated mask

Absorber pattern

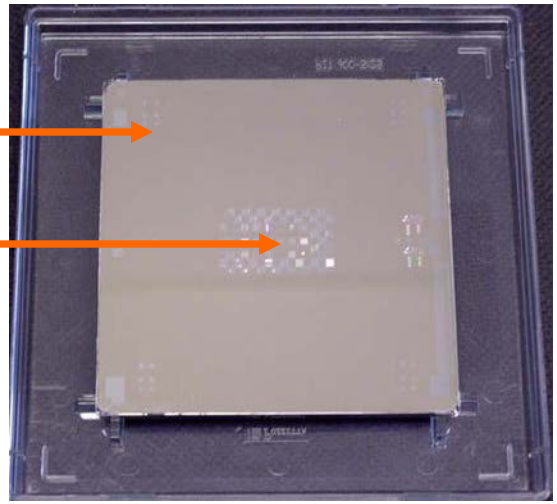

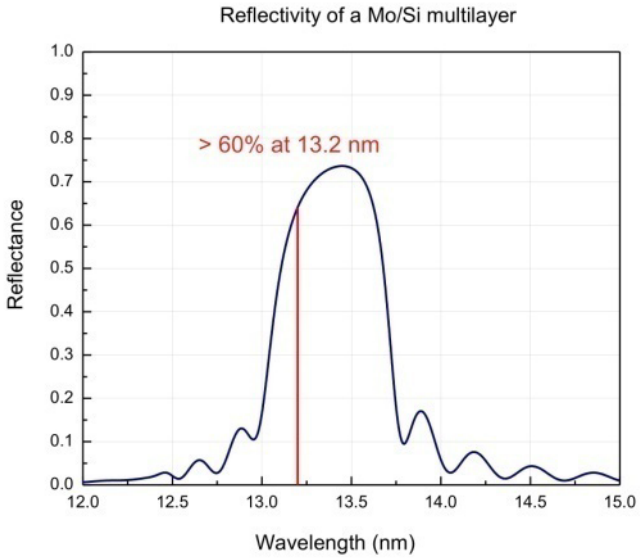

Phase defects

Mo/Si multilayers

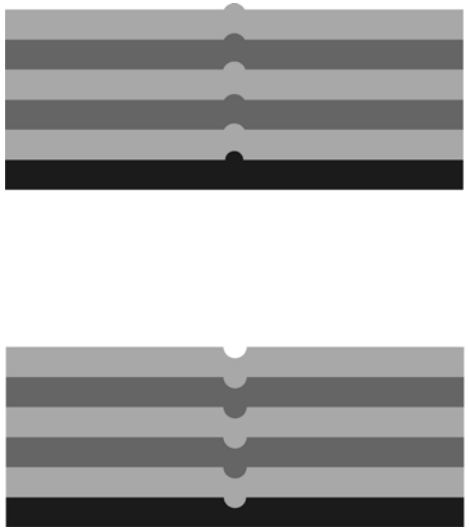

Absorption defects

Currently: 0.3 defects/cm^2
Goal: 0.003 defects/cm^2

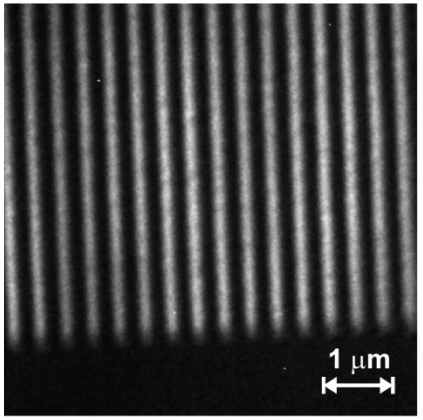

Block copolymer masks

- Phase separation of incompatible block copolymers

e.g., polystyrene and polybutadiene

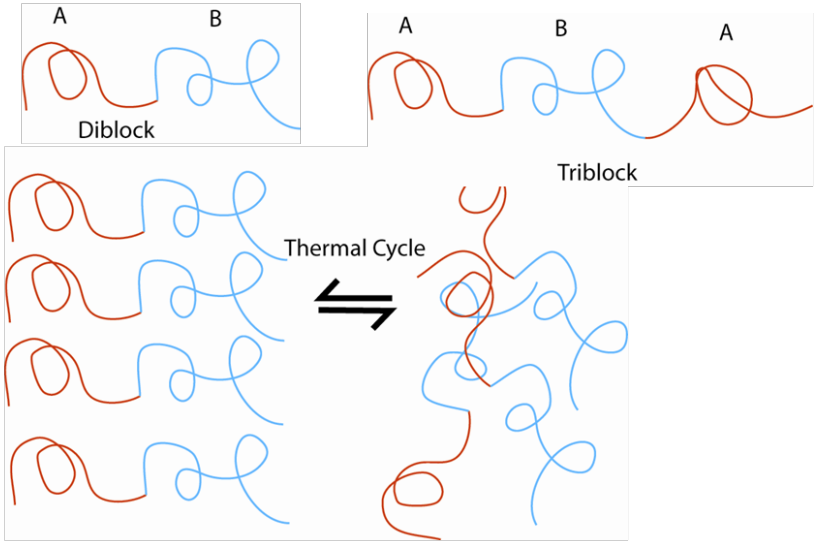

Copyright Stuart Lindsay (2008)

Immiscible polymers phase-separate into an ordered domain structure. The size and structure depends on the length of the polymer chain and of the nature of the polymer

Self assembled lithography

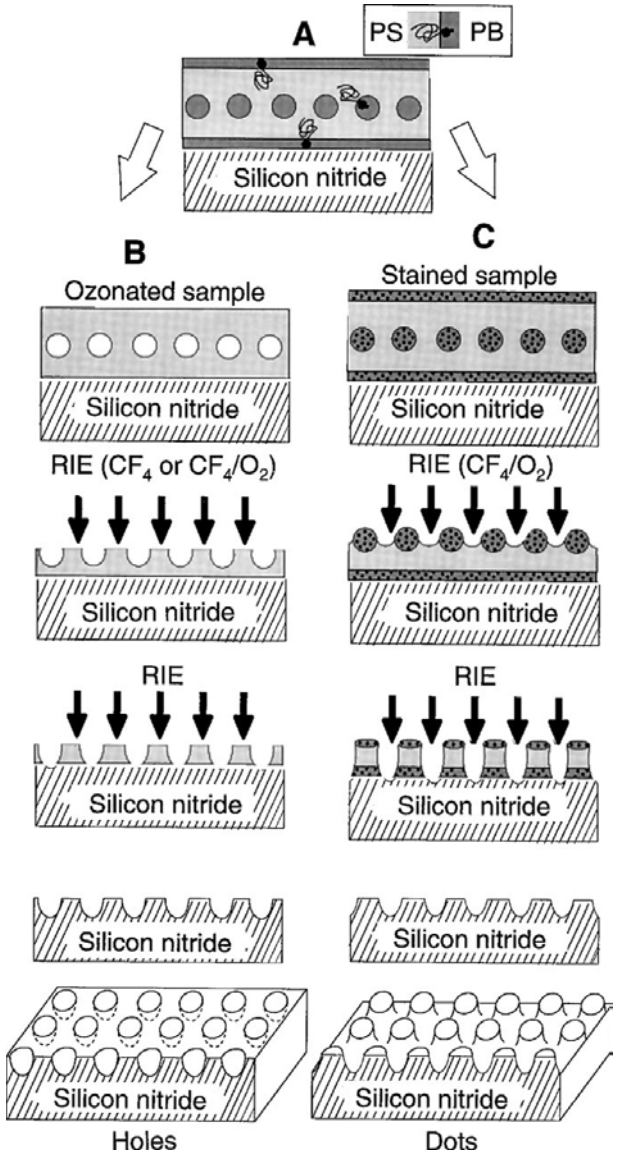

Structures made with block-copolymer masks

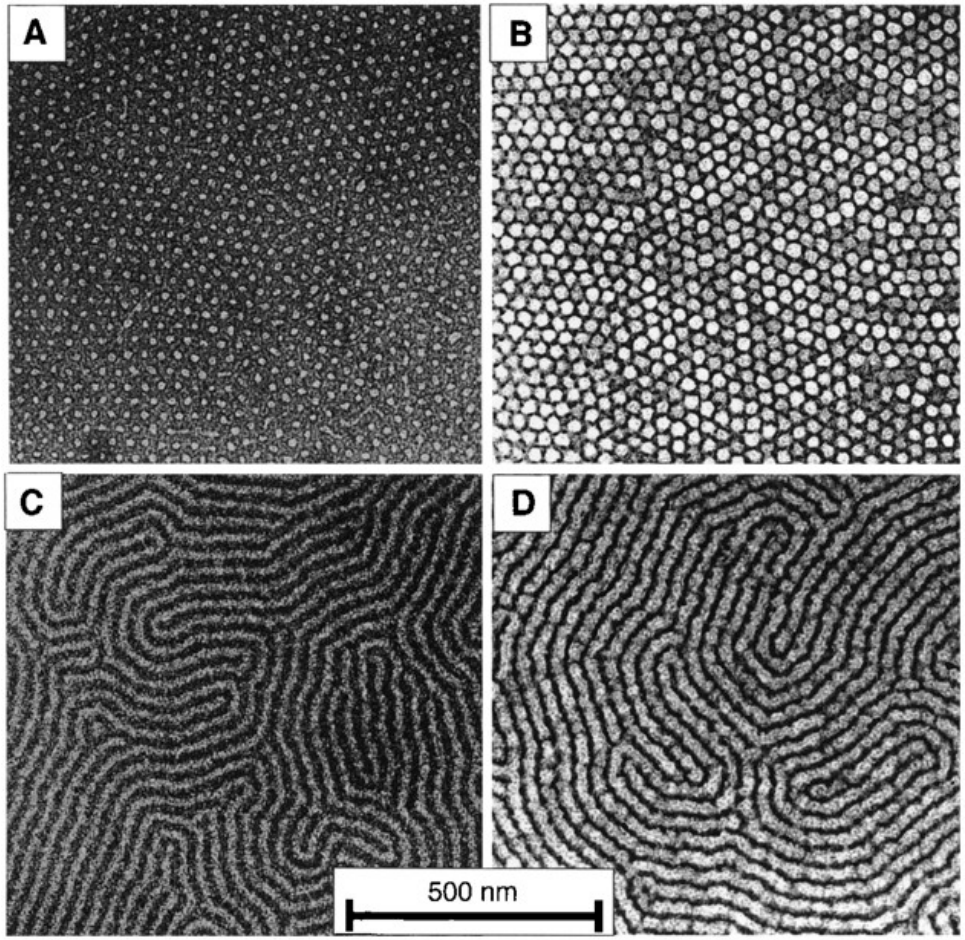

TEM images showing (A) a spherical micro-domain monolayer film after removal of poly butadiene by ozone treatment, (B) the resulting array of holes in silicon nitride after RIE, (C) cylindrical microdomains in which the darker regions are osmium stained poly butadiene domains and (D) the resulting cylindrical pattern etched into the silicon nitride surface.

Focused Ion Beam

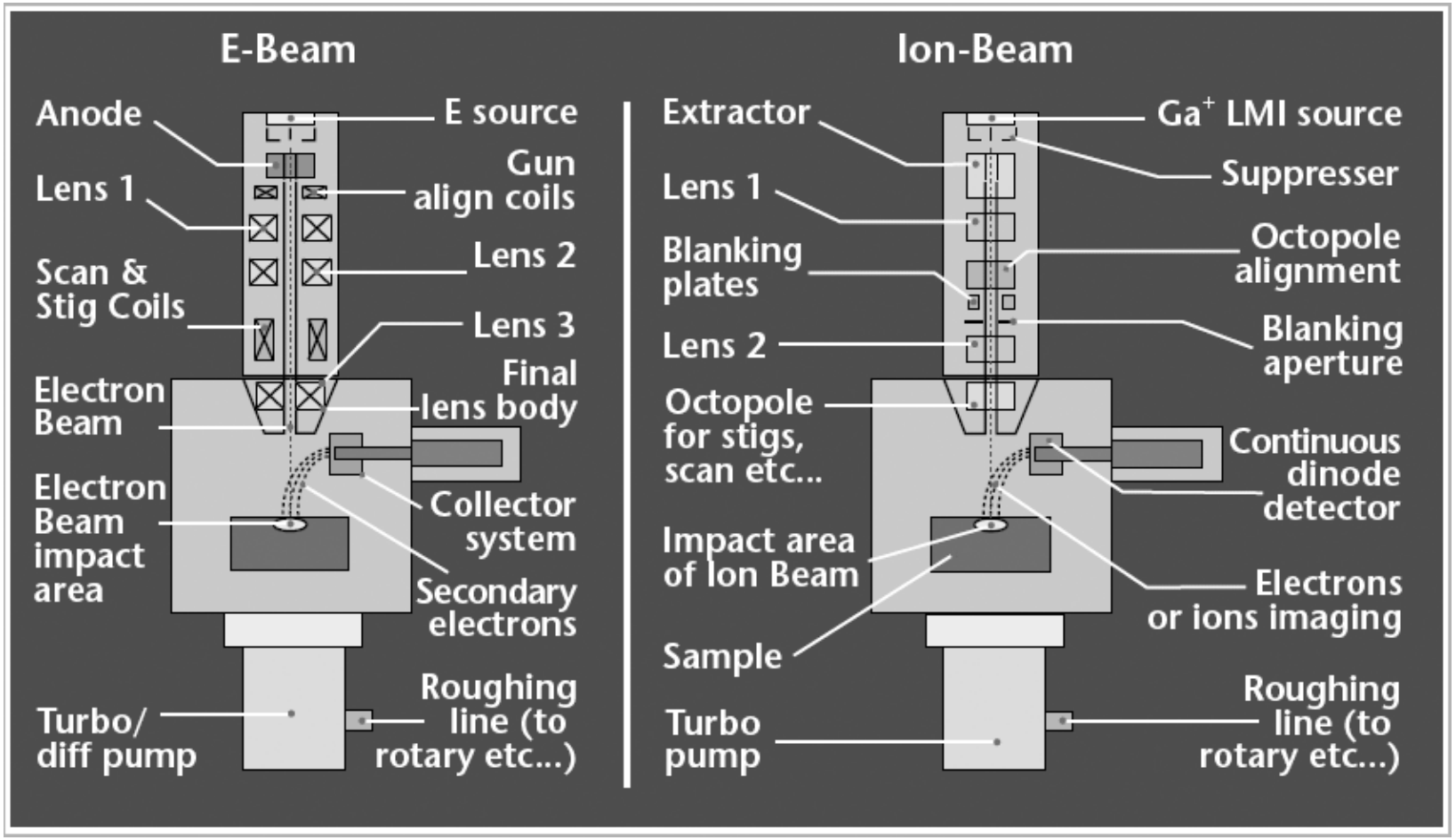

Focused Ion Beam

Ga liquid metal source and reservoir

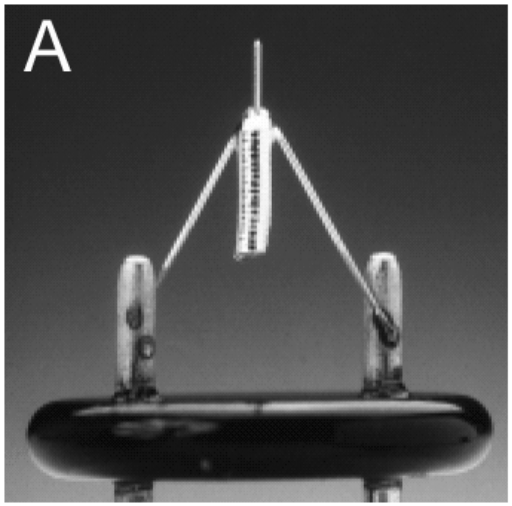

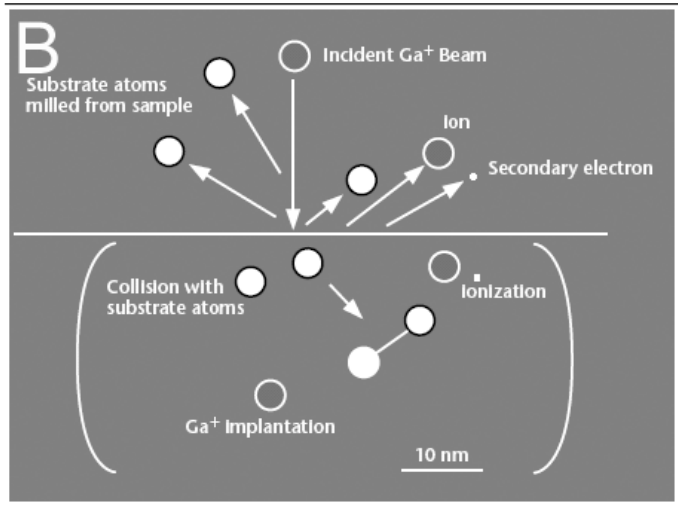

(Courtesy of FEI)

Interactions of Ga ions and atoms/molecules in the sample

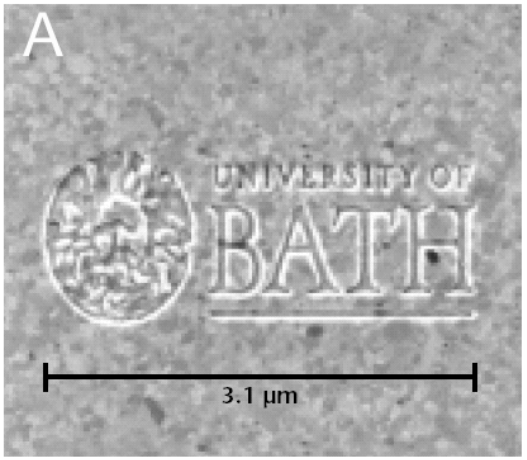

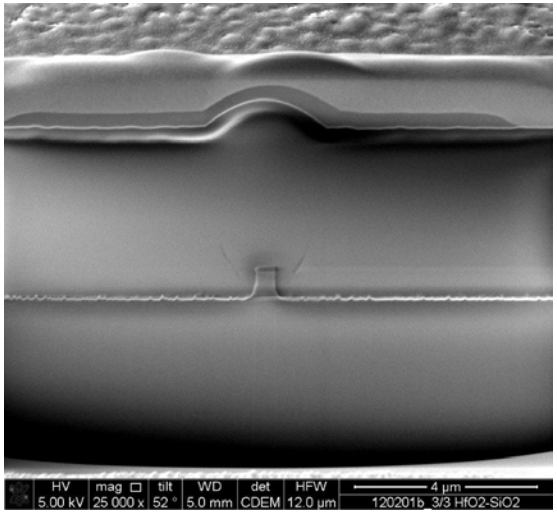

Examples of ion milling with FIB.
A) Lithography; B) 1um defect in covered with a Silica layer µm thick

Stamp Technology

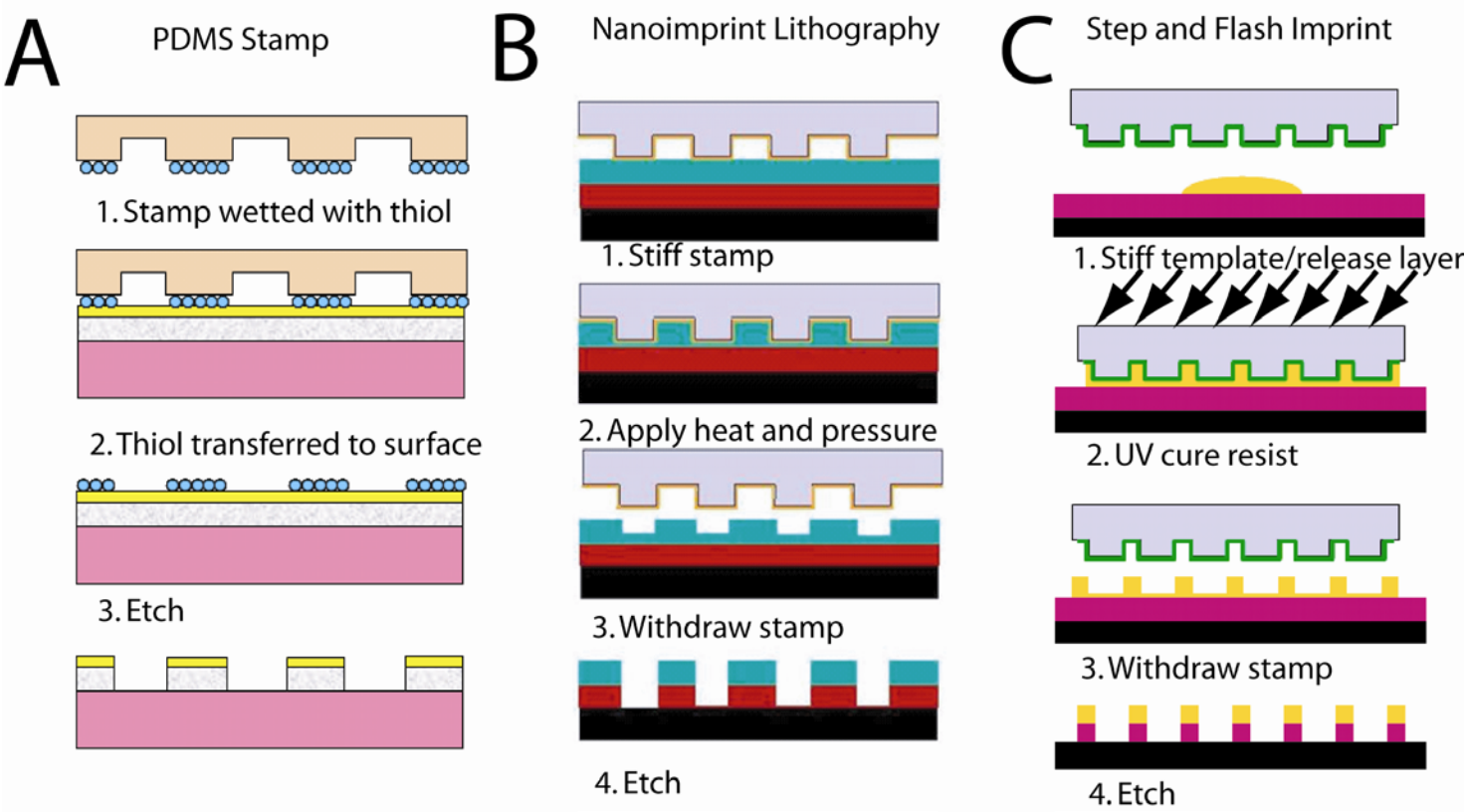

Replication methods are referred as “soft lithographies” because they rely in a soft elastomer to achieve intimate conformal contact between the master and the sample.

Advantages: 1) patterning of curved surfaces; 2) the use of materials that are incompatible with photoresists or developers, 3) large area fabrication.

Mold is made is Si wafer by e-beam lithography. A) PDMS poured into mold and cured. The resulting Silicone rubber is poured away from the mold. It is used to transfer patterns into coated substrates.

Edge lithography

In this technique the edges of a structure become the feature in the resulting pattern.
Near field phase shifting photolithography is a contact lithography but includes a mask made out an elastomer to achieve a better contact with the photoresist. The mask induces a phase shifts in the illumination that produces in the surface of the photoresist an interference pattern.

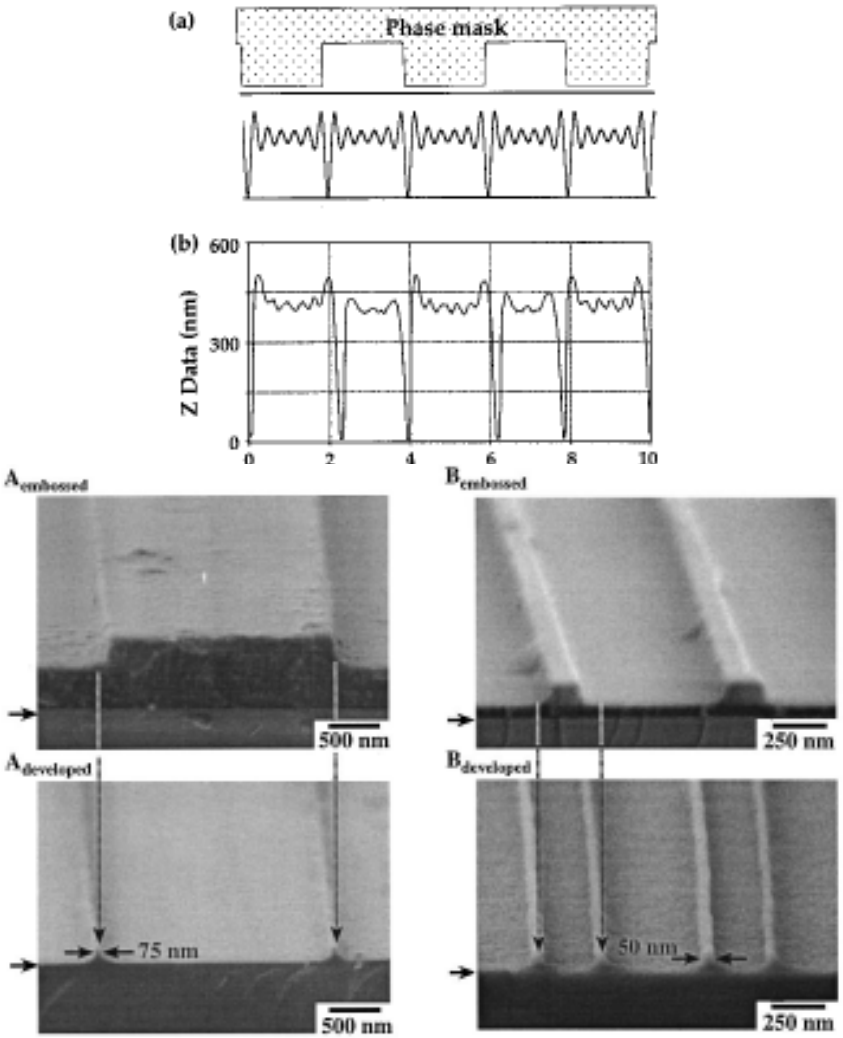

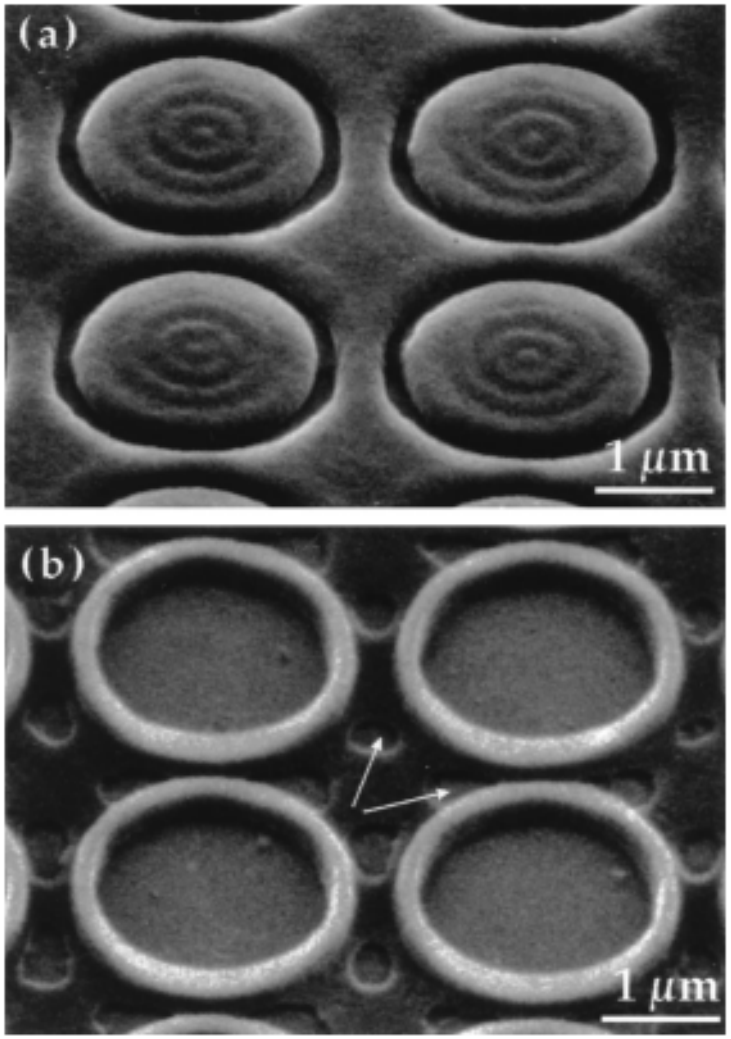

Three dimensional patterning

Examples carving of a surface by ablating material, laser induced deposition of precursor compounds and photoinduced polymerization of a liquid polymer.
A recent technique is writing based on two photon absorption (TPA). With this technique, photo-polymerization only occurs in small volumes corresponding to the focal spot of a laser beam where the intensity is high enough to produce absorption of two photons.

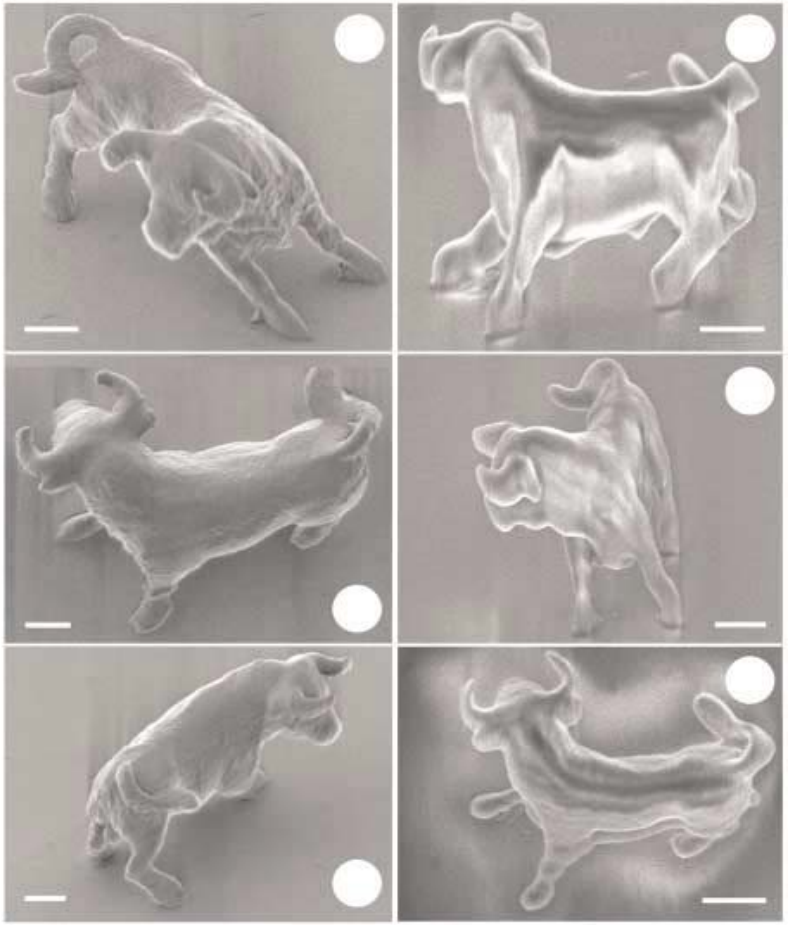

EUV interferometric lithography using a Lloyd mirror

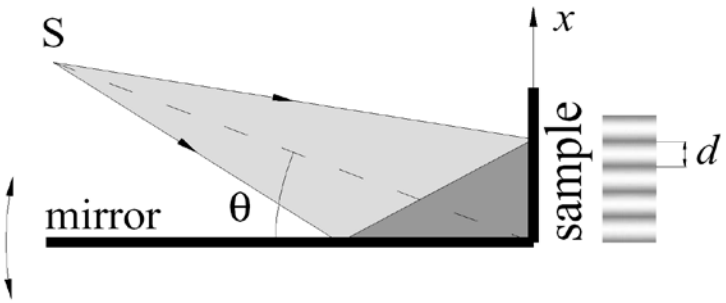

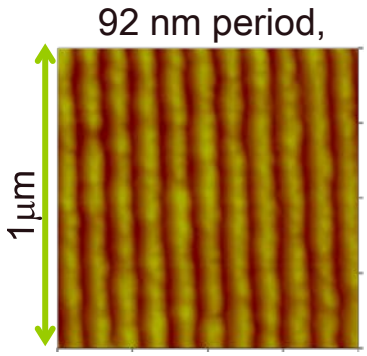

~ 12.5 nm

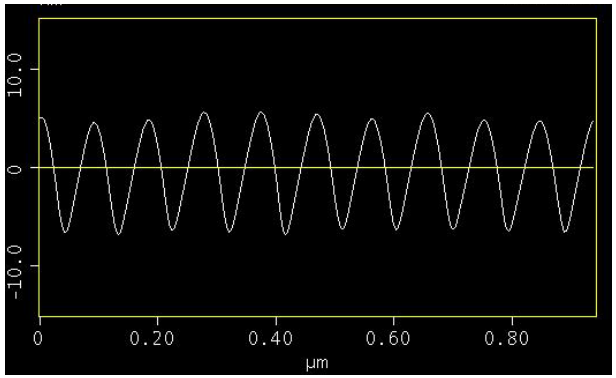

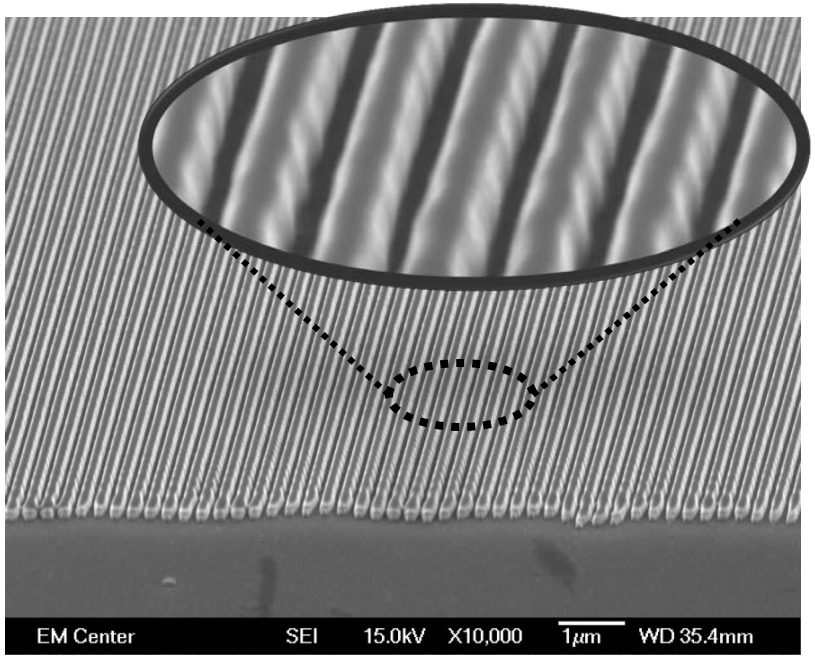

90 nm lines and spaces fabricated in Au

M. Marconi, CSU

Holographic patterning and interferometric lithography

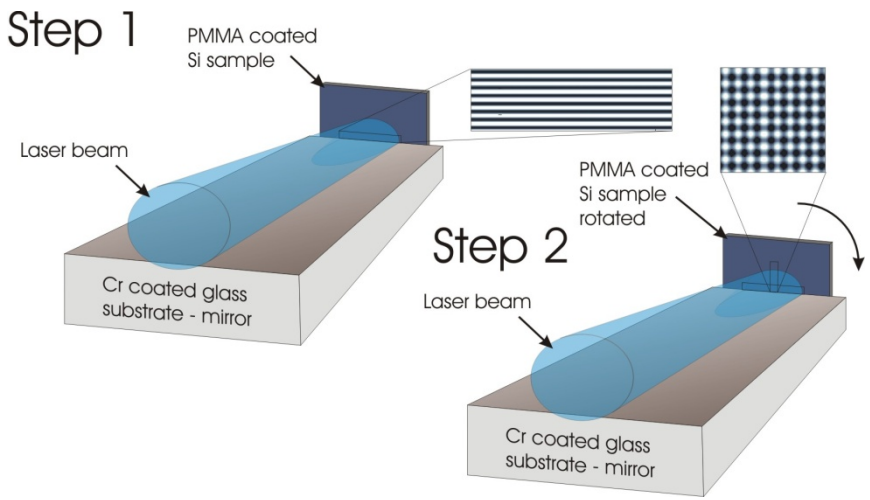

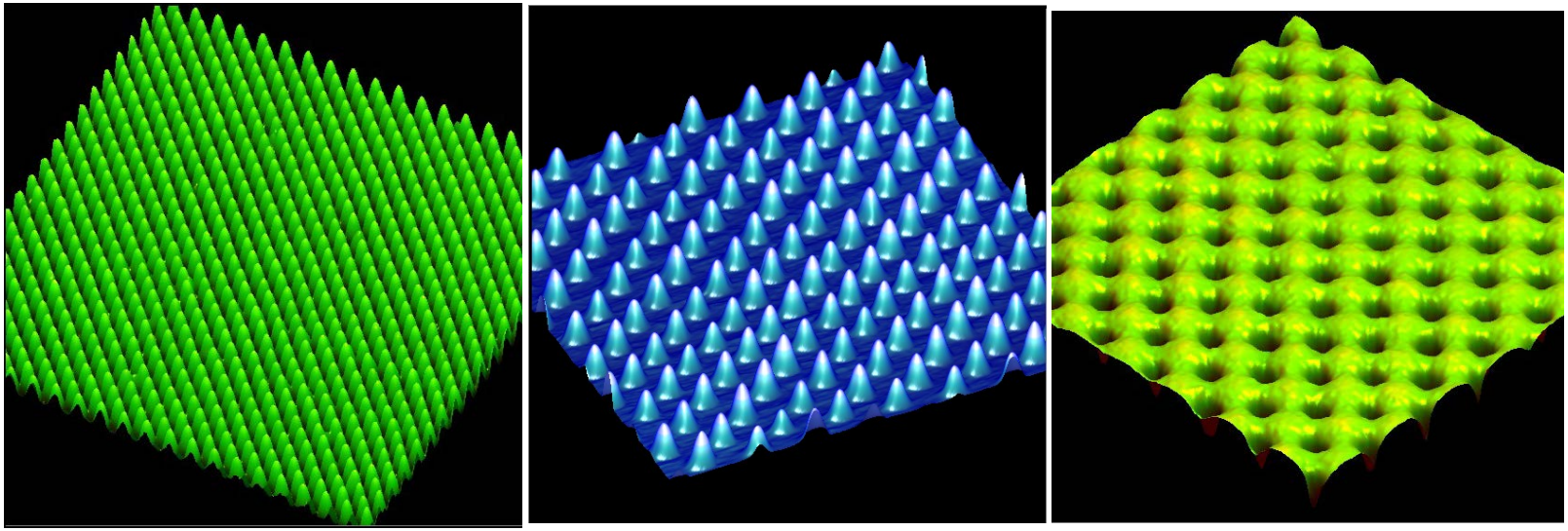

EUV Nanopatterning tool

EUV Ne-like Ar Capillary discharge 46.9 nm laser

- High average power: up to 3 mW
- High pulse energy: 0.1 mJ –0.8 mJ @4 Hz
- Spectral bandwidth: $\Delta\lambda/\lambda = 10^{-4}$
- Beam divergence: $\theta = 4.5$ mrad

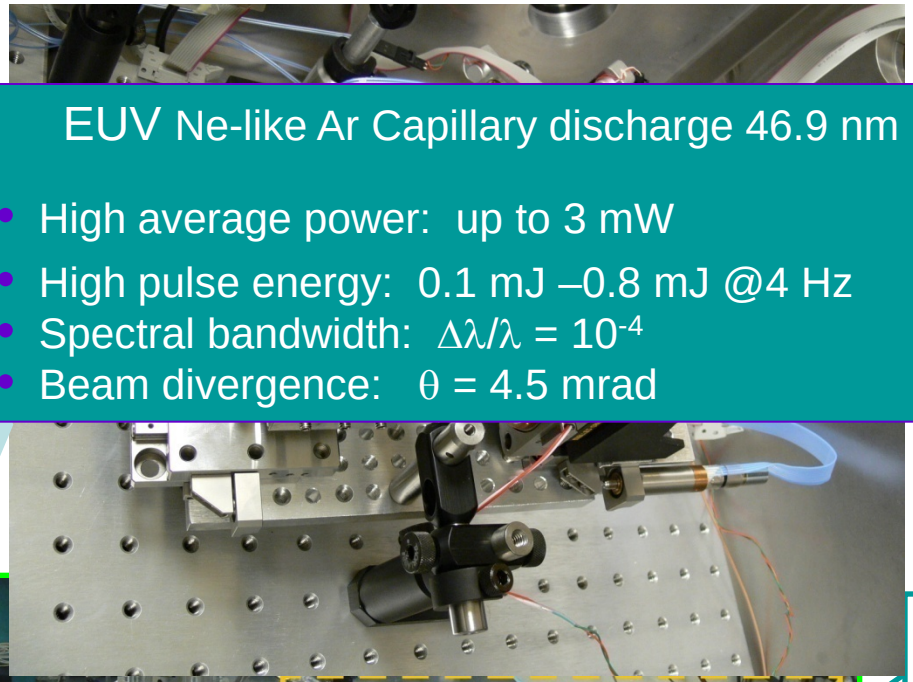

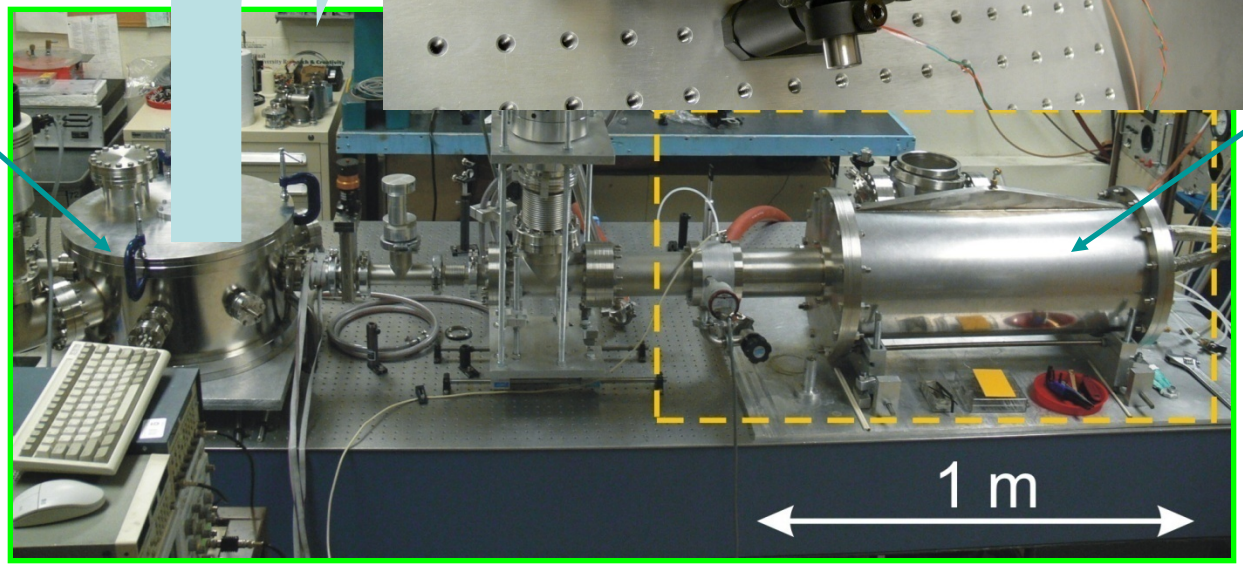

Experiment chamber

Capillary discharge EUV laser

Talbot coherent imaging lithography

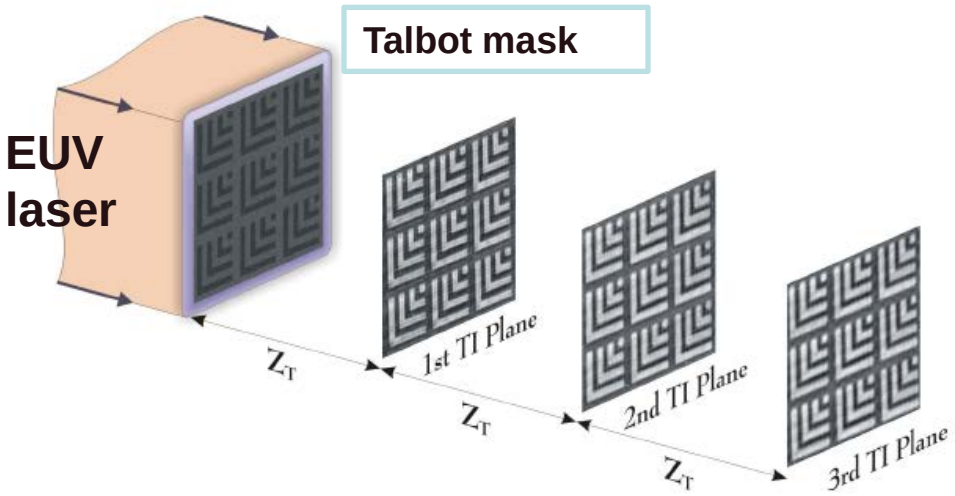

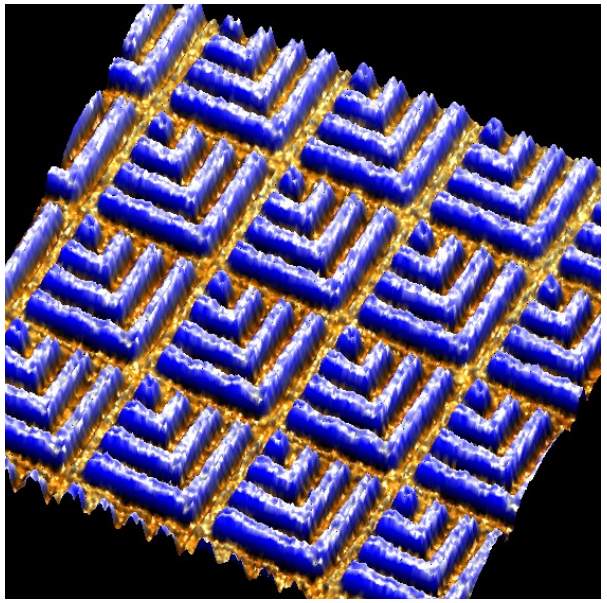

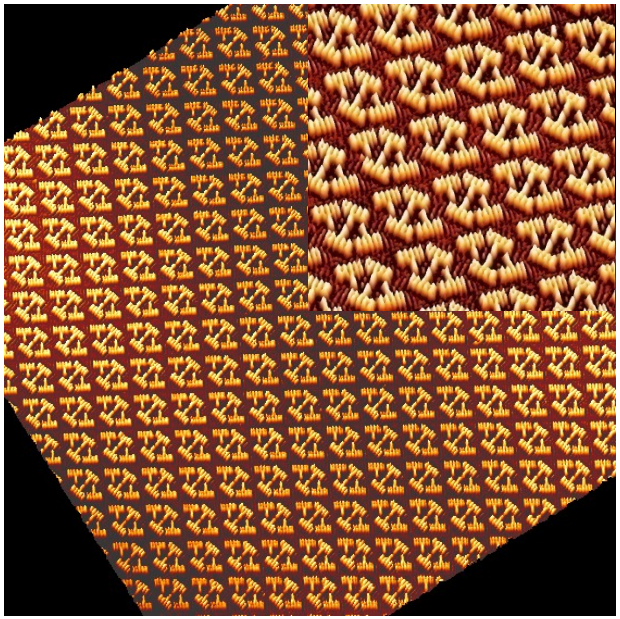

Direct printing of arbitrary patterns with nanometer resolution
Over areas only limited by illuminated region in mask

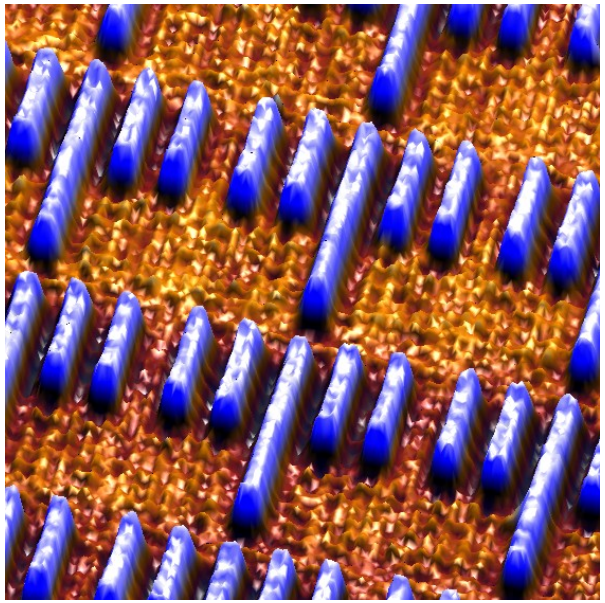

Talbot coherent imaging lithography prints defect free 1-to-1 replicas of the mask

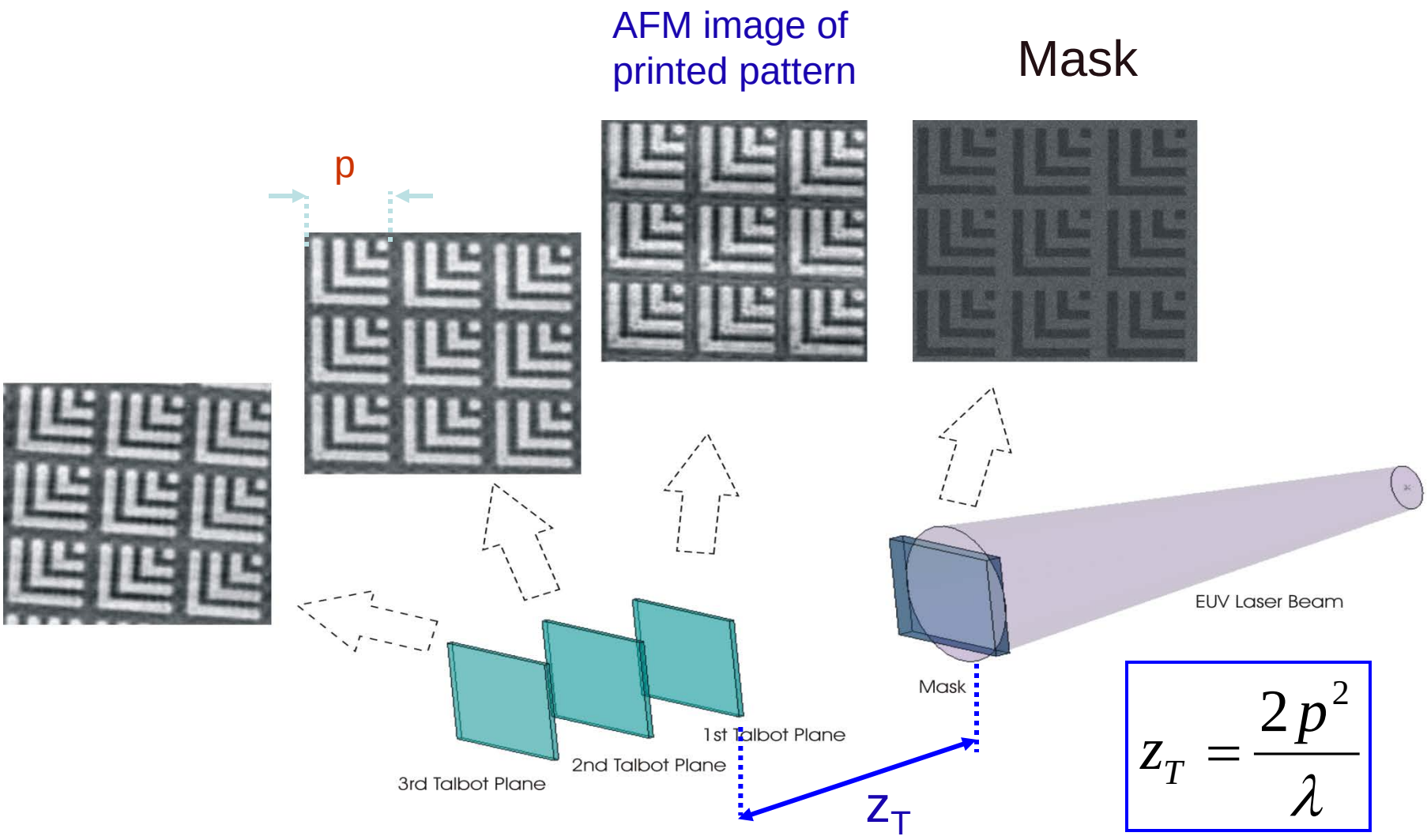

$$z_T = \frac{2p^2}{\lambda}$$

For λ = 46.9 nm, p=4.8 μm, z_T= 1 mm

Experimental set up

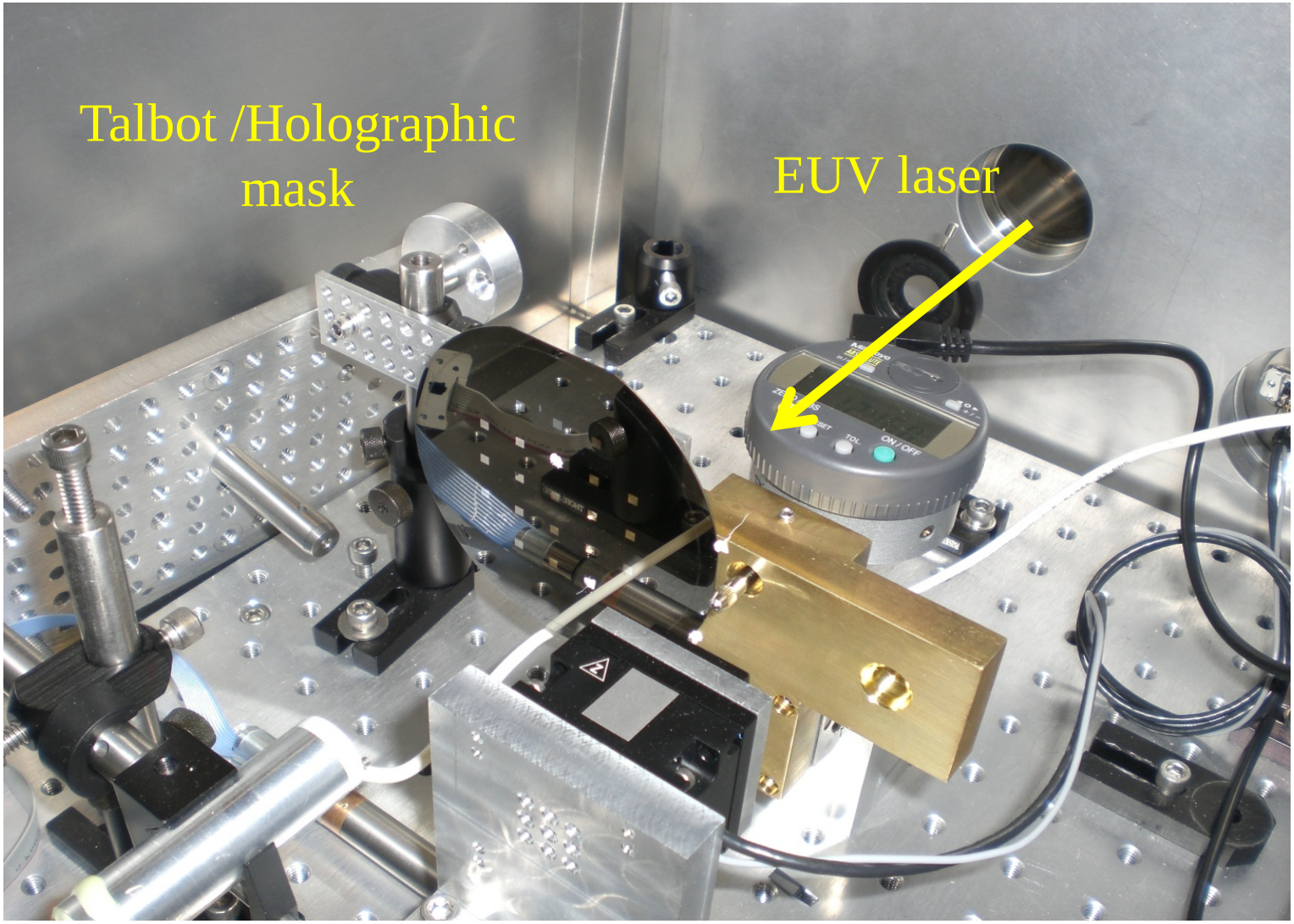

Arbitrary patterns can be printed over large area with a spatial resolution of ~ 100 nm in exposures of about 1 minute

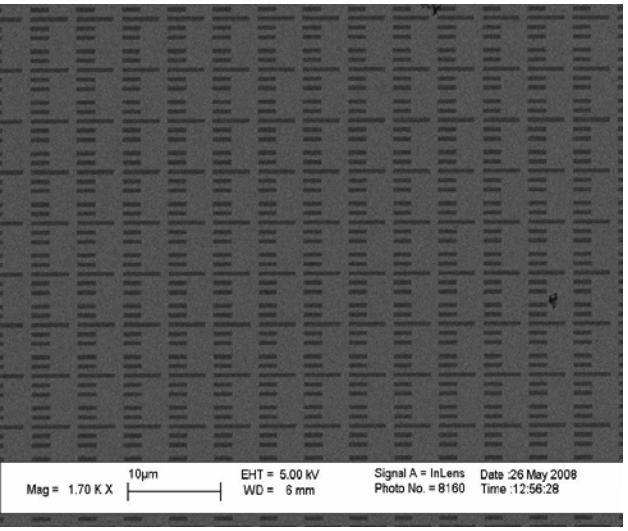

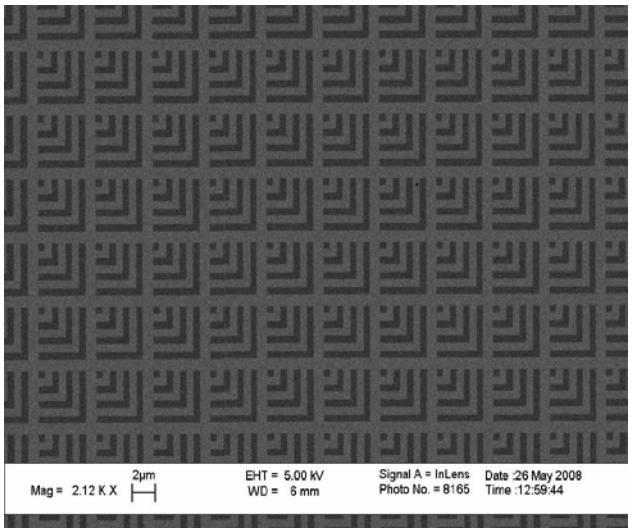

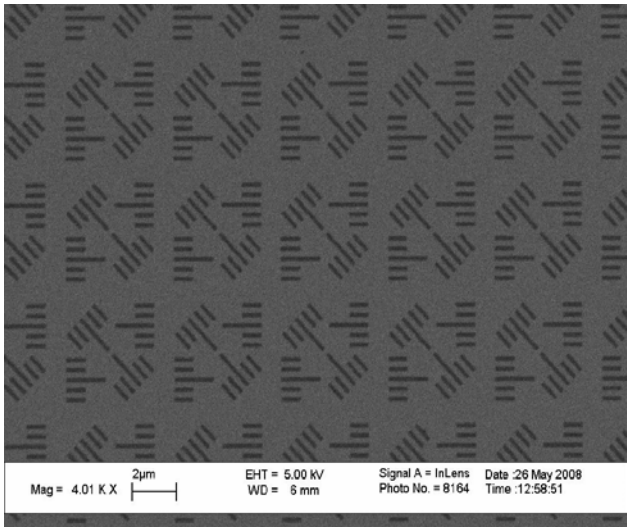

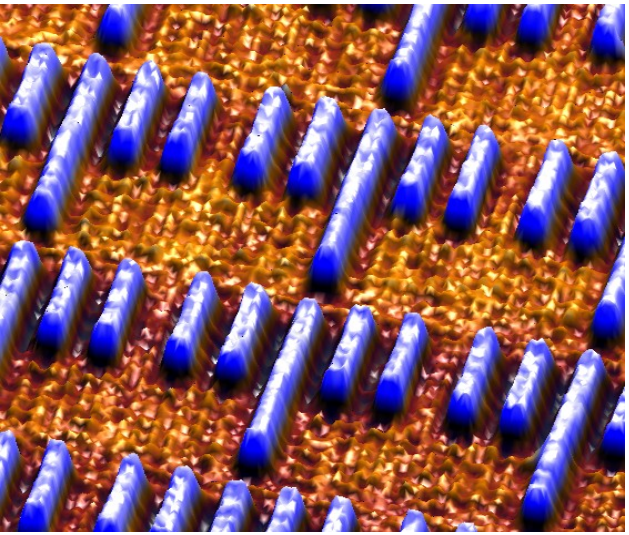

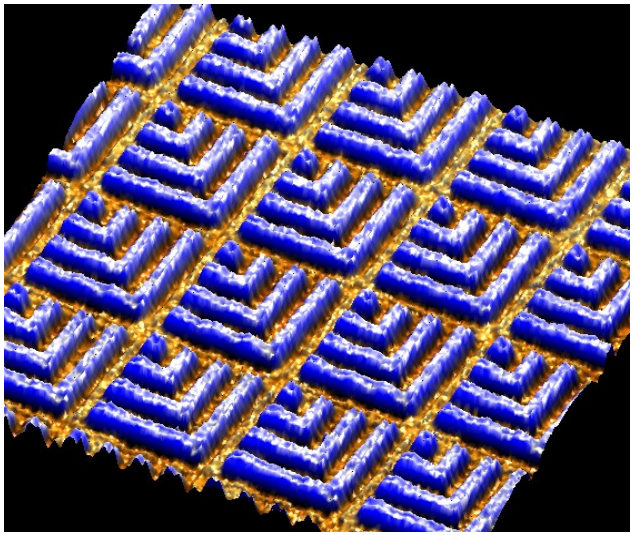

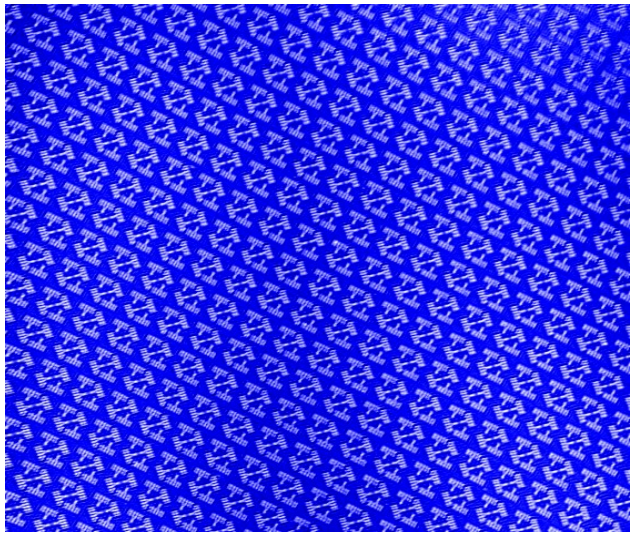

p=500 nm

A. Isoyan et al, JVST B 2010

Talbot Lithography is non contact and offers defect free printing

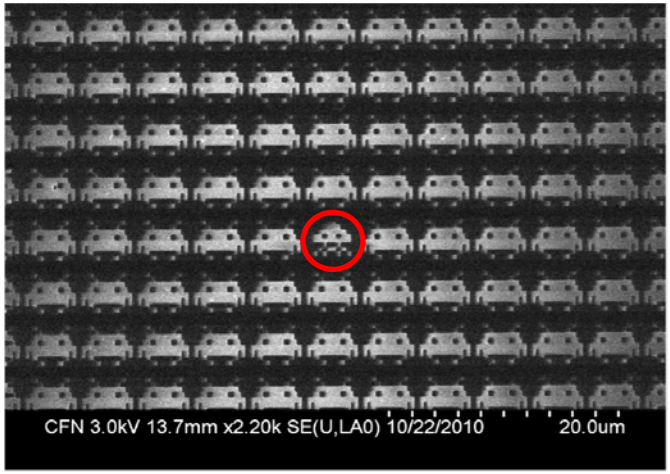

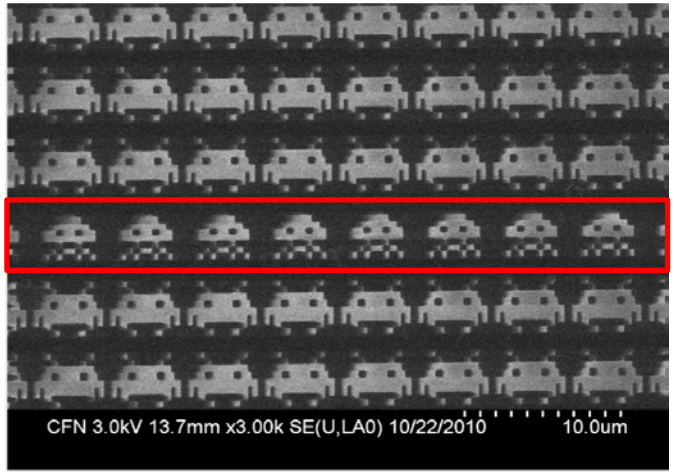

Talbot masks with “defects”

The mask with 1% defects (left) prints a defect free replica (right). The dashed line indicates the row that in the print corresponding to the row with defects in the mask

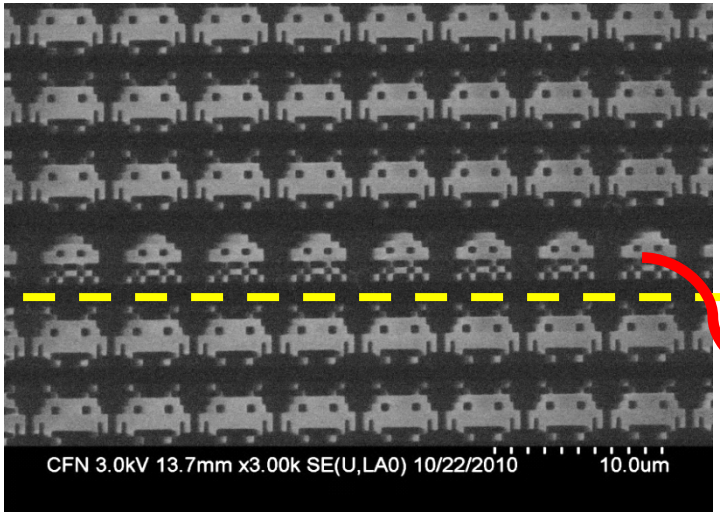

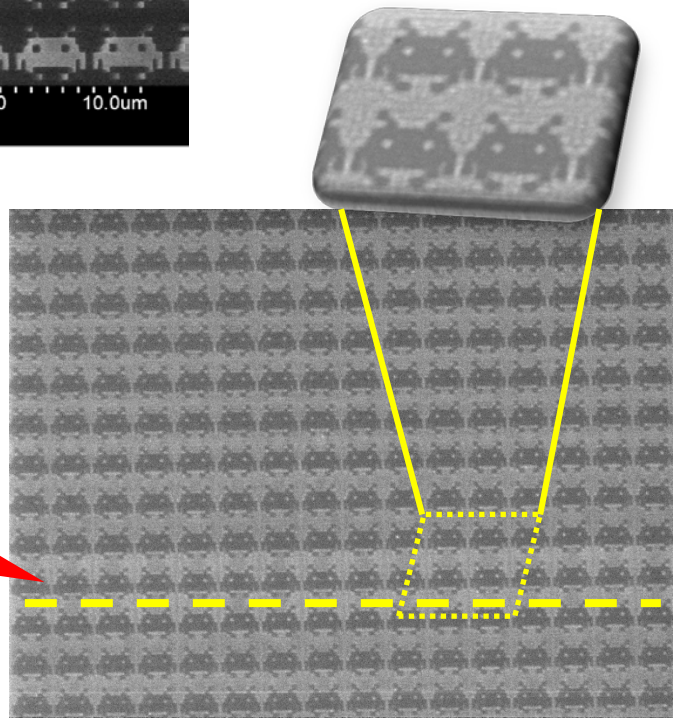

Summary

EUV laser nanopatterning tool exploits high coherence of the laser to print >100 nm features using

Interferometric Lithography

Talbot Imaging Lithography – (optical nano-imprint)

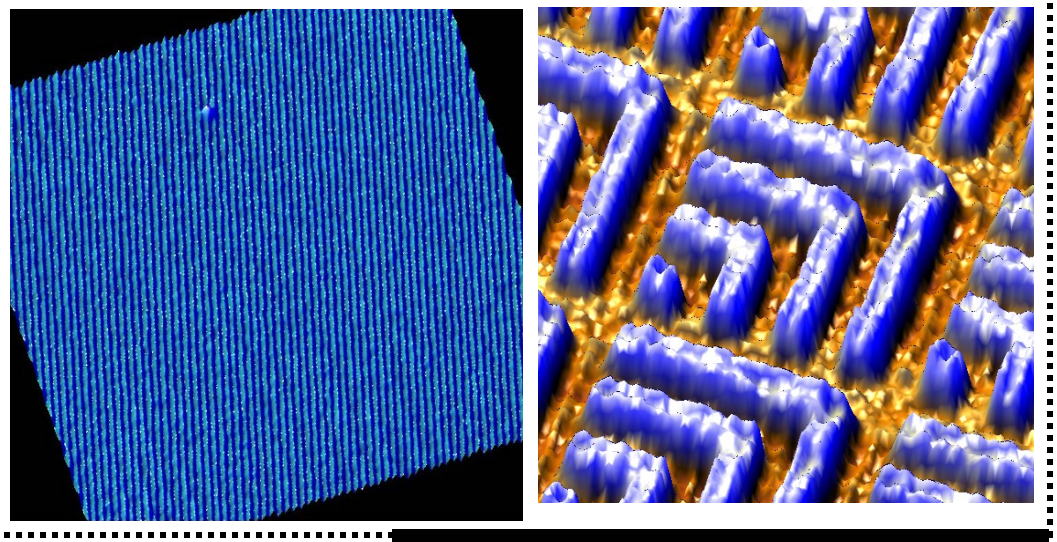

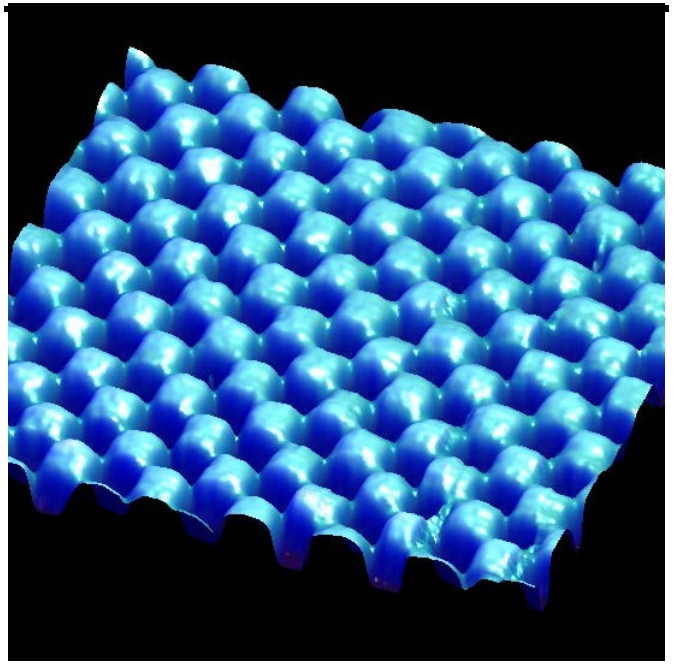

- Compact and reliable set up
- Versatile: printing different periodic and arbitrary motifs
- Very short exposure times (tens of seconds to few minutes)
- Printed area in each exposure is a fraction of a square millimeter

Highly monodispersed core–shell particles created by solid-state reactions

V. Radmilovic, C. Ophus, E. A. Marquis, M. D. Rossell, A. Tolley,
A. Gautam, M. Asta and U. Dahmen
Nature Photonics vol 10, pp. 710, 2011

Precipitation hardening in metals is a thermal process whereby precipitates or 'second phase particles' are created within a matrix. These particles prevent motion or creation of dislocations and in turn reduce plasticity of materials.

Ostwald ripening (OR): In a supersaturated solution, nuclei form and growth proceeds by controlling supersaturation. OR is a process in which the larger nuclei grow at the expense of the smaller ones.

THE AUTHORS IN THIS PAPER SHOW THAT **OR** IS NOT ALWAYS DOMINANT AND THAT PLAYING WITH SOLUBILITY OF MATERIALS, IT IS POSSIBLE TO MAINTAIN A NARROW PARTICLE SIZE DISTRIBUTION. THIS IS IMPORTANT TO DEVELOP NEW ALLOYS THAT CAN RETAIN MECHANICAL PROPERTIES AT HIGH TEMPERATURES

The material system the authors use is **Al-Sc-Li -**

Crystal Structure – $L1_2$ face centered cubic

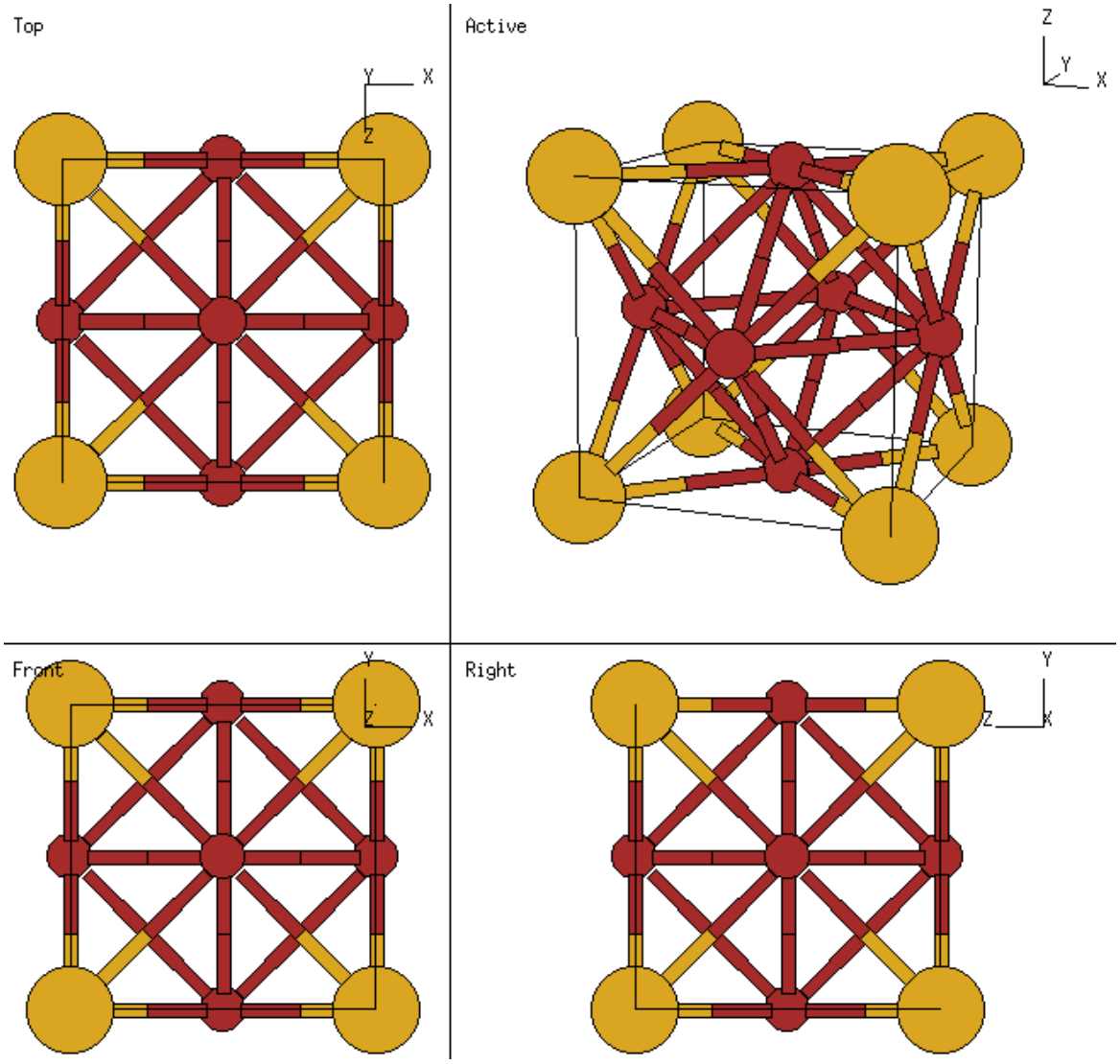

Alloy: Al with 8.5% of Li and 0.11% of Sc.
Sc is the most potent strengthener of Al
Li: lightest material
Both form Al3X intermetallic phases with FCC structure
The Li enhances nucleation of Al3Sc cores – Al3Sc is stable
Al3Li are metastable

Heat treatment 1 – Anneal at 450 C to nucleate ordered Al3Sc phase on Al matrix
Heat treatment 2 – Anneal at 190 C to create the Al3Li core – the Al3Li wets the surface of the Al3Sc core – same crystal structure leads to no lattice mismatch.

Coarsening rate (agglomeration) is much slower than OR would predict.

Figure 1: Size distributions of precipitates in AlLiSc alloy measured with TEM.

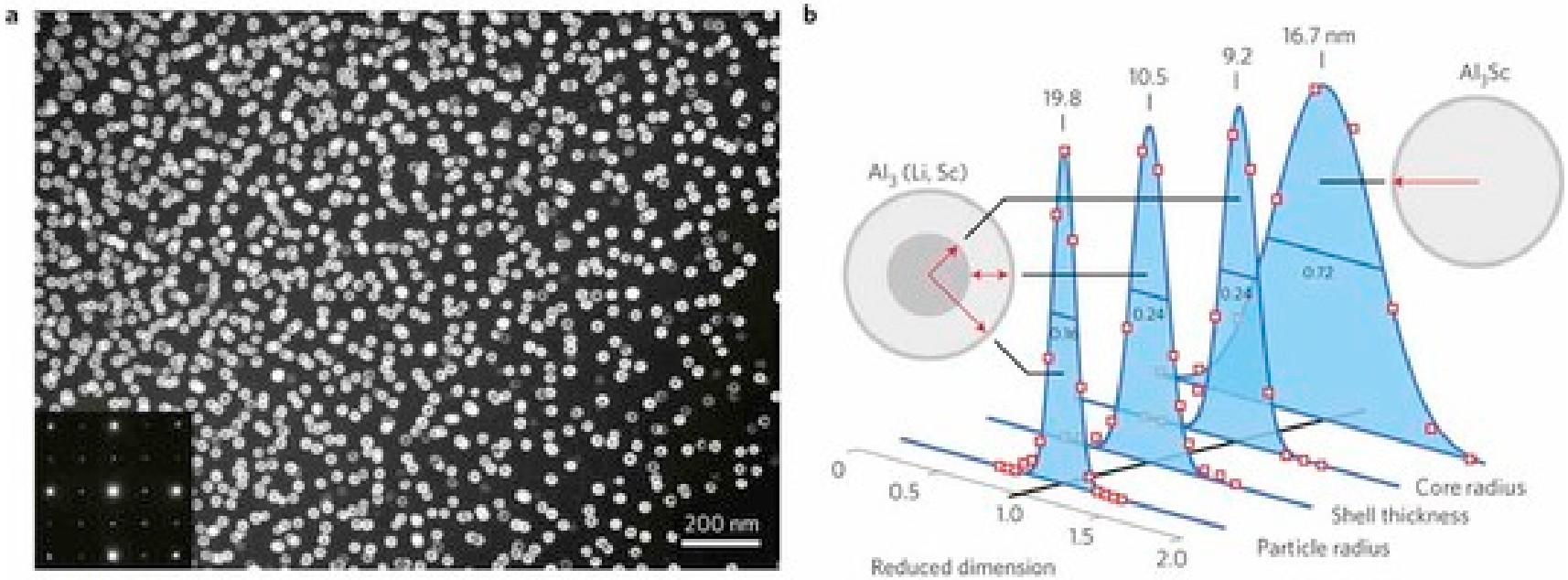

Dark field micrograph of an AlLiSc alloy, showing a remarkably uniform distribution of core–shell precipitates with L12 structure. The selected area diffraction pattern inset shows strong fcc reflections and weaker L12 superlattice reflections in a square pattern typical of an 〈001〉 crystal orientation. (b) Particle size distributions comparing core, shell and core–shell sizes in the present alloy with the much broader distribution of a typical AlSc binary alloy. FWHM divided by mean shown on each distribution.

Mean core radius: 9.2 nm
Shell thickness: 10.5 nm
Total radius: 19.8 nm

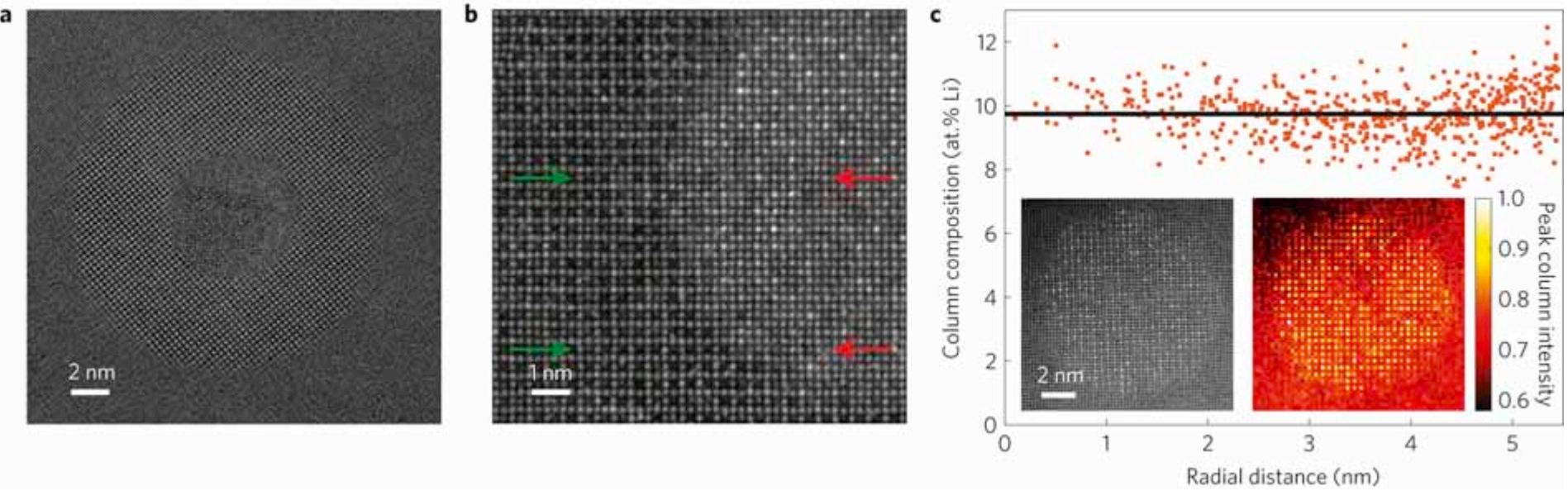

Figure 2: Characterization of a single Al_3(Li,Sc) core–shell precipitate in Al.

a, High resolution TEM micrograph. (b), HAADF image of the core–shell interface; arrows show perfect alignment of the (Sc, Li) sublattice (red arrows) in the core with the Li sublattice (green arrows) in the shell. c, Li composition in atomic columns obtained from intensity measurements normalized to the local neighborhood of the Al sublattice in the core region. HAADF – high angle annular dark field TEM

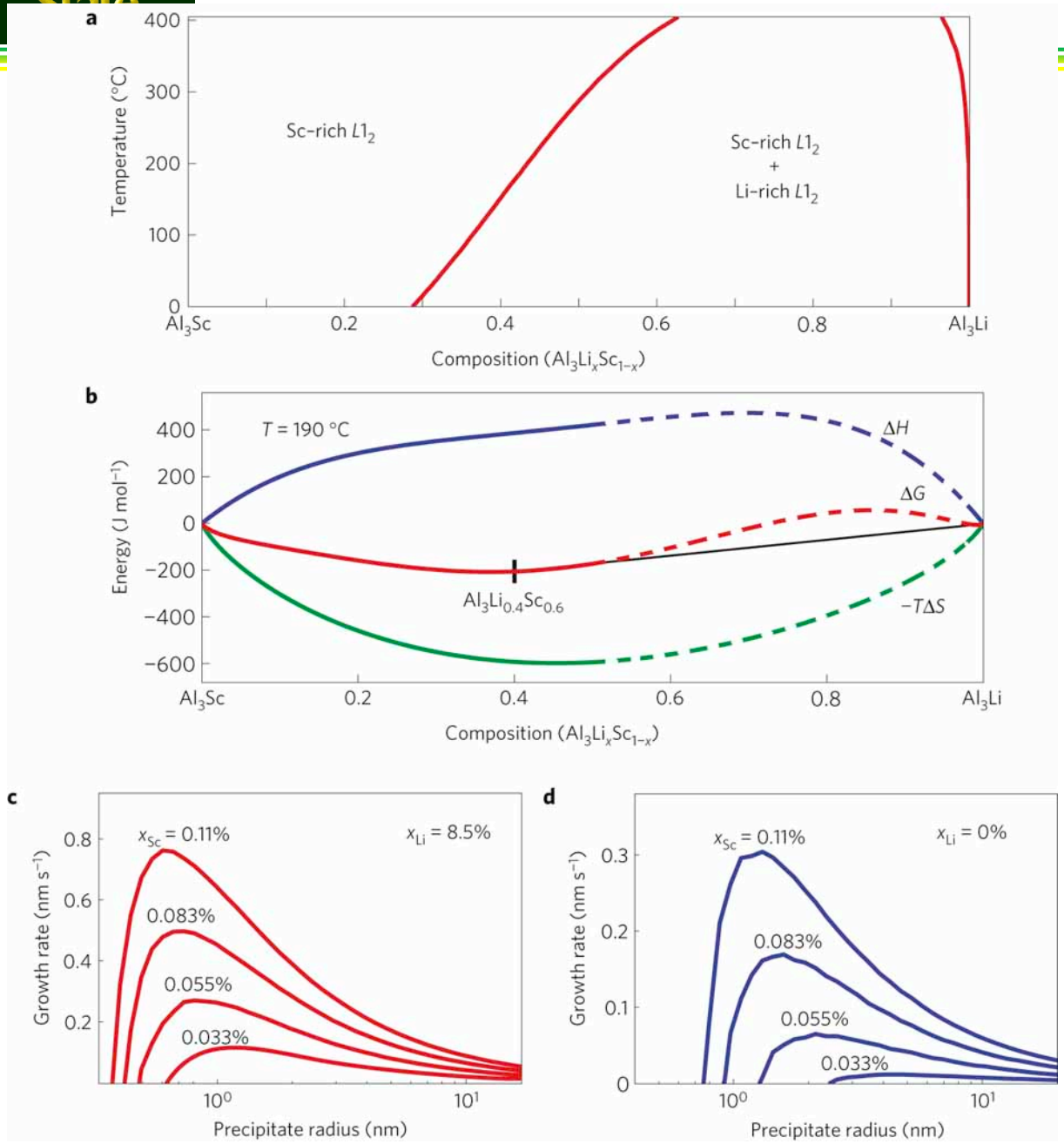

Figure 3: Thermodynamic and kinetic modelling of $Al_3(Li,Sc)$ precipitation.

Calculated phase diagram of Al_3Sc–Al_3 Li pseudo-binary system and **b**, energies at 190 °C. **c**,**d**, Growth kinetics of $Al_3(Li,Sc)$ (**c**) and Al_3Sc (**d**) plotted as a function of precipitate radius and matrix Sc solute concentration. x_{Li} a nd x_{Sc} refer to the matrix solute concentrations.

Explanation of narrow size distribution obtained uses Kuehmann, Voorhees theory that states:
Particles grow or shrink at a rate determined by the solute diffusion in the matrix phase.

During the first heat treatment: Adding Li to AlSc decreases energy barrier to nucleation and accelerates nucleation rate of Al3Sc by 5 orders of magnitude. (Increase Sc concentration- supersaturation)
Li increases growth rate
Li lowers the critical radius (dr/dt=0)

To keep the distribution narrow, the annealing time is set not too long – in this way agglomeration is prevented.

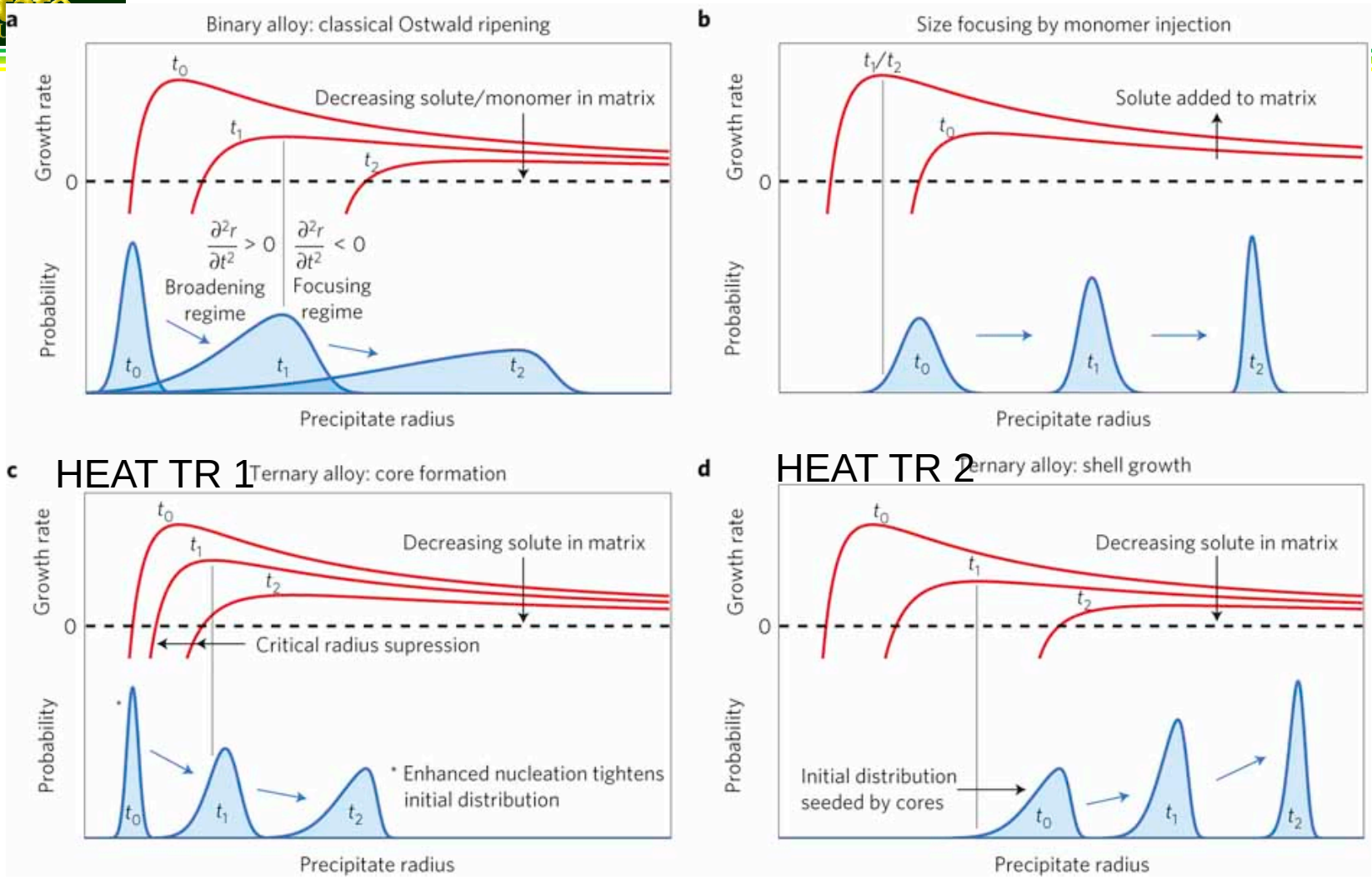

Figure 4: Comparison of the evolution of precipitate sizes using the method described in this study with classical Ostwald ripening and an alternate route used in colloid synthesis. Precipitate growth rates and size distributions as a function of size are shown for three time steps for a, classical Ostwald ripening in a typical binary alloy, b, size focusing in a colloidal solution using solute injection17, c, core formation and d, shell growth used in this study. The vertical divider line separates the broadening from the focusing regime for time t1.

POTENTIAL FOR

FORMATION OF NARROW SIZE PARTICULATES WITH CONSIDERABLY LOW ONSET FOR CORSENING – THIS WOULD RESULT IN MICROSTRUCTURES WITH INCREASED HIGH TEMPERATURE STABILITY

TAILORING PROCESS COULD LEAD TO BIMODAL DISTRIBUTION IN SIZE

Two dimensional structures: Self assembly

Molecules or small components as small particles are spontaneously organized: chemical reactions, electrostatic attraction and capillary forces.

Self assembled monolayers are molecular assemblies that are formed spontaneously by the immersion of an appropriate substrate into a solution of an active surfactant in an organic solvent.

A self assembly surfactant molecule is composed by three parts

- Head group that provides the most exothermic process by chemisorption to the surface of the substrate.
- A chain: exothermic interactions between chains in different molecules is through van der Waals interactions and typically are one order of magnitude smaller than the molecular chain that produces the attachment to the surface.
- Terminal functionality.

Self assembly monolayers consists of ordered and closely packed molecular assemblies that have a two dimensional crystalline like structure, though there exists a lot of defects.

Forces includes hydrophobicity, hydrophilicity, electrostatic forces, capillary forces and chemisorption.

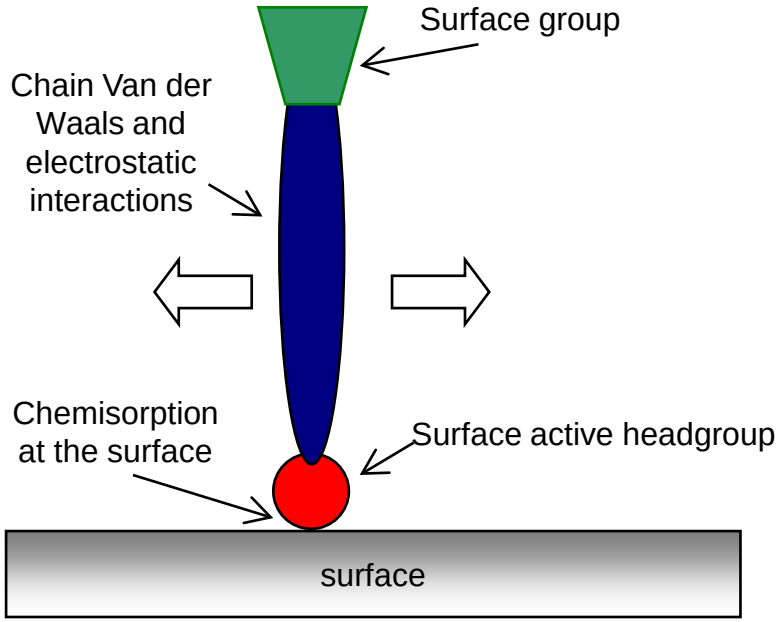

Two dimensional structures: Langmuir Blodgett films

Are monolayers and multilayers of amphiphilic molecules transferred from the liquid gas interface (commonly water/air interface) onto a solid substrate

Molecules insoluble in water with one part hydrophobic and a part hydrophilic are called amphiphilic. These molecules are located in the water/air interface, with the hydrophobic part residing in the air or in a non polar solvent.

The LB technique is unique as these monolayers established in the liquid interface can be transferred to different substrates.

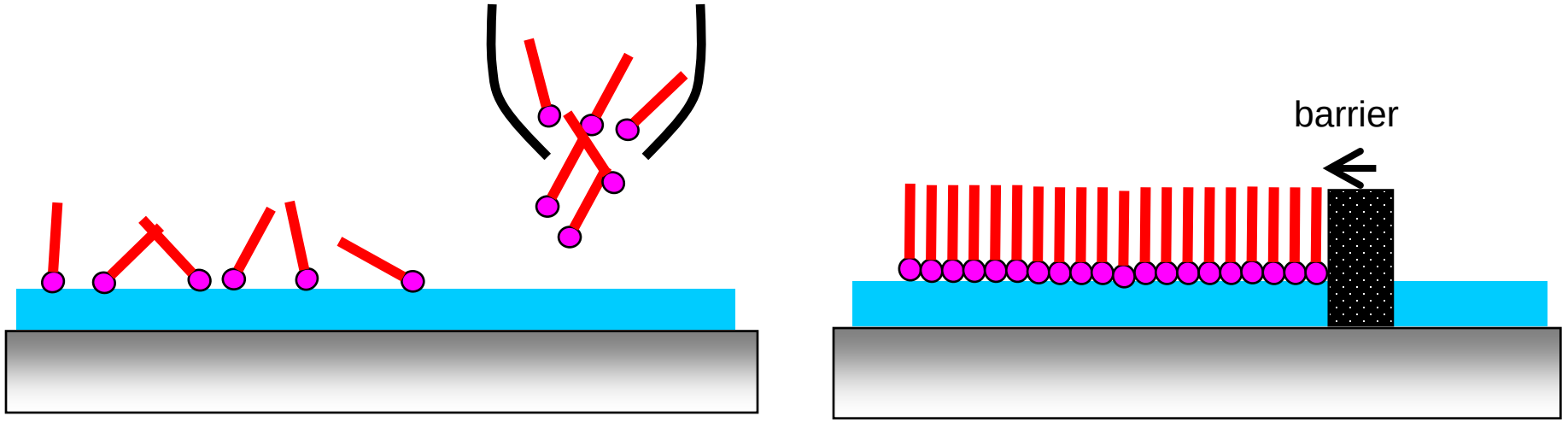

The drop of an amphiphilic molecule in a volatile solvent in spread on the water-air interface of a sample. The solvent evaporates. The barrier moves to compress the molecules and align them on the surface

Two dimensional structures: Langmuir Blodgett films

To transfer monolayers from the water/air interface to the substrate, the most common method is the vertical deposition.

Another to transfer a monolayer to a substrate is the Schaefer's method or horizontal lifting. This method is very well suited to transfer very rigid films

Thermal stability and order-disorder transitions are two important issues for any practical application of the LB films.

LB films allow the possibility to design and construct stable organic super-lattices.

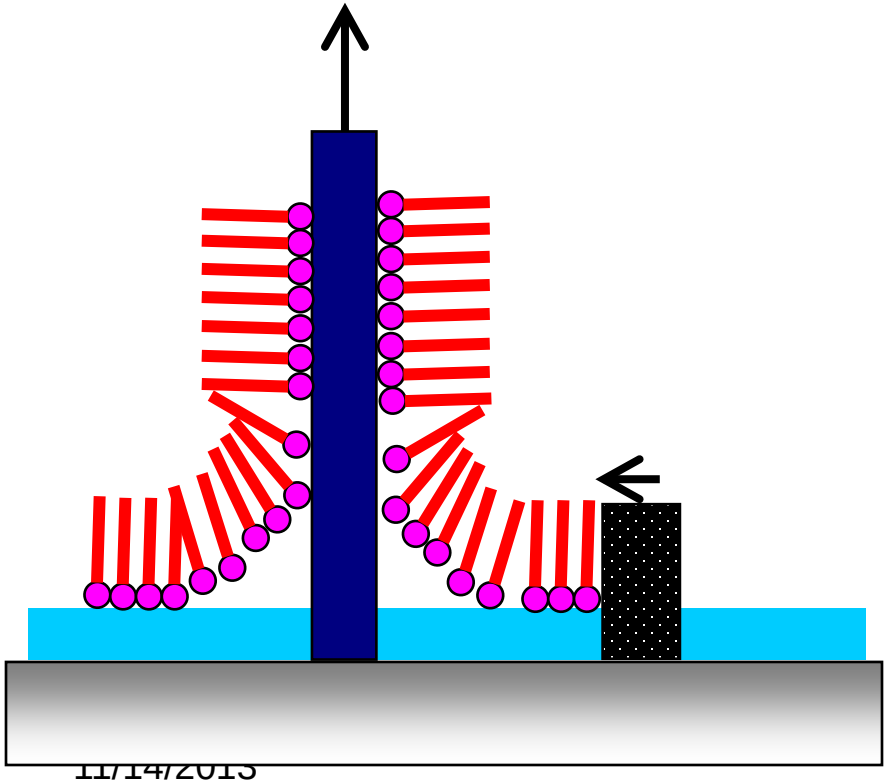

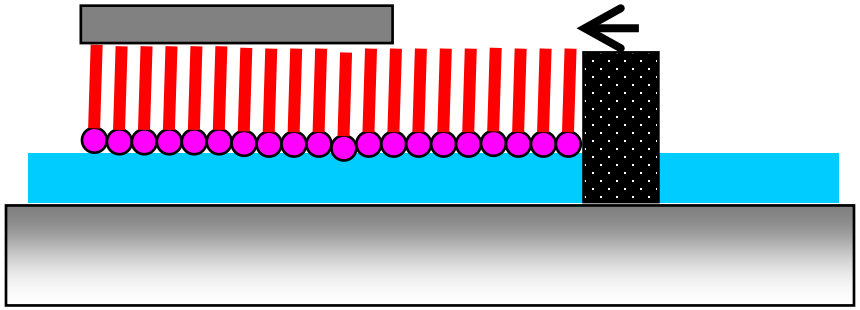

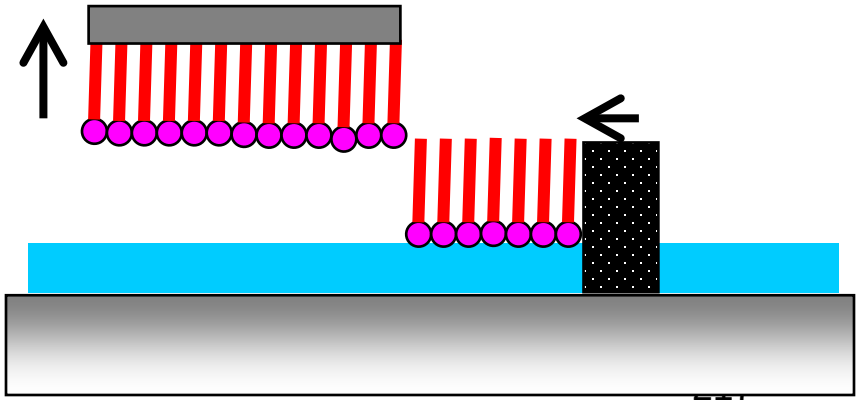

Self Assembly

This is a “bottom-up” approach. The final structure is achieved when the ensemble of the building blocks reaches its minimum free energy state in which the attraction and repulsion interactions between the components in the surface are well balanced.
The building blocks can be divided in three categories depending on its size: molecular self assembly, nanoscale particles (such as colloidal particles) and meso to macro scale dimension objects.
In the first category the interaction forces are based on electrostatic, hydrophobic or Van der Waals interactions, etc.. In the second and third categories, the organized assembly of blocks rely on external forces as gravity, electric or magnetic fields.

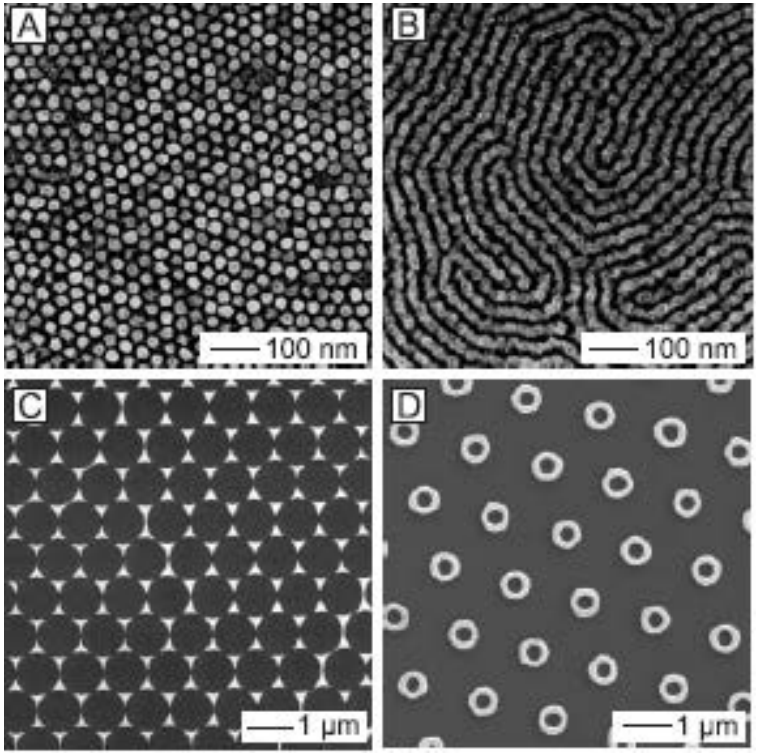

Self Assembly

Phase-separated block copolymers

Block copolymers consists of two or more immiscible polymer fragments jointed by a covalent bond. BC can auto-arrange in large domains which typical size depends on the preparation of the sample and on the characteristics of the particular polymers used.

Nano-sphere lithography

This method uses a monodispersed spherical colloid that are assembled on a surface into a form of a closed packed monolayer with hexagonal symmetry. This monolayer can serve as a mask for subsequent processing of the surface.

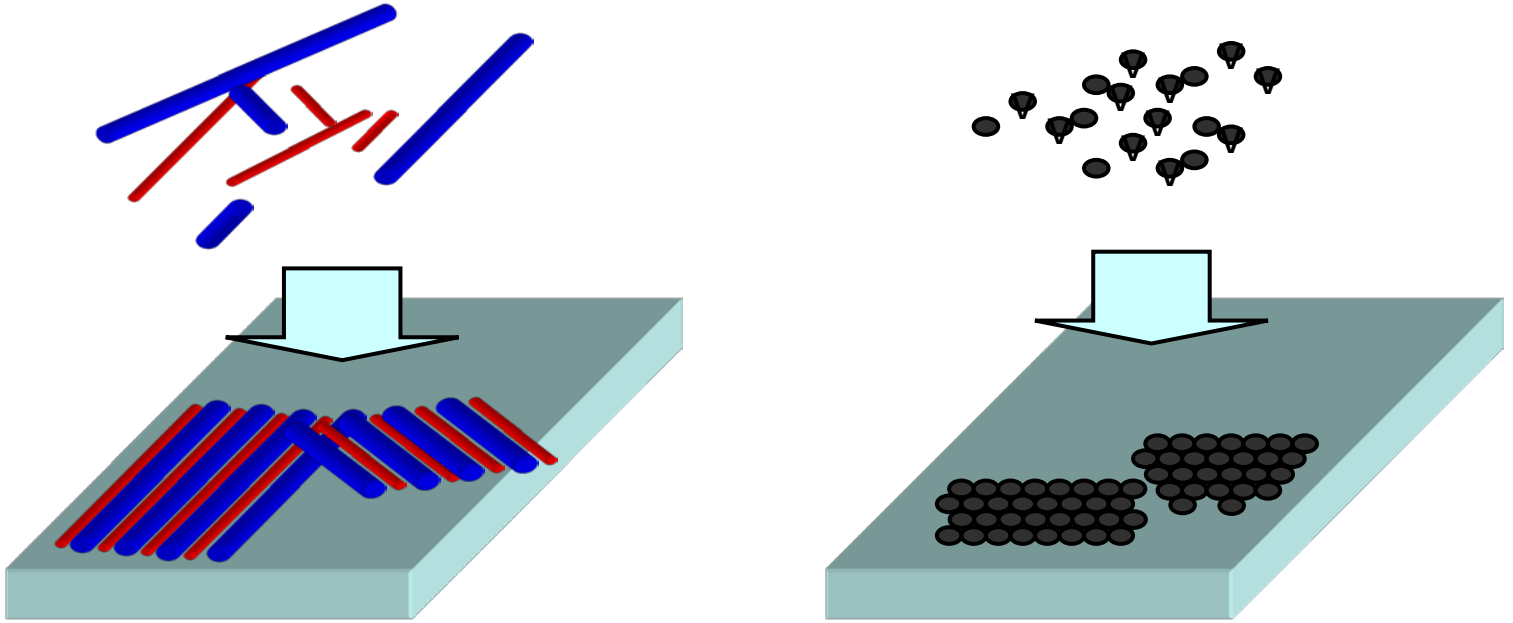

NANOSTRUCTURE CHARACTERIZATION

Scanning tunneling microscope

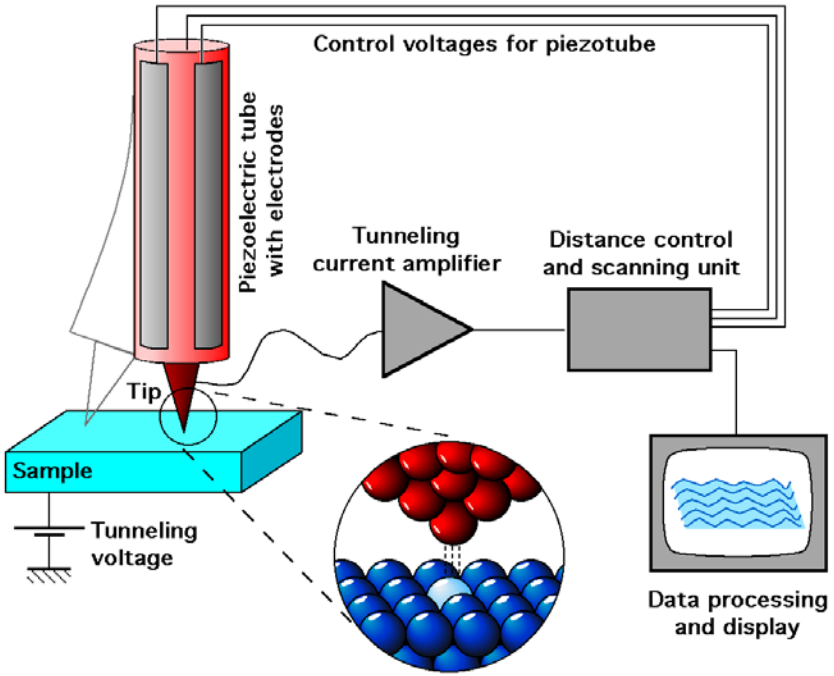

Concept of this apparatus: a fine metallic tip is brought close the surface of the sample (typically few nanometers). When a voltage is applied between the surface and the tip a tunneling current is established. Measuring this small tunneling current it is possible to accurately inspect the surface of the sample with atomic resolution. This is the simple and effective idea that deserved a Nobel Prize.

With tip/surface voltages between 1 mV to 4 V, tunneling currents between 0.1 nA and 10 nA were measured with an exponential dependence with the sample/tip distance. STM can therefore be used to inspect surfaces with atomic resolution.

The current and the sample-tip separation d are related by: $I \approx V \; e^{-2Kd}$

In fact the current is related to the density of states in the tip and the sample

This topography is usually referred as “STM” topography, which is actually a convolution of the topography of the sample with the density of states in the two electrodes (tip and sample).

Scanning tunneling microscope

The tips are made simply by pulling metal wires (typically 200 to 250 microns in diameter) using pliers.

A more consistent way to fabricate tips is using electrolysis. When the tip becomes very thin, it breaks living a very sharp tip appropriate to be used in the STM. The electrolytic bath is usually a solution of NaOH.

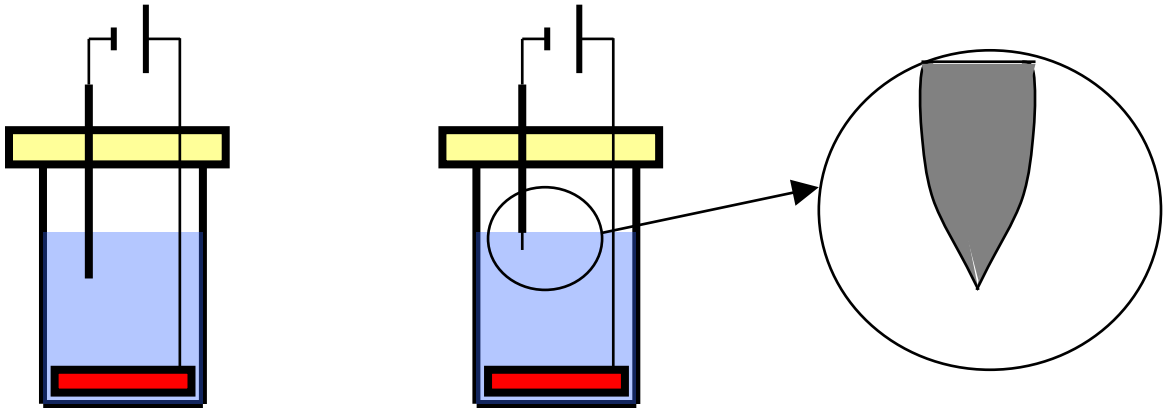

Tunnel Current

To characterize the tunneling current let us consider the gap between the sample and the tip produces a potential barrier of height U. The wave function Ψ(z) associated with a particle of energy E less than U is given by

$$\Psi(z) = \Psi(0)\ e^{-kz}$$

$$k = \sqrt{2m(U-E)}\Big/\hbar$$

The probability of a particle being inside the barrier is proportional to

$$\left|\Psi(0)\right|^2 \exp(-2kz)$$

For a metal tip, since the tip-sample polarization (or bias) is very small in normal operation, the quantity (U – E) can be directly replaced by Φ the work function of the metal. The value of Φ represents the height of the tunnel barrier between a tip and the metal surface.

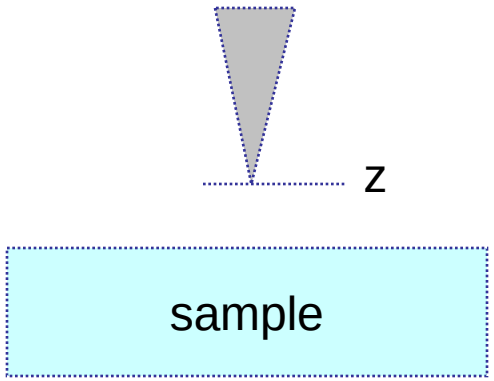

For metals (tip or sample) used in STMs (W, Pt, Au, Si, etc), Φ is of the order of 5 eV, which means that the factor k is of the order of 1 A^{-1}.

From the last equation, it can be seen that the current varies by a factor of about 10 per Armstrong unit.

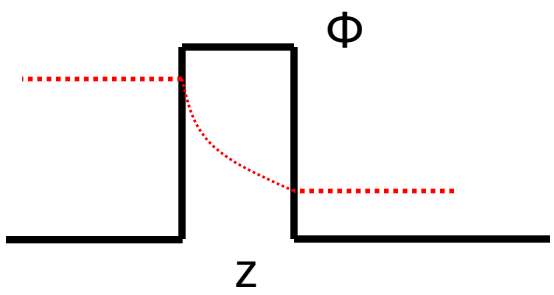

Resolution

The spatial resolution of the STM depends on the tip and the relevant sample states. A simple approach is to assume that there is only one atom at the very end on the tip which participates in the tunneling current. One also assumes that the tip wave function is

$$|\Psi|^2 \propto \frac{\exp(-2kr)}{r^2} \qquad r = \sqrt{x^2 + z^2}$$

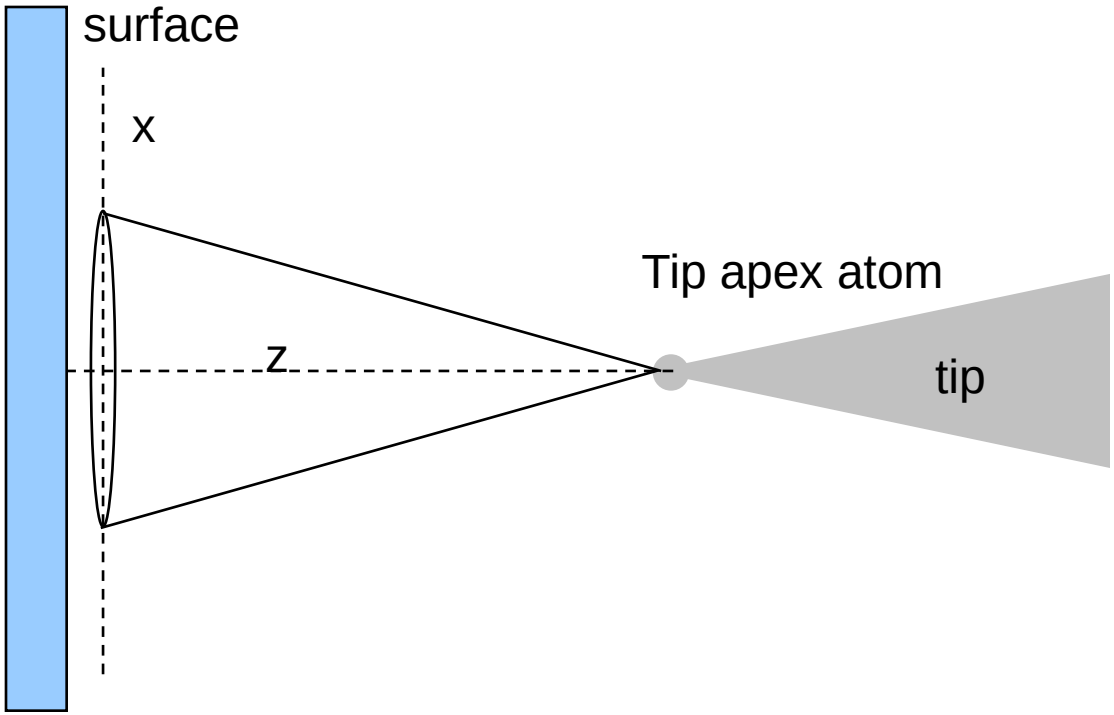

Resolution

Assuming that z is much bigger than x the squared amplitude of the wave function in a plane close to the surface S can be approximated by a Gaussian function of x

$$|\Psi|^2 \approx \frac{\exp(-2kz)}{z^2}\exp\left(-\frac{kx^2}{z}\right)$$

This shows that the amplitude decreases with the lateral displacement x. The full width at half maximum of the Gaussian is

$$\Delta x = \sqrt{\frac{2z}{k}}$$

With $k \approx 1\,A^{-1}$ and z given in angstrom units the resolution is of the order of $1.4\sqrt{z}\ A$.

The distance between the tip and the surface is effectively z = d + R, where d is the tip-sample distance and R is the curvature of radius of the tip.

Consequently the best possible spatial resolution is given by $1.4\sqrt{R}\ A$.

The practical problem here is to know the radius of curvature of the tip.

In fact the tunneling current is often due to small protuberances with very small radius, which explains the images obtained with atomic resolution.

The nature of the wave function of the tip also influences the resolution.

Contrast

The contrast of the observed image depends on the measurements conditions, in particular the tip to sample distance. An approximate formula for the contrast is

$$\Delta z \approx \frac{2}{k} \exp\left[-2z \left(\sqrt{k^2 + \frac{\pi^2}{a^2}} - k \right) \right]$$

For large lattice periods, i.e. $a >> \pi/k$ the contrast is high and almost independent of the distance.

Typically, for Φ = 4 eV, the contrast tends to 1.6 A for a = 12 A.

However when $a << \pi/k$ the contrast tends to $\Delta z \to \exp\left(-\frac{\pi^2 \, z}{a^2 \, k} \right)$

a: lattice constant of sample

Tip - sample interactions

When the tip is brought near the surface, the tip-sample interaction increases and it becomes possible to tear atoms from the surface and manipulate the adsorbed atoms (adatoms) by sliding them across the surface. The different possibilities are

Pulling mode. This mode uses the attractive forces between the tip and the adatom. The tip is positioned above the adatom and then brought towards the surface. The tunnel current increases. The tip is then moved horizontally. The current subsequently falls off until the adatom undertakes a hop towards the tip, while remaining on the surface. The current increases once more and the procedure continues.

Pulling mode

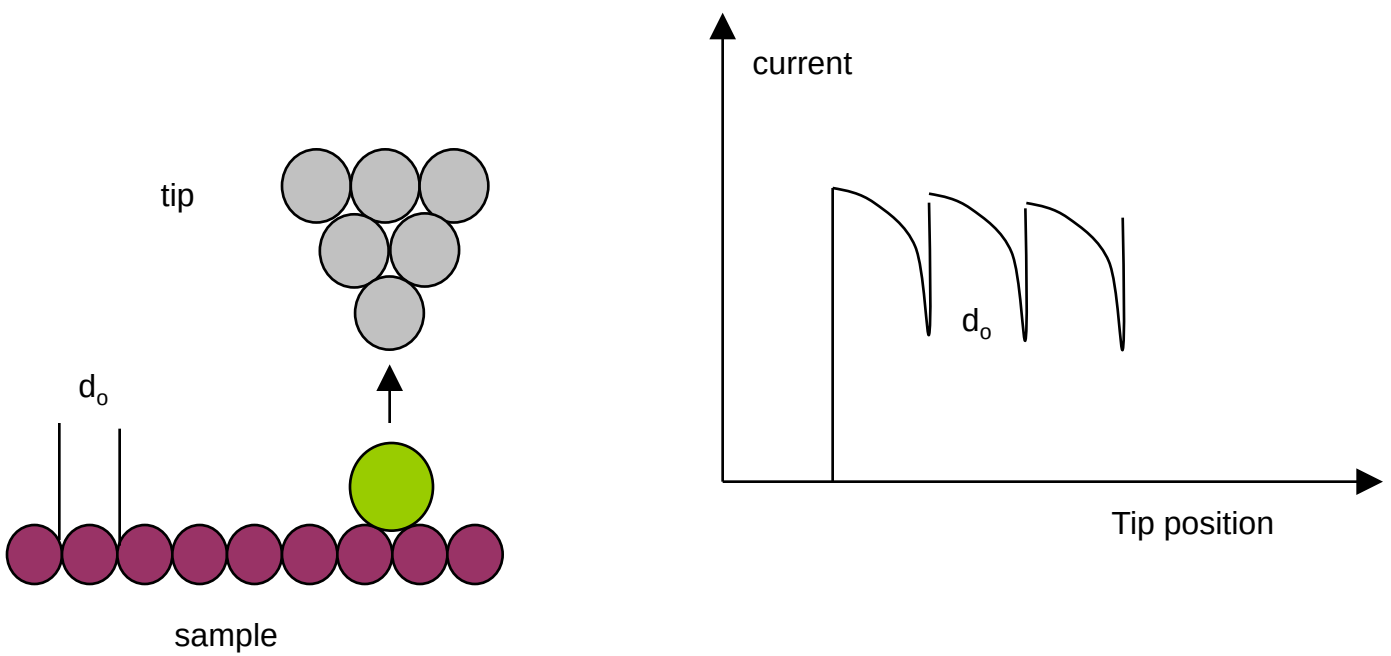

Tip - sample interactions

Pushing mode. This is similar to the pulling mode except that it makes use of repulsive forces between the tip and the adatom. The tip is brought towards the surface and moved horizontally towards the atom. The latter jumps to the neighboring surface site. The current falls abruptly and the procedure continues

Sliding mode. In this mode the forces between the tip and the adatom are attractive, but the tip is so close to the surface that the adatom is attached onto it. As the tip approaches, the current increases and the adatom jumps onto the tip and remains there. When the tip moves horizontally parallel to the surface the current is related to the surface topography as seen by the tip with the attached adatom. Finally the tip is withdrawn and the adatom falls back onto the surface

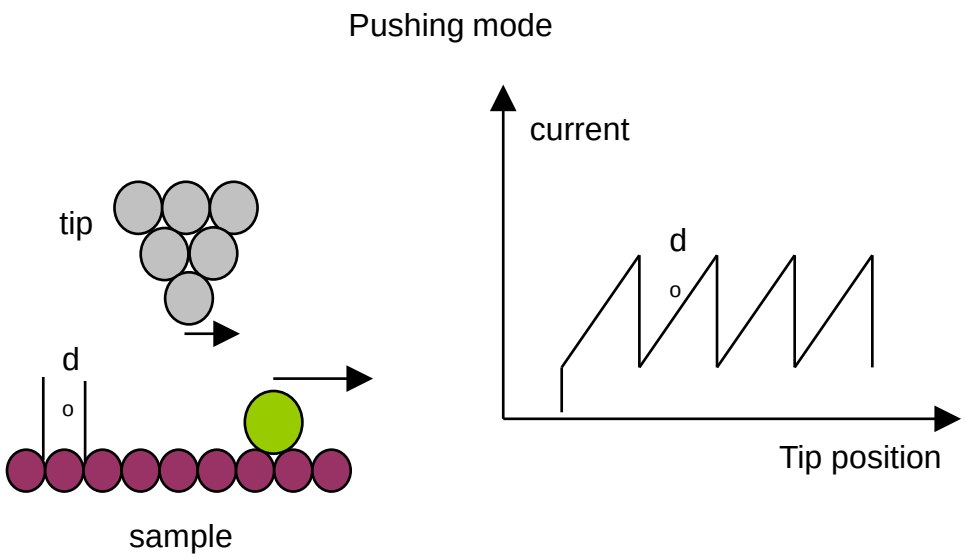

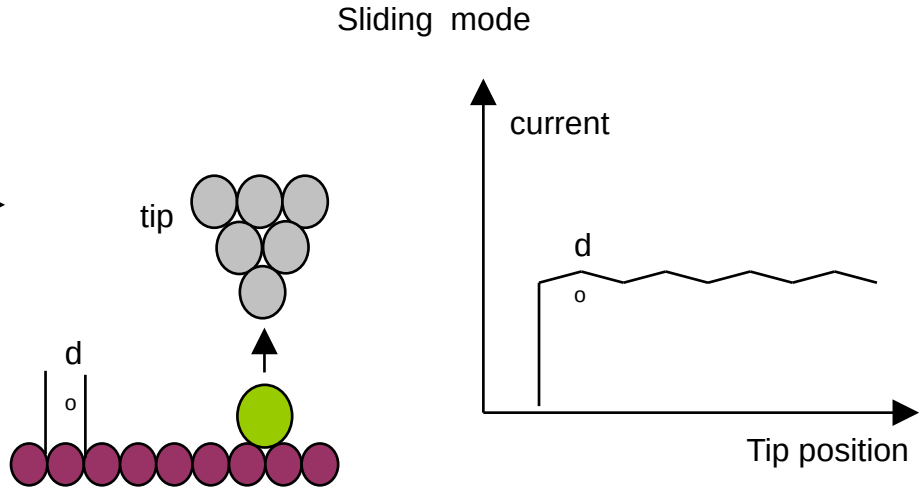

Tip - sample interactions

With these manipulation modes it is possible to move single atoms on the surface of a crystal. With this atomic manipulation technique it was possible to arrange organized arrays of molecules or to fabricate a “quantum corral” where the interference of the wavefunctions of the atomsis evident in the STM image.

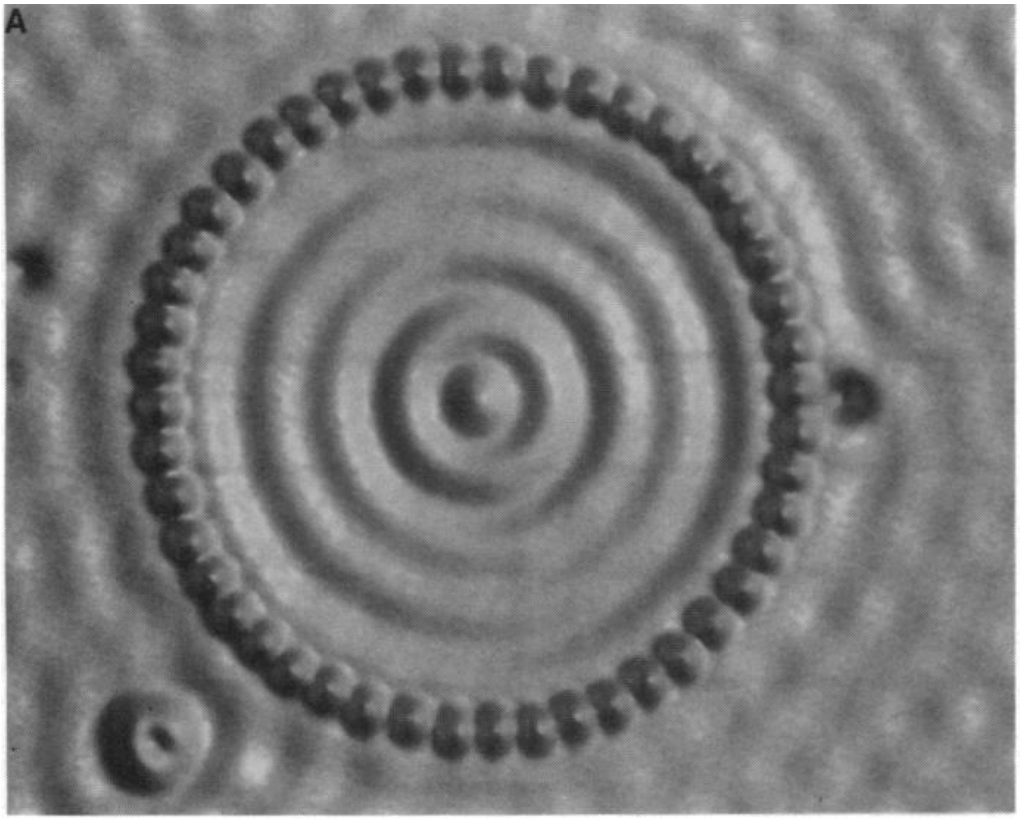

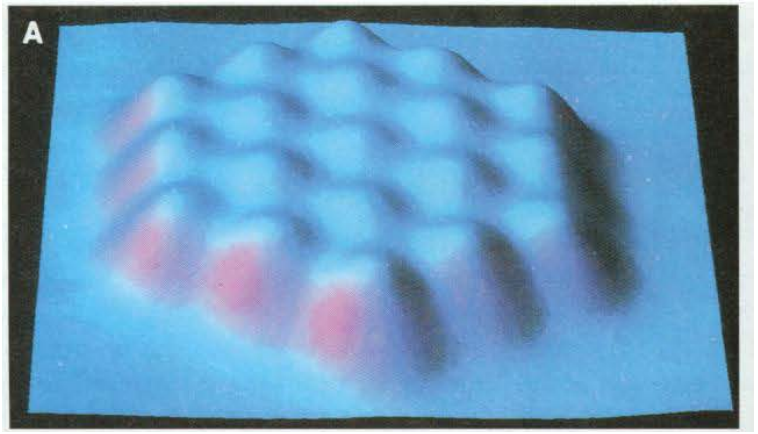

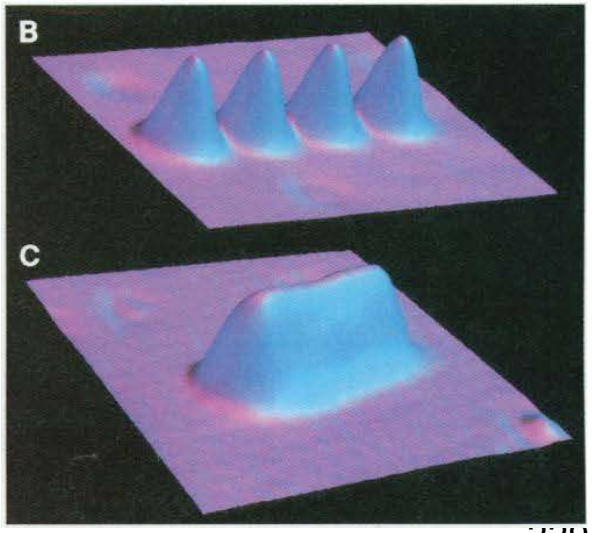

Atomic force microscopy

The atomic force microscope (AFM) is without doubt the most widely used instrument among the local probe devices. It gives quick access to a wide range of surface properties including mechanical, magnetic, electrical, and other properties with good spatial resolution. Furthermore, it can operate in air, vacuum or solvent. The AFM can provide invaluable aid in the study of materials, chemistry and physical chemistry, but it is also used for basic research.

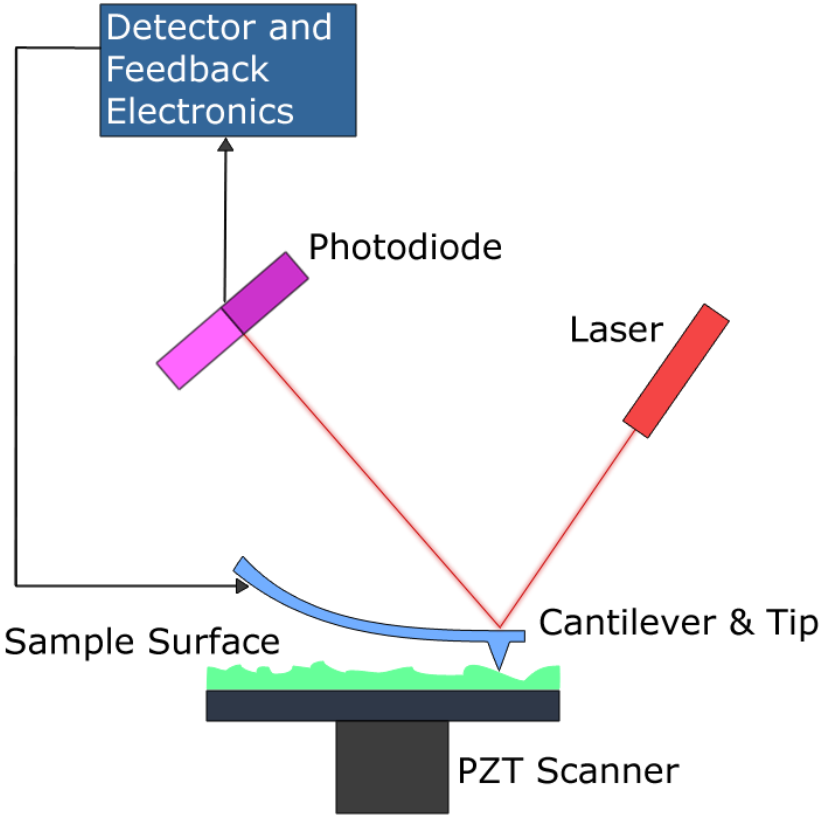

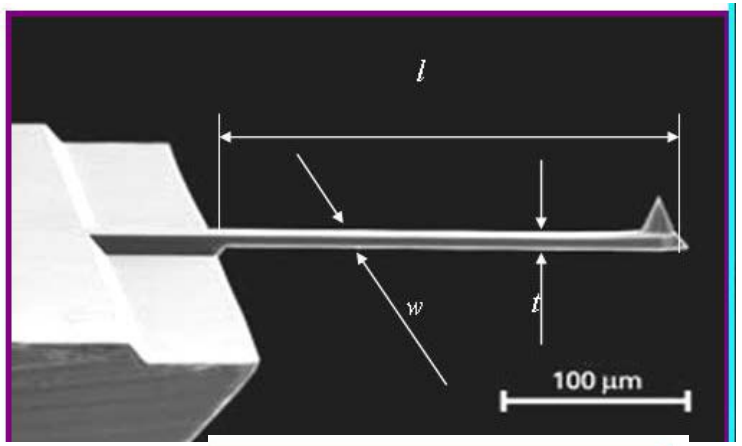

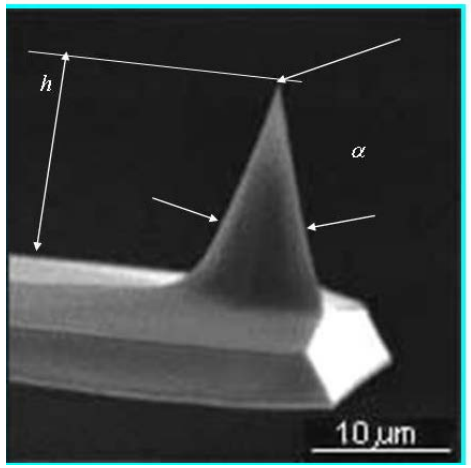

Imaging Modes

Suppose that the sample is made from a non-deformable material.
The tip-sample interaction can be described as shown below.

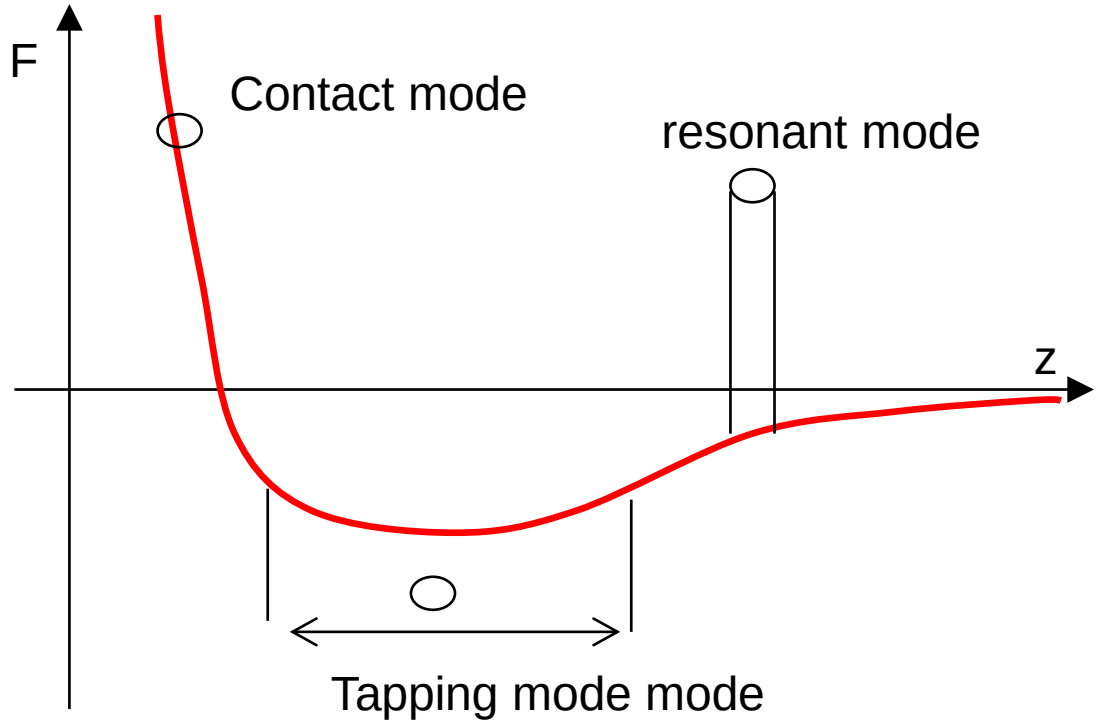

The interaction is attractive at large distances (typically beyond a few tenths of nanometers) due to van der Waals forces and repulsive at very short range due to the impenetrability of the electron clouds associated with the two surfaces.

The different imaging modes are contact mode, friction mode, resonant mode and tapping mode

Image resolution

The vertical resolution of the AFM images is always very good. It is basically limited by the accuracy of the piezoelectric actuators that move the sample (or the tip).
However the lateral resolution has to be considered in great detail.
Suppose that the AFM works in contact mode as a perfect tactile sensor passing over a non deformable surface. The geometric effects due to the finite size of the tip complicate the analysis of the images and the evaluation of the resolution in the lateral direction. Although it is not exactly applicable one can say that the image is the convolution of the surface profile with the tip.

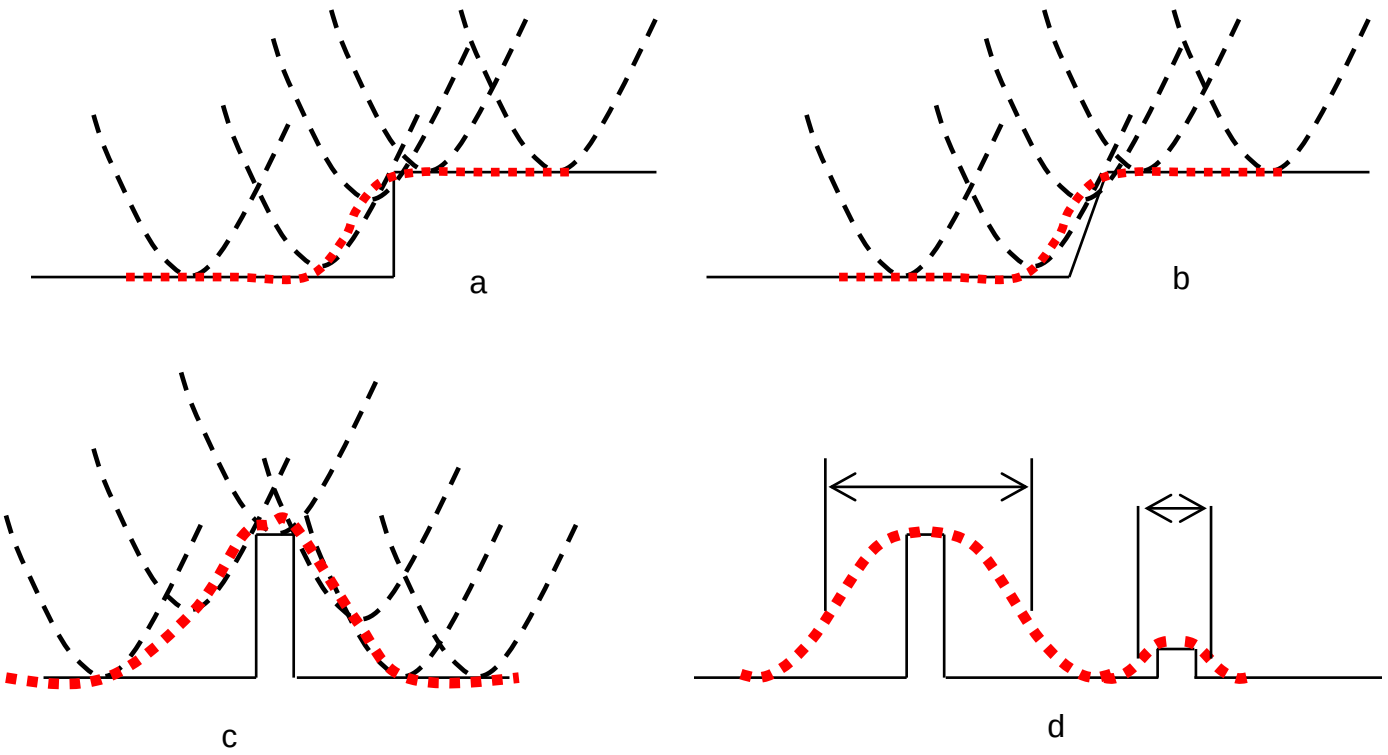

Contact mode

The contact mode can be described on the basis of the so call force curve that represents the variation of the cantilever deflection as a function of the sample height.

In these curves the deflection angle of the cantilever is plotted as a function of the distance z between the tip and the surface.

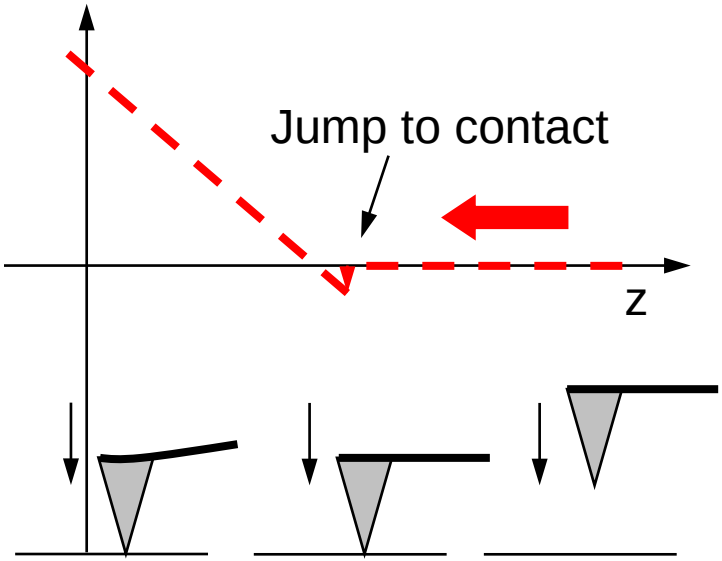

APPROACH

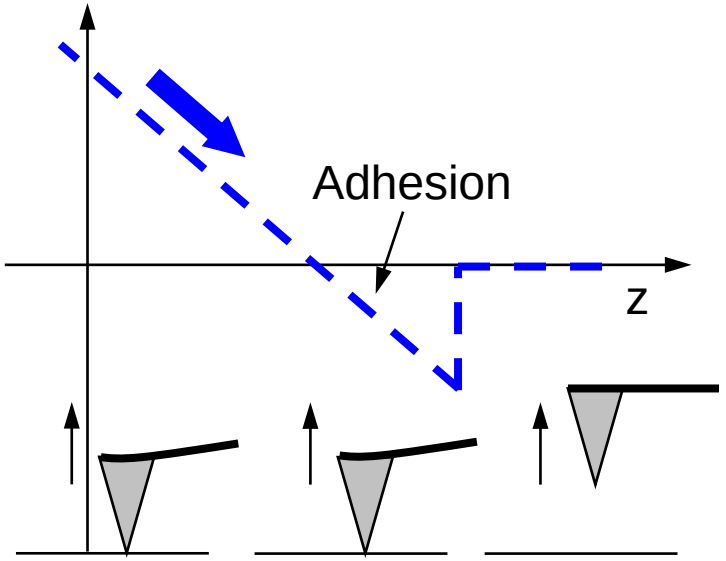

RETRACT

The adhesion effect is manifested through the “hysteresis” of the force curve. It is caused by a combination of van der Waals forces, electrostatic forces, capillary forces in liquids, etc..

These interactions are then modified by the pH, ionic forces and so on. So it is possible to use a very sensitive AFM to sense the physics-chemistry characteristics of a surface.

Contact mode

If the surface of the sample is deformable, once the tip is pressed towards the surface it can penetrate the sample surface
Once contact has been established, the tip is pressed against the material by the elasticity of the cantilever.
It may penetrate the surface so the observed deflection will be smaller than expected in a rigid material. The deflection will depend both on the stiffness of the cantilever and the surface.
If the sample is viscoelastic, the curve will distort when one modifies the operating frequency, tip shape, maximal penetration in the material, and so on.

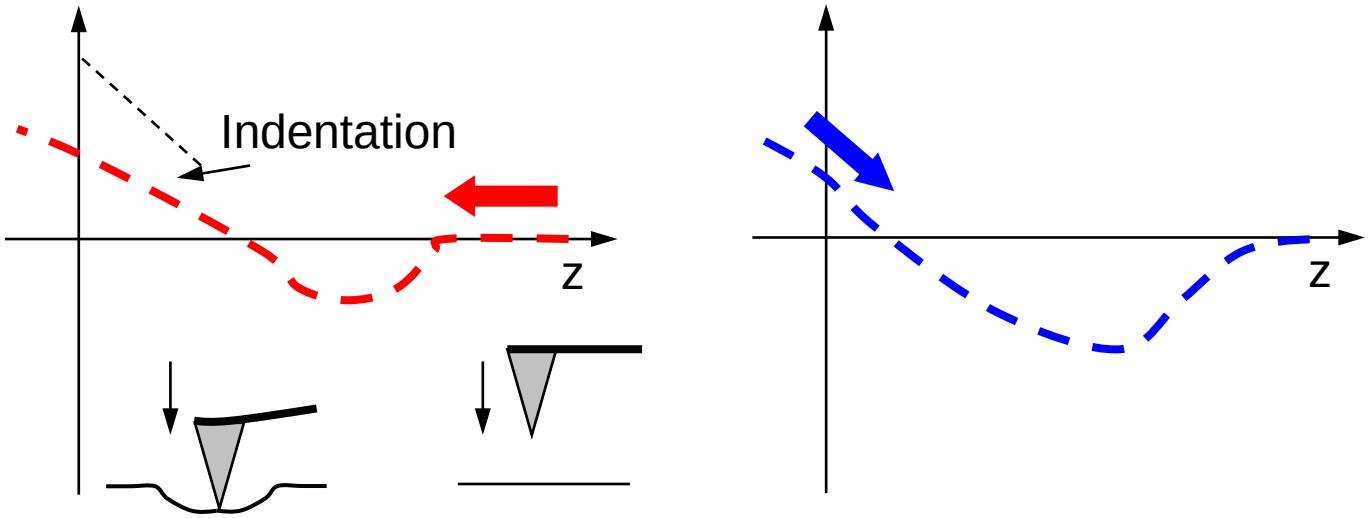

APPROACH

RETRACT

Resonant modes

The cantilever is a beam clamped at one end, is a very good mechanical oscillator. Dissipation mainly caused by the viscosity of the ambient medium.

The resonant frequency is modified by the tip-surface interactions. Two techniques are used.

1. Drive the cantilever at a fixed frequency close to the resonant frequency and follow the variation of the amplitude and possibly also the phase. This technique is often called amplitude modulated AFM (AM-AFM)
2. Set up a phase locked loop which holds the vibration amplitude and phase difference at pre-assigned values. The servo controlled system then begins to self oscillate and its resonance frequency is continuously monitored. This dynamic mode is called frequency modulated AFM (FM-AFM)

The equation that describes de displacement of the cantilever is

$$\ddot{x} + 2\beta\dot{x} + \omega_0^2\, x = \gamma \cos\omega t + \frac{f(D,t)}{m}$$

where x is the position of the oscillator, ω_0 is the resonant frequency, γ is the amplitude of the excitation at the frequency ω; β is the dissipation term such that the quality factor is given by

$$Q = \omega_0 / 2\beta$$

where m is the effective mass of the oscillator determined by $\omega_0 = k/m$

and k is the stiffness of the cantilever.

The function f(D,t) is the tip-sample interaction, where D is the tip-sample separation when the cantilever is not deflected.

Resonant modes

The simplest case occurs when the interaction force depends only on the tip-sample separation D+x. More complex behavior is observed if dissipation comes into play due to adhesion, viscosity or capillarity. Even in the simple case described by $f(D,t) \equiv F(D+x)$

the equation governing the system is not generally linear.

$$\ddot{x} + 2\beta\dot{x} + \omega_0^2\, x = \gamma \cos\omega t + \frac{F(D+x)}{m}$$

Linear resonant mode: corresponds to a non dissipative interaction and a very low amplitude oscillation far from the sample surface (X<<D). Expanding the interaction to first order in x the former equation gives:

$$\ddot{x} + 2\beta\dot{x} + \omega_0^2\, x = \gamma \cos\omega t + \frac{F(D)}{m} + \frac{F'(D)}{m}x$$

F'(D) is the gradient of the force at the central position of the oscillation.

The constant term shifts the rest position of the tip $F(D)/k$ which is generally negligible compared with the oscillation amplitude. We thus obtain a new equation expressed relative to the new mean position

$$\ddot{x} + 2\beta\dot{x} + \left(\omega_0^2 - \frac{F'(D)}{m}\right)x = \gamma\cos\omega t \quad \longrightarrow \quad \omega_0^{2\,\prime} = \omega_0^2\left[1 - \frac{F'(D)}{k}\right]$$

Non-linear (tapping mode)

If the tip oscillates close to the surface, or if the amplitude of the vibration is large, a first order approximation is not longer valid.

In this case the oscillator is non linear. However the deflection remains quasi sinusoidal.

$$\ddot{x} + 2\beta\dot{x} + \omega_0^2\, x = \gamma\cos\omega t + \frac{f\left(D,t\right)}{m} \longrightarrow x = A\cos\left(\omega t - \varphi\right)$$

The tip-sample interaction causes energy dissipation, which can be calculated as follows:

Energy dissipated in one cycle:

$$U_{diss} = \oint f\left(D,t\right)dx$$

$$U_{diss} = Am\gamma\left(\frac{2A\beta\omega}{\gamma} - \sin\varphi\right)$$

Applications to nanotechnology

Oxidation of Si in air under the AFM tip in intermittent contact one can produce linear oxide structures of width 15 nm and height about 1 nm. By chemical etching then Si nanowires can be fabricated .

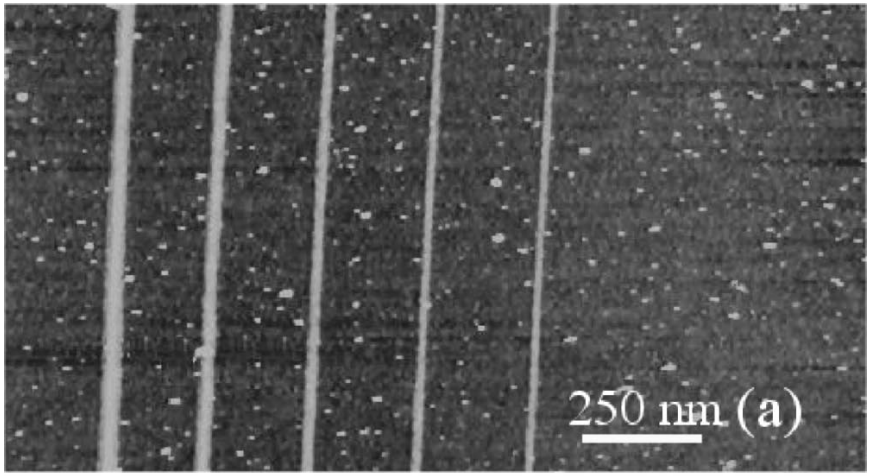

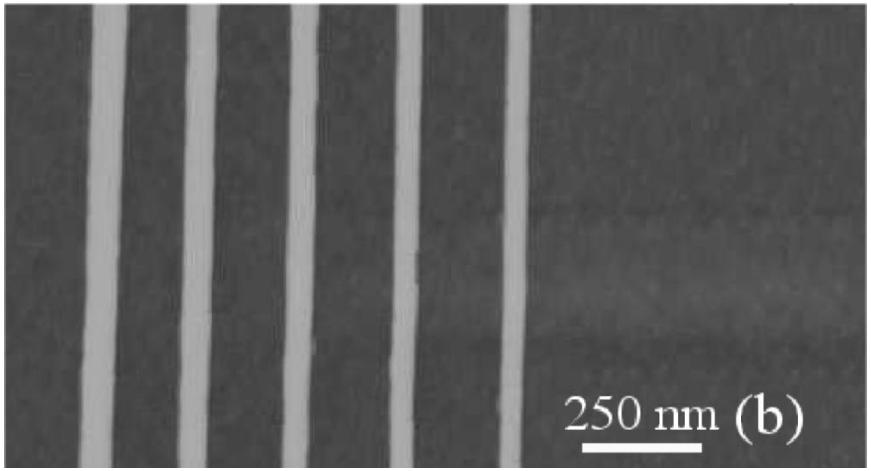

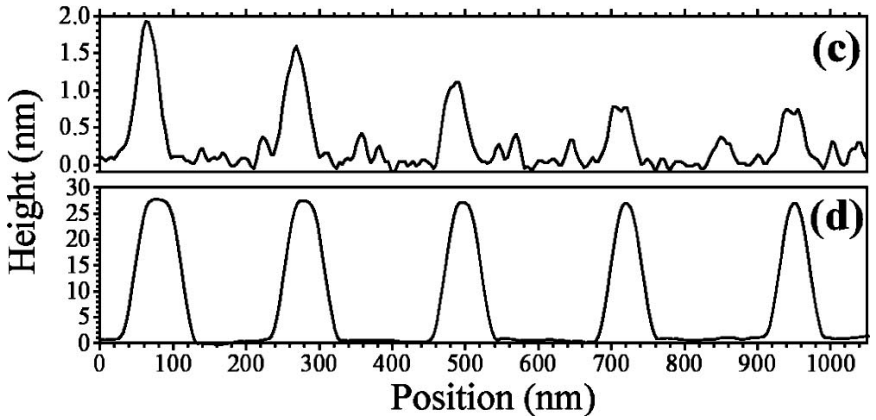

Applications to nanotechnology

Write with the AFM tip like the nib of a fountain pen. After dipping the tip into a thiol solution, the gold sample sample-tip contact is used to transfer molecules though the water meniscus whence they form a self-assembled lattice. A line thickness of 30 nm can be obtained by this simple procedure.

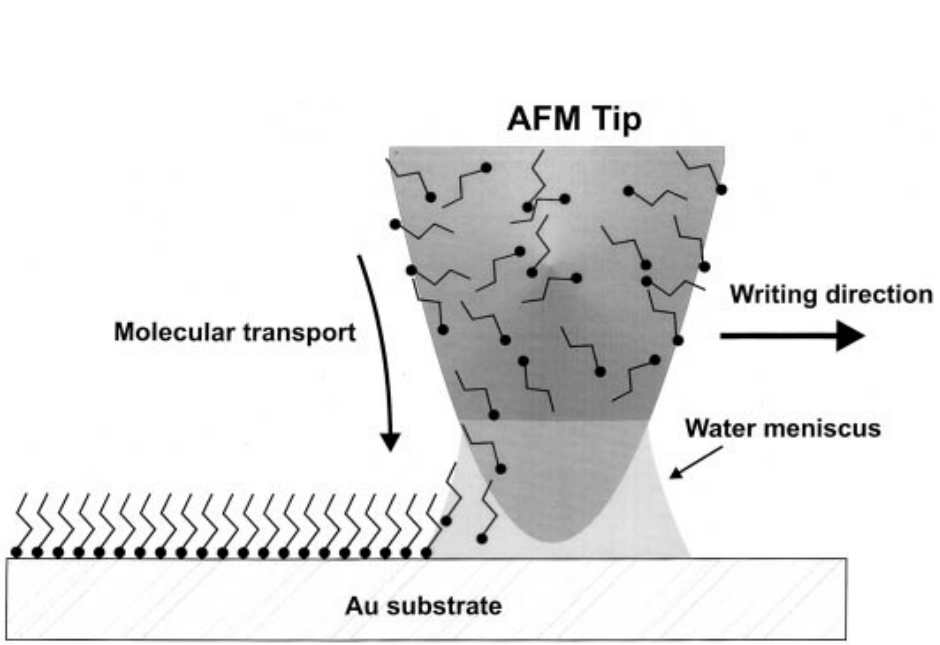

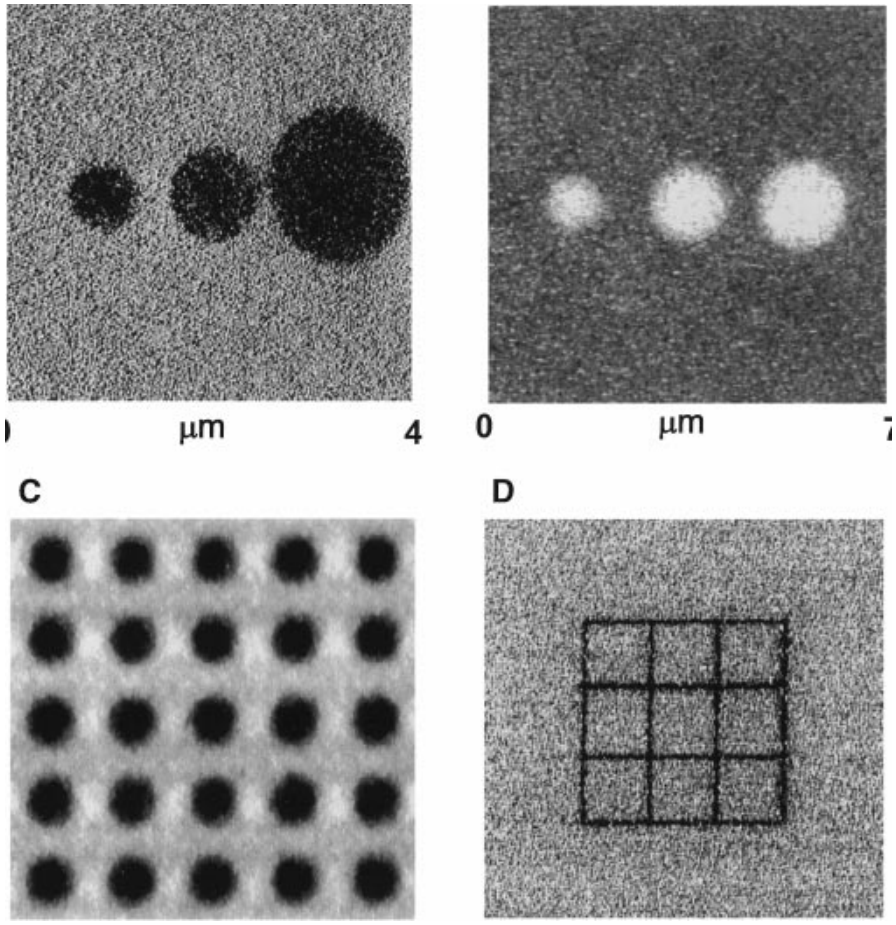

MOTIVATION

There are many types of microscopes- each with unique characteristics and specific applications

Microscope Type	Detect	Resolution	Contrast
visible light	transmitted light	500 nm	bright field
		500 nm	phase contrast
	scattered light	500 nm	dark field
	fluorescence	50 – 500 nm	label
electron microscope (TEM)	scattered electrons	0.1 – 1 nm	heavy metal stain
scanning electron micr. (SEM)	secondary electrons	3 – 10 nm	surface relief
scanning tunneling micr. (STM)	tunneling current	0.1 nm	surface atoms
scanning force micr. (AFM)	force on probe tip	0.5 nm	surface relief
X-ray projection microscope	transmitted X-rays	>1000 nm	absorption
X-ray microscope (TXM)	transmitted X-rays	25 nm	absorption
		25 nm	phase contrast
scanning X-ray microscope (STXM)	transmitted X-rays	25 nm	absorption
			XANES (chemical)
nanoprobe	fluorescence	30 nm	elements
	diffraction	30 nm	strain

Resolution of optical systems depends on the wavelength

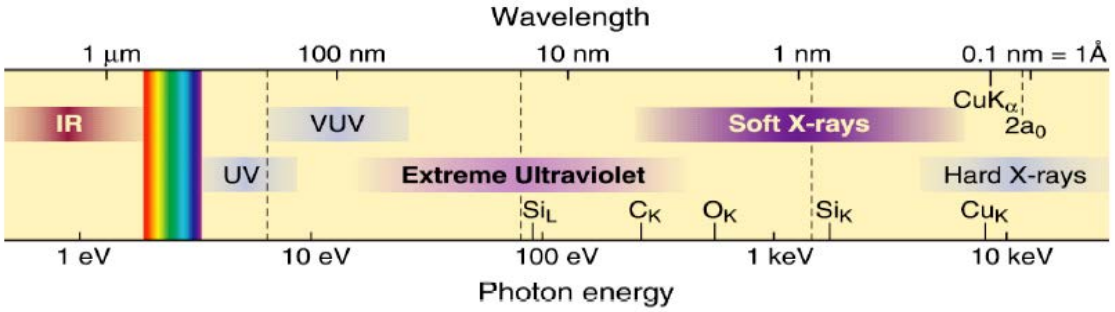

$$\text{Spatial Resolution} = \frac{k\lambda}{NA}$$

visible light

λ = 500 nm

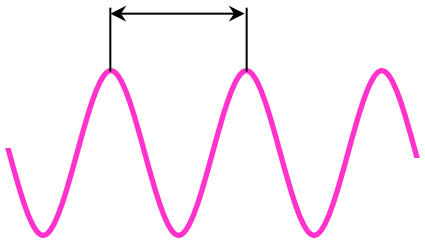

Extreme ultra-violet and soft x-ray light

λ = 1 - 50 nm

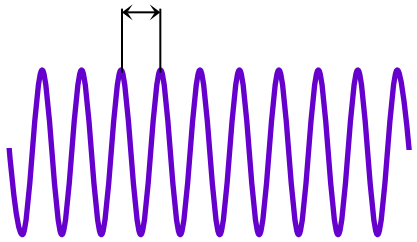

EUV and SXR microscopy can potentially resolve full-field images with 10-100x smaller features than conventional visible microscopy

Anatomy of a full field optical microscope

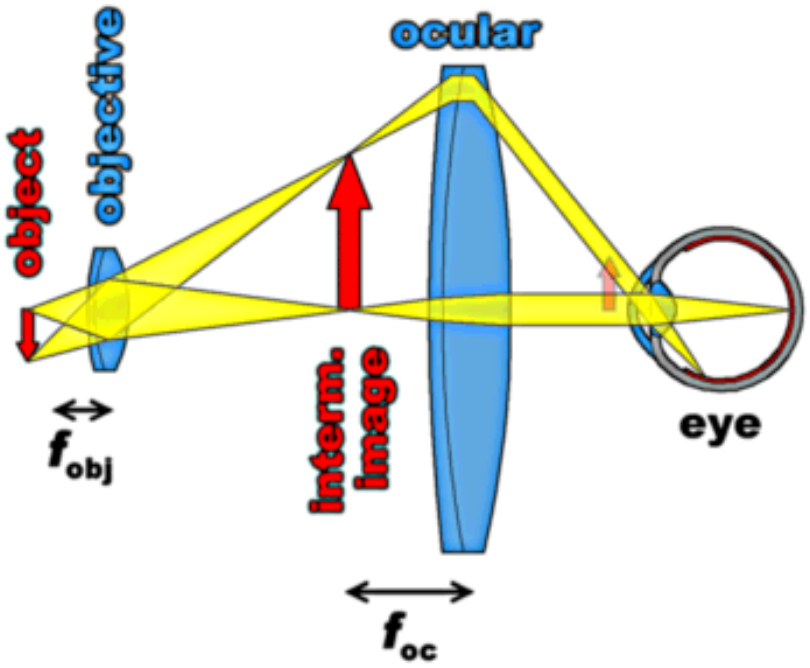

$$\text{Resolution} = \frac{k_1 \lambda}{NA_{obj}}$$

λ: wavelength of the illumination
NA: numerical aperture of the objective

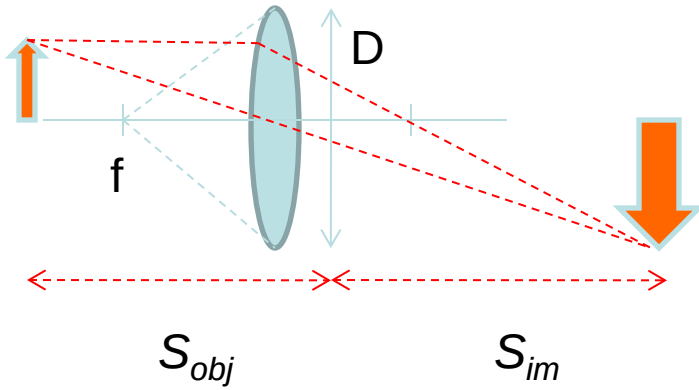

$$NA = \frac{D}{2f}$$

$$\frac{1}{f} = \frac{1}{s_{obj}} + \frac{1}{s_{im}}$$

http://www.molphys.leidenuniv.nl/monos/smo/index.html?basics/microscopy.htm

Anatomy of a full field optical microscope

In the visible region of the electromagnetic spectrum, the objective and condenser are typically made out of glass. It is the curvature of the lens, diameter and the refractive index (n) of the material that determines the focal length and numerical aperture of the lens. Furthermore, the lens material is transparent to the illumination.

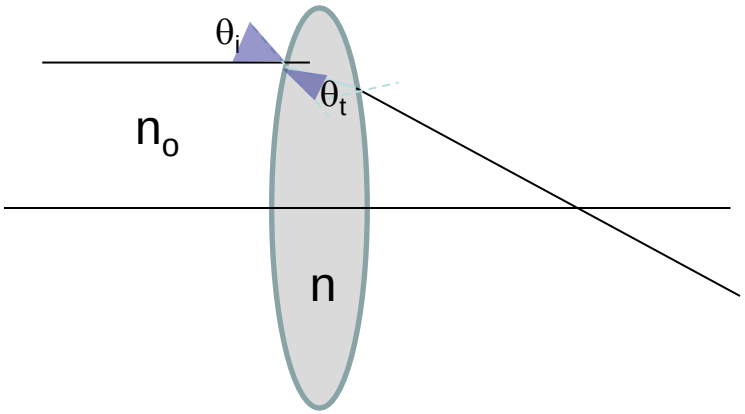

At each interface Snell's law must be satisfied (Boundary conditions for E and H)

$$n_o \sin\theta_i = n \sin\theta_t$$

where

$n(\lambda)$ Dispersion – oscillator model

Table of refractive index for different materials
http://www.luxpop.com/

Spatial resolution and contrast determine quality of the image

Resolution:
Capability to discern between two close objects

Tricks:
Use shorter wavelength
Immersion

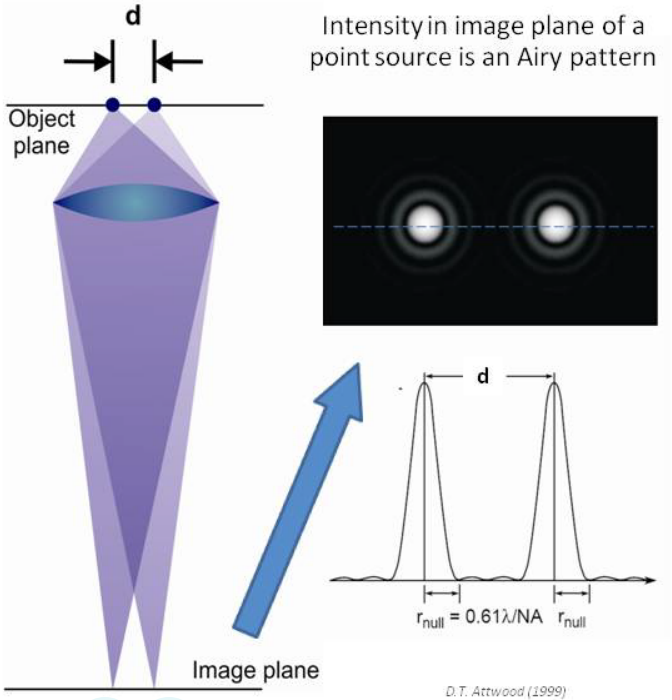

$$\text{Resolution} = \frac{k_1 \lambda}{NA_{obj}}$$

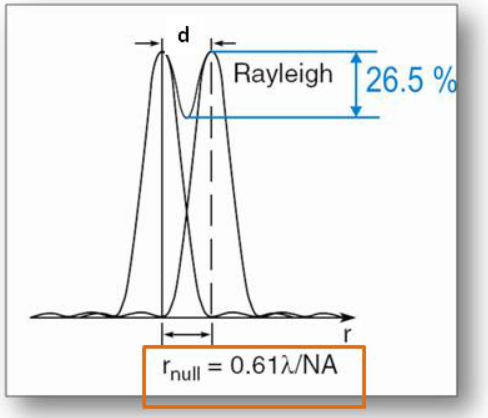

Modulation:

$$\frac{I_{max} - I_{min}}{I_{max}} = 0.265$$

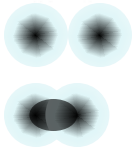

Resolved

Not Resolved

Contrast:
This depends on the Optical response of the materials at the specific wavelength of the illumination

Tricks
Labeling
Use of different wavelengths

How can the spatial resolution of microscopes be improved to image smaller objects?

$$\text{Resolution} = \frac{k_1 \lambda}{NA_{obj}}$$

1. Increase NA

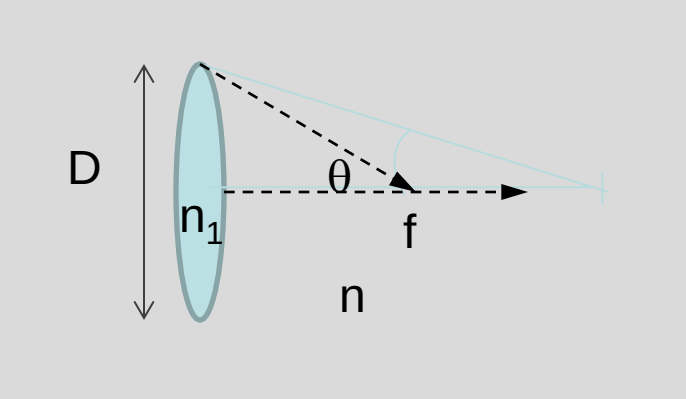

D: lens diameter
f: focal length
n: refractive index

$$NA = n \sin\theta$$

$$NA = n \sin(a \tan(\frac{D}{2f})) \approx n \frac{D}{2f}$$

NA=1 when lens is immersed in air

Use of a high index matching fluid can increase NA to 1.4

This technique is used in lithography of integrated circuits -@ λ=193 nm prints 40 nm features

2. Vary k_1

k_1 is a constant that depends on the illumination
Its value is 1.2 for incoherent illumination. (full period)
Some microscopes employed structured illumination

How can the spatial resolution of microscopes be improved to image smaller objects?

$$\text{Resolution} = \frac{k_1 \lambda}{NA_{obj}}$$

3. Use shorter wavelength illumination

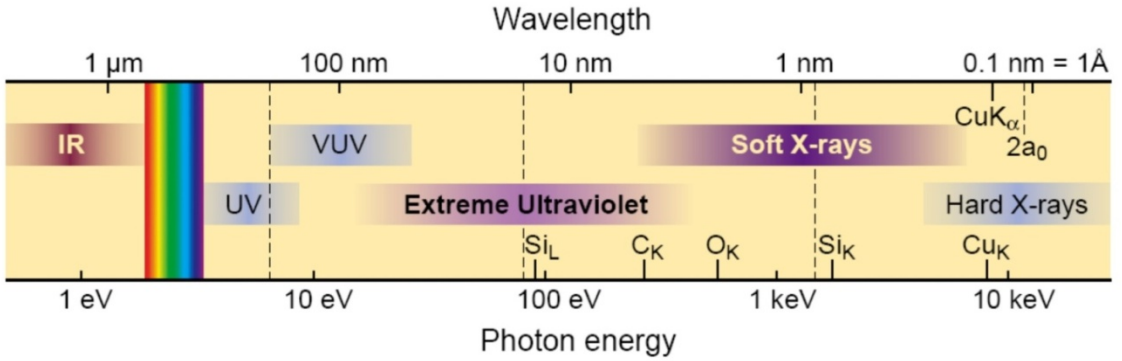

D.T. Attwood, "SXR and EUV Radiation"

'Can write smaller patterns'
'Can see smaller features'

Visible microscopy

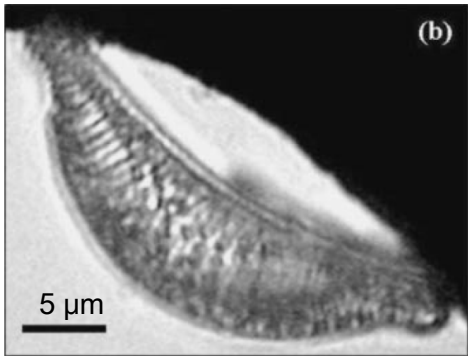

λ = 400 -700 nm
Res > 200 nm

EUV/SXR microscopy can potentially resolve full-field images with 10-100x smaller features than conventional visible microscopy

THIS IS THE APPROACH THAT WILL BE DISCUSSED IN CLASS

EUV/ SXR microscopy

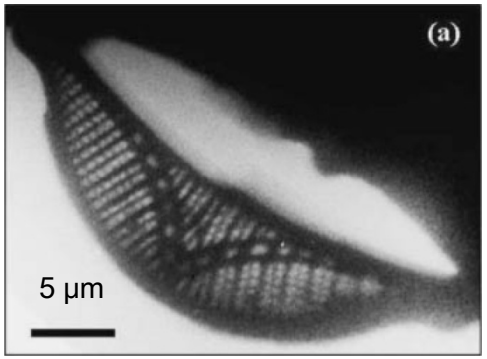

λ = 3.2 nm
Res < 100 nm

CONTRAST IN IMAGING SYSTEMS reflects how much light is absorbed/reflected

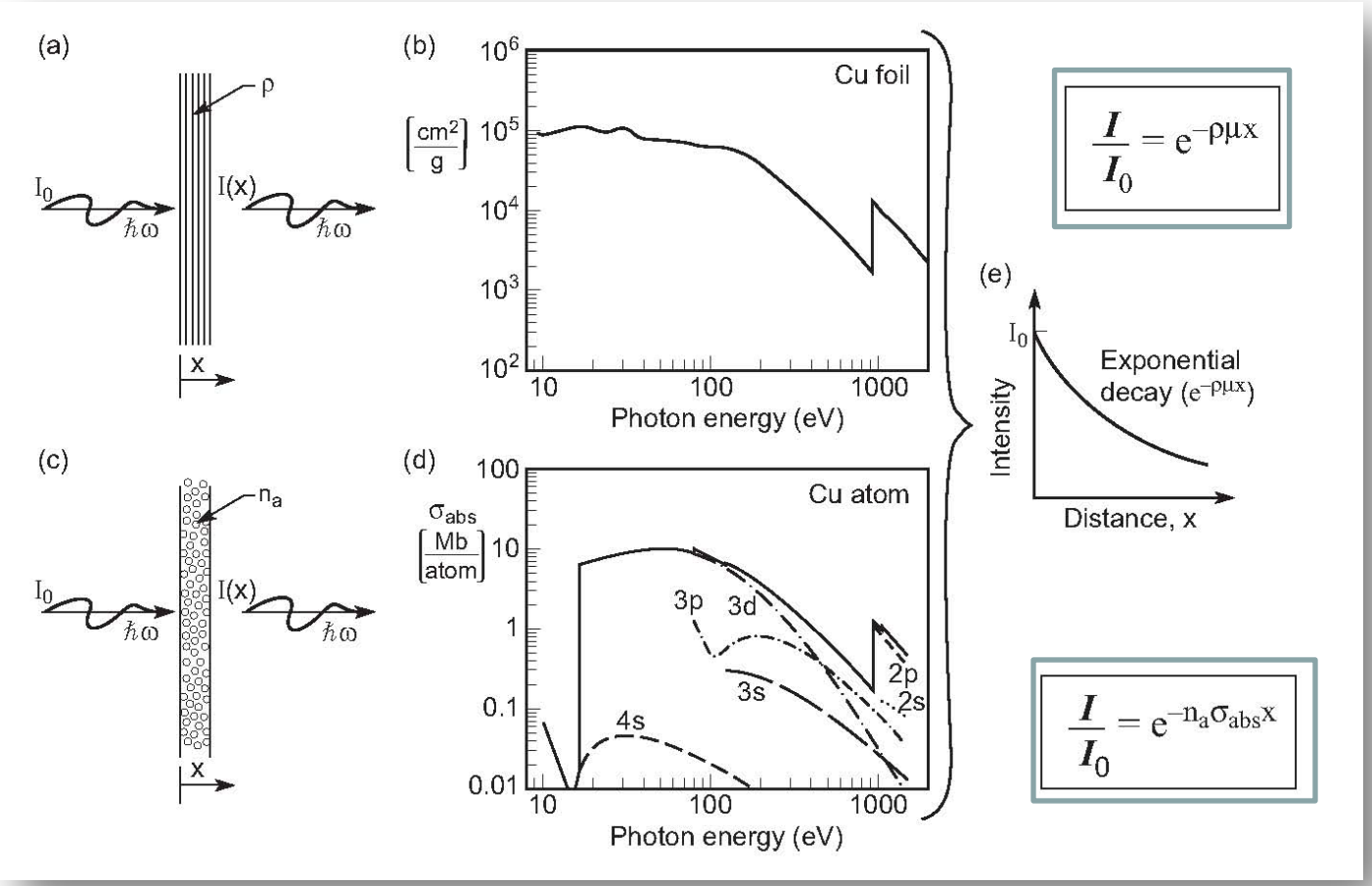

Fig. 1.8 – Soft X-rays and extreme ultraviolet radiation – D. Attwood, Cambridge 1999

Photo-absorption
- increases with thickness
- varies material to material

ρ: mass density
μ: energy and material dependent absorption coefficient
σ: photo-ionization cross-section (microscopic/atomic representation of absorption process)

In visible range, valence electrons determine the absorption response.
At EUV/SXR wavelengths, core electrons come into play

Large number of atomic resonances exist in EUV/SXR

Numerous atomic resonances exist in the EUV/SXR region

- **Strong absorption**
  - **Requires special optics**
  - **Vacuum environment for light to propagate over large distances**
- \+ **Elemental specificity/ Natural enhanced absorption contrast**

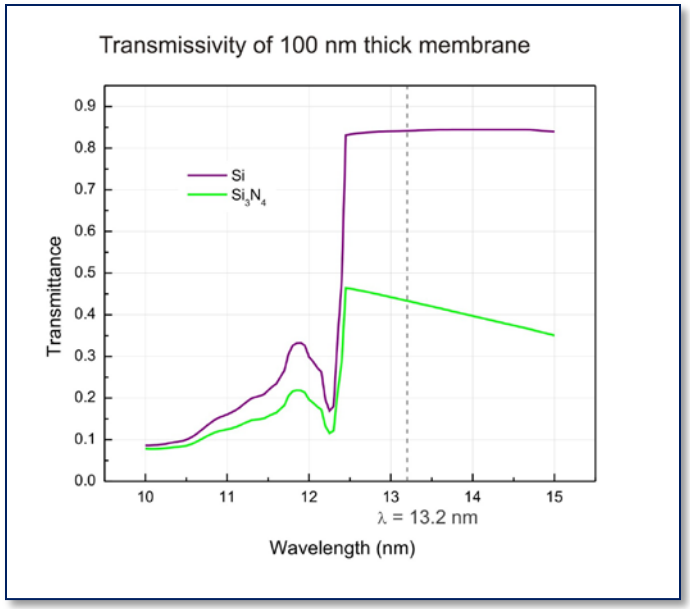

"Water window"

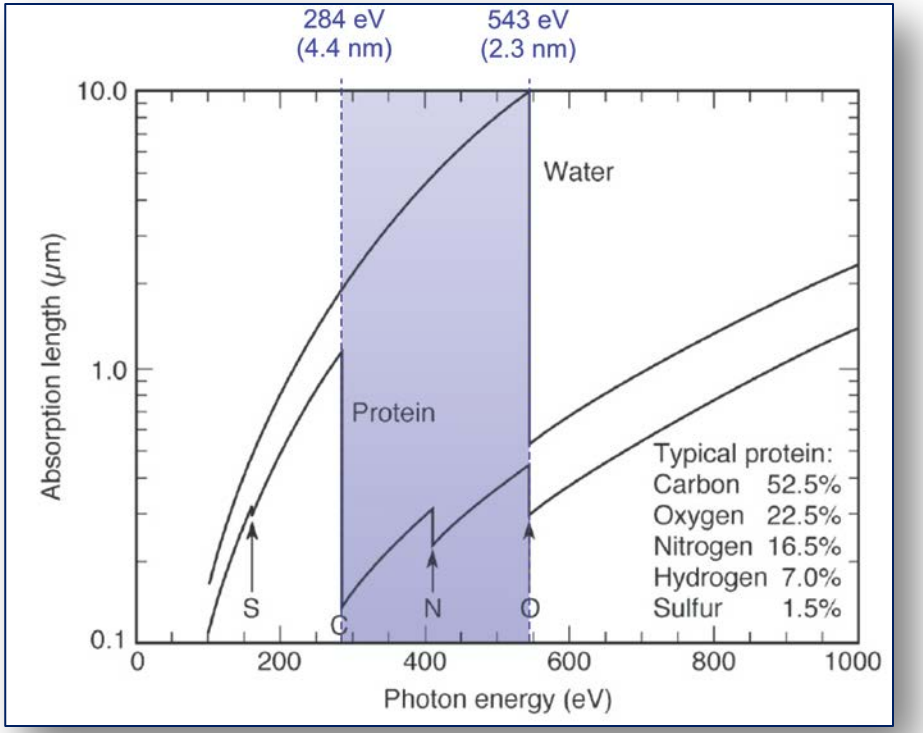

Atomic resonances- interaction of EUV/SXR light with core electrons -also affect refractive index.

$$n(\omega) = 1 - \delta + i\beta \quad (3.12)$$

$$\delta = \frac{n_a r_e \lambda^2}{2\pi} f_1^0(\omega) \quad (3.13a)$$

$$\beta = \frac{n_a r_e \lambda^2}{2\pi} f_2^0(\omega) \quad (3.13b)$$

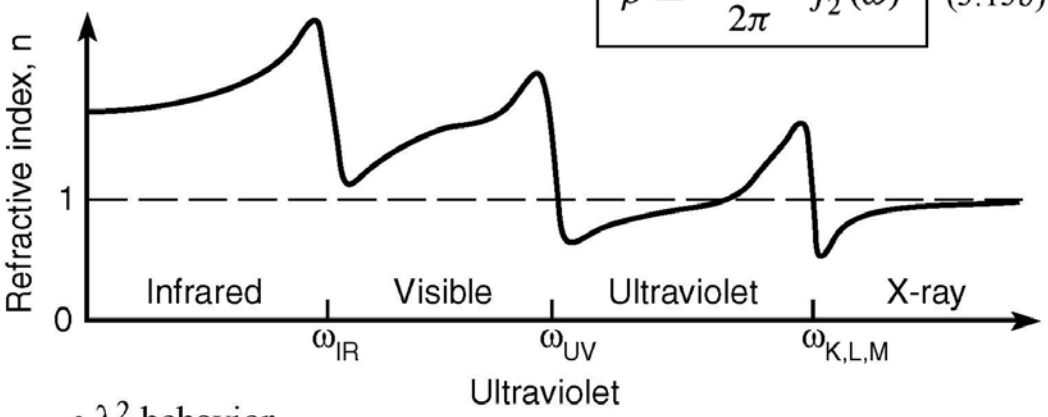

- λ^2 behavior
- δ & $\beta << 1$
- δ-crossover

δ, β are small quantities
For Carbon, at a wavelength of 0.4 nm, δ=4.9 10^{-5} and β=5.7 10^{-7}.

n is practically equal to 1 – Has consequences for wave propagation

$$E(\vec{r}) = \underbrace{E_o e^{-i(\omega(t-r/c)}}_{vacuum\ propagation} \underbrace{e^{-i(2\pi\delta/\lambda r)}}_{phase-shift} \underbrace{e^{-i(2\pi\beta/\lambda r)}}_{decay}$$

Fig. 3.1 Refractive index vs frequency – Soft X-rays and extreme ultraviolet radiation – D. Attwood, Cambridge 1999

Phase contrast

If the sample has largely uniform density and thickness, it is often desirable to make use of **phase contrast**. The phase depends on the optical properties of the sample, and can provide contrast even if absorption is minimal or has little spatial variation. Zernike phase contrast is implemented in X-ray microscopes much as in the light microscope, using a strategically placed "phase ring". This technique is used widely for biological materials

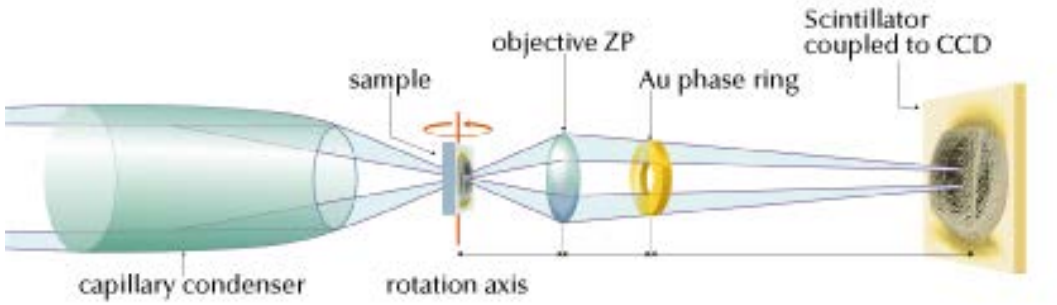

Image contains phase information in the form of interference

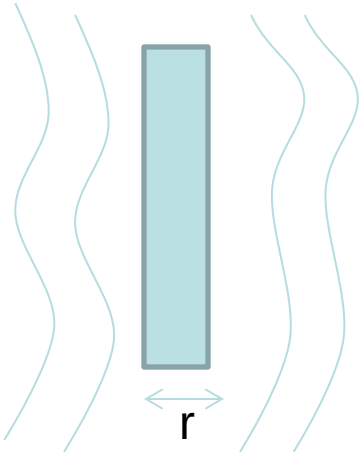

$$\Delta\phi = \frac{2\pi\delta}{\lambda r}$$

Lens tissue paper- Phase contrast image

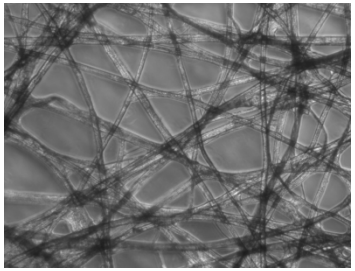

http://www.xradia.com/technology/microscopes/types-of-xray-microscopes.php

http://en.wikipedia.org/wiki/File:Paper_Micrograph_Phase.png

Multilayer coatings can be coated on many different surfaces. Magnetron sputtering is typically used. It is very challenging to make these multilayers and to make optics with no aberrations

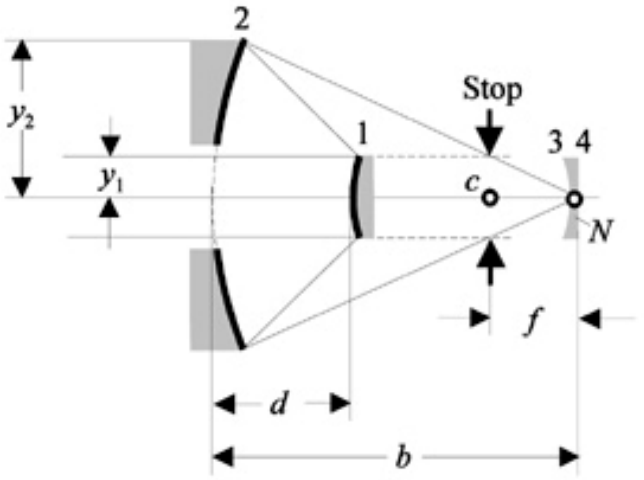

A common geometry that is used is the Schwarszchild – it consists of two curved mirrors that focus the light into

To eliminate aberrations the two mirrors have to be perfectly aligned.
d=2f

We use a lens of this configuration at λ=46.9 nm. The lens surfaces are coated with Sc/Si multilayers that reflect ~45% at this wavelength.

Specifications:

Diameter M_1	D_1 = 50 mm
Diameter M_2	D_2 = 10.8 mm
Focal distance	f = 27 mm
Num. Aperture	NA = 0.18
Throughput	T = 13%

All EUV microscopes use diffractive optics as objective, and many also as condenser. Fresnel zone plate are circular diffractive elements that focused light by diffraction – most efficient is the 1st order diffraction.

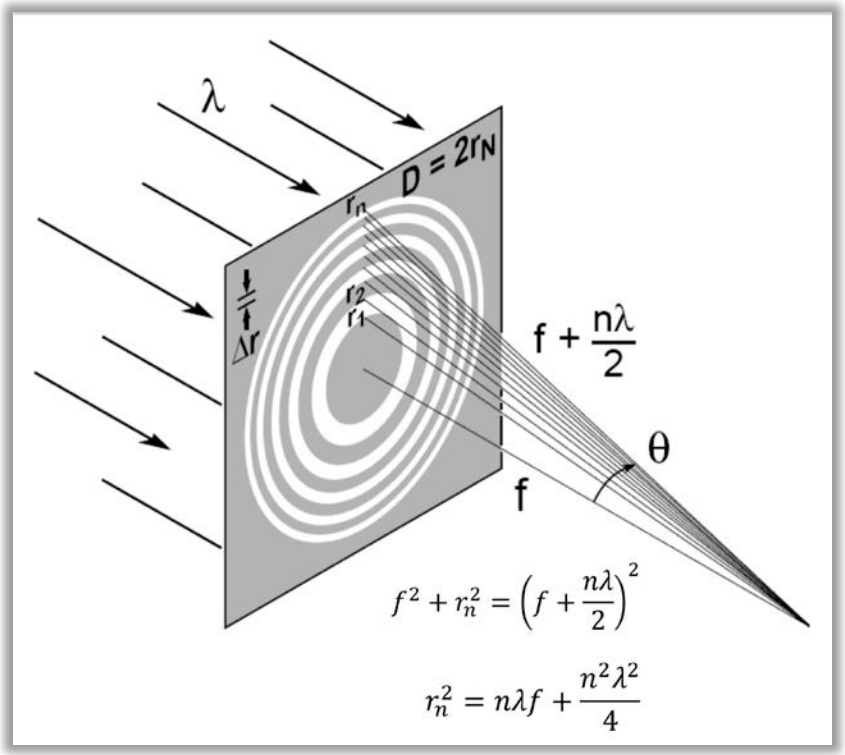

D. T. Attwood, "Soft X-rays and Extreme Ultraviolet Radiation." (Cambridge Univ. Press, New York, 1999).

$$NA = \frac{\lambda}{2\Delta r}$$

$$resolution = k_1 \frac{\lambda}{NA_{obj}} = 2k_1\Delta r$$

$$f = \frac{4N(\Delta r)^2}{\lambda}$$

$$DOF = \pm\frac{1}{2}\frac{\lambda}{(NA_{OZP})^2} = \pm\frac{2(\Delta r)^2}{\lambda}$$

For free aberration operation

$$\frac{\Delta\lambda}{\lambda} \le \frac{1}{N}$$

Highest resolution ZP demonstrated have 12 nm outer zone width (W. Chao et al, OE 2010)

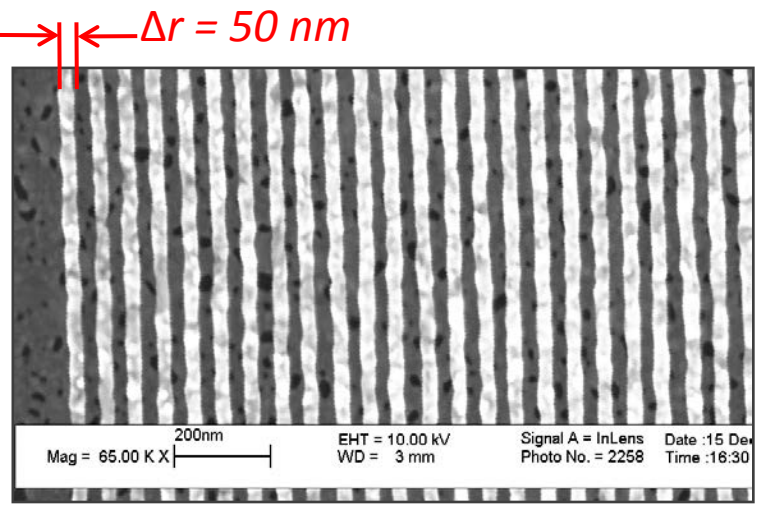

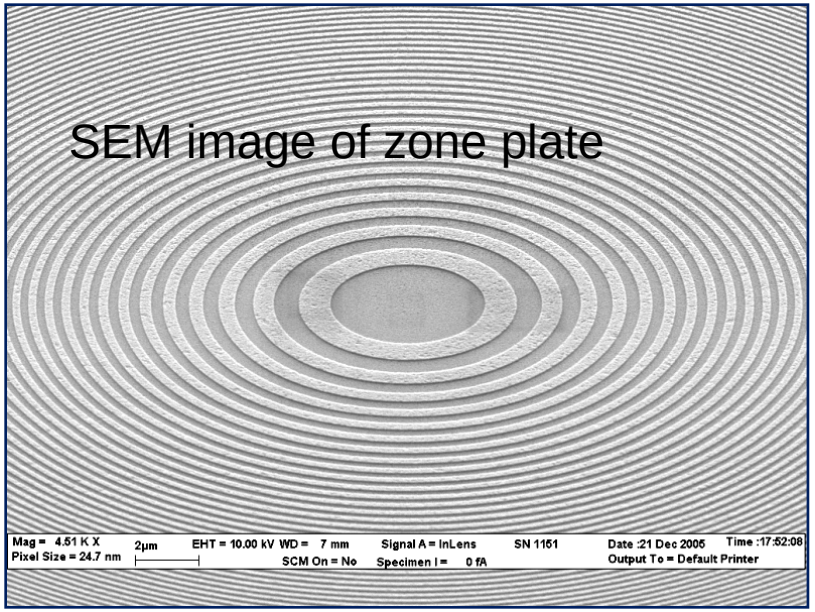

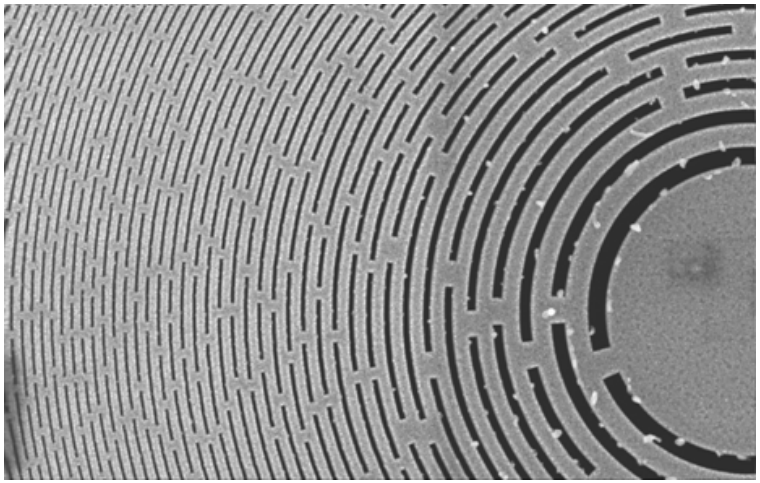

Free-standing zone plates in which Si2N5 membrane was removed. were fabricated to improve efficiency at λ=46.9 nm

EUV/SXR sources

Laboratory facilities where experiment is taken to the source

Synchrotron – emission at many wavelengths selectable with monochromator. Low average power, 500 MHz repetition rate, ps pulse duration (ALS-Berkeley, Wisconsin, Brookhaven)

Free Electron Laser – wavelength selectable, high peak power, fs pulse duration (FLASH Hamburg (EUV/SXR), ACLS Stanford (X-rays)

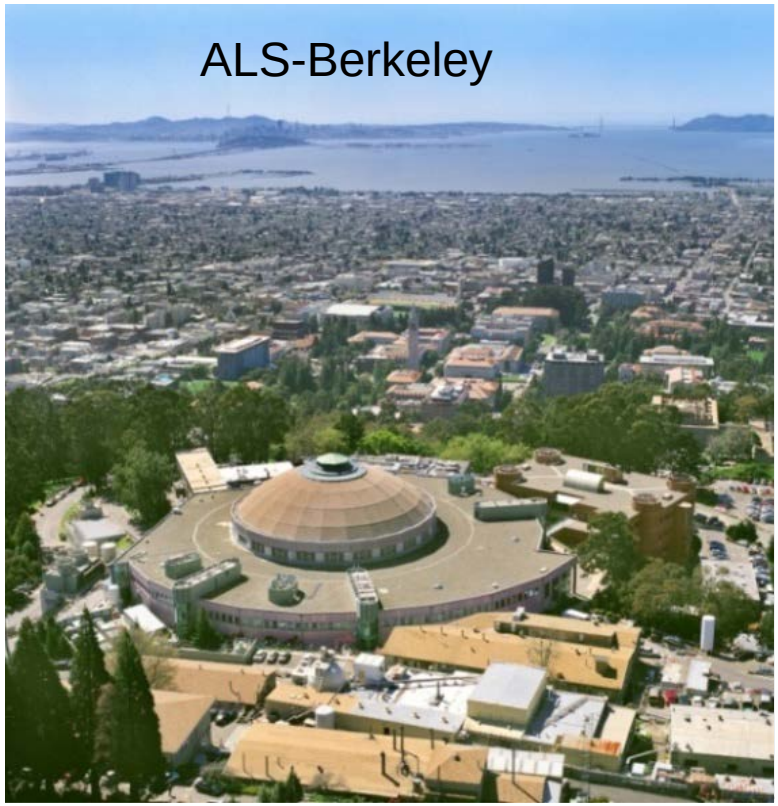

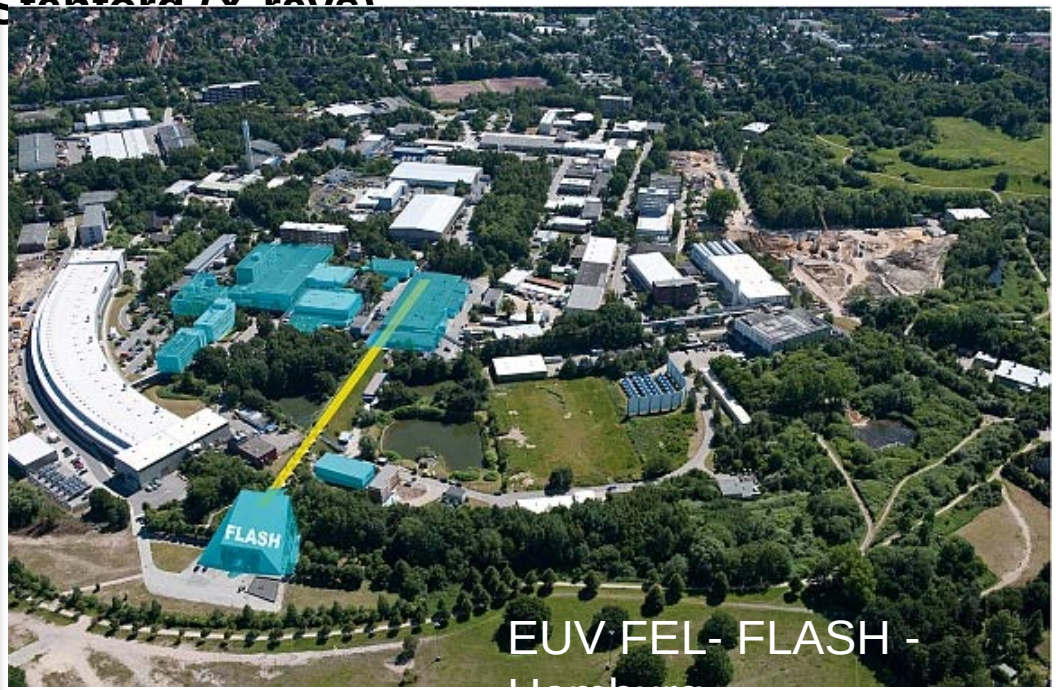

mer School – 2010

A Single Storage Ring Serves Many Scientific User Groups

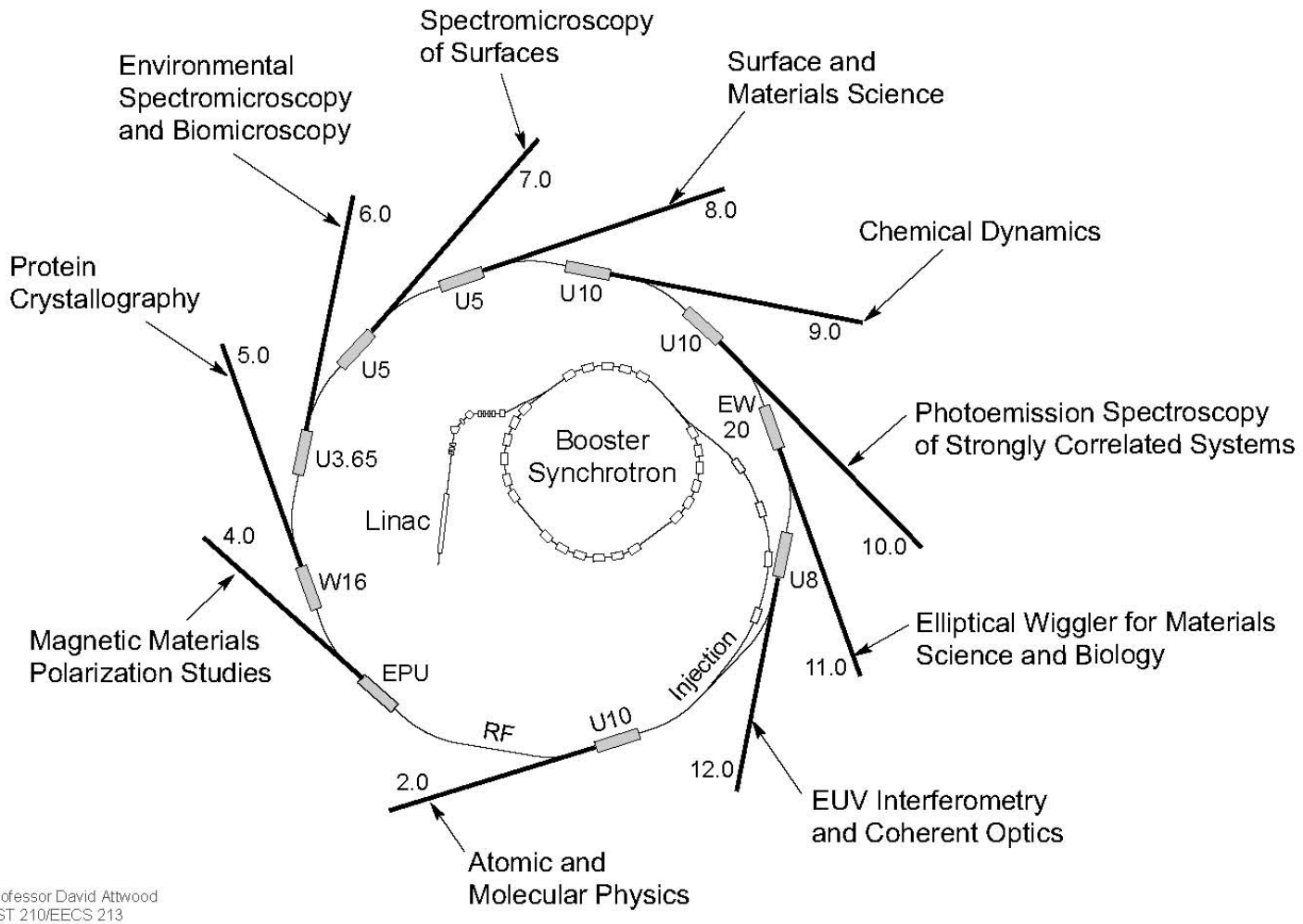

Different type of EUV/SXR microscopes

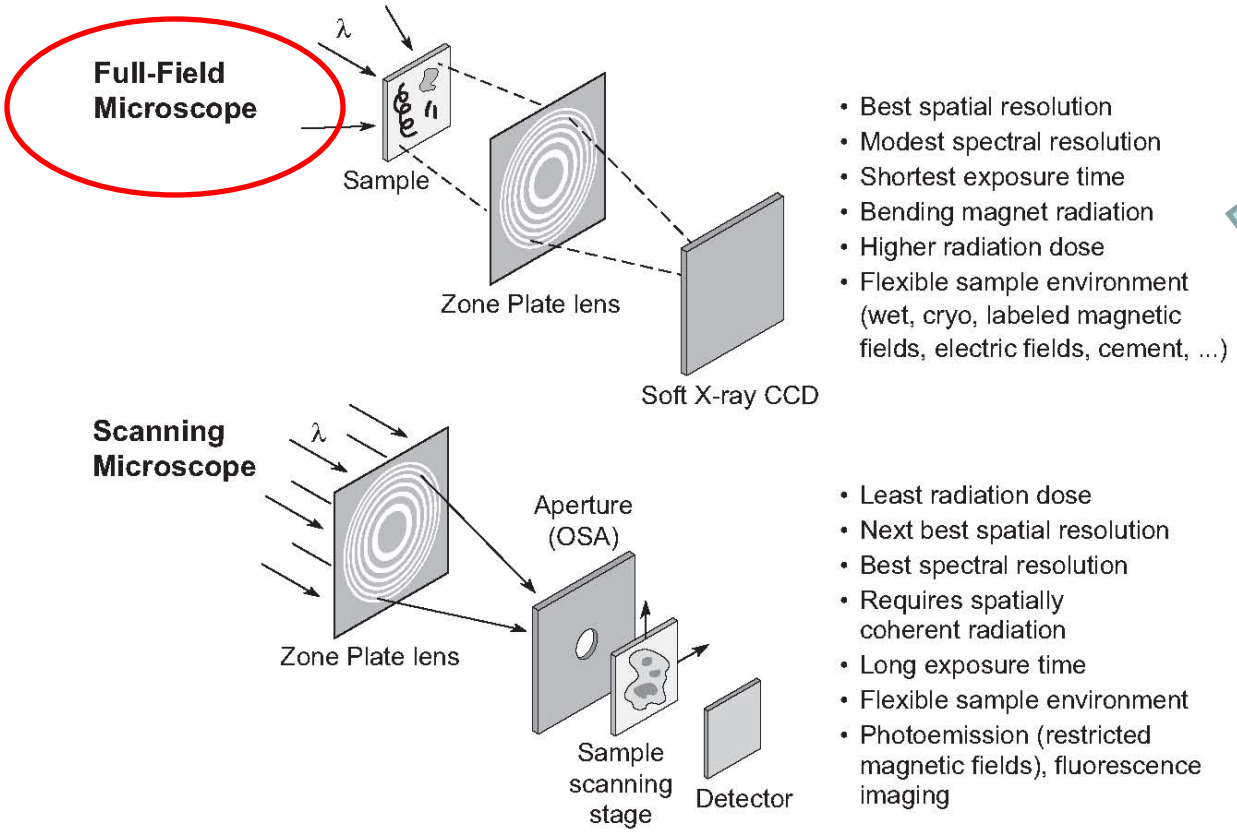

Professor David Attwood
Univ. California, Berkeley

Zone Plate Microscopy and Applications, EE290F, 12 April 2007

Ch09_F21modif_Nov05.ai

Bright field
Contrast due to absorption of light in sample

Dark field
Contrast comes from light scattered by the sample

Large facilities of bright EUV-SXR-XR laser pulses are being developed worldwide

EXTREME LIGHT INFRASTRUCTURE (Czech Republic

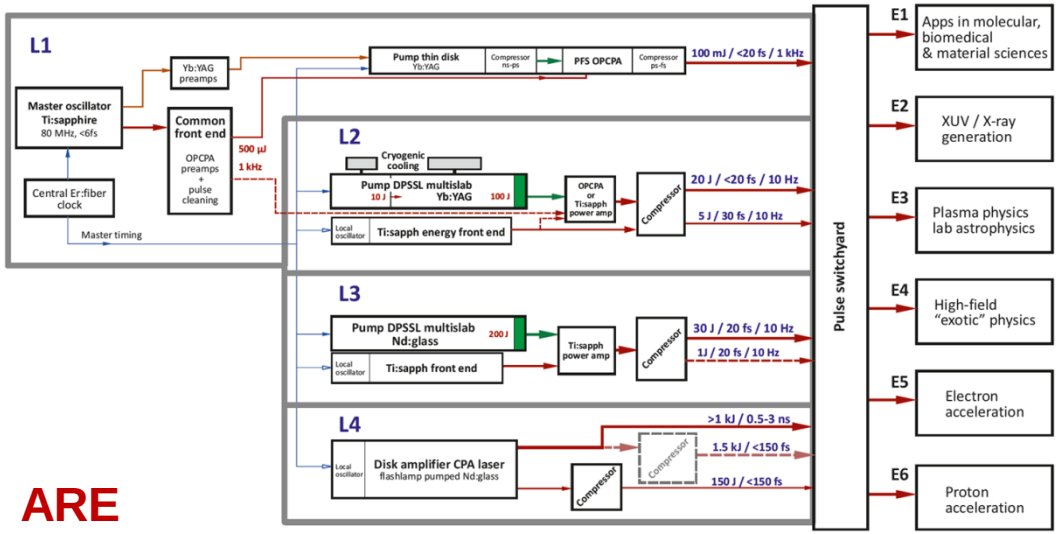

NEW EUV SXR SOURCES ARE OPENING PATH TO NEW SCIENCE

New high repetition rate table-top EUV-SXR lasers provide exciting alternatives for new applications on a table-top

Table top EUV/SXR lasers offer

- High pulse energy (μJ-mJ)
- High monochromaticity
- High peak spectral brightness

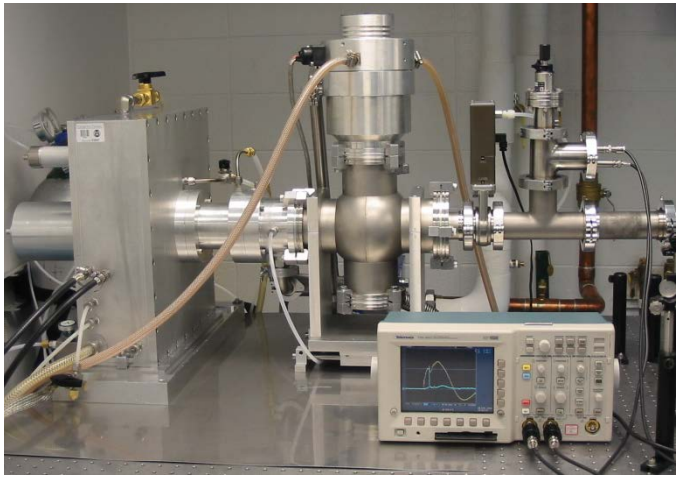

Discharge pumped EUV laser
Wavelength λ = 46.9 nm
Energy per pulse: 0.1 mJ (10^{12} ph/s)
Pulse duration: ~1.5 ns
Repetition rate: up to 15 Hz
Tailored spatial coherence
Used for NANO-IMAGING AND NANO-PATTERNING and NANO-PROBING

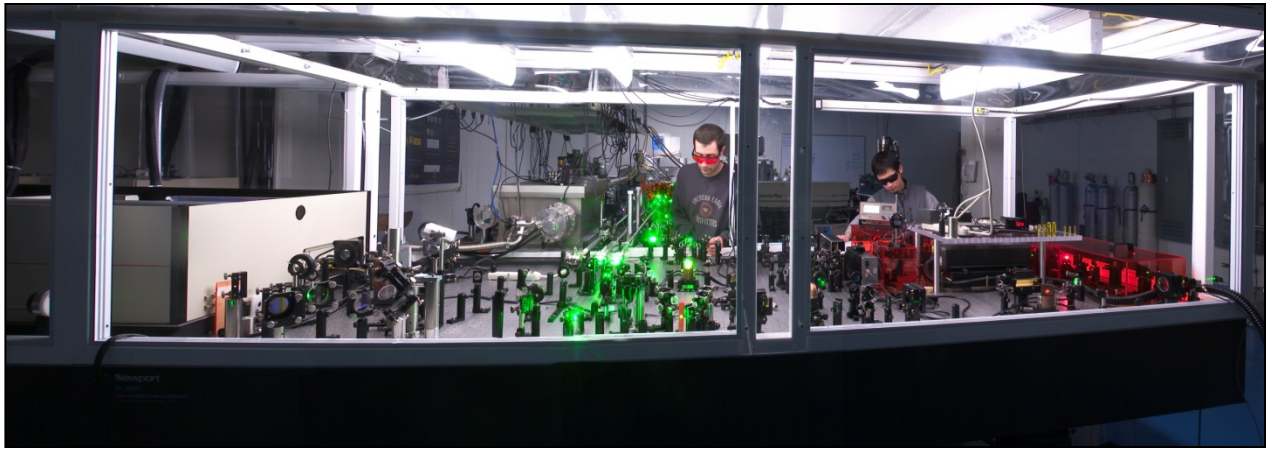

Laser pumped EUV laser
Wavelength λ = 13.2 nm
Energy per pulse: 10 μJ (10^{11} ph/s)
Pulse duration: ~1 ps
Repetition rate: up to 5 Hz
Used for NANO-IMAGING

Nanoscale resolution table-top full field EUV microscopy test-beds

λ = 46.9 nm
Imaging of nanostructures

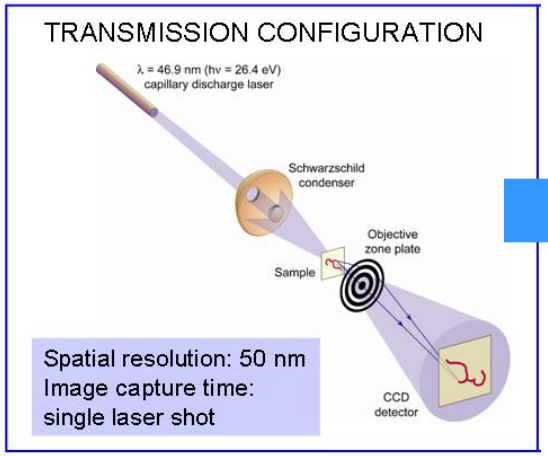

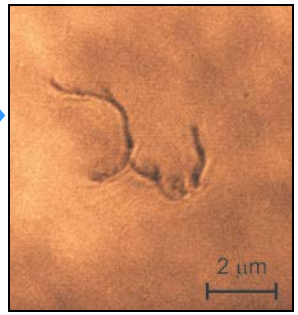

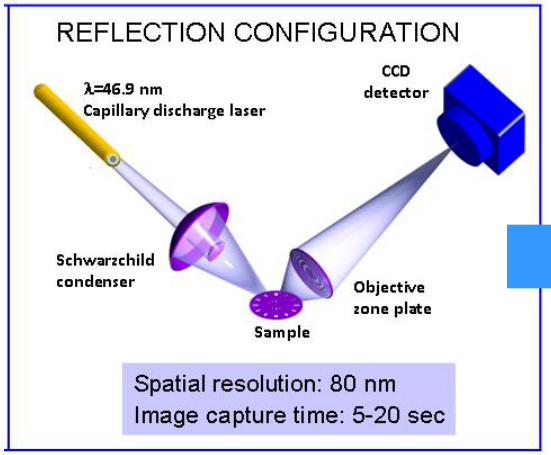

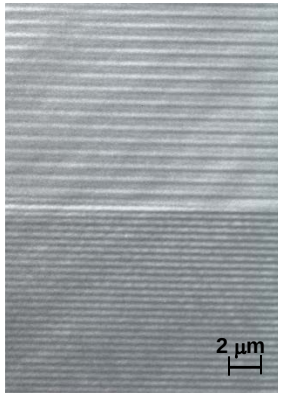

λ = 13.2 nm
Actinic defect inspection

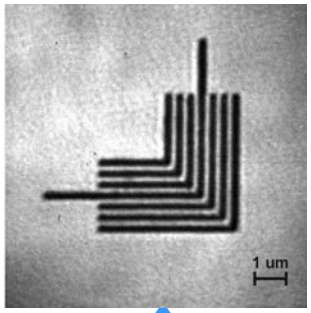

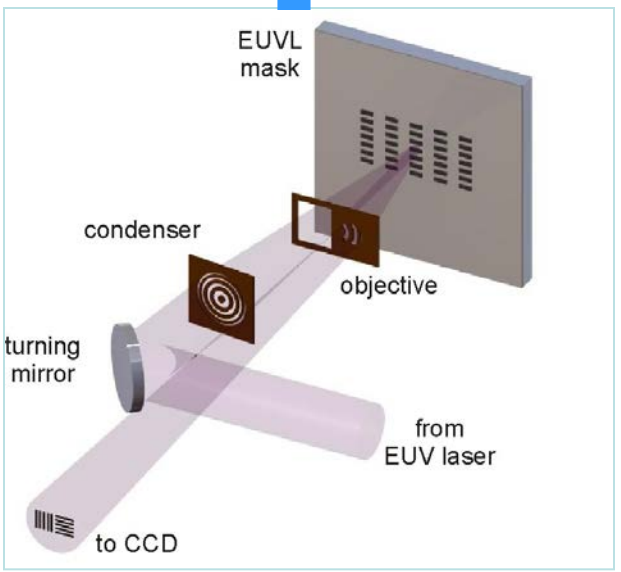

Spatial resolution: 55 nm
Image capture time: 20 sec

Goal: to enable the demonstration of laser-based table-top high resolution imaging systems

Important factors for compact microscopy systems

- Spatial resolution
- Image acquisition time
- Illumination uniformity and overall image quality

Two full field microscopes have been demonstrated each with distinct requirements

λ=46.9 nm

Strong absorption requires implementation of free standing zone plates.

λ=13.2 nm

Geometry of illumination requires novel designs of condenser and objectives.

λ= 46.9 nm microscope fits on a 8'x4' optical table

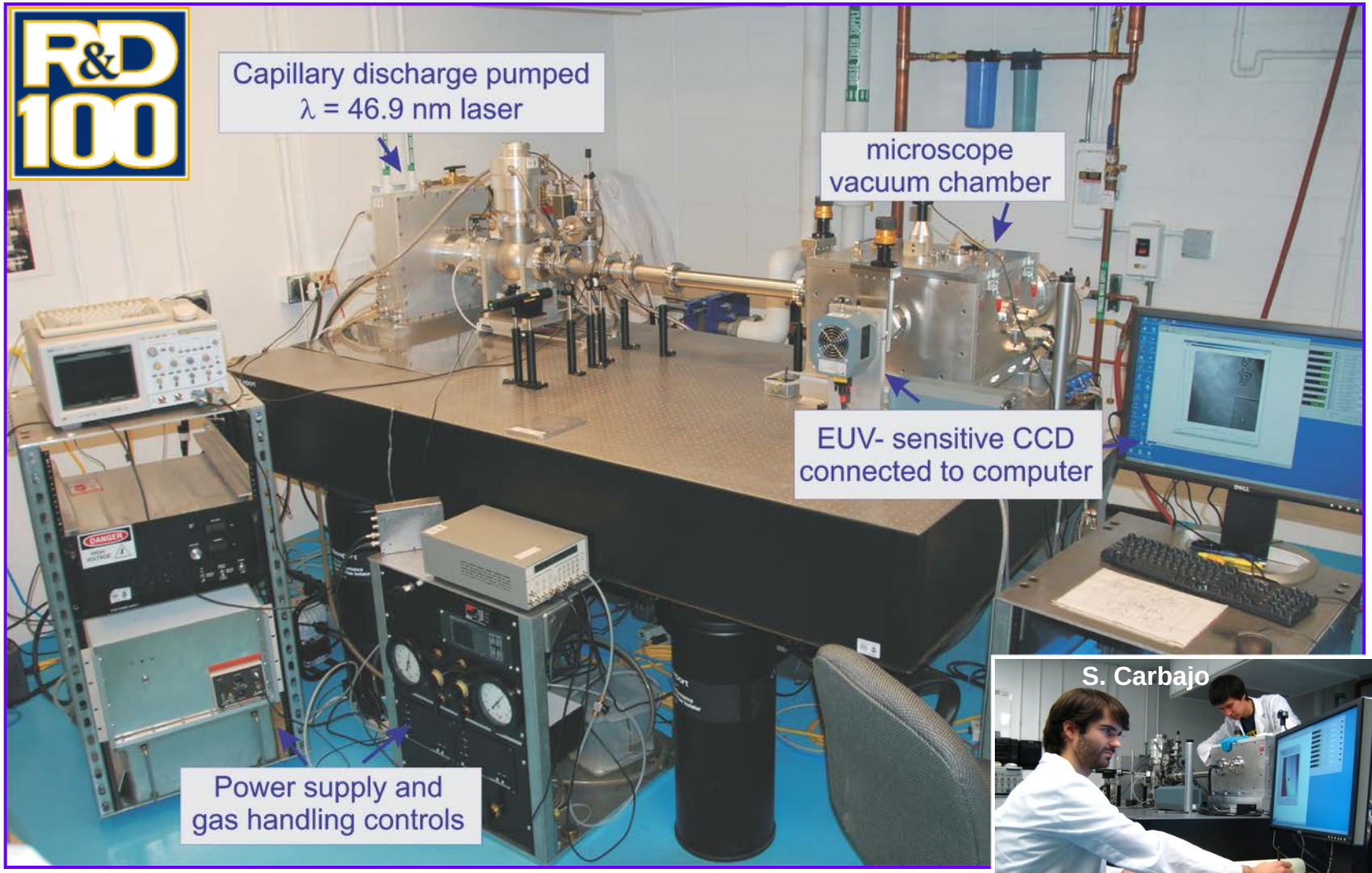

λ= 46.9 nm full field microscope operates in transmission and reflection configurations

TRANSMISSION CONFIGURATION

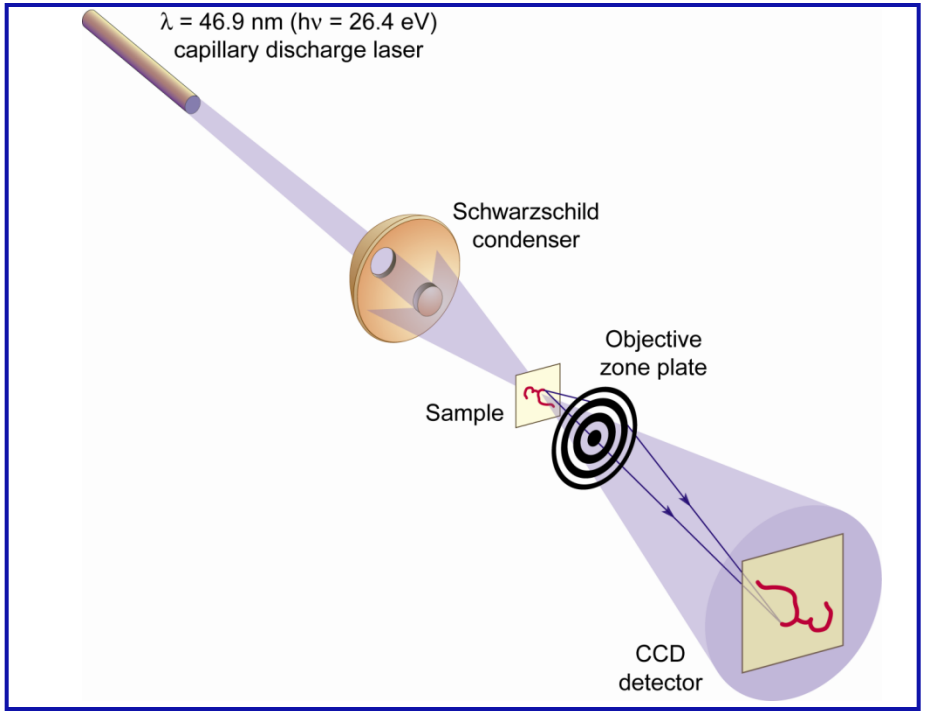

REFLECTION CONFIGURATION

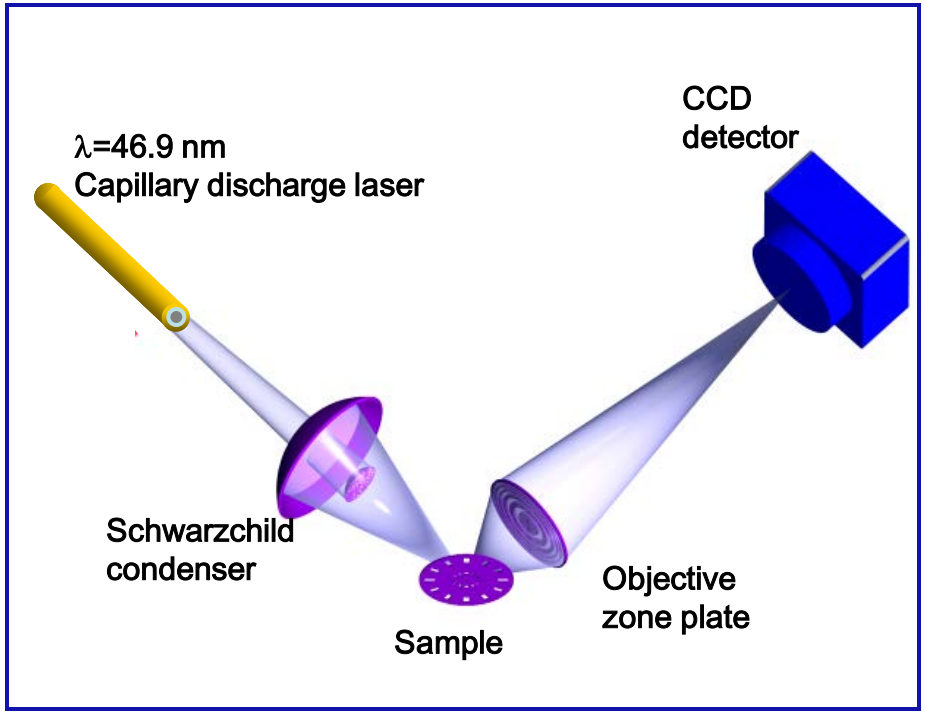

Spatial resolution: 50 nm

Image capture time: single laser shot

Spatial resolution: 80 nm

Image capture time: 5-20 sec

Objective zone plates for the λ=46.9 nm microscope

Zone plate equations:

$$D = 4N\,\Delta r$$

$$f = \frac{4N(\Delta r)^2}{\lambda}$$

$$\mathrm{NA} = \frac{\lambda}{2\,\Delta r}$$

$$\mathrm{DOF} = \pm\frac{1}{2}\frac{\lambda}{(NA_{OZP})^2} = \pm\frac{2(\Delta r)^2}{\lambda}$$

$$\mathrm{Res} = k_1\frac{\lambda}{NA_{OZP}} = 2k_1\Delta r$$

Δr = 70 nm, N = 1785	**Δr = 120 nm, N = 1042**	**Δr = 200 nm, N = 625**
500 μm	500 μm	500 μm
0.75 mm	1.23 mm	3.41 mm
0.34	0.20	0.12
± 0.21 μm	± 0.62 μm	± 1.7 μm
Expected Resolution: 42-70 nm	**Expected Resolution: 72-120 nm**	**Expected Resolution: 120-200 nm**

FTh – A1 – Introduction to X-Ray Optics – D. Attwood

Freestanding grating patterns are imaged to assess spatial resolution of the microscope

EUV/SXR image

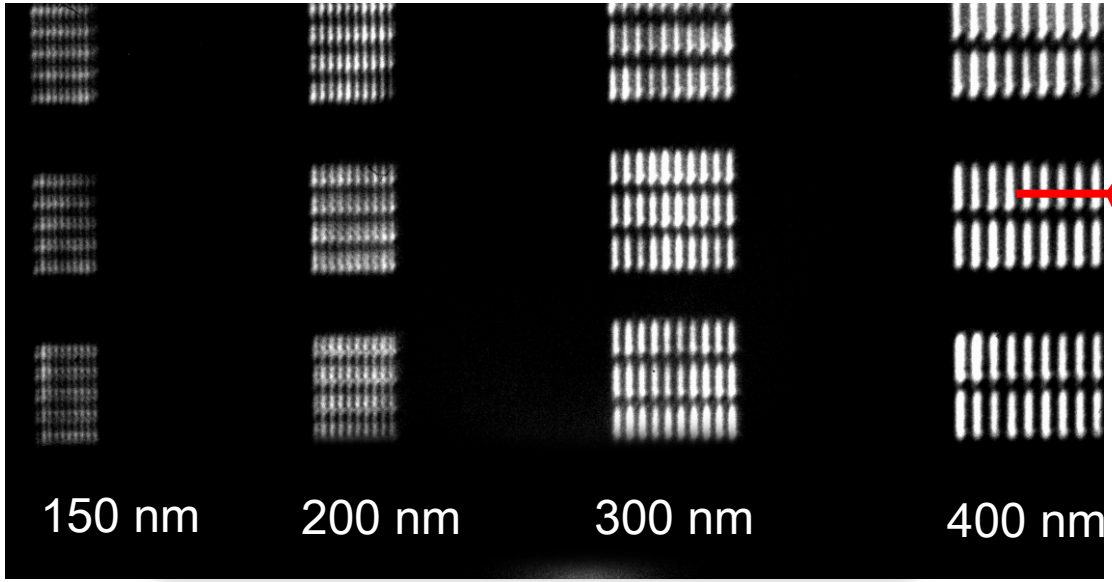

NA= 0.19 zone plate, exposure time 20 seconds

Image intensity lineout

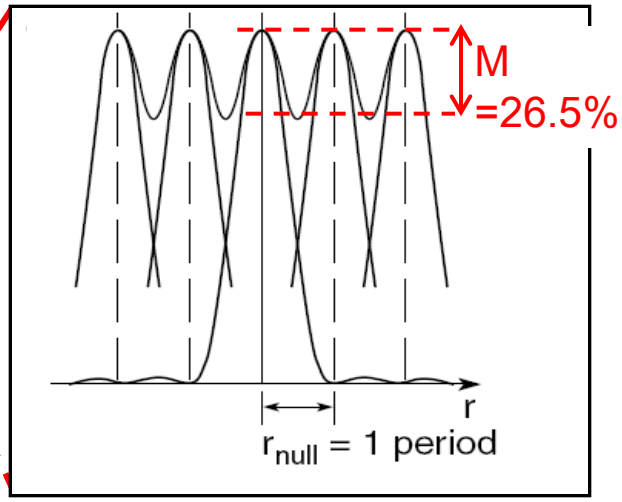

$$M = \frac{I_{max} - I_{min}}{I_{max}}$$

$$\text{Res.} = k_1 \frac{\lambda}{NA_{obj}} \rightarrow 26.5\%\ \text{modulation}$$

Modulation transfer function constructed for all three objective zone plates from single shot images

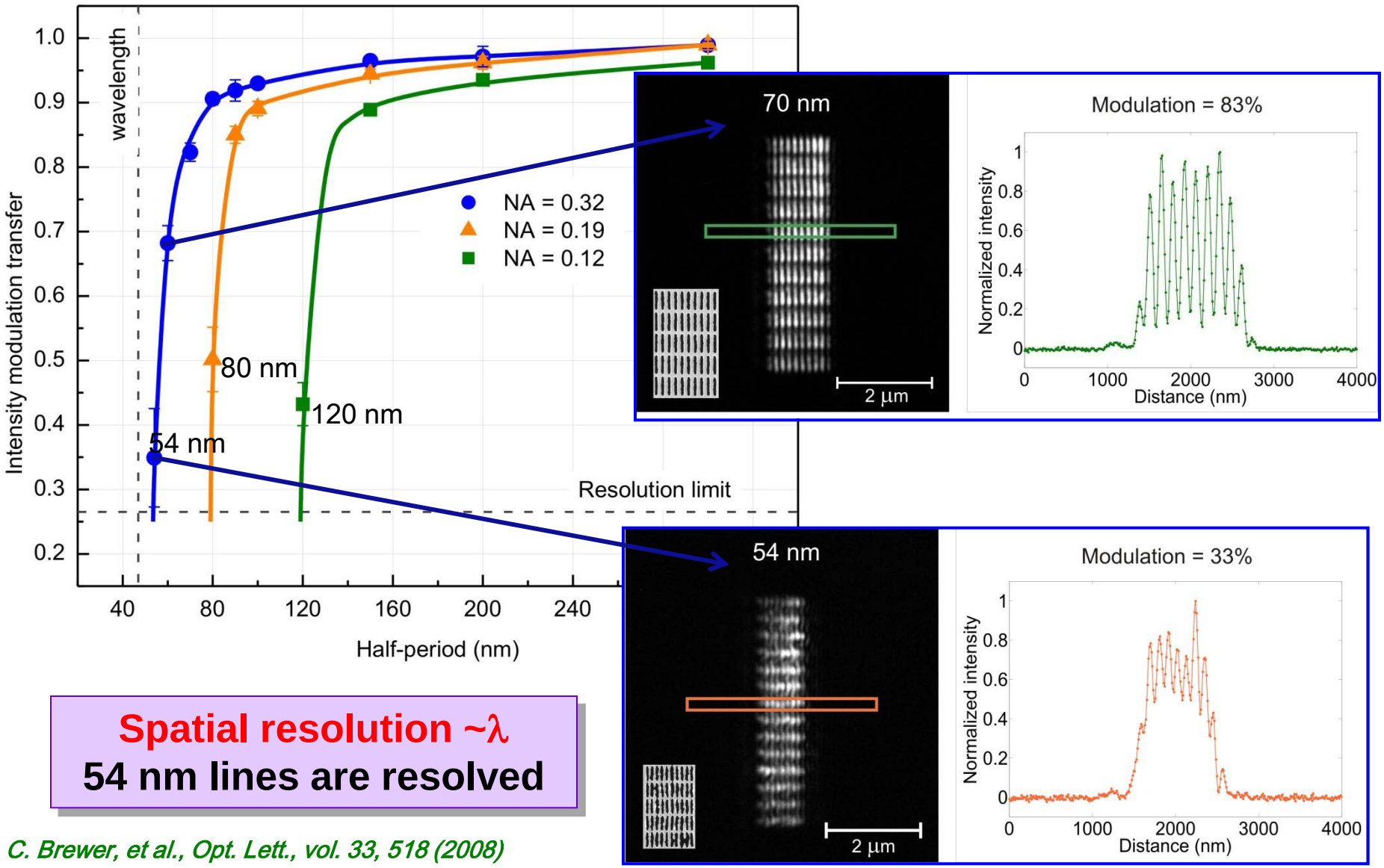

Spatial resolution ~λ
54 nm lines are resolved

C. Brewer, et al., Opt. Lett., vol. 33, 518 (2008)

EUV microscope captures images of nanostructures with very high resolution

TRANSMISSION
NA=0.32 (M~1000)

200 nm half period diatom

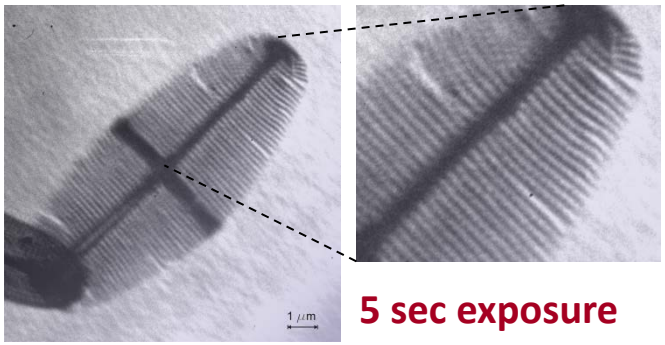

5 sec exposure

50 nm carbon nanotube

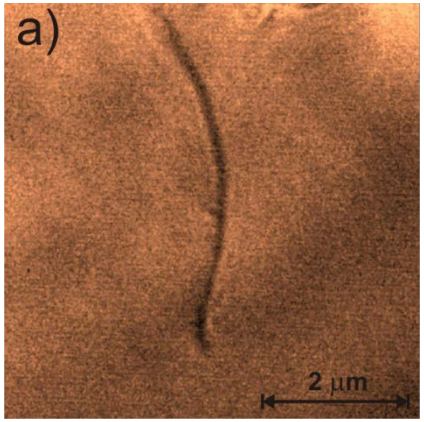

Single shot, 1.5 ns exposure

C. Brewer, et al, Opt. Lett. ***33****, 518 (2008)*

REFLECTION
NA=0.12 and 0.19 (M~250)
5-20 sec exposures

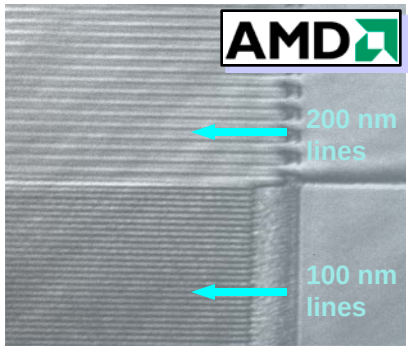

Partially Processed semiconductor chip

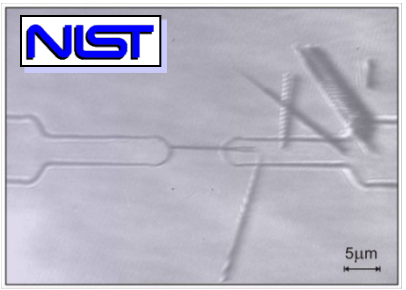

100 thick GaN nanowire between Al contacts

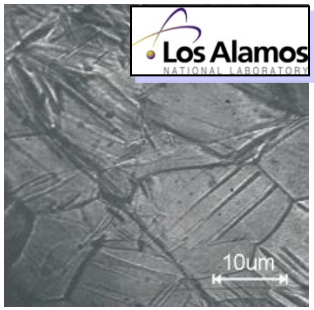

Zirconium surface

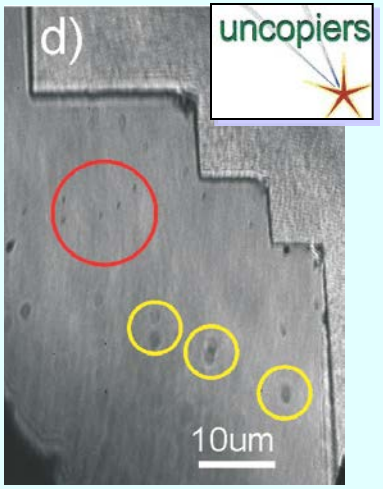

Collaborative Project with industry

Crosscheck Particle Scout monitoring system by imaging 100 nm Au nanodots on Si wafer

Movies of Nano-scale Dynamics on a Table-top

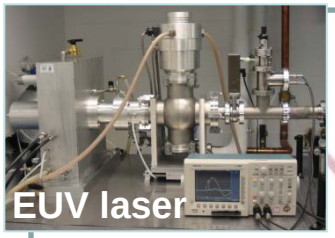

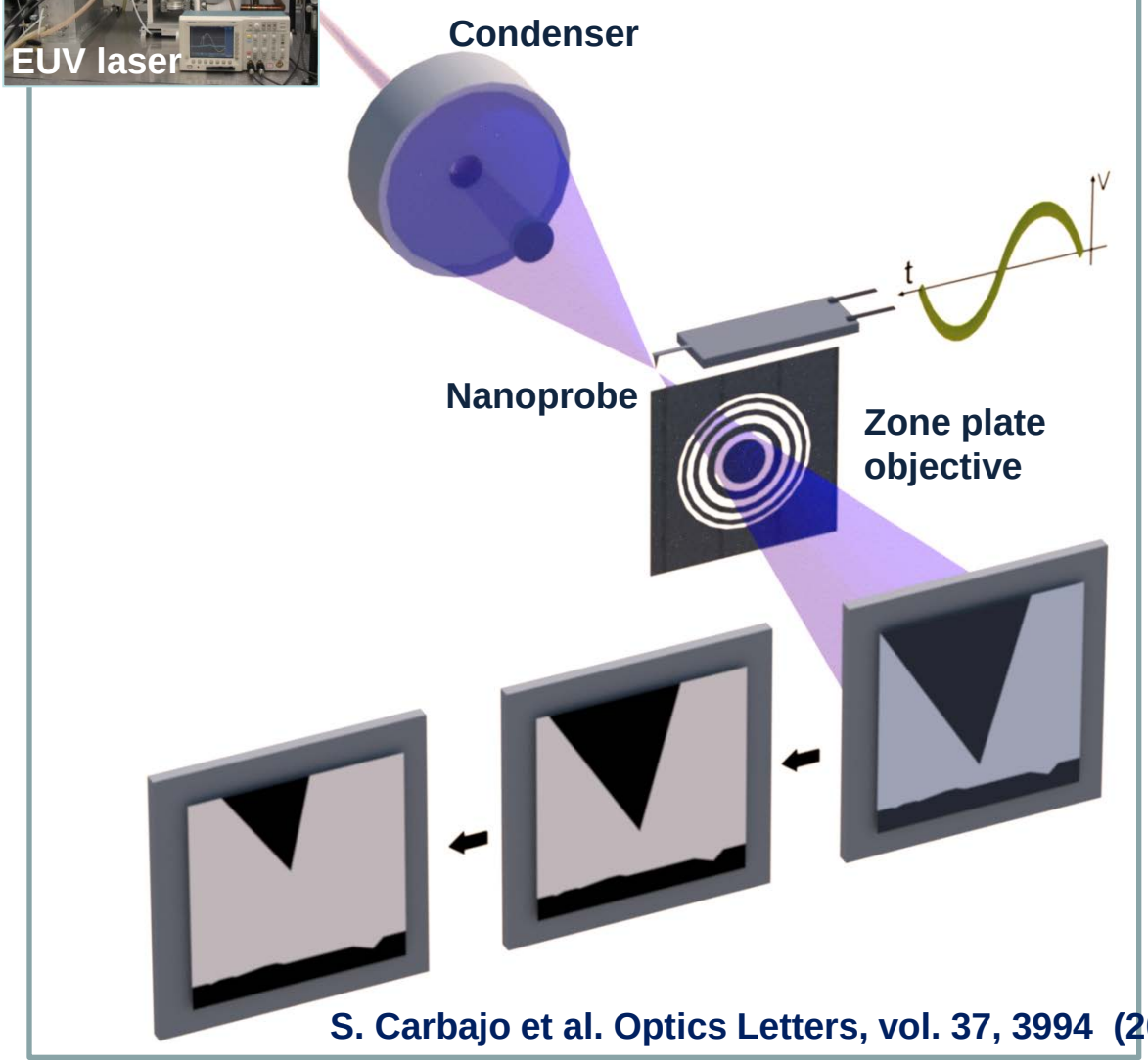

S. Carbajo et al. Optics Letters, vol. 37, 3994 (2012)

Magnetic force microscope tip interaction with stray magnetic field

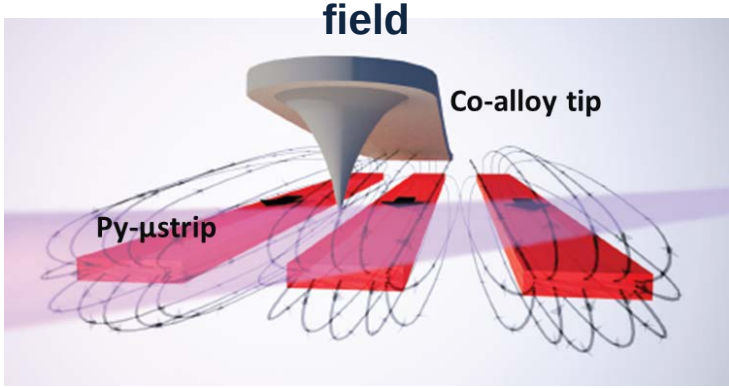

Movie of oscillating nano-tip

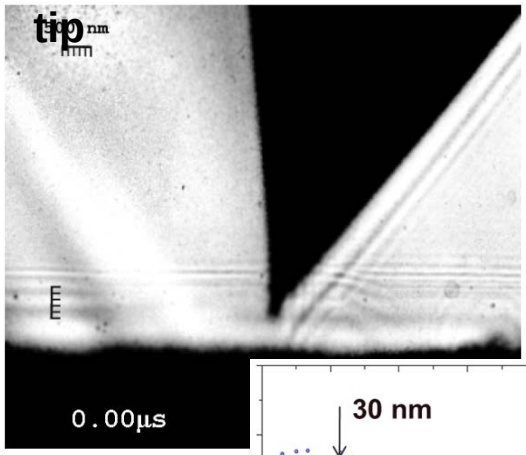

Detected variations of 30 nm in the amplitude of the tip oscillation

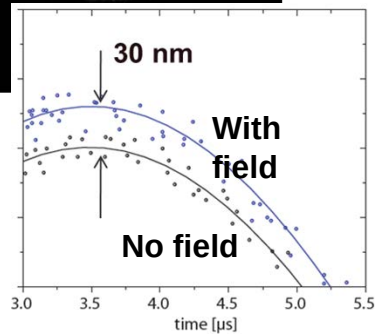

First demonstration of Image plane holography in EUV

RAW IMAGE

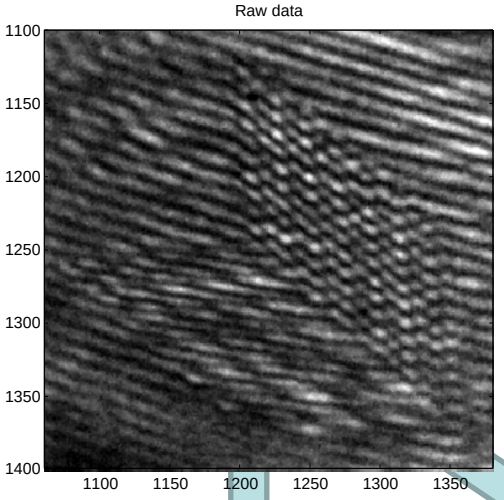

Schematic of setup

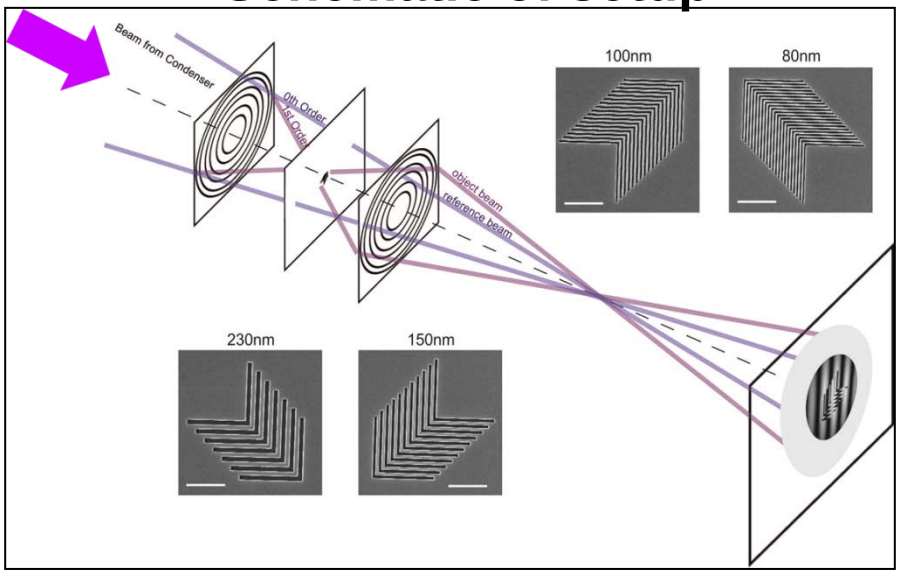

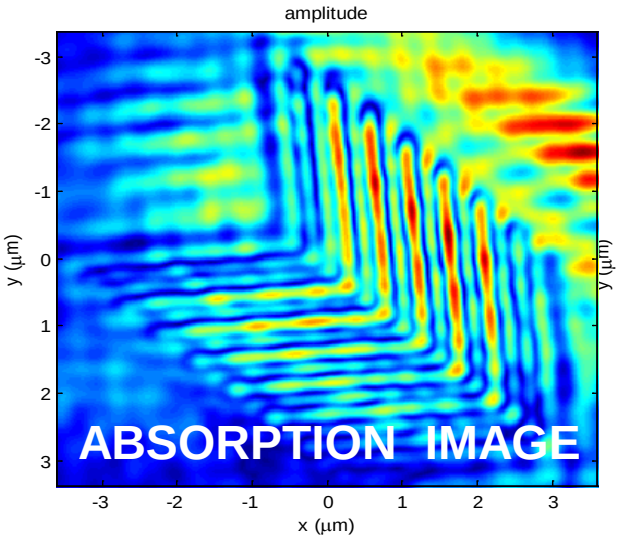

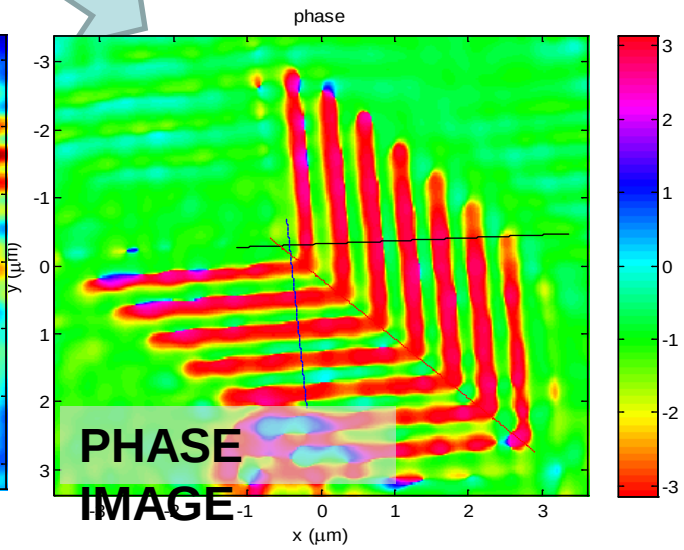

Phase difference of (2.3±0.3) rad corresponds to of (100±15) nm thick Si

J. Nedjl, I. Howlet, C. Menoni
Czech Republic – USA team

Single Shot EUV Fourier Holography: Towards the realization of nano-scale holographic movies

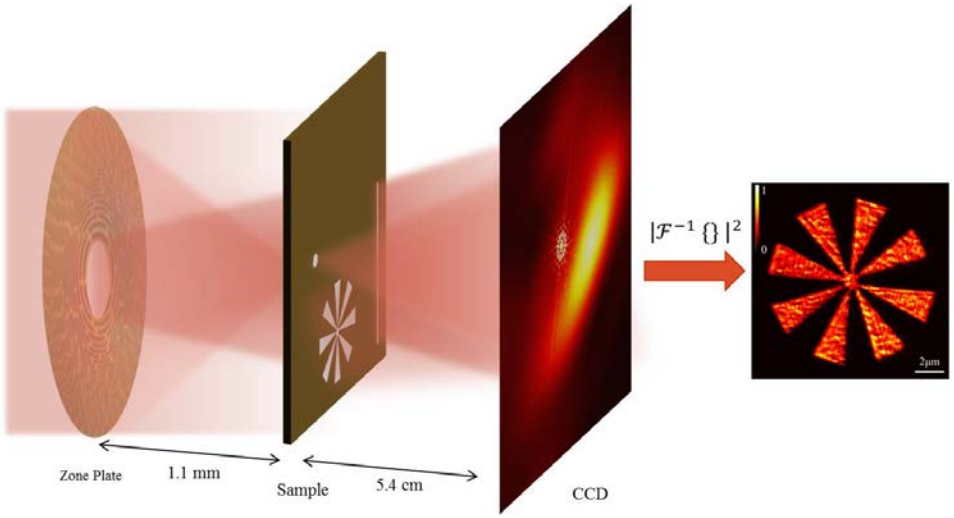

The large photon flux of the highly coherent table top EUV lasers allows for "flash" holographic imaging with spatial resolution of ~100nm and temporal resolution of 1ns.

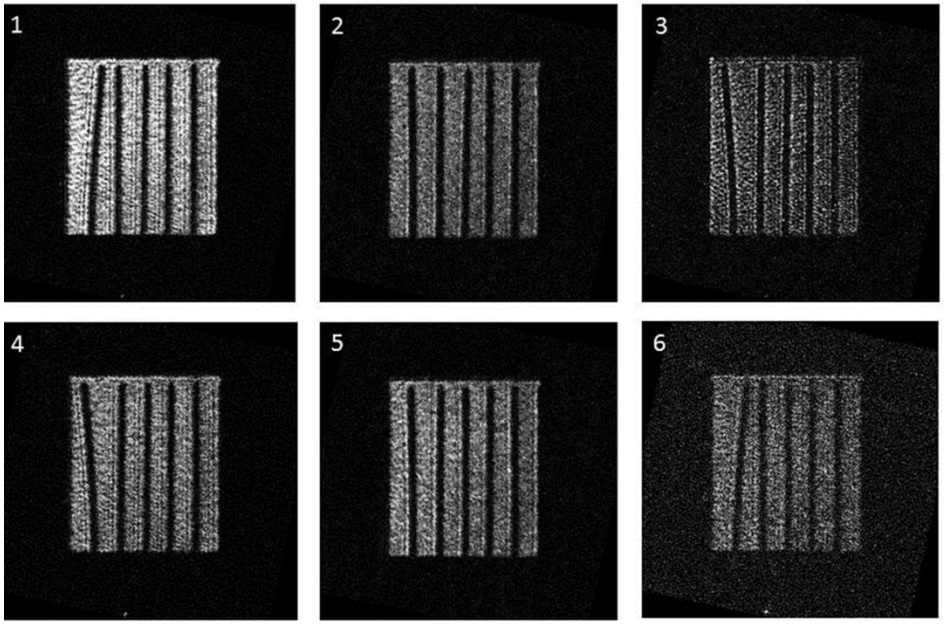

Frames from the motion picture of an array of 200 nm thick nanopillars

N. Monserut & P. Wachulak(Poland), M. Marconi

Recording and digitizing the hologram

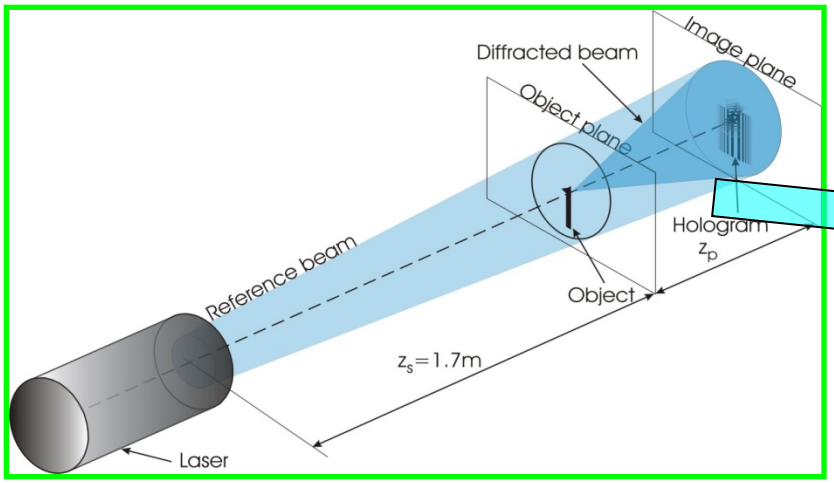

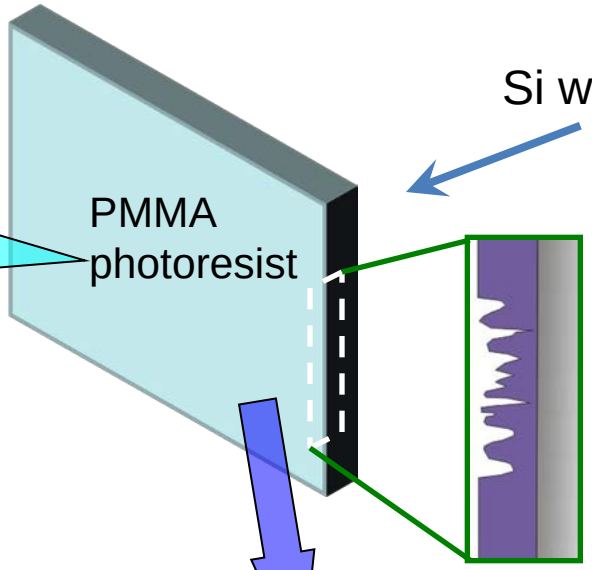

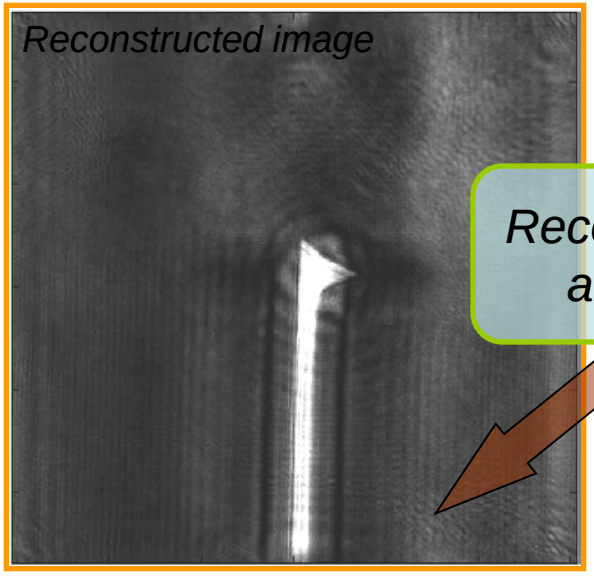

Reconstruction algorithm

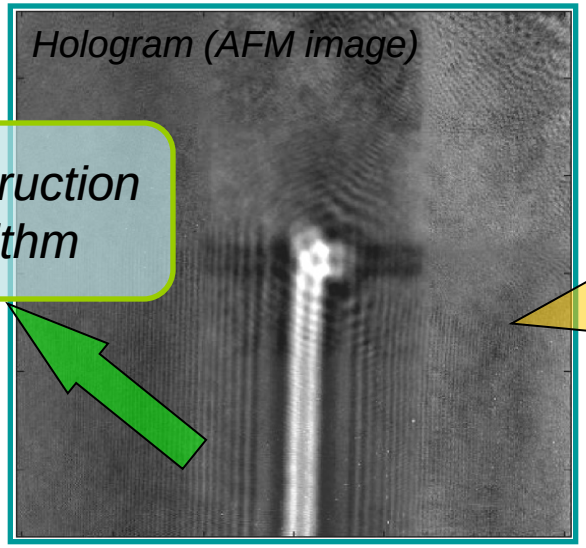

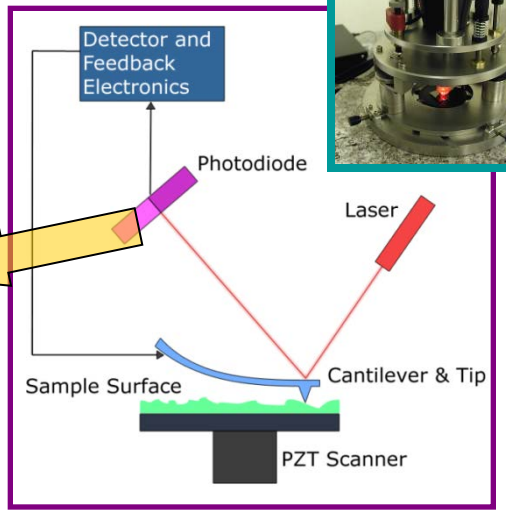

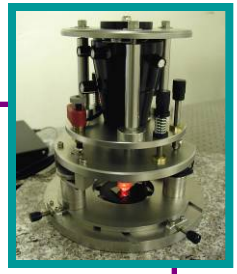

3D information: "numerical" optical sectioning

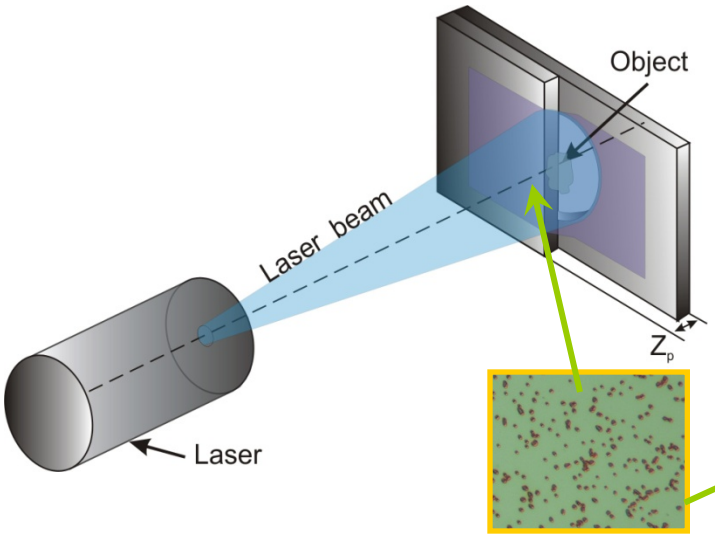

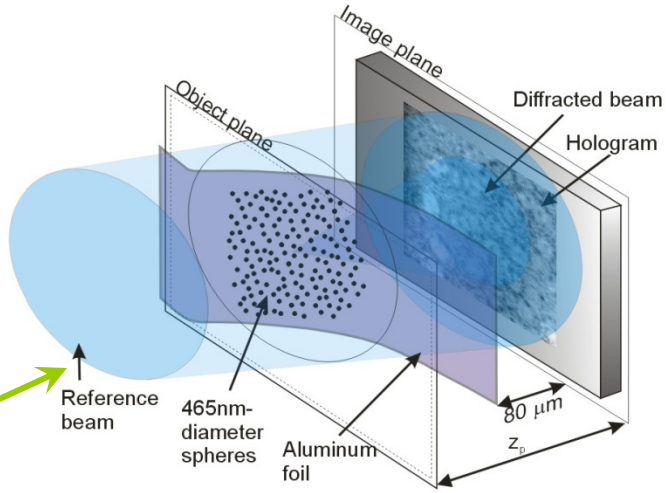

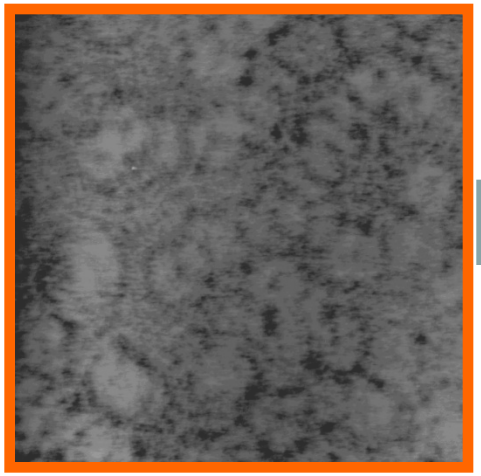

hologram

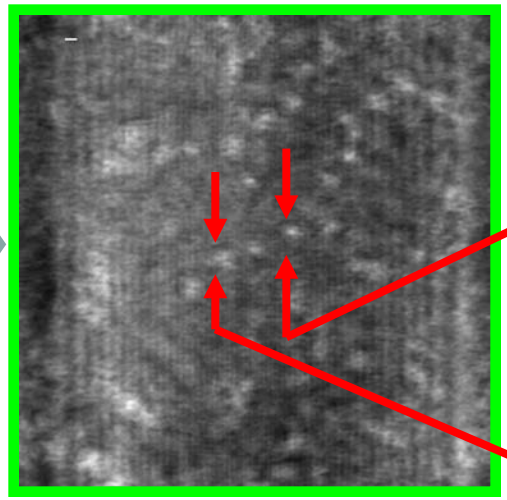

reconstruction

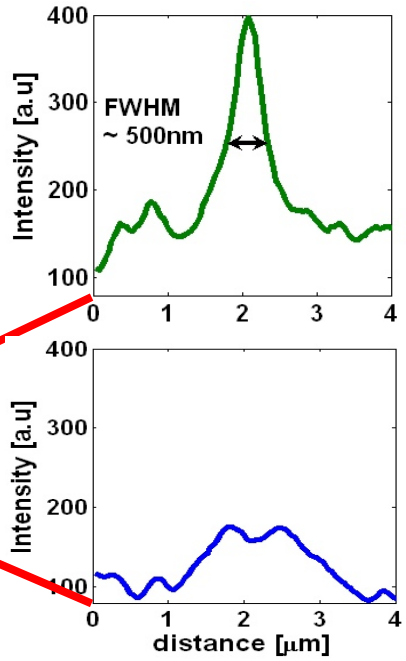

Mapping a surface

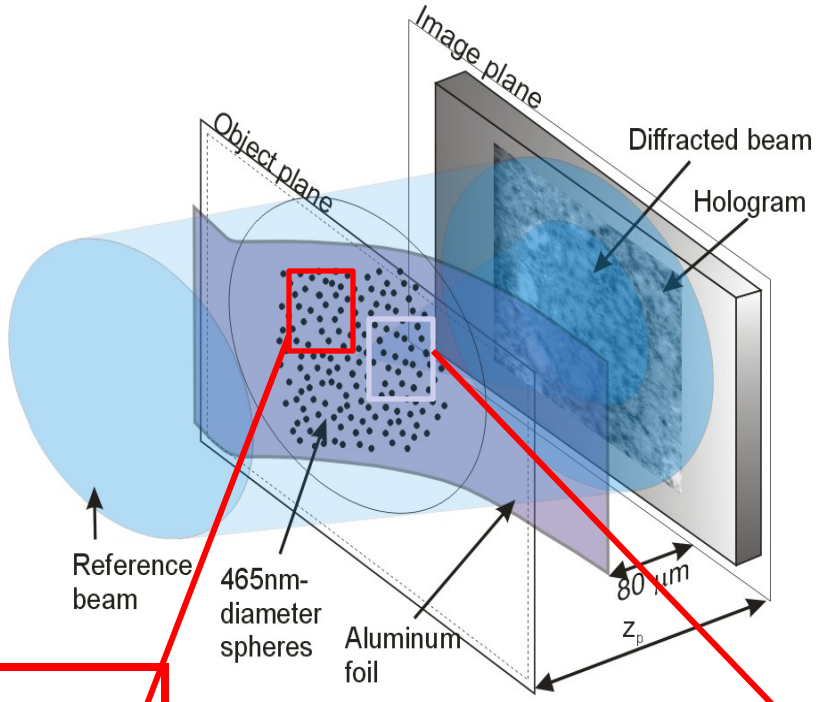

"Numerical" optical sectioning allows to reconstruct 3D information

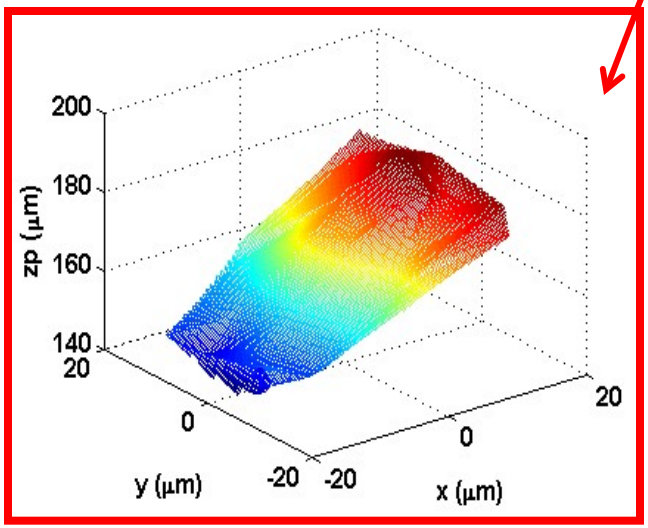

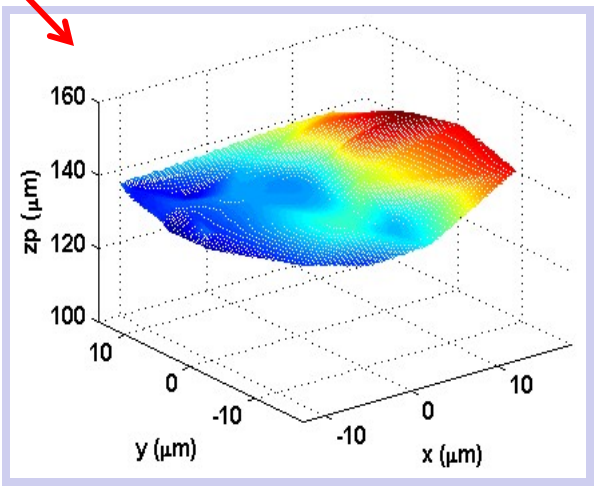

P. W. Wachulak, et al.Optics Express **15**, 10622-10628, (2007).

Wavelength resolution holography

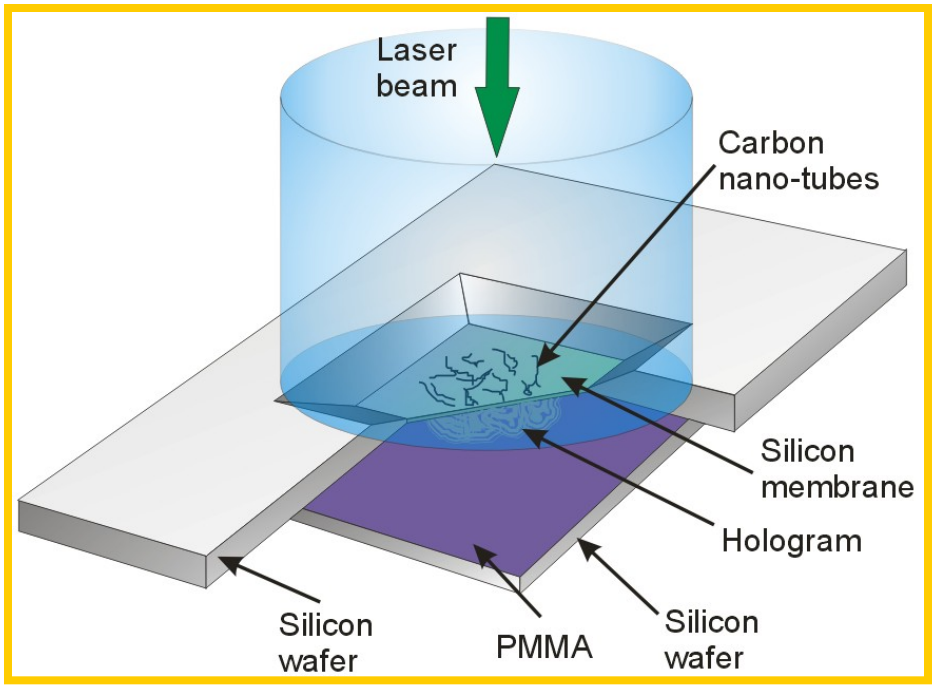

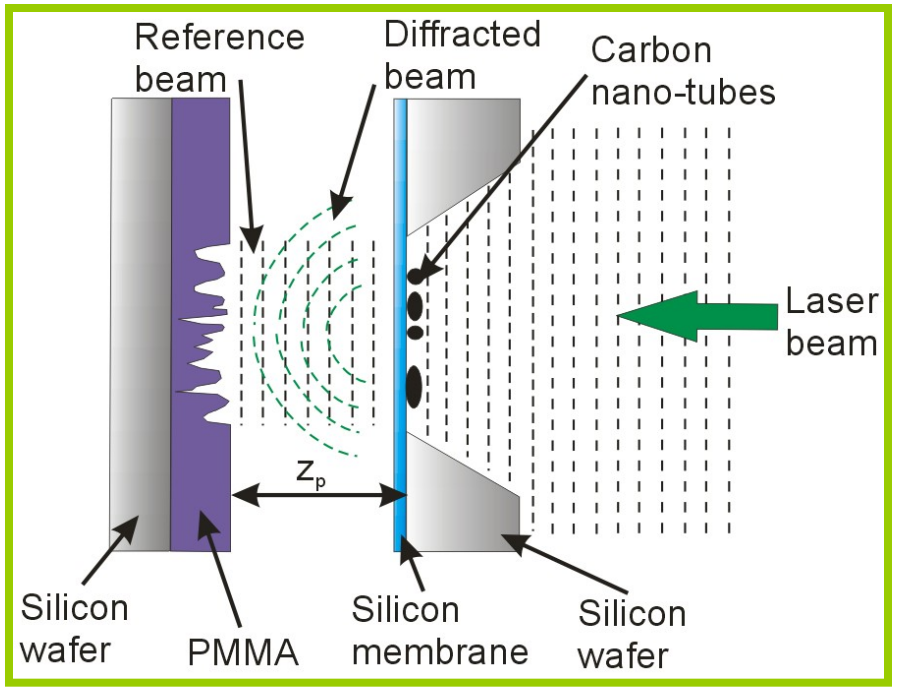

Object :

Multi-Wall Carbon Nanotubes :

- Thickness 30- 50 nm
- Length 10-20μm

Experimental details:

- z_p ~2.5 - 4 μm
- Laser-object distance z_s =75cm
- Laser shots = 150
- Dose = 53mJ/cm^2

Hologram and reconstruction 30-50 nm CNT

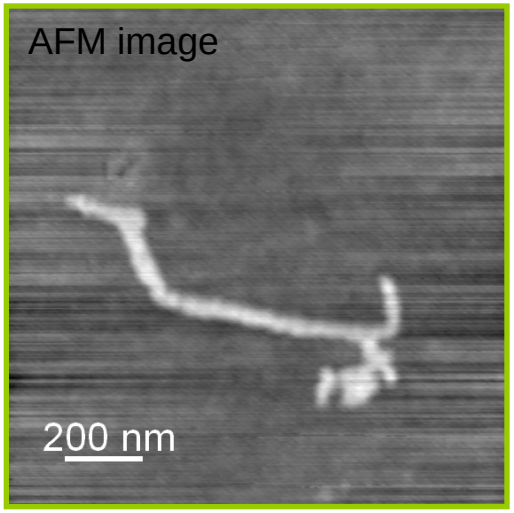

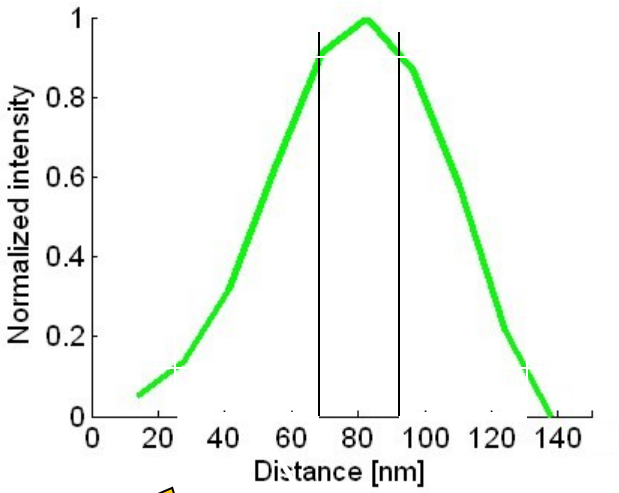

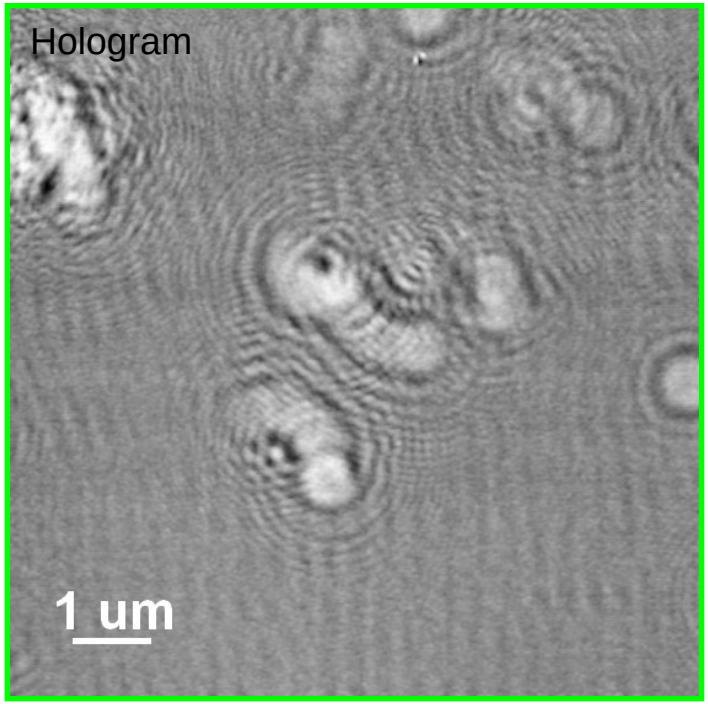

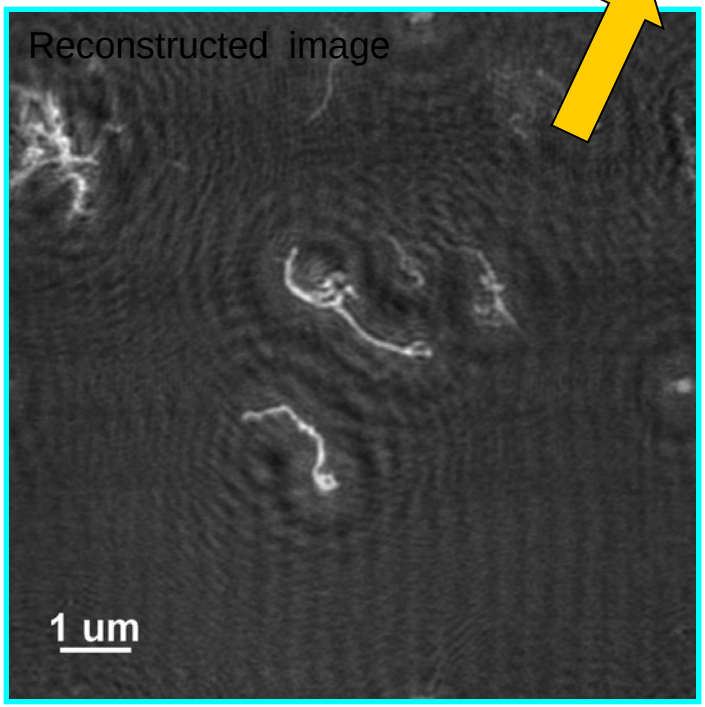

45nm 38nm

- z_p = **3.94 μm**
- pixel size = **9.7nm**

High numerical aperture tabletop soft x-ray diffraction microscopy with 70-nm resolution

Richard L. Sandberg,* Changyong Song,† Przemyslaw W. Wachulak,‡ Daisy A. Raymondson,* Ariel Paul,* Bagrat Amirbekian,† Edwin Lee,† Anne E. Sakdinawat,§ Chan La-O-Vorakiat,* Mario C. Marconi,‡ Carmen S. Menoni,‡ Margaret M. Murnane,*¶ Jorge J. Rocca,‡ Henry C. Kapteyn,* and Jianwei Miao†

PNAS January 8, 2008 vol. 105 no. 1, 24- 27

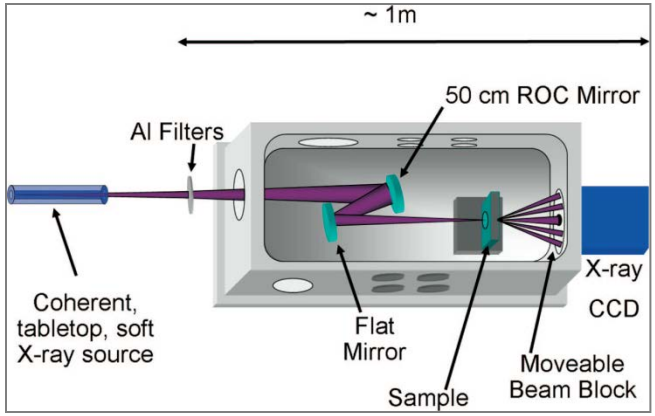

Set up: uses as illumination either λ=46.9 nm laser or λ=29nm harmonic of Ti:Sa

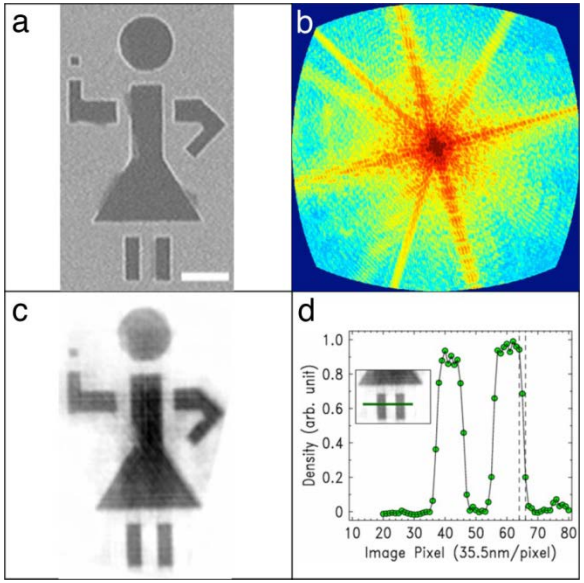

a) SEM image of object; b) diffraction pattern; c) reconstructed image; d) resolution test of coherent imaging at λ=46.9 nm

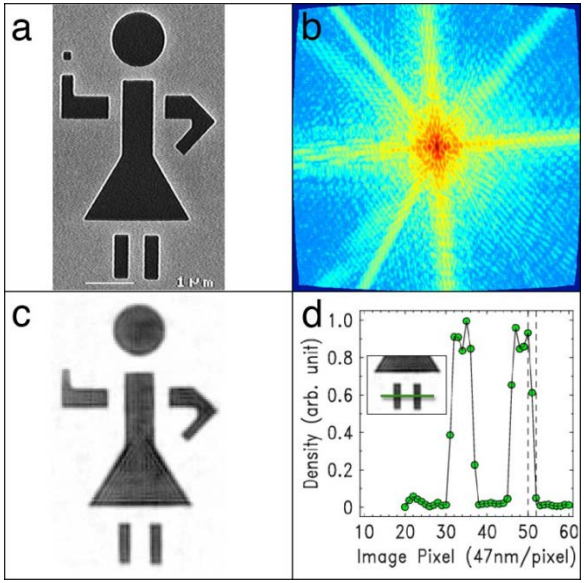

a) SEM image of object; b diffraction pattern; c) reconstructed image; d) resolution test of coherer imaging λ=

Microscope for table-top defect inspection in EUV lithography masks

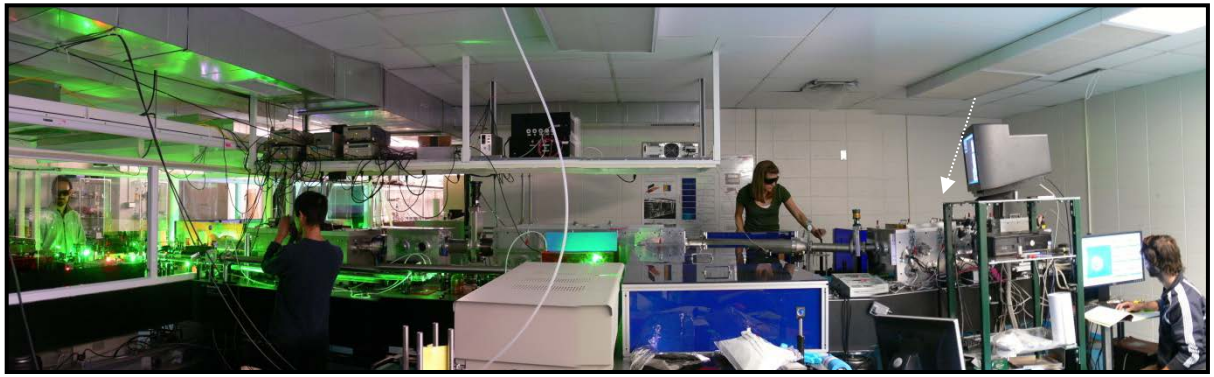

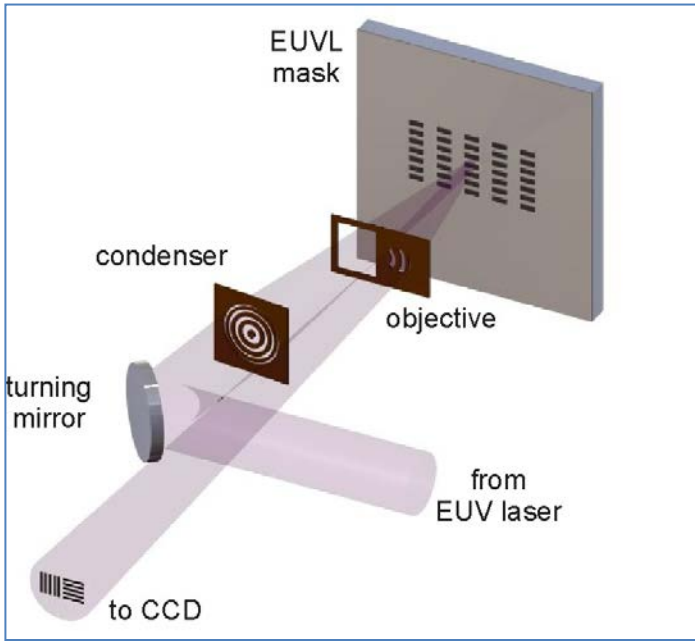

Resonant illumination enables detection of defects at the surface and buried within Mo/Si coatings in extreme ultraviolet lithography masks

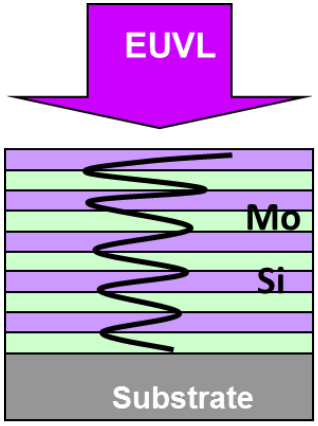

At-wavelength images of EUV lithography masks

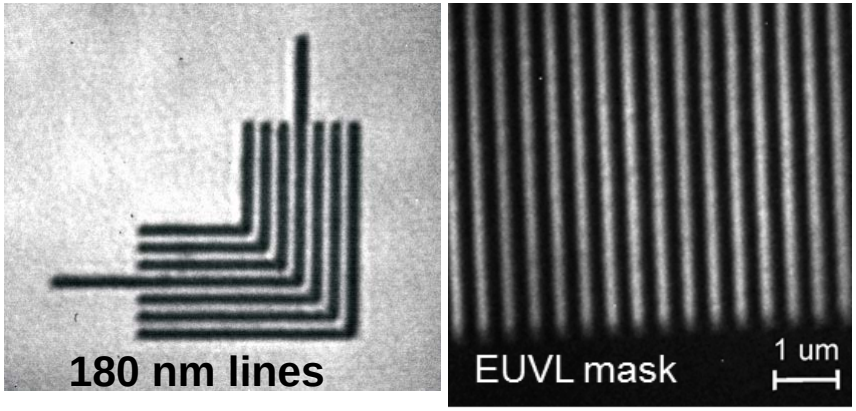

Image analysis provides line-edge roughness, a critical metric of mask quality

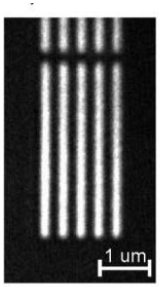

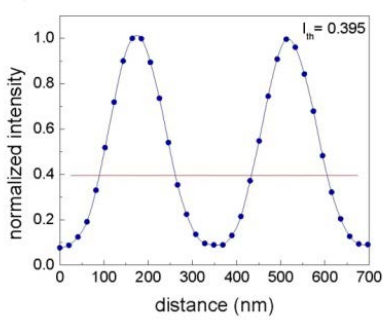

F. Brizuela et al, Optics Letters vol. 34, 271, (2009)
F. Brizuela, et a. Optics Express, Vol. 18, 14467 (2010)

λ=13.2 nm microscope: Mask illumination emulates EUVL stepper

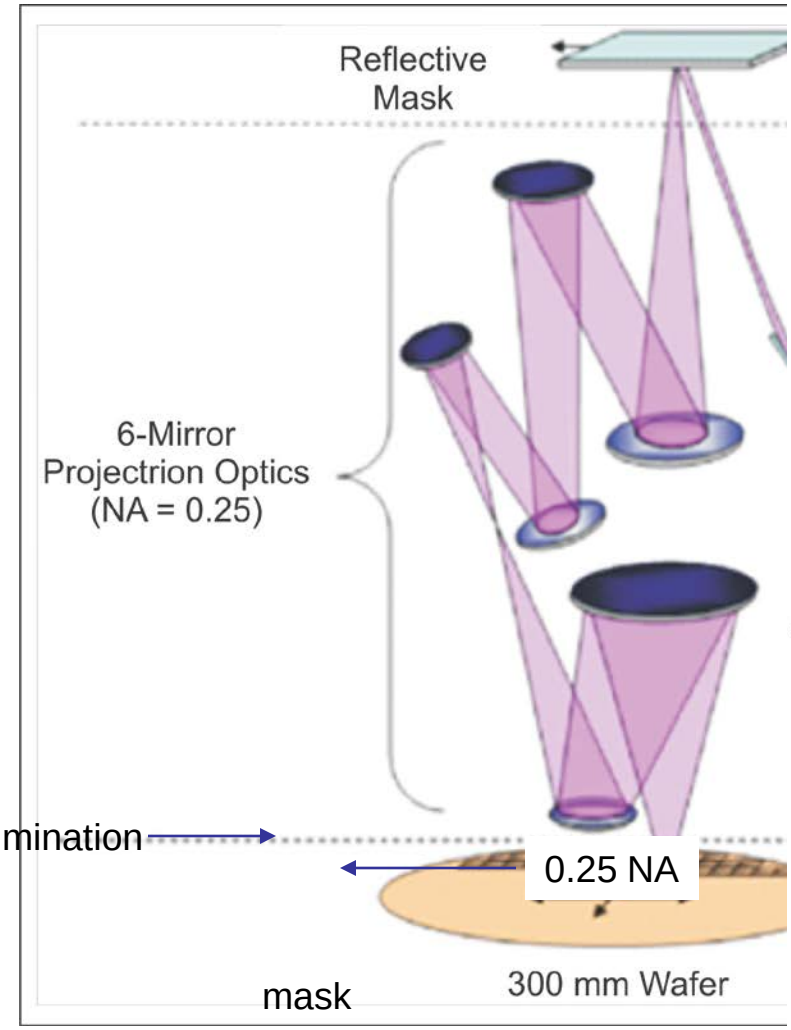

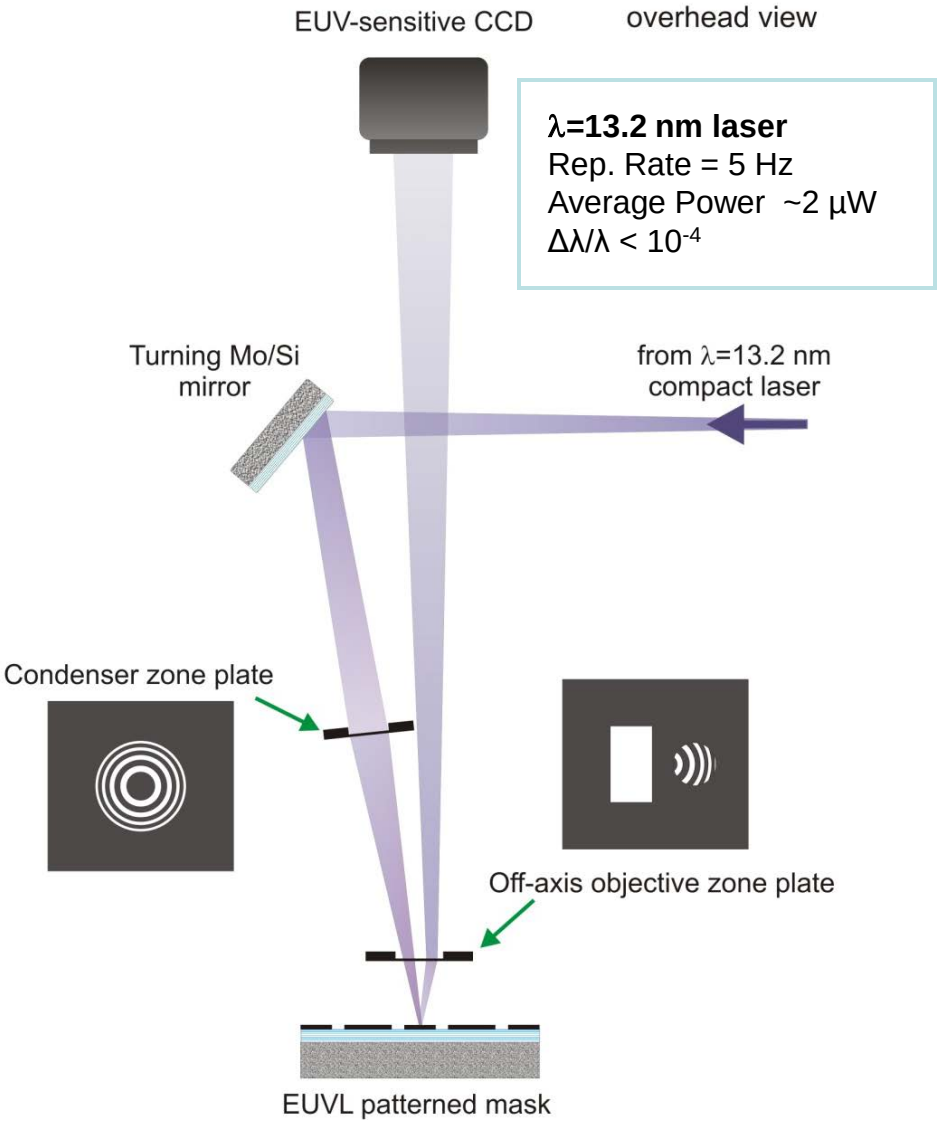

11/14

2010 results - Improved illumination allows to obtain high quality images for line edge roughness analysis

EUV Image of elbow patterns on a EUVL mask with CD = 180 nm
Exposure: 90 sec

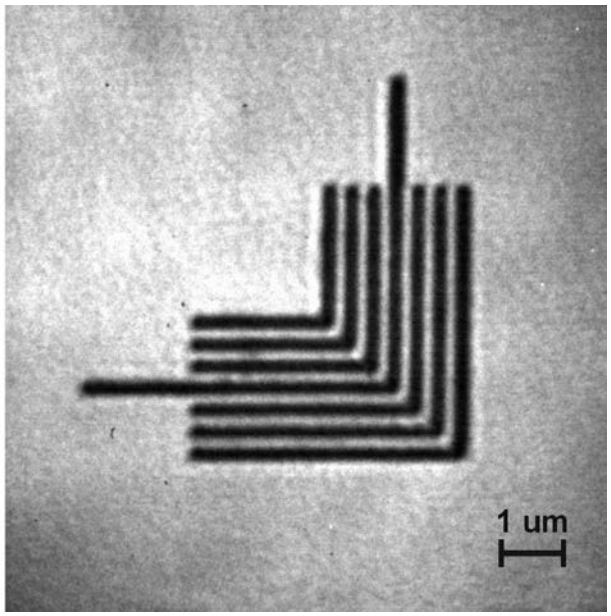

EUVL mask image of lines with CD=200 nm pattern
Exposure: 90 sec

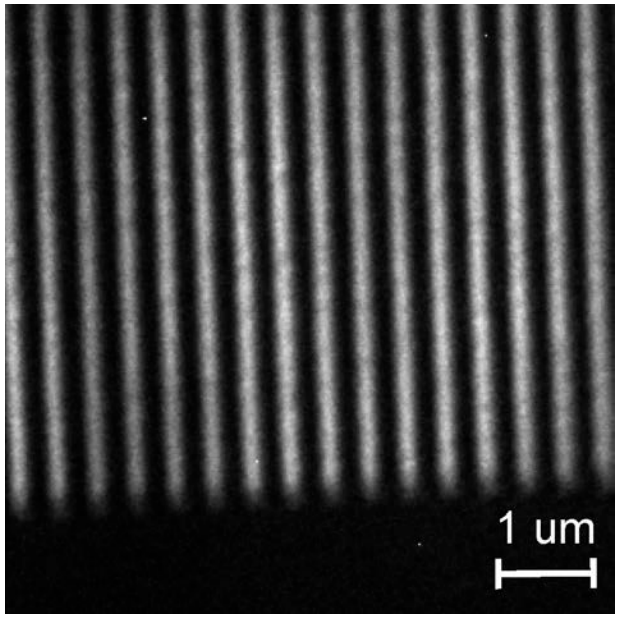

GLOBALFOUNDRIES

TABLE TOP EUV MICROSCOPE CAN TEST EUVL MASK PATTERN AND DEFECT PRINTABILITY INDEPENDENT OF RESIST RESPONSE

High quality EUV images reliably allow to obtain line-edge roughness (LER) on EUVL mask

CD=175

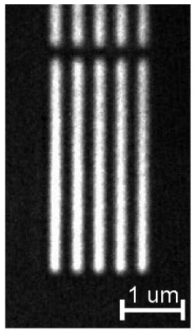

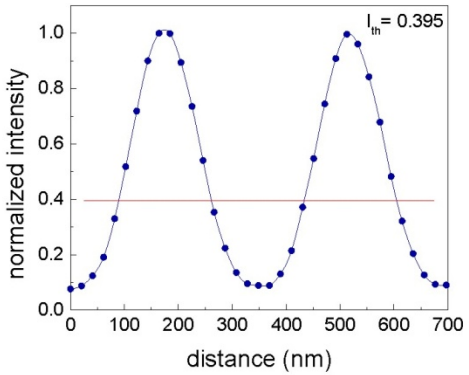

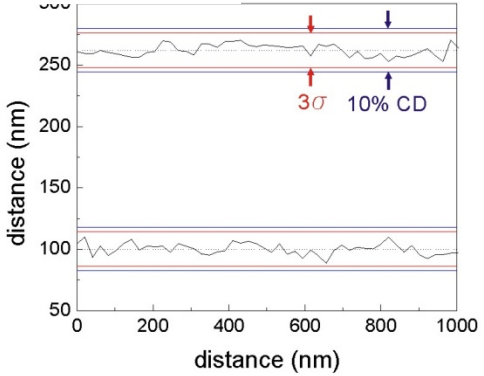

CD=225

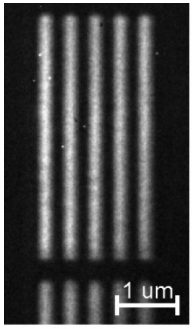

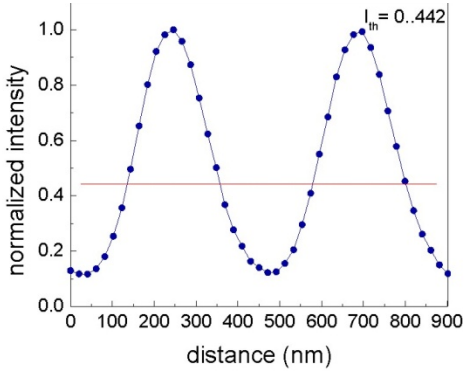

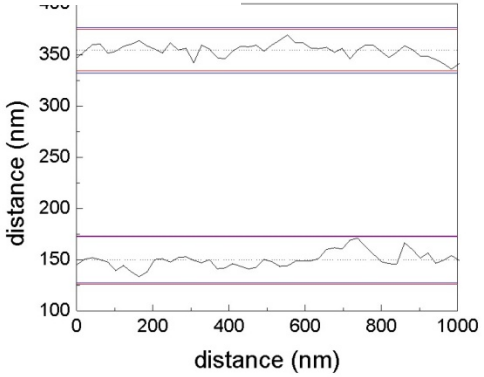

CD (nm)	I_{th}	NILS	LER (nm)	LER/CD
175	0.395	3.58	13.55	0.078
225	0.442	3.32	20.86	0.093

F. Brizuela, Optics Express 2010

No chemical fixatives or contrast enhancement reagents were used to image these cells

Organelle Details Imaged with Cryogenic Preservation and High Spatial Resolution

BERKELEY LAB

Cryo x-ray microscopy of 3T3 fibroblast cells

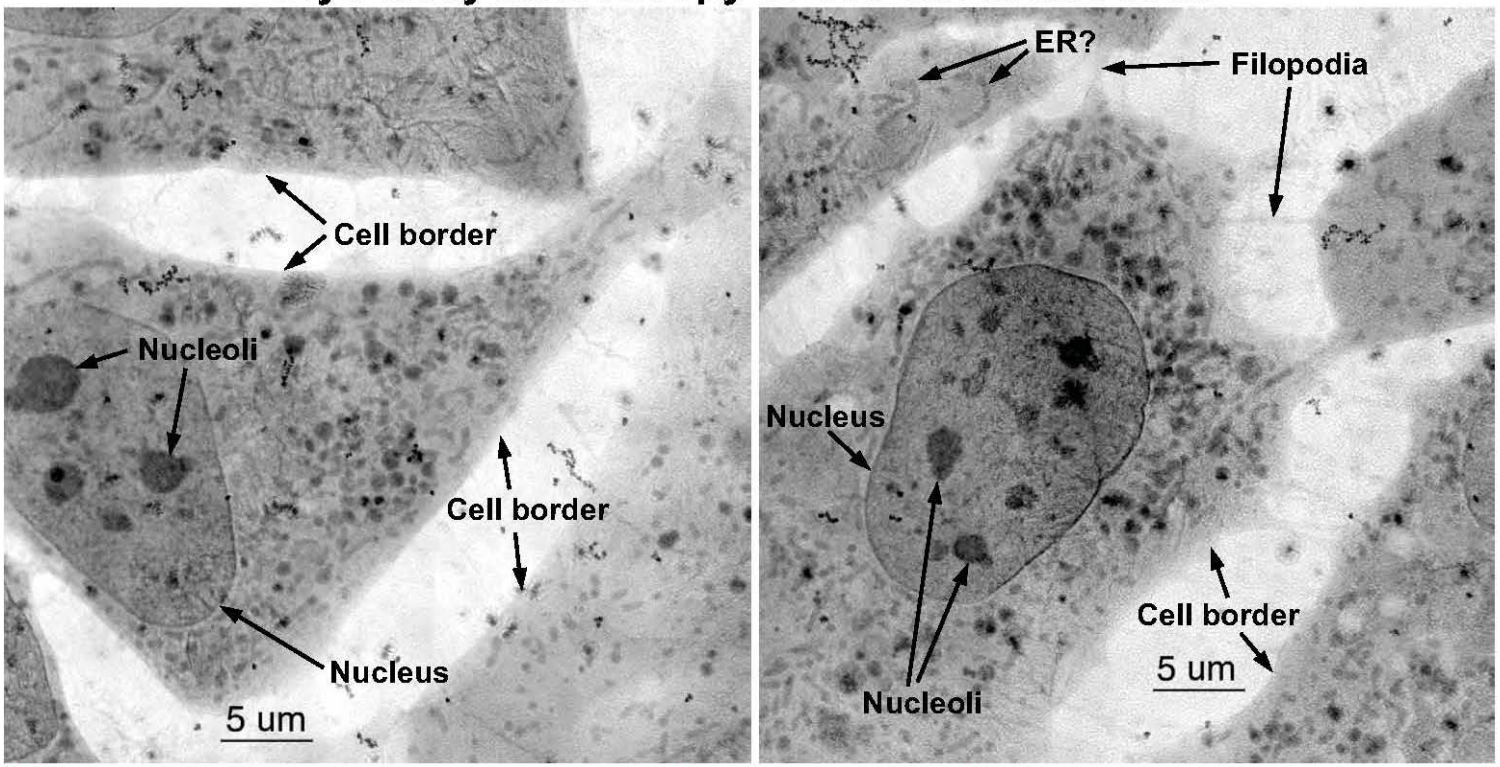

C. Larabell, D. Yager, D. Hamamoto, M. Bissell, T. Shin (LBNL Life Sciences Division)
W. Meyer-Ilse, G. Denbeaux, L. Johnson, A. Pearson (CXRO-LBNL)

nanoXCT: Schematic and Challenges

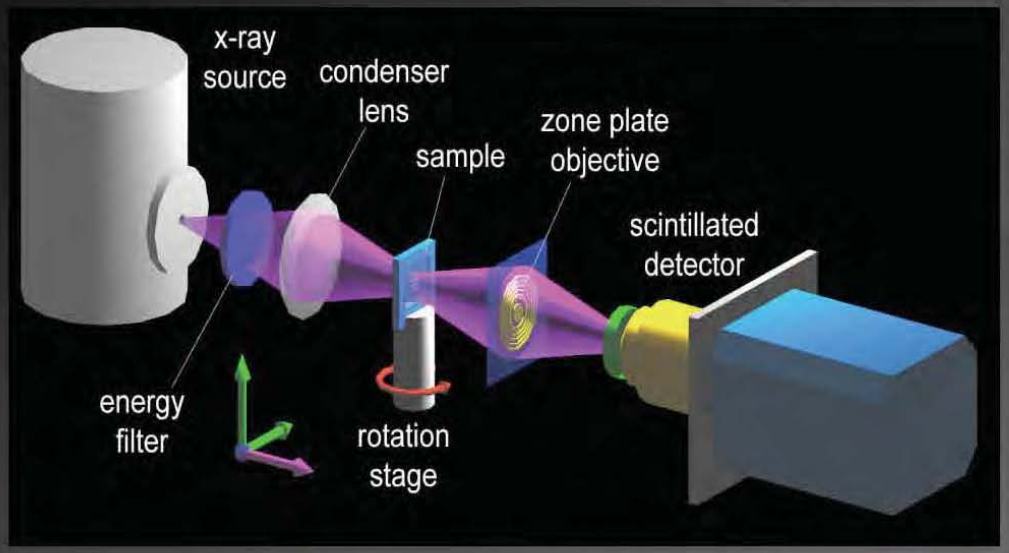

X-ray Zone-plate Lens

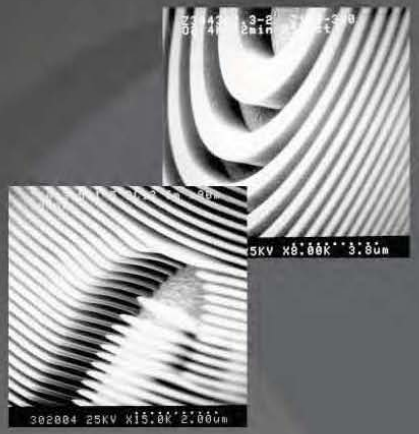

Challenges for achieving nm scale resolution:

- High resolution objective lens: limiting the ultimate resolution
- High numerical aperture condenser lens:
- Detector: high efficiency for lab. source and high speed for synchrotron sources
- Precision mechanical system

Nano-tomography

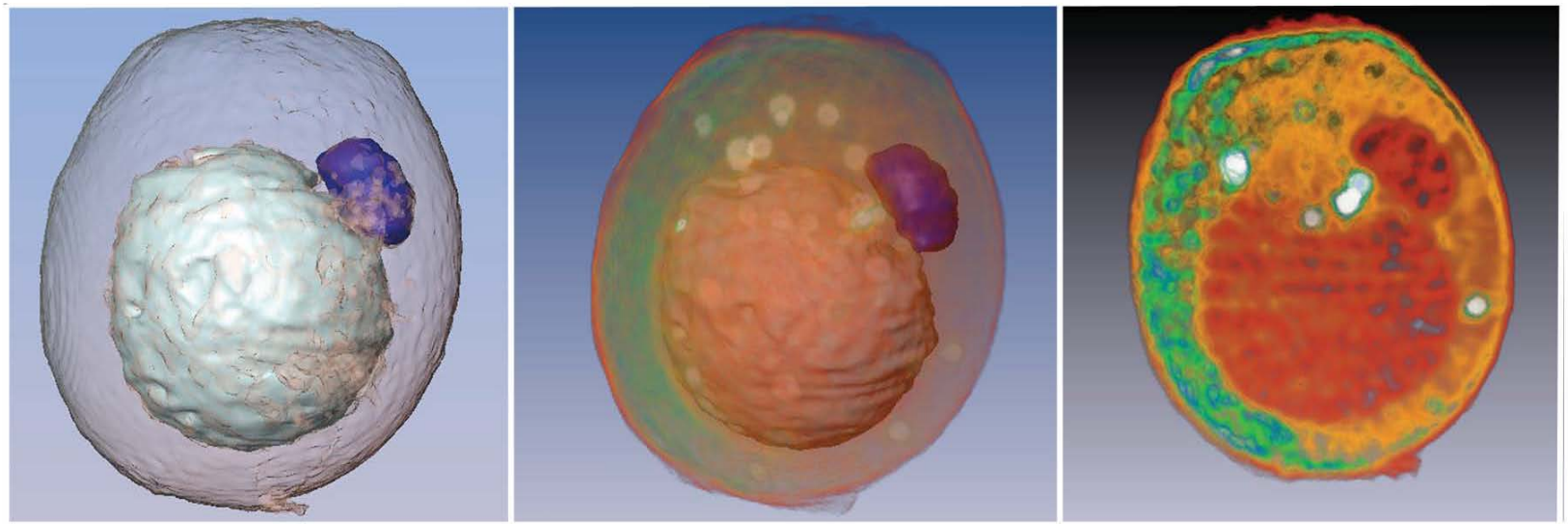

C.A. Larabell & M.A. Le Gros (2004). Molecular Biology of the Cell, 15(3), 956-962

Summer School – 2010

Lensless imaging of whole biological cells with soft X-rays

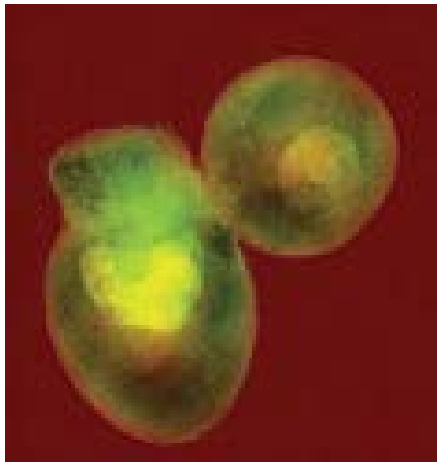

High-resolution x-ray diffraction microscopy of specifically labeled yeast cells

Johanna Nelson[a],[1], Xiaojing Huang[a], Jan Steinbrener[a], David Shapiro[b], Janos Kirz[b], Stefano Marchesini[b], Aaron M. Neiman[c], Joshua J. Turner[a], and Chris Jacobsen[a],[d],[e]

Procc. Nat. Acad. 0910874107

A pair of yeast cells imaged at very high resolution using coherent soft x-rays at the Advanced Light Source's beamline 9.0.1. The coherent (laser-like) beam of penetrating x-rays allows a computer to reconstruct the cells' internal structures from a diffraction pattern, without focusing the light with a lens.

Abstract: We report here the highest resolution (11–13 nm) x-ray diffraction micrograph of biological specimens, and a demonstration of molecular-specific gold labeling at different depths within cells via through-focus propagation of the reconstructed wavefield. The lectin concanavalin A conjugated to colloidal gold particles was used to label the α-mannan sugar in the cell wall of the yeast *Saccharomyces cerevisiae*. Cells were plunge-frozen in liquid ethane and freeze-dried, after which they were imaged whole using x-ray diffraction microscopy at 750 eV photon energy.

http://esciencenews.com/articles/2010/04/27/lensless.imaging.whole.biological.cells.with.soft.x.rays

EUV Laser Ablation/Ionization Nano-Mass Spectrometry

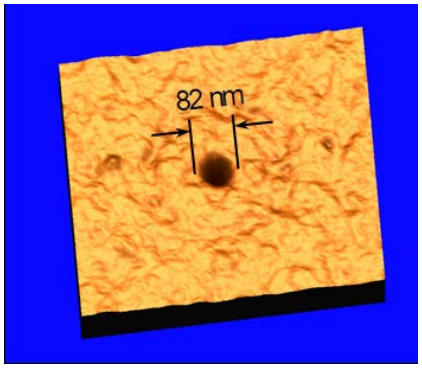

82 nm diameter, 10 nm deep crater in resist

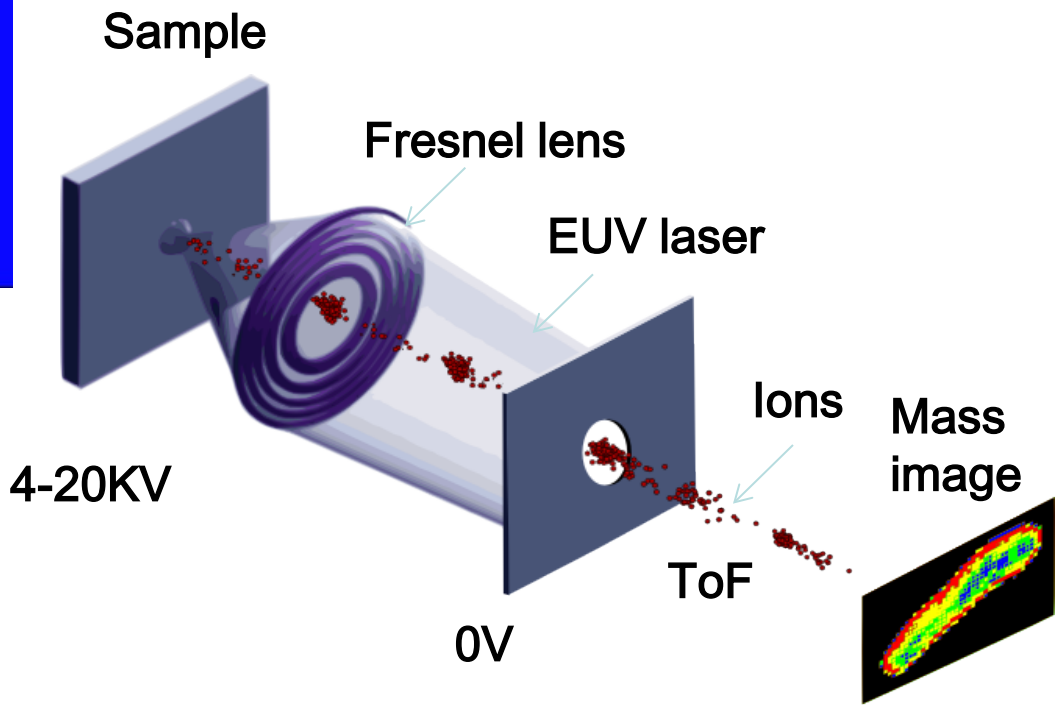

- **EUV laser pulses are focused onto specimen**
- **The focused laser ablates the material and simultaneously ionizes the fragments in the ablation plume**
- **Ions are extracted into the Time of Flight mass spectrometer**

I. Kuznetsov, J. Filevich, C. Menoni

3D imaging nano-mass spectrometry system

EUV Optics
Fresnel zone plate
0.16 NA

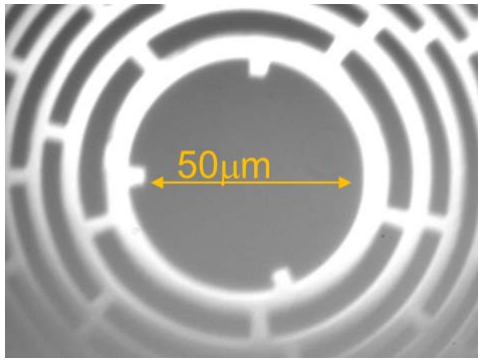

EUV laser
Wavelength : 46.9 nm
- **Energy per pulse > 0.010 microjoule**
- **Repetition rate: 12 Hz**
- **Pulse duration ~1.5 ns**

S. Heinbuch Optics Express vol. 13, 4050 (2005)

EUV optics engineered by W. Chao and E. Anderson at Center of X-Ray Optics, LBL.

E.H. Anderson, IEEE J. Quantum Electronics, vol.42, 27, 2006

Results: Biological compounds
Single shot mass spectrum of Alanine

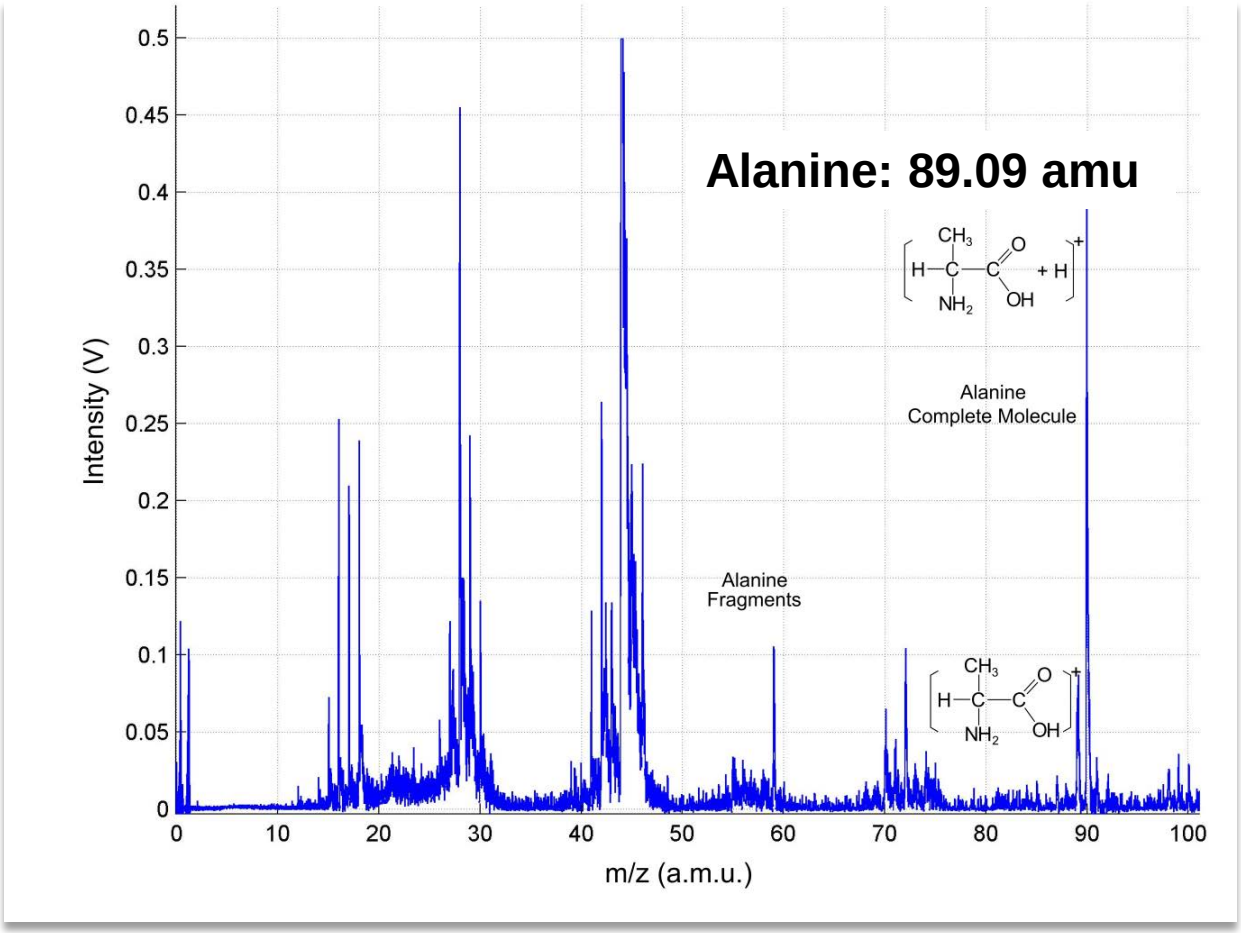

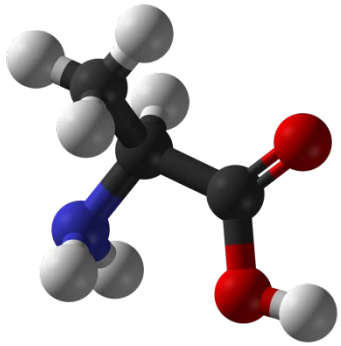

- Parent molecule and fragments observed

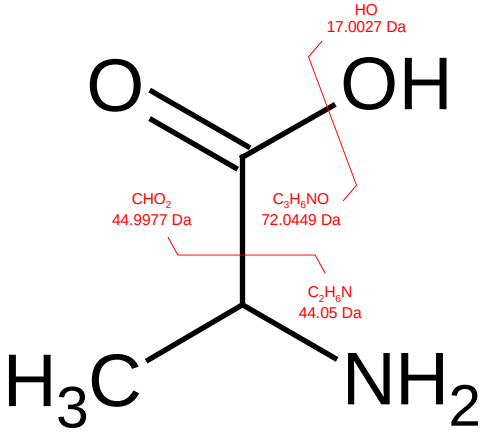

Monoisotopic Mass = 89.047678 Da
[M+H]+ = 90.054955 Da

High sensitivity signal from ~100 a-moles of analyte

Results

2D imaging with 154 nm lateral resolution

Microscope Image

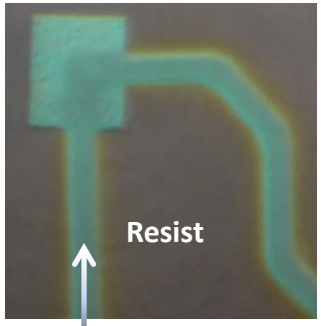

Trench with ITO at bottom

Resist

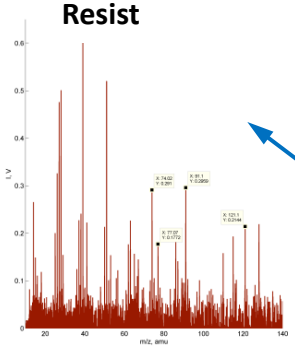

ION IMAGE

40 pixel x 40 pixel

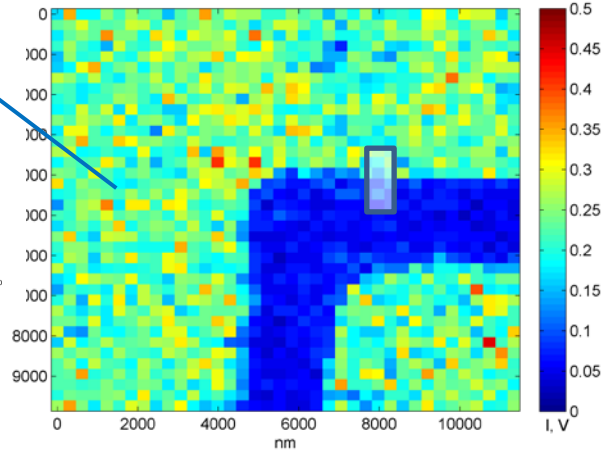

AFM IMAGE

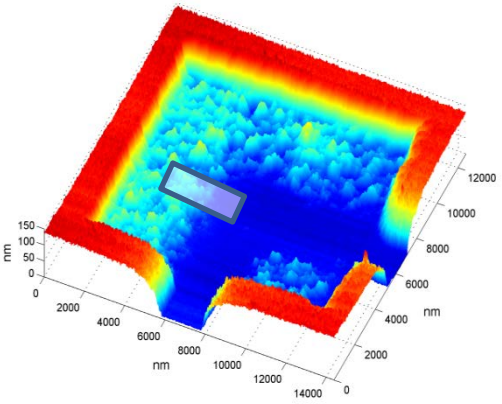

AFM profile of the resist edge

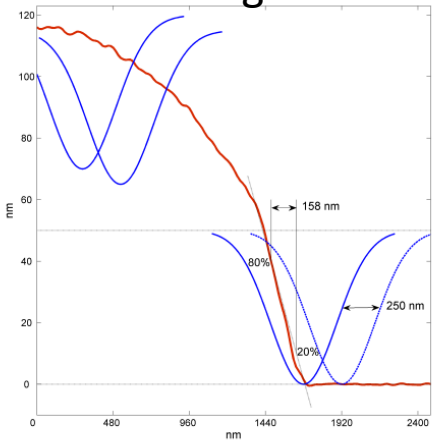

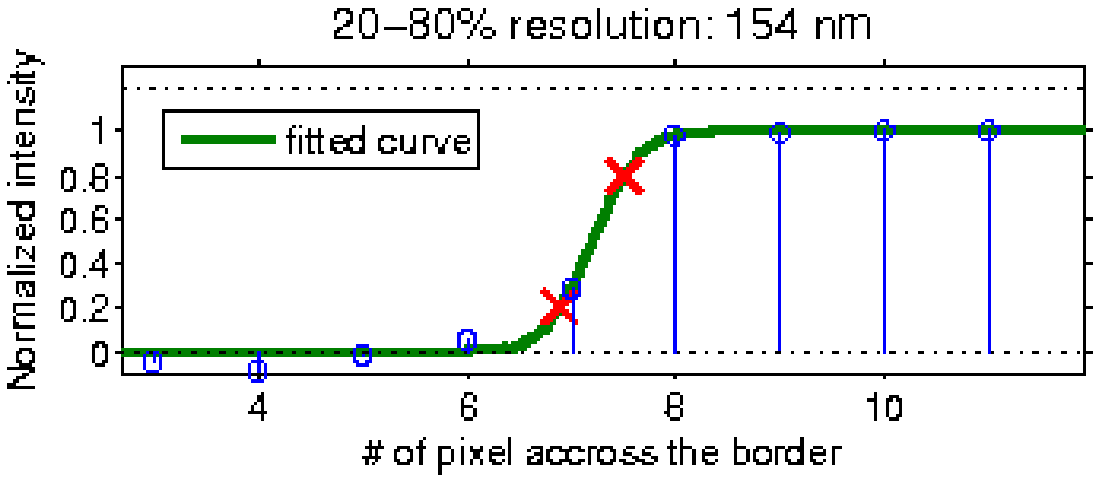

What is the overall goal on this project?

To develop a mass spectrometry imaging system capable to map molecular composition on single cells, on a single atmospheric aerosol; trace detection of metals in bio-organics…….

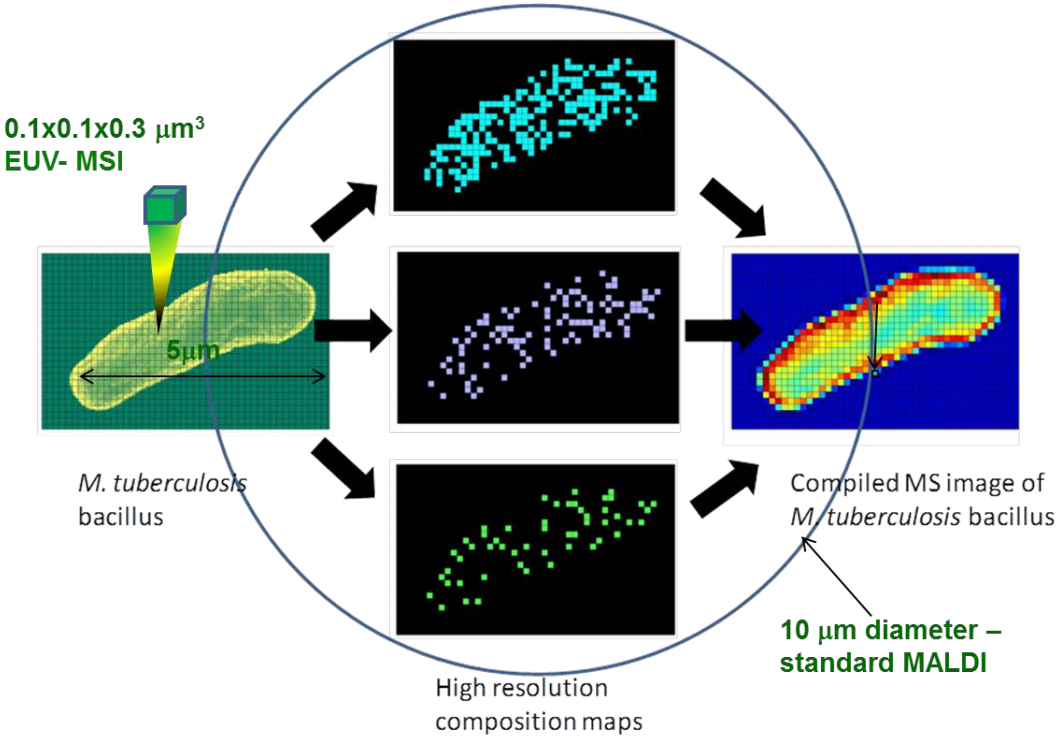

Challenges:

- To control molecular fragmentation
- To increase sensitivity to detect single ions.

Increased resolution will be exploited to investigate chemical changes in in a *single Mycobacterium tuberculosis* bacterium at the subcellular level

Fast Freeze Cryo Fixation Strongly Mitigates Radiation Dose Effects

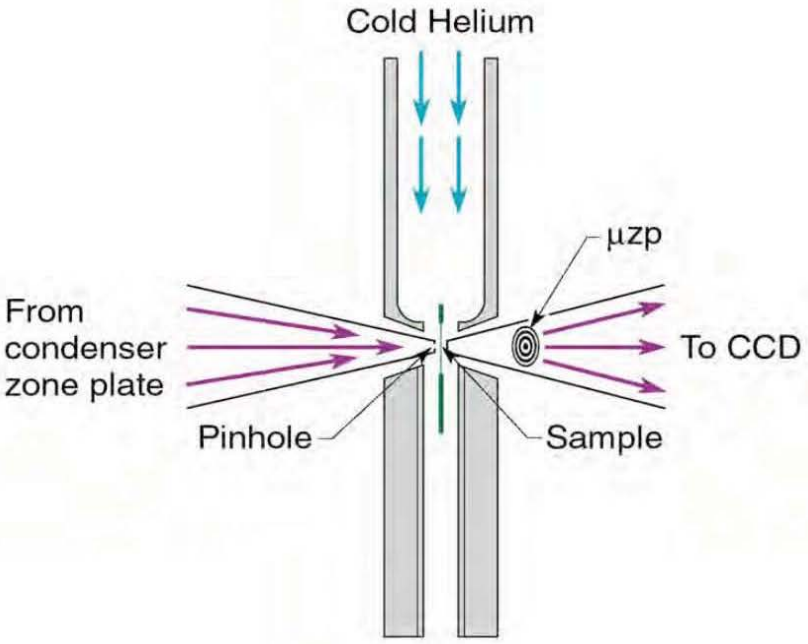

Helium passes through LN, is cooled, and directed onto sample windows

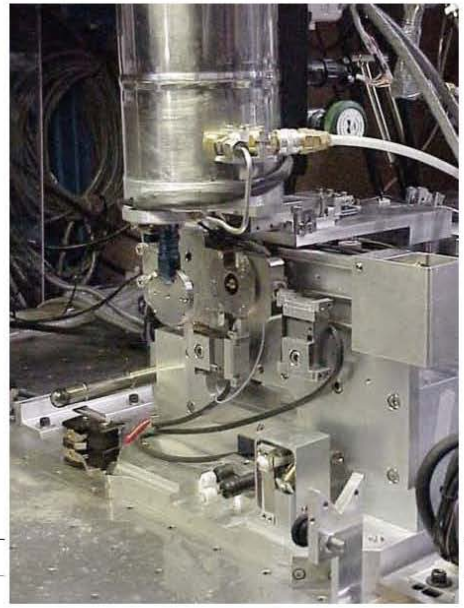

Fast Freeze

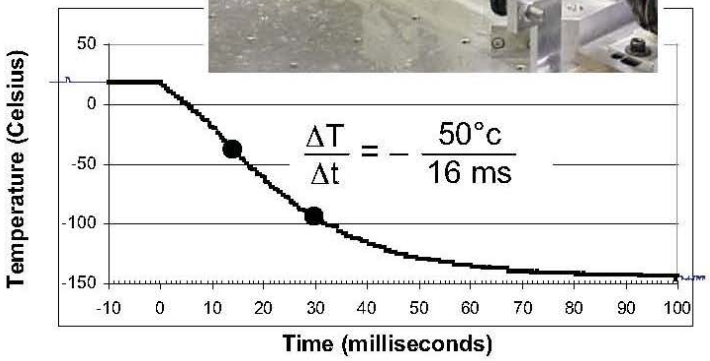

W. Meyer-Ilse, G. Denbeaux, L. Johnson, A. Pearson (CXRO-LBNL)

Motivation: Modern magnetic materials consist of nm thick layers of metal/oxides –unpatterned and patterned . Their dynamics plays a crucial role in technological applications.

The New Paradigm: Smaller and Faster

Examples: Magnetic Devices in Computers

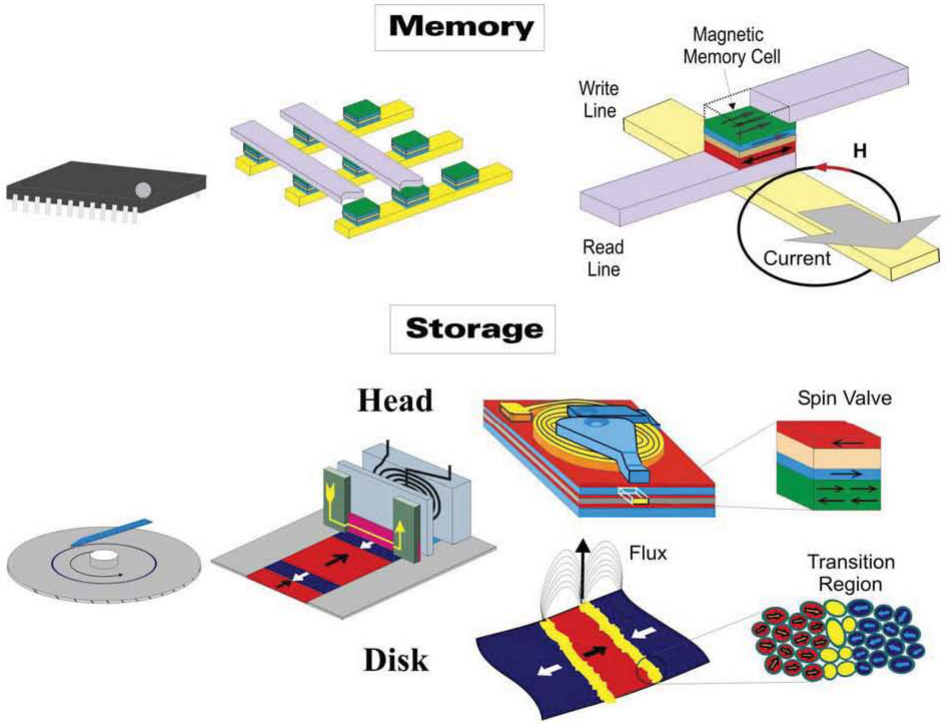

Future: < 100 nm, < 1 nsec → Ultrafast Nanoscale Dynamics

What does it take to explore advanced magnetic materials and phenomena ?

General requirements:	*Technique requirements:*
see the invisible	nanoscale spatial resolution
separate spin and orbital contributions	sensitive to s-o coupling
study thin films and interfaces	large cross section for "signal"
look below the surface	depth sensitivity
distinguish components	elemental (chemical) specificity
resolve dynamic motions	time resolution < 1 nanosecond

…. x-rays

Capability to polarize light

Summer Schoo

X-rays to probe magnetic materials need sufficient photon energy to reach atomic resonances

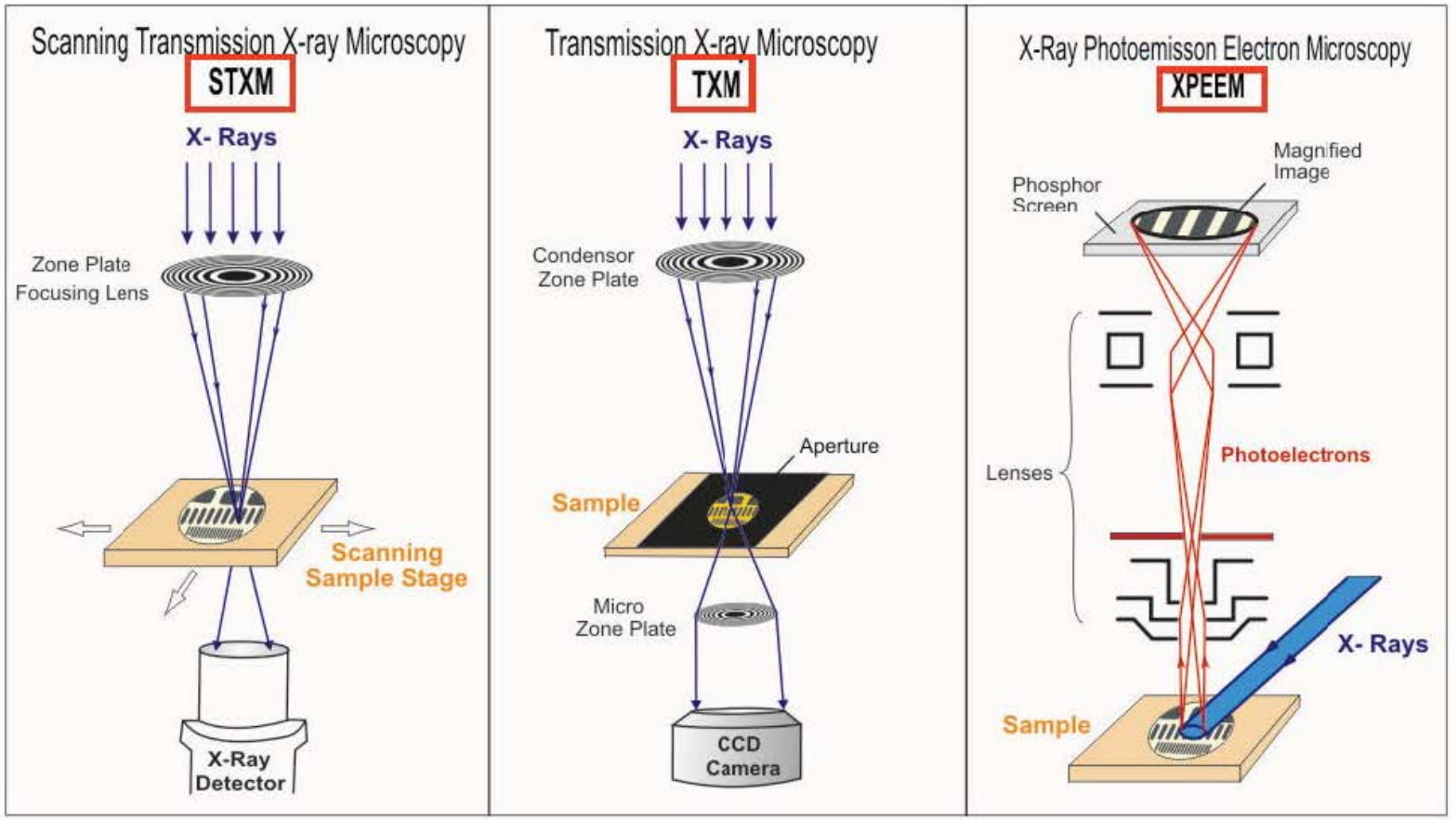

Present resolution in the 20 - 40 nm range

x-rays in / x-rays out – bulk like sensitivity
x-rays in / electrons out – near-surface sensitivity

Summer School – 2010

Imaging of Thermomagnetically Written Bits in MO Media

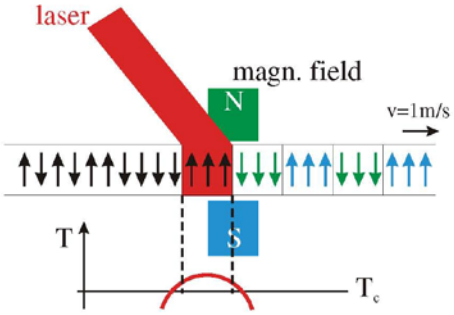

100 nm lines & spaces →

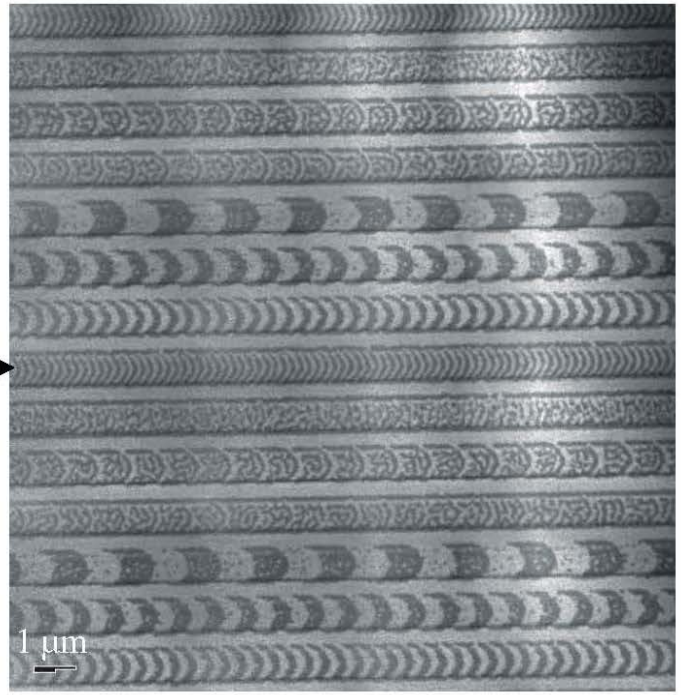

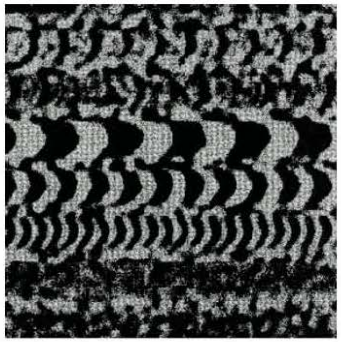

MFM-image

$SiN(70\ nm)/Tb_{25}(Fe_{75}Co_{25})_{75}(50\ nm)/SiN(20\ nm)/Al(30\ nm)/SiN(20\ nm$

P. Fischer et al., Wuerzburg; N. Takagi et al., Sanyo; G. Denbeaux et al., CXRO/LBNL

Summer School – 2010

Magnetic phase contrast with Fourier Optics

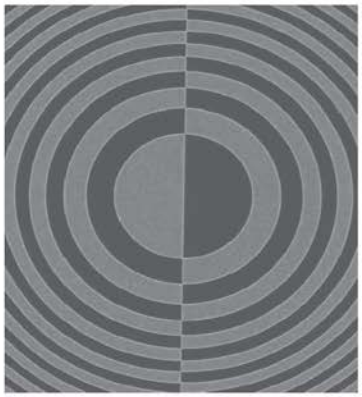

C. Chang, et al., Appl. Optics 41, 7384 (2002)

- XOR pattern = zone plate + transmission grating
- direct measurement of real and imaginary parts of (f´ and f´´)
- differential phase contrast objective

sample: 59nm $Gd_{25}Fe_{75}$

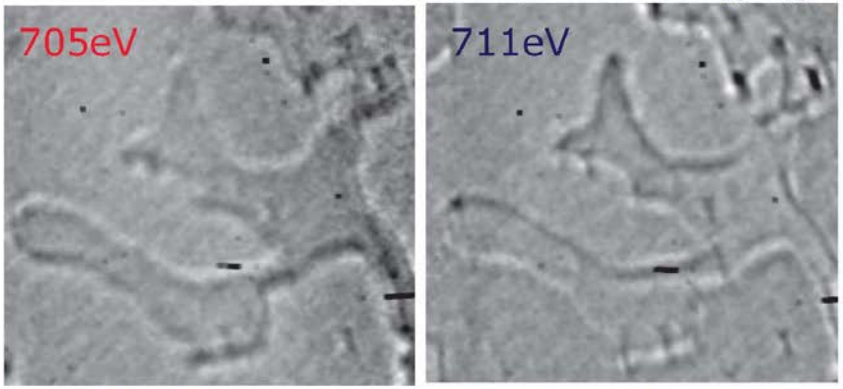

C. Chang, A. Sakdinawat, P. Fischer, Optics Letters 31(10) (2006) 1564-1566

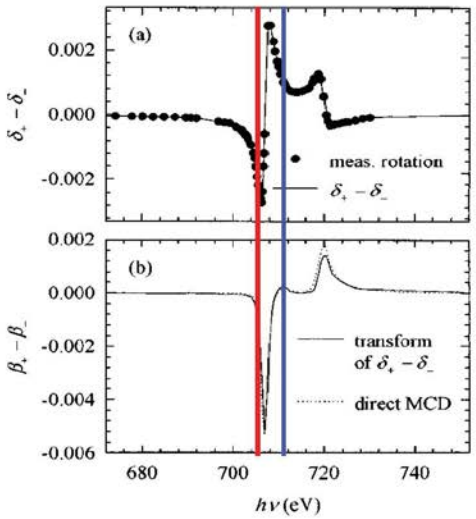

J. Kortright, S.-K. Kim, PRB 62 (2000) 12216

Peter Fischer

EE 290F Synchrotron Radiation for Materials Science Applications April 17, 2007

59

Summer School – 2010

Electron Microscopes TEM

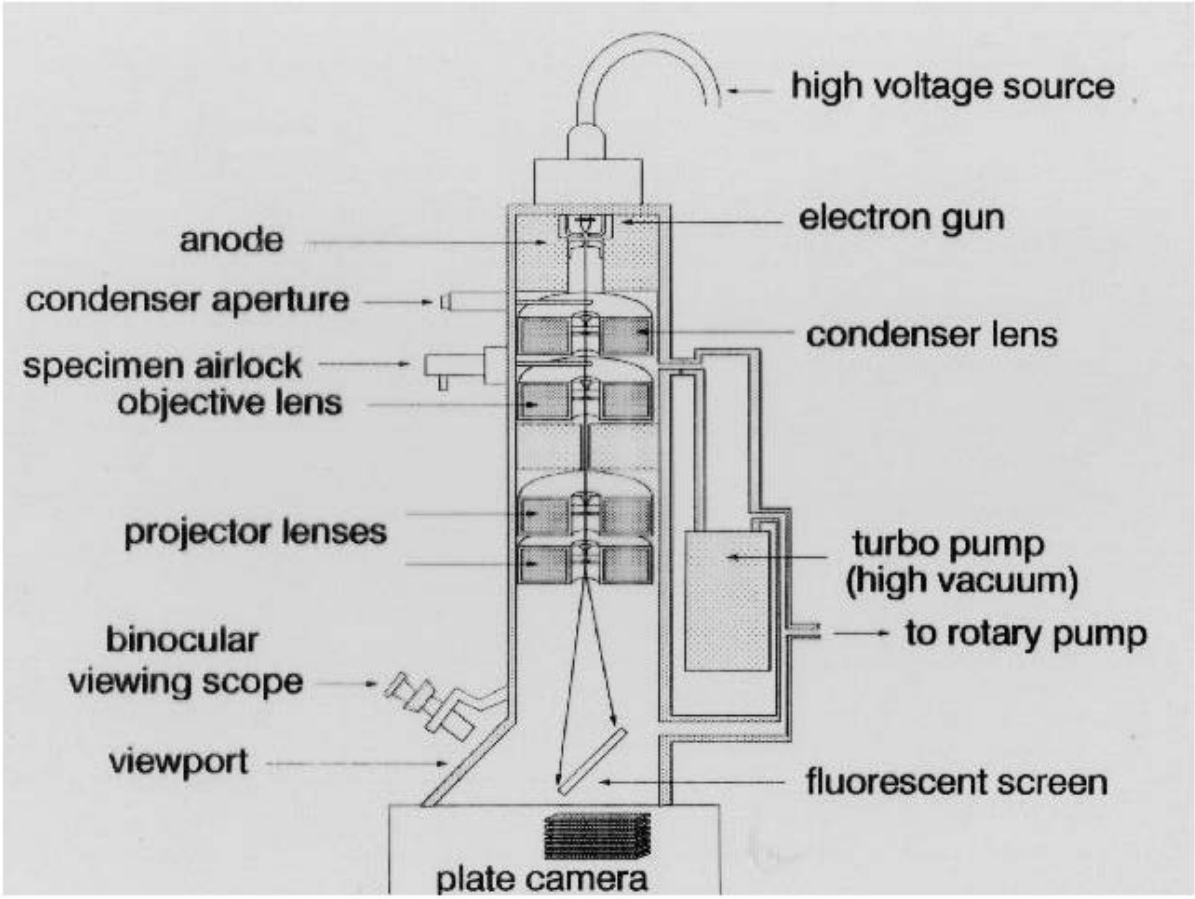

http://www.fei.com/products/

The resolution of the TEM is limited by spherical and chromatic aberration, but a new generation of aberration correctors has been able to overcome this problem. Software correction of spherical aberration has allowed the production of images with sufficient resolution to show carbon atoms in diamond separated by only 0.89 ångström (89 picometers) and atoms in silicon at 0.78 ångström (78 picometers) at magnifications of 50 million times. The ability to determine the positions of atoms within materials has made the high resolution TEM (HRTEM) an indispensable tool for nano-technologies research and development in many fields.

The Electron Microscope

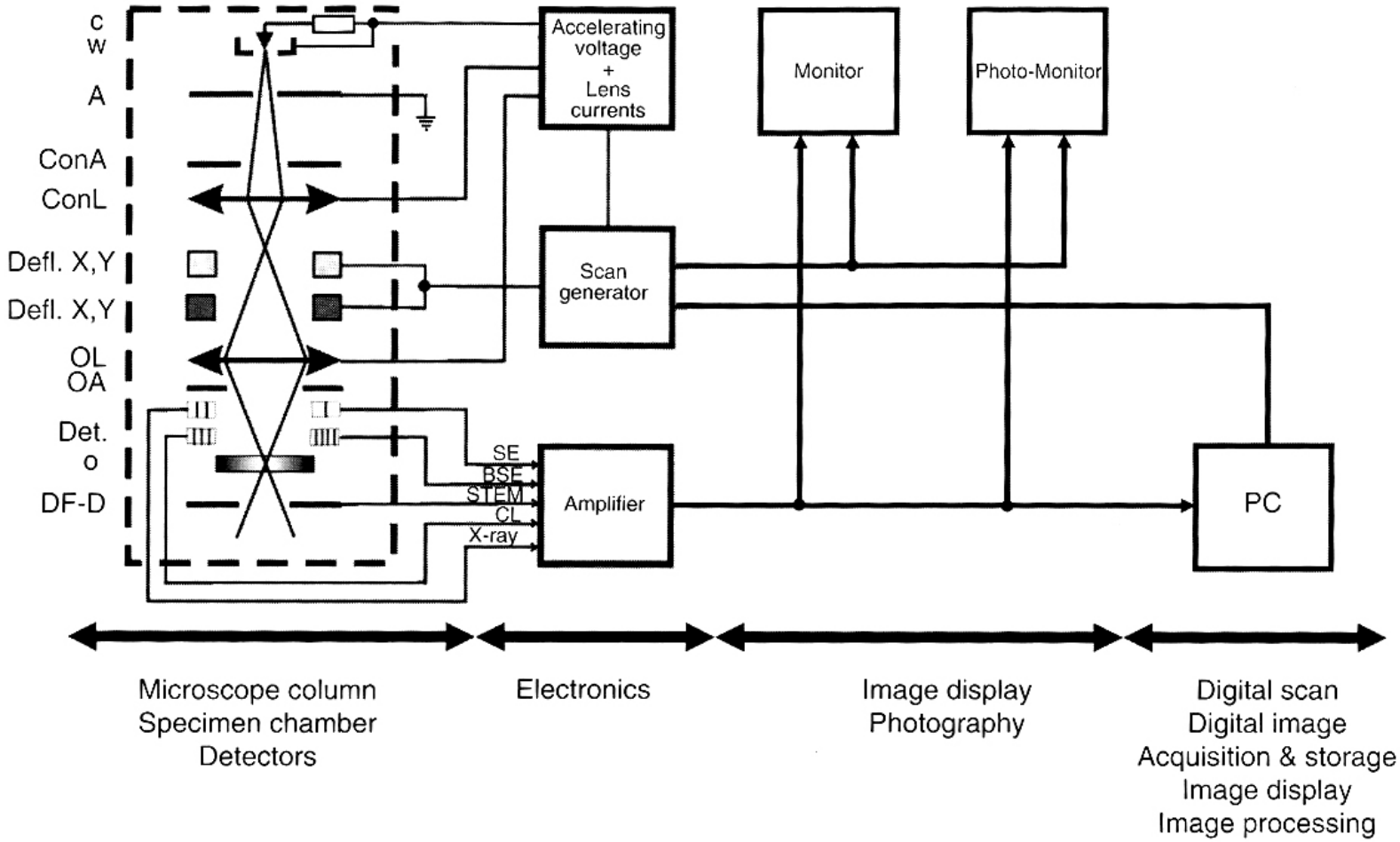

Reprinted from R. Reichelt, Scanning electron microscopy, in Science of microscopy, P.W. Hawkes and J.C.H. Spence, Editors. 2007, Springer: New York. p. 133-272. with kind permission of Springer Science+Business Media. Courtesy Professor Rudolf Reichelt

Electron Guns

Richardson Law for Thermionic emission

$$J = \frac{4\pi me}{h^3}(k_B T)^2 \exp - \frac{\phi}{k_B T}$$

Work function of electrons in metal

Field emission:

E- field at the sharp tip of a TEM. This calculation assumes the tip to be a sphere of radius a. Fields of 10^10 V/m are possible. In the presence of these field, electrons escape by tunneling. Field emission is preferred to thermoionic emission because it produces a monoenergetic e-beam.

$$E = \frac{1}{4\pi\varepsilon_0}\frac{Q}{a^2} = \frac{V}{a}$$

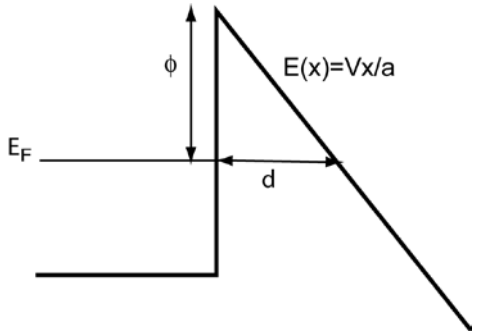

$$J \propto E^2 \exp - \left(\frac{4\sqrt{2m}}{3e\hbar}\frac{\phi^{\frac{3}{2}}}{E} \right)$$

Focusing electron beams

$$m\ddot{\mathbf{x}} = -e\mathbf{v} \times \mathbf{B} - e\mathbf{E}$$

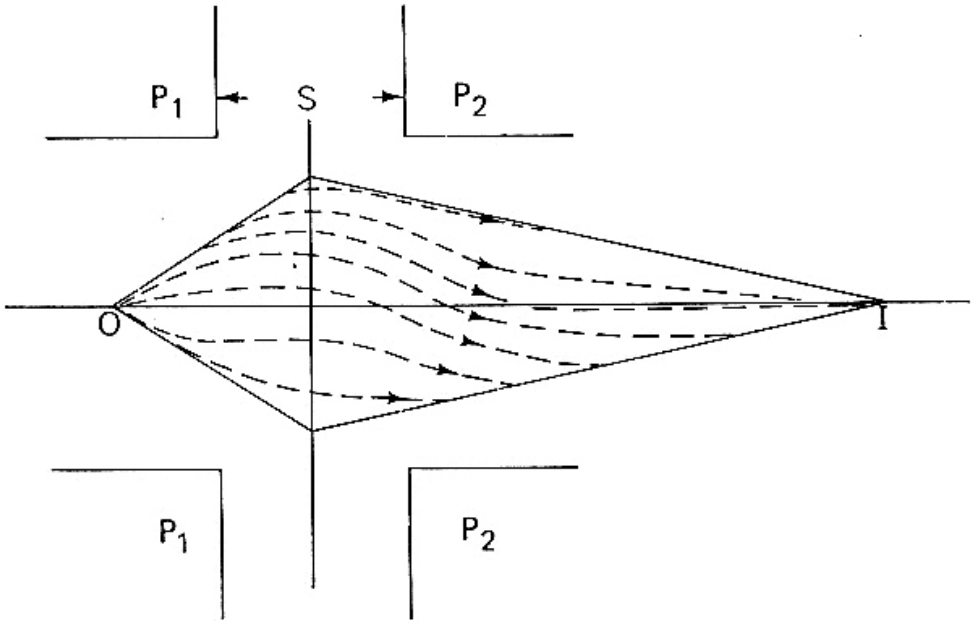

Magnetic lens

Electrons spiral around B-field lines. B field is directional along the axis of the microscope. Electrons with a velocity component perpendicular to B are forced to move towards the axis, creating a focus.

Electron wavelengths

Classical

$$\lambda = \frac{h}{\sqrt{meV_0}}$$

5kV = 0.17A

Relativity:

$$V_r = V_0 + \left(\frac{e}{2m_0 c^2} \right) V_0^2$$

5% error at 100kV

Wave-like effects have to be considered when operating at high voltages to achieve high resolution. Contrast limits resolution. So in high resolution imaging TEM, extremely thin samples are used. These samples are placed in grids with holes. Contrast is obtained by interference of beams that go through the samples and the hole.

Sample preparation for TEM

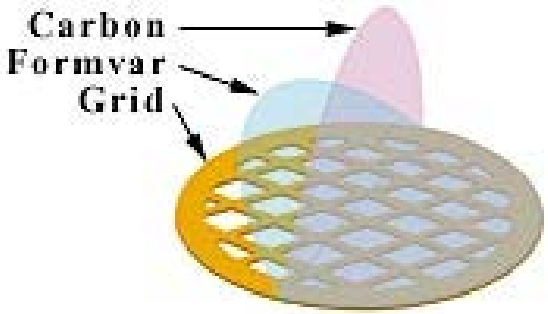

Mesh

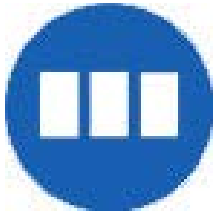

Mesh holder

Thickness of Support Films
The following is a guide to the relative thickness of the support films. The actual thickness varies depending on a number of factors during the deposition process.

1. Formvar Layer, measured with a Tencor Alpha-Step 200 profilometer:
   All Formvar Films - 30 to 60nm.
2. Carbon Layer, measured with a Film thickness Monitor during evaporation:
   On Formvar Stabilized with Carbon - 5 to 10nm
   On Carbon Type-A - 15 to 25nm
   On Carbon Type-B - 15 to 25nm
   On Ultrathin Carbon Type- A - 3 to 4nm
   On Ultrathin Carbon Film over Holey Carbon Film - under 3nm

http://www.tedpella.com/supflm_html/suptflm.htm

Resolution

- Electron scattering volume in SEM
- Atomic resolution possible as phase contrast in TEM

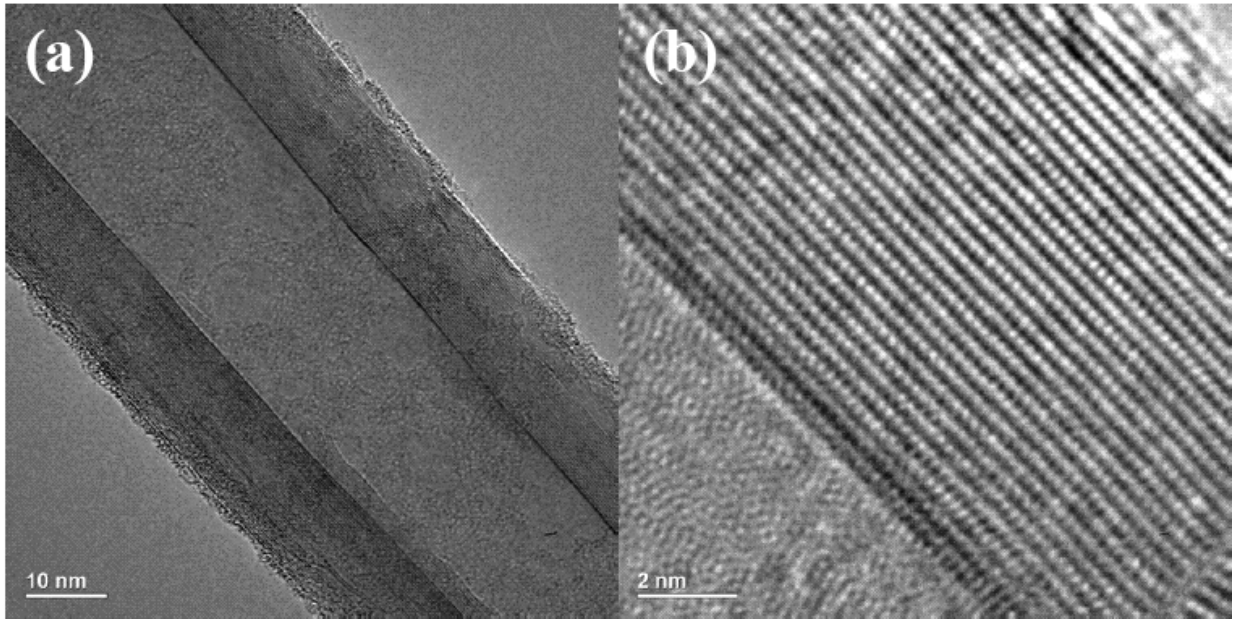

(Reprinted with the permission of Cambridge University Press. Courtesy of Mario Miki-Yoshida et al.)

Imaging is by phase contrast

Electron Microscopes TEM

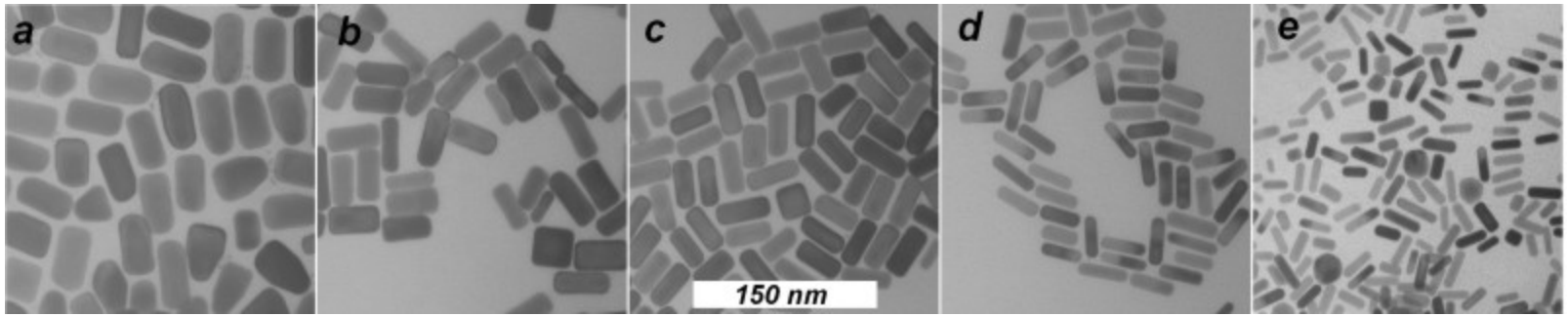

Au nanorods

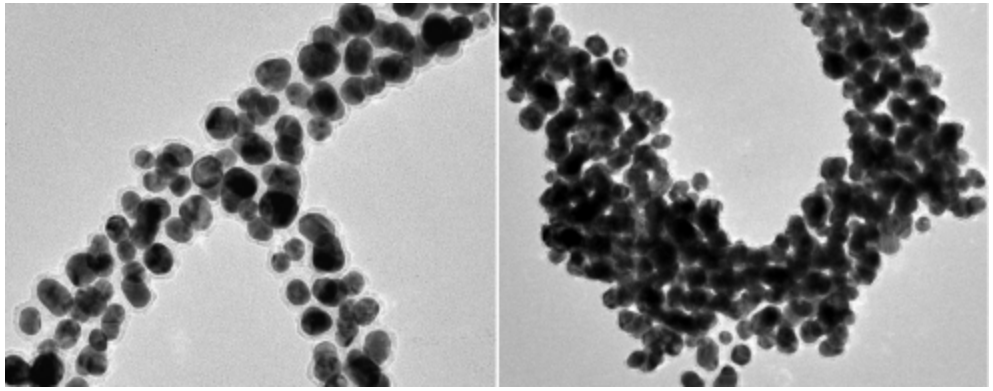

MW C nanotubes

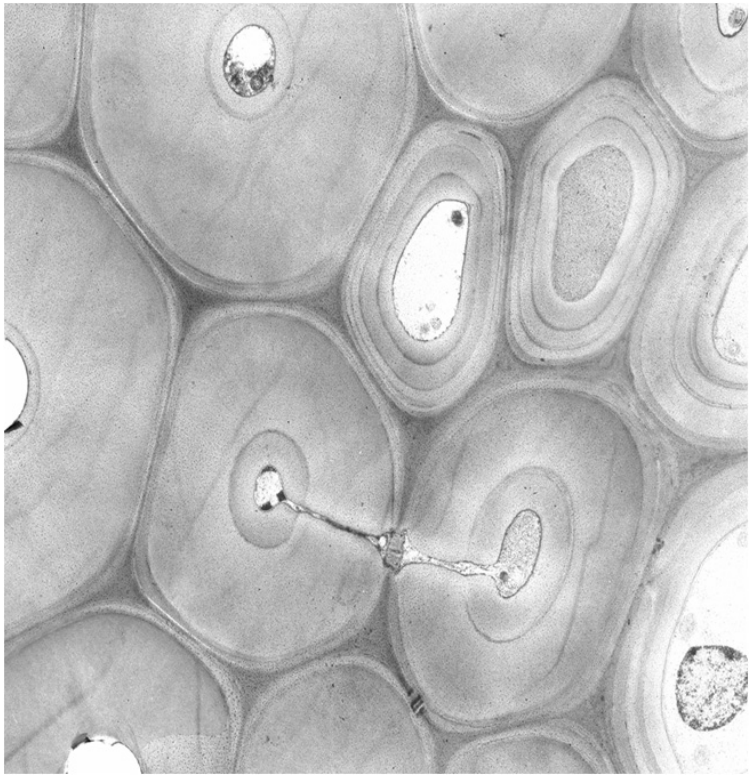

Bamboo cells

Transmission electron microscopy: a textbook for materials science. Imaging
By David Bernard Williams

Where is electron microscopy going???

TIME RESOLUTION

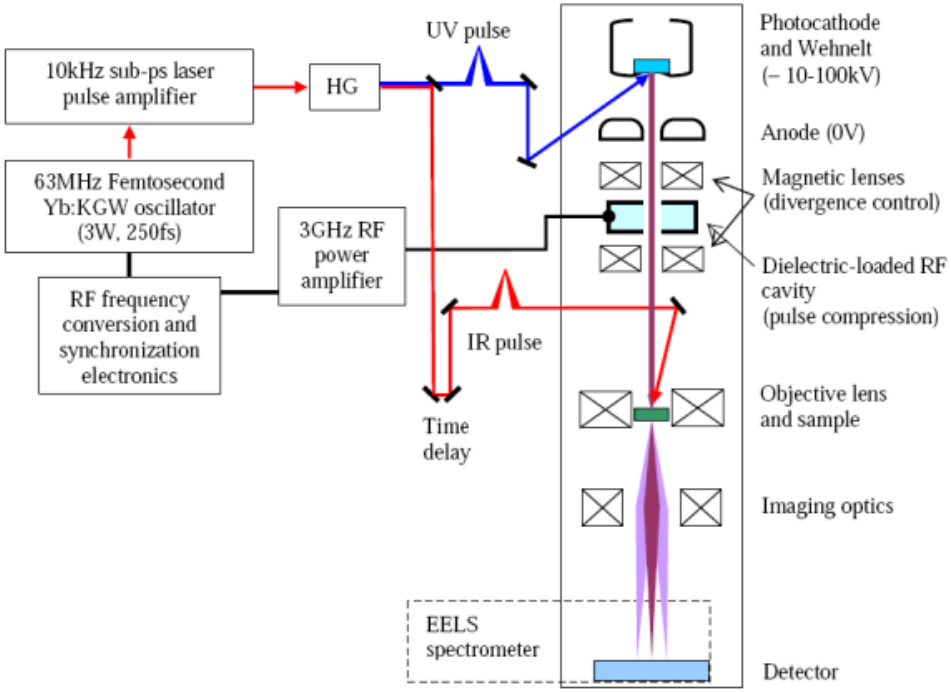

http://ultrafast.phy.uic.edu/research/ultrafast-electron-microscopy

4D SCANNING TEM

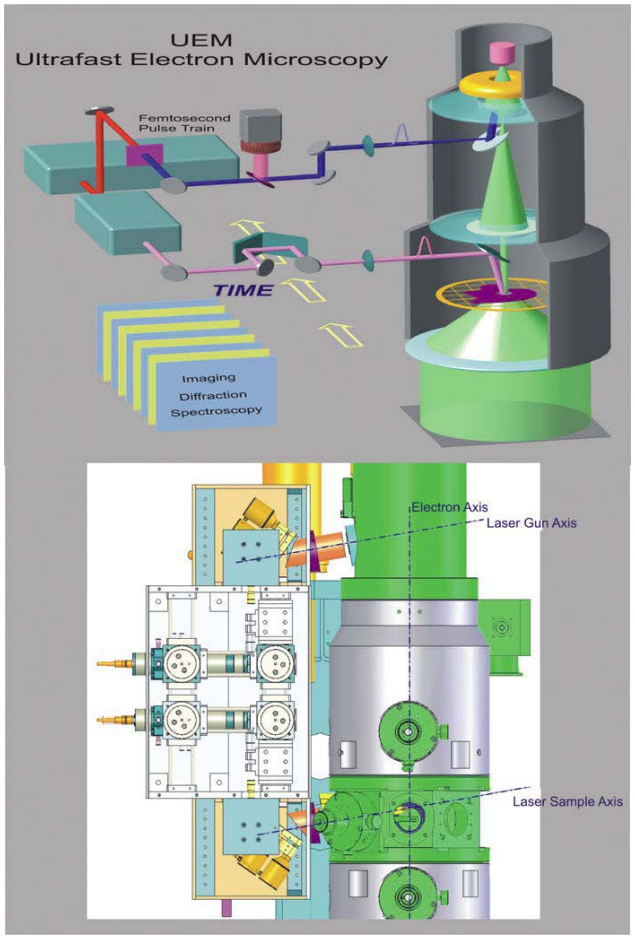

AH ZEWAIL Annu. Rev. Phys. Chem. 2006. 57:65–103

EXAMPLES OF TIME RESOLVED IMAGING

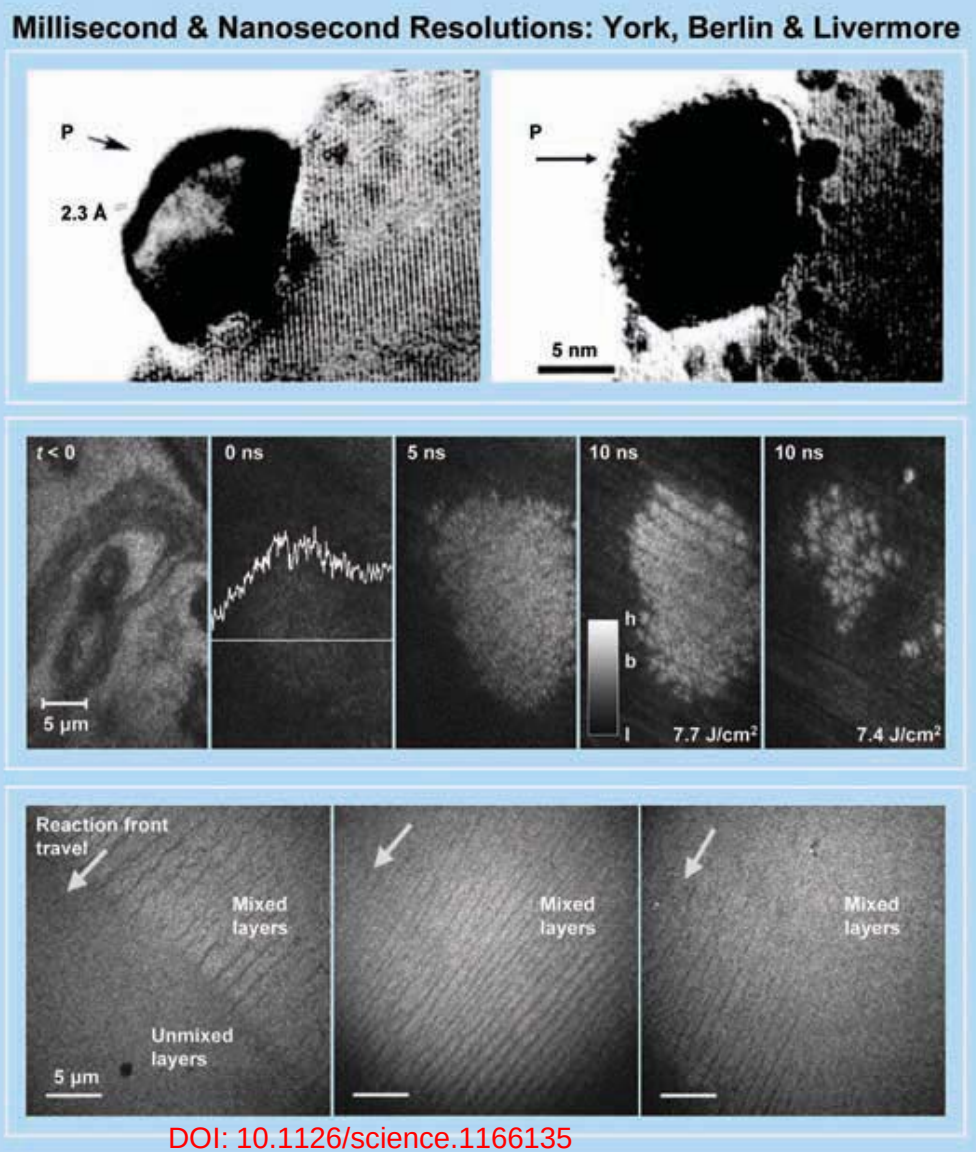

DOI: 10.1126/science.1166135
Science 328, 187 (2010);

Millisecond and nanosecond imaging by the groups at York, Berlin, and Livermore. Displayed at the top is the work from the group of Gai (32). Shown are
in situ atomic-resolution environmental TEM images of Pt/titania catalyst activated
in hydrogen at 300°C, with the atomic planes resolved (2.3 Å) in the Pt particle (P). The same particle is shown at 450°C, also in hydrogen, demonstrating the growth of Ti-oxide overlayer and development of Pt clusters. Such an experiment
can be ramped at 30 frames per second. The middle panel depicts single shots of explosion in a nickel film acquired with nanosecond resolution. The pattern at time
t = 0 indicates the intensity change across the line shown with the bar (at t < 0) giving the micrometer scale. At t = 10 ns, the bar reflects the change in the transmitted intensity of initial liquid (l), bubbles (b), and final hole (h). The fluence is very high (~8 J/cm2). This panel is adapted from (55) of the Berlin group. In the
lower panel, shown is the resolution of a reaction front on the microsecond time scale, displaying a transient behavior in the mixed layers. This panel is adapted from the work at LLNL (35).

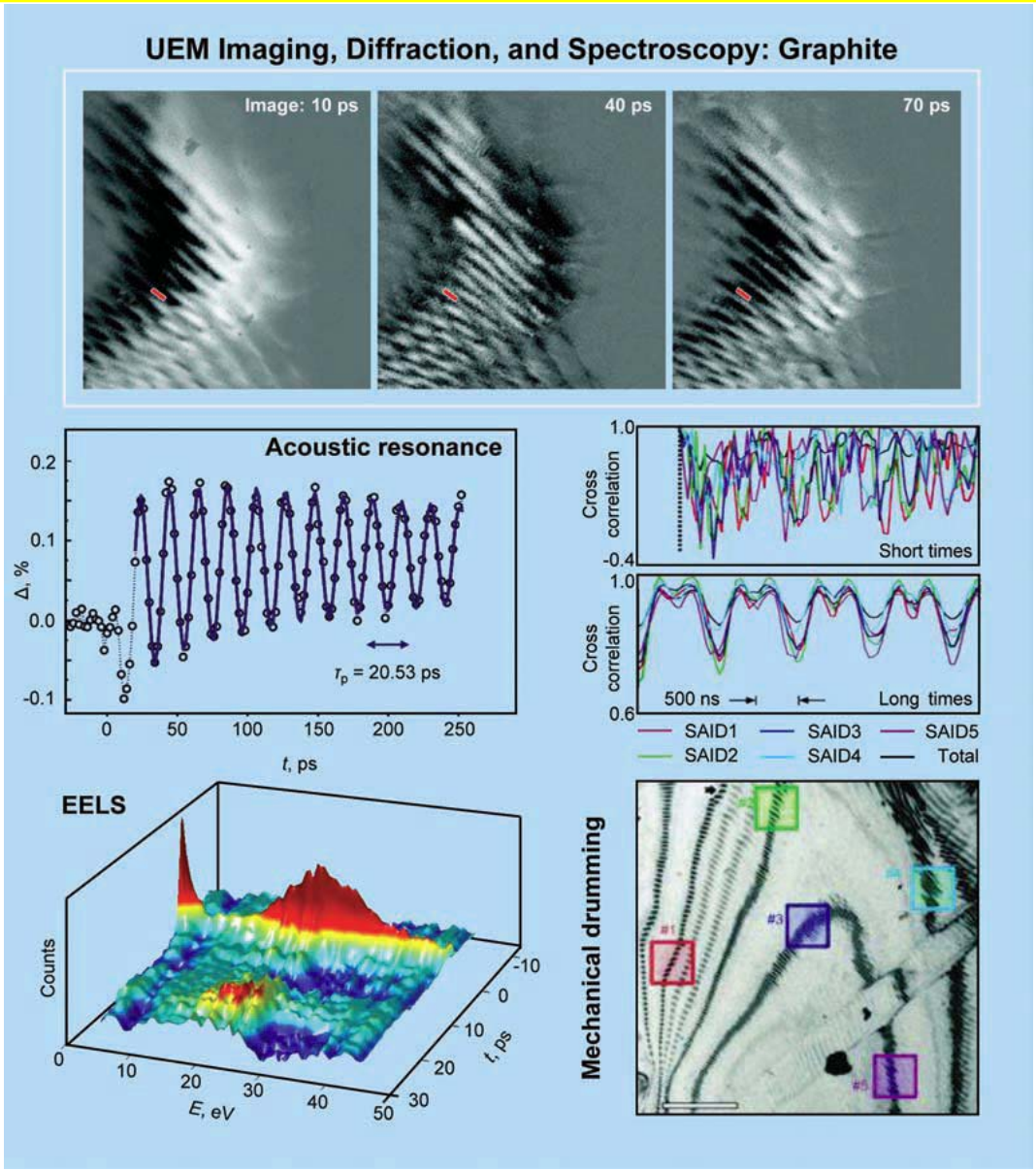

UEM imaging, diffraction, and spectroscopy of graphite: a prototypical case study. Shown are three frames for the change in the image with time (upper panel), the observed acoustic resonance (center left), the FEELS contour map (lower left), and the drumming resonance observed at longer times (lower right and center right). The selected area image dynamics (SAID) display the observed local resonances. See text and (10, 11, 39, 56); the values discussed in the text for resonance frequencies, Young's moduli, and the speed of sound are given in (56).

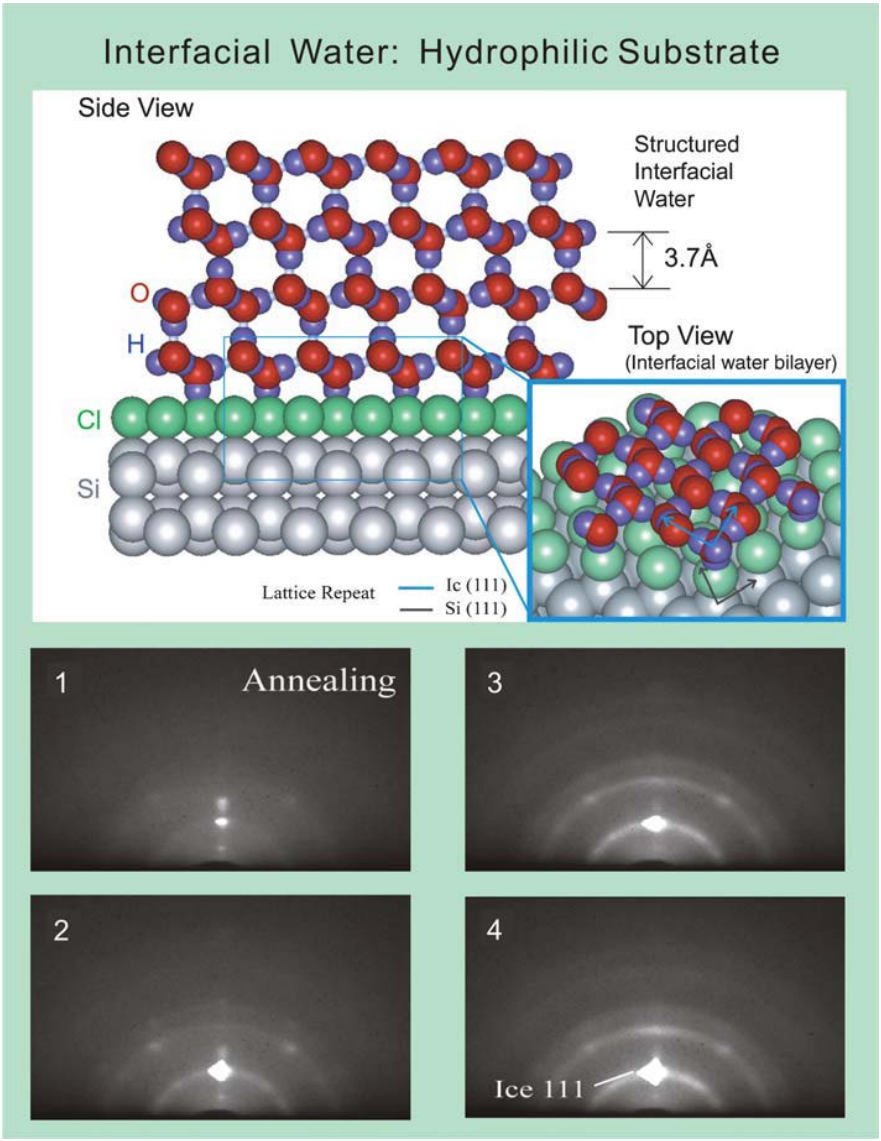

Ultrafast electron crystallography studies of interfacial water on a hydrophilic substrate. The coexistence of crystalline and polycrystalline structures (Bragg spots and Debye-Scherer rings) are clear in the patterns.

Scanning electron microscope

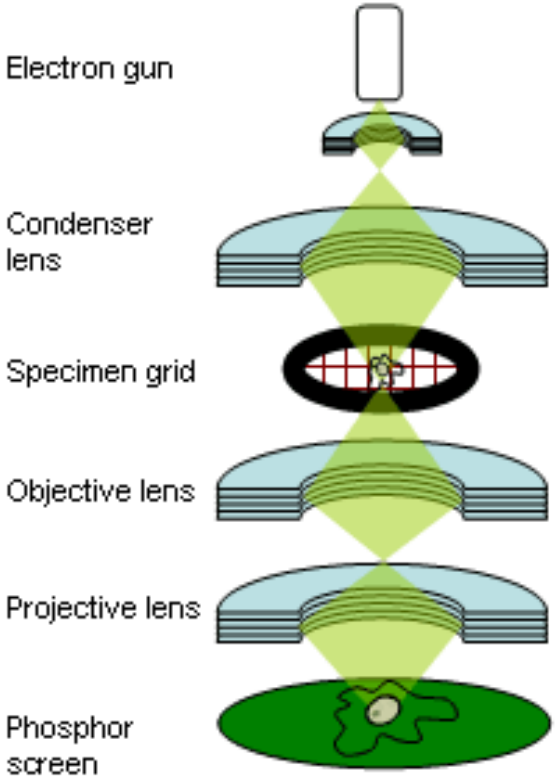

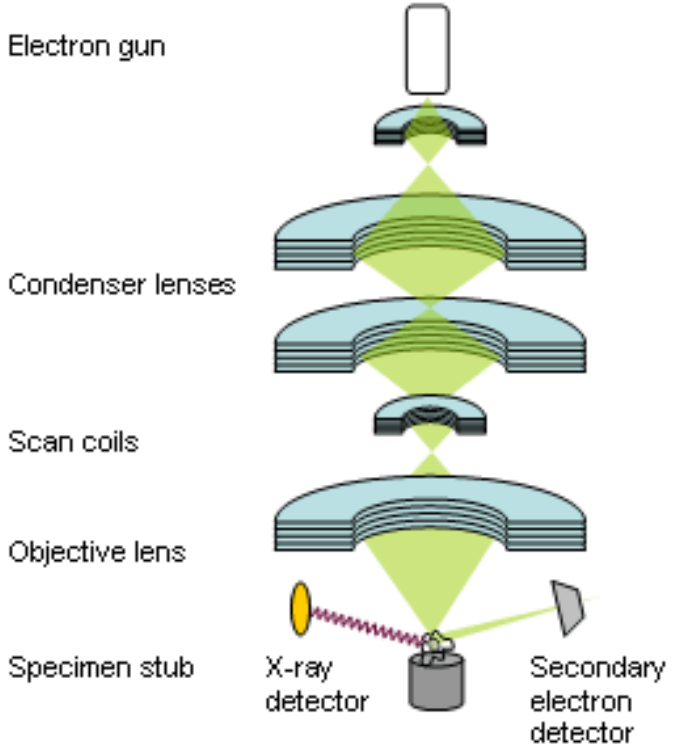

The electron beam, which typically has an energy ranging from a few hundred eV to 50 keV, is focused by one or two condenser lenses into a beam with a very fine focal spot sized 1 nm to 5 nm. The beam passes through pairs of scanning coils in the objective lens, which deflect the beam in a raster fashion over a rectangular area of the sample surface. Through these scattering events, the primary electron beam effectively spreads and fills a teardrop-shaped volume, known as the interaction volume, extending from less than 100 nm to around 5 µm into the surface.

Scanning electron microscope

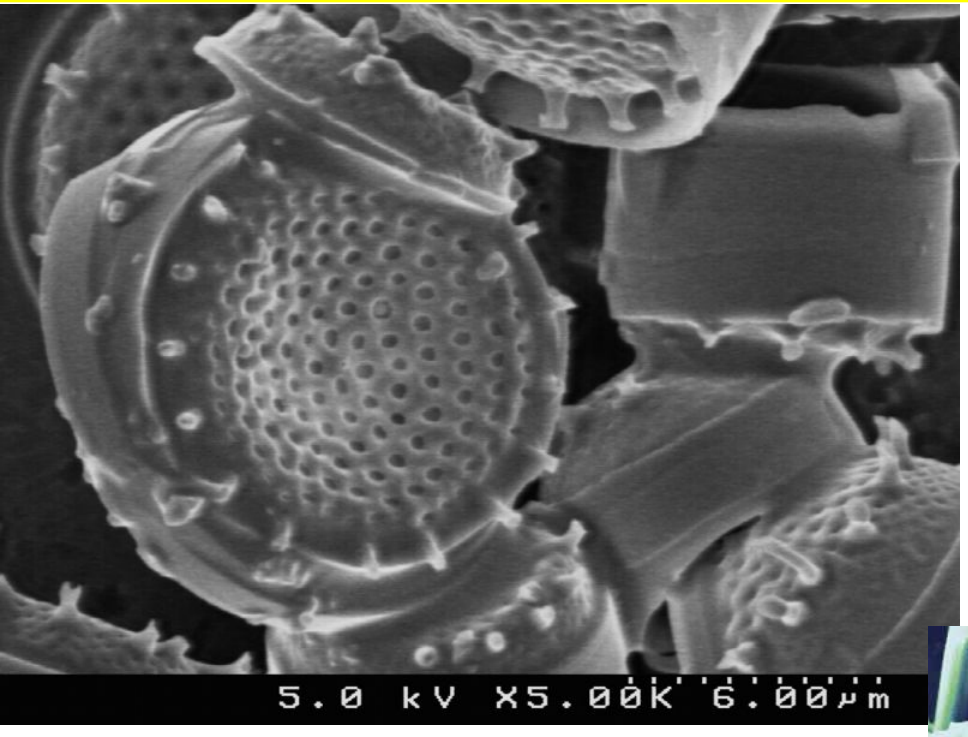

diatom

C nanorods

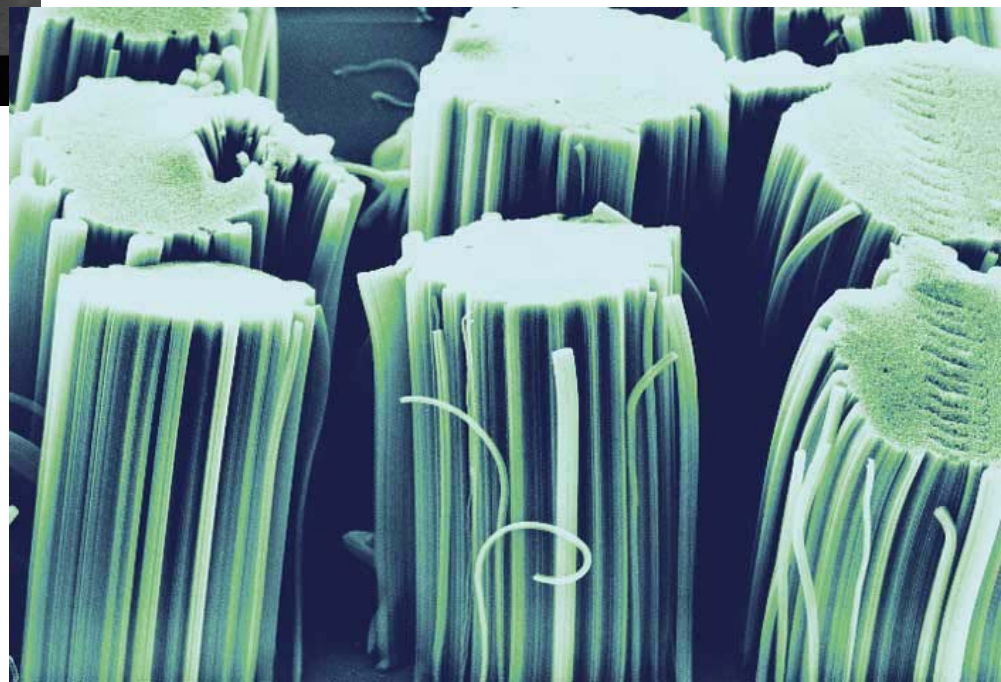

ALLOWS ONE TO IMAGE 'WET' SAMPLES

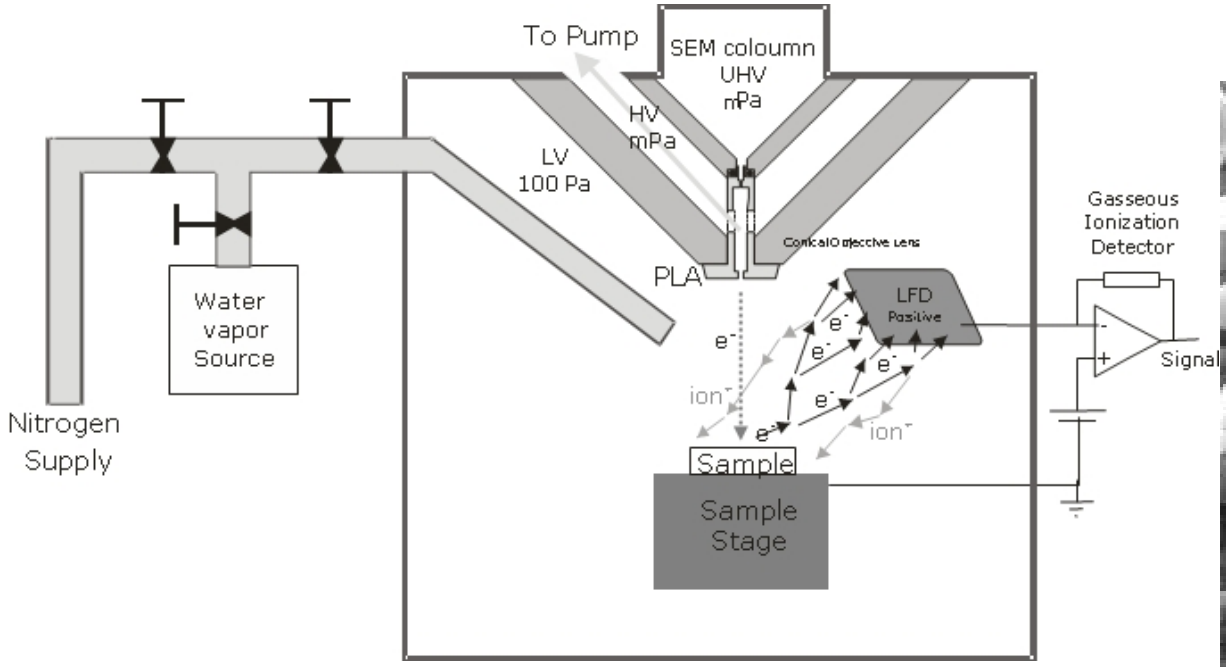

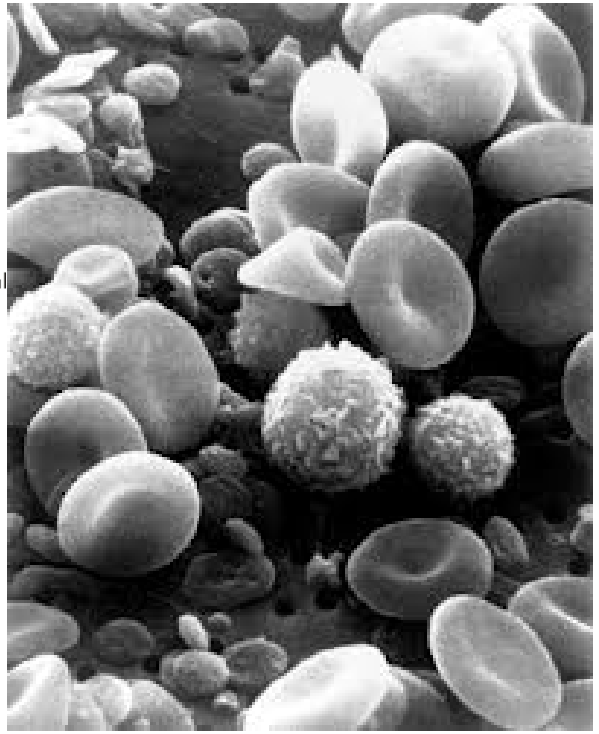

ESEM uses a proprietary Environmental Secondary Detector (ESD) which can function in non-vacuum environment instead of Everhart-Thornley (ET) detector used in SEM. The ESD uses the principle of gas ionization. By applying a positive potential of a few hundred volts to the detector, the secondary electron emitted by the sample when interacts with electron beam is attracted to detector. As the electrons accelerate in the detector field, they collide with gas molecules. The resulting ionizations create additional electrons, amplifying original secondary electron signal, and positive ions. The detector collects secondary electron signal and passes it directly to an electron amplifier. In nonconductive samples the positive ions created in gas ionization process are attracted to the sample surface and they effectively suppress charging artifacts.

IMAGE OF BLOOD CELLS

http://dmohankumar.wordpress.com/2010/04/28/environmental-scanning-electron-microscope-%E2%80%93esem/

Resolution, near field and far field

Consider a diffraction grating with grating interval p, The grating diffracts the beam and produces diffraction orders 0, ±1, ±2, etc.. which emerge at angle i such that

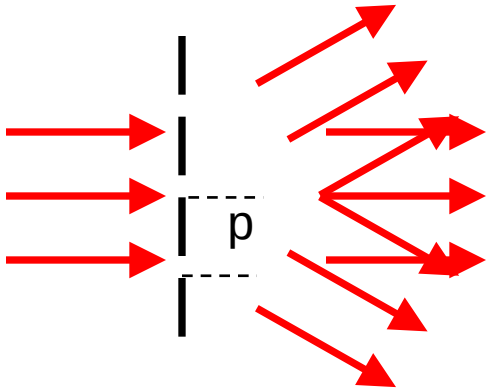

$$\sin i = \frac{k\lambda}{p}$$

k is an integer

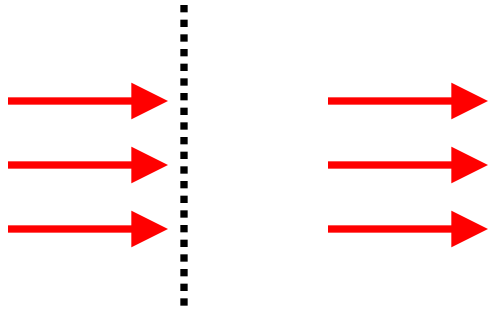

If p < λ only the order zero propagates. The information indicating that the object is periodic still exists but remains localized close to the surface in the form of the so called **evanescent waves.** The resolution of the image produced by an optical system depends on the transfer function that is determined by the maximum spatial frequency that the optical system can transmit. A simple diffraction calculation shows that for a microscope objective, the resolution in absence of aberrations is given by

$$\rho = \frac{1.22\,\lambda}{2n\sin u} = \frac{1.22\,\lambda}{NA}$$

Near Field Optics

A plane wave which illuminates a slit of width $a >> \lambda$ emerges almost parallel to its direction of incidence. If a decreases, the beam diverges, i.e. the projection of the wave vector $\mathbf{k_a}$ onto the plane of the slit increases.

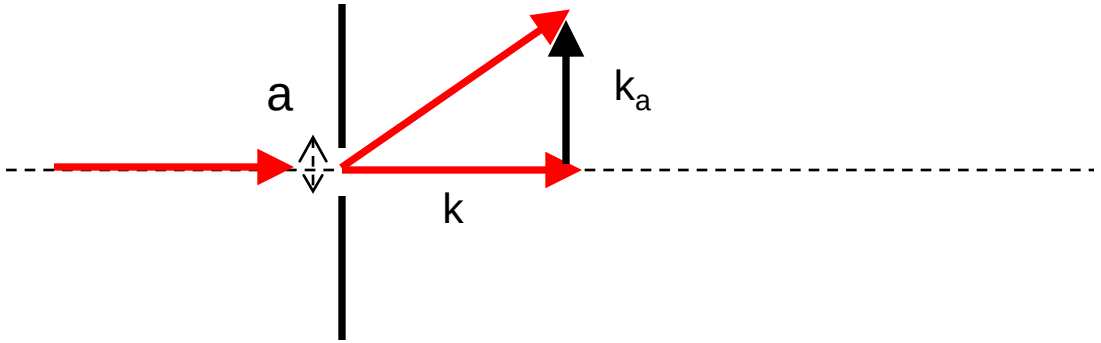

This projection reaches the value $2\pi/\lambda$ when $a = \lambda/2$, where the light fills the whole half space.

If we continue to decrease the slit size, no more information regarding the slit width can be retrieved from the diffracted light. That means that the information indicating the size of the slit does not propagate and cannot be retrieved from, for example, the angular distribution of the diffracted beam.

Conclusion: to obtain an "optical" image with electromagnetic waves of wavelength λ with better resolution than $\lambda/2n$ we must pick up the evanescent waves that are close to the object we want to image.

Photon scanning tunneling microscope (Near field optical microscope –NSOM)

Frustration of evanescent fields: by analogy with the tunnel effect in quantum mechanics the evanescent wave existing at the surface of an object when there is a total reflection that can be frustrated by the presence of a third medium.

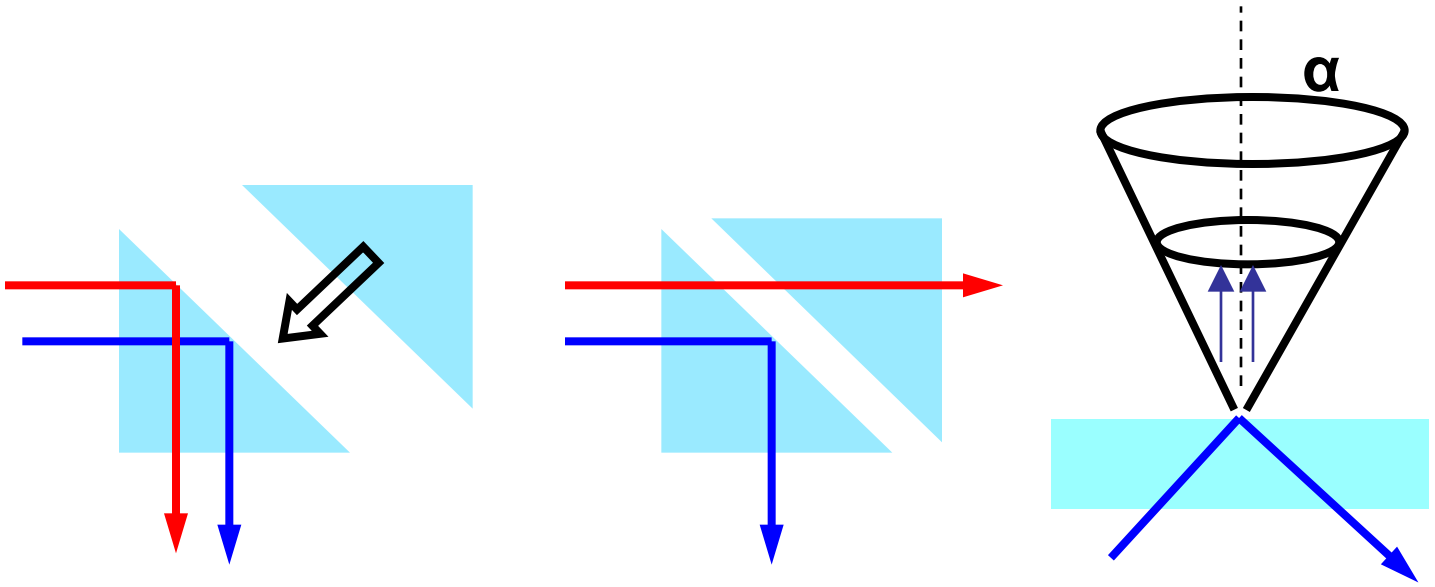

When a conical tip is brought to the vicinity of the surface the evanescent field is locally coupled into the tip. This is the set up used in the *photon scanning tunneling microscope* . The very end of the tip acts as a small scattering object of dimensions <<λ.

Photon scanning tunneling microscope

There is no simple way to calculate the polarization of the conical object in an non uniform fields. However if the dielectric constant is close to unity, the magnitude of the polarization can be found to be

$$P = \varepsilon_0 \left(\varepsilon_r - 1\right) E\, V$$

V: volume
E: electric field intensity

$$P = \int_0^Z dv(z)\, \varepsilon_0 \left(n^2 - 1\right) E_0\, e^{-z/S}$$

S: decay length

$$dv(z) = \pi\, r^2\, dz = \pi\, z^2\, \tan^2\alpha\, dz$$

$$P = 2\pi\, S^3\, \tan^2\alpha$$

$$2S^3\, \tan^2\alpha$$

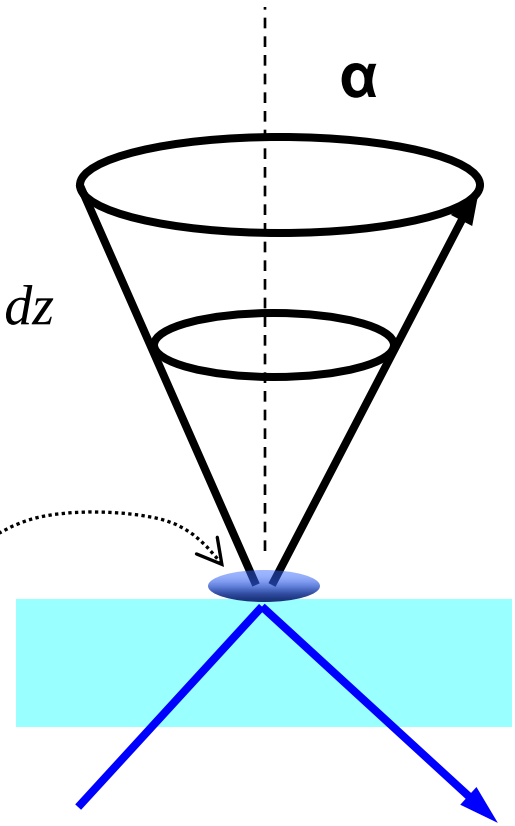

The power collected by the probe

$$W = \frac{1}{4\pi\varepsilon_0}\frac{\omega^4\, P^2}{3c^2}$$

Photon scanning tunneling microscope

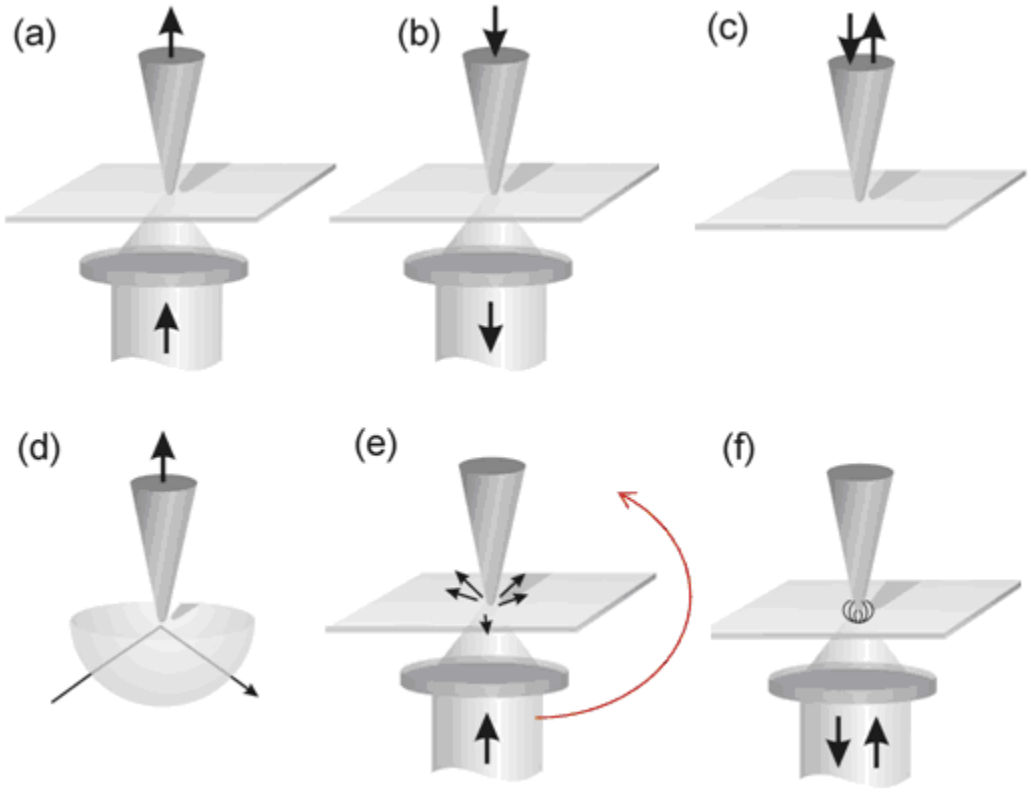

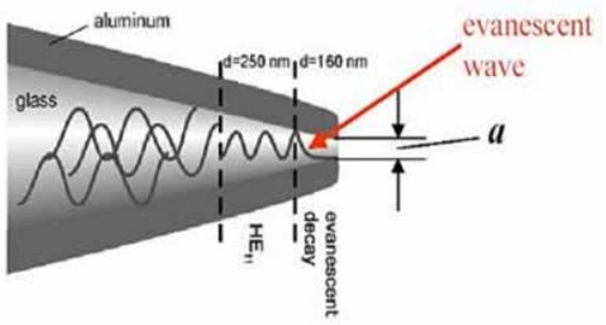

The evanescent field is detected with a tapered fiber optic and directed to a photon counter detection system.

Light can be scattered from the evanescent field by other probe tips, such as a force microscope tip on a cantilever (e). In the Plasmon Near-Field Microscope, surface plasmons are generated at the surface of a sample on a thin film metallic substrate, and scattered by a probe tip (f).

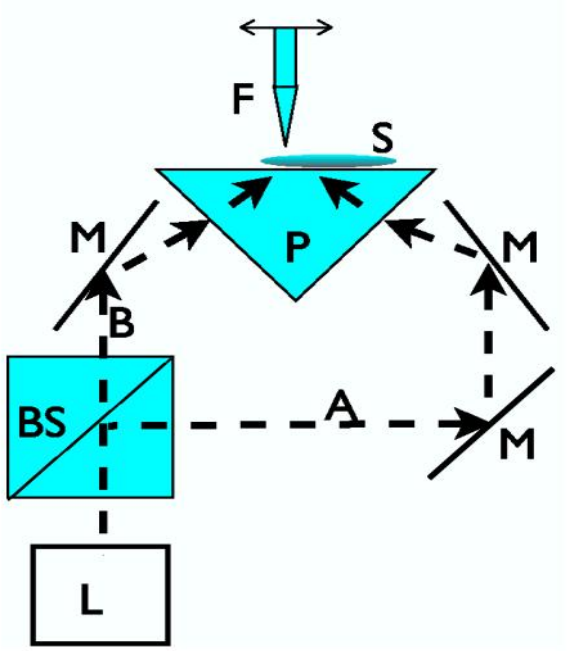

Photon scanning tunneling microscope

Feedback Mechanisms: to approach the surface with the tapered fiber in a controlled manner. The resolution of an NSOM/SNOM measurement is defined by the size of the point light source used. This point source is typically **50-100 nm.** The distance between the point light source and the sample surface is usually controlled through a feedback mechanism that is unrelated to the NSOM/SNOM signal. A- Shear force feedback, or tuning fork feedback, the straight tip is mounted to a tuning fork, which is then oscillated at its resonance frequency. The amplitude of this oscillation is strongly dependent on the tip-surface distance, and it can be effectively used as a feedback signal. B-Normal force feedback (the standard feedback mode used in AFM), it is possible to perform experiments in contact and in intermittent contact mode. This feedback mechanism is only possible with cantilevered, tapered optical fibers and with AFM cantilevers with holes.

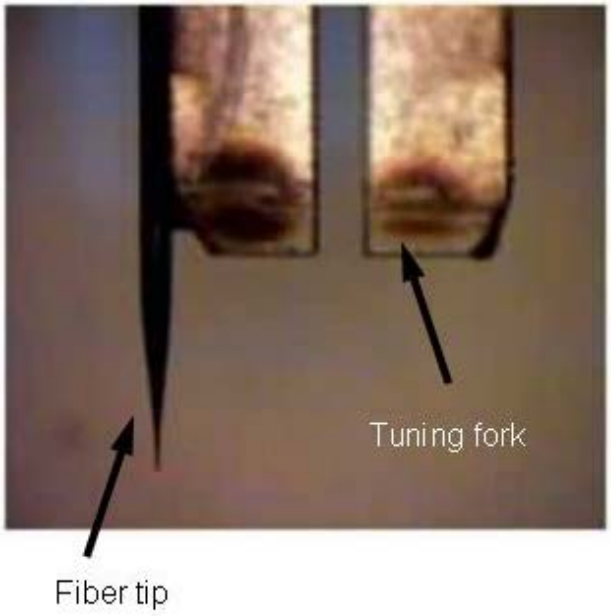

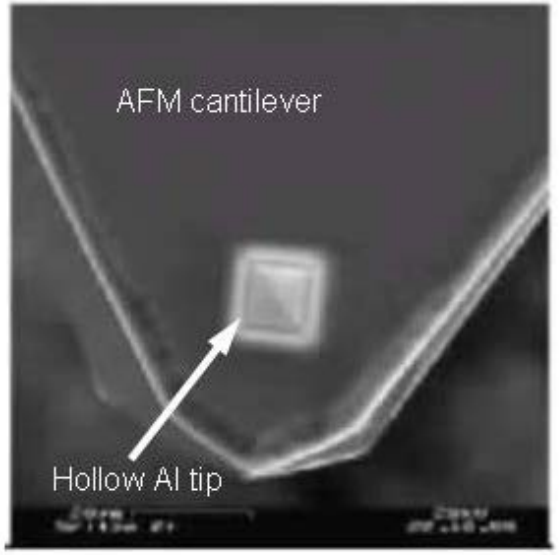

- Limits of conventional Optics:

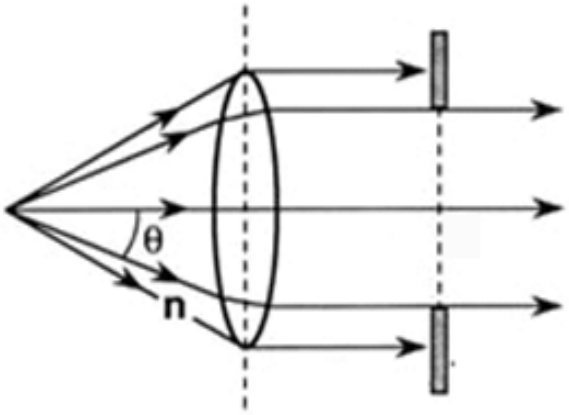

$$r = \frac{\lambda}{2NA} \qquad NA = n\sin\theta$$

ca. 0.5 microns in air

Fluorescence

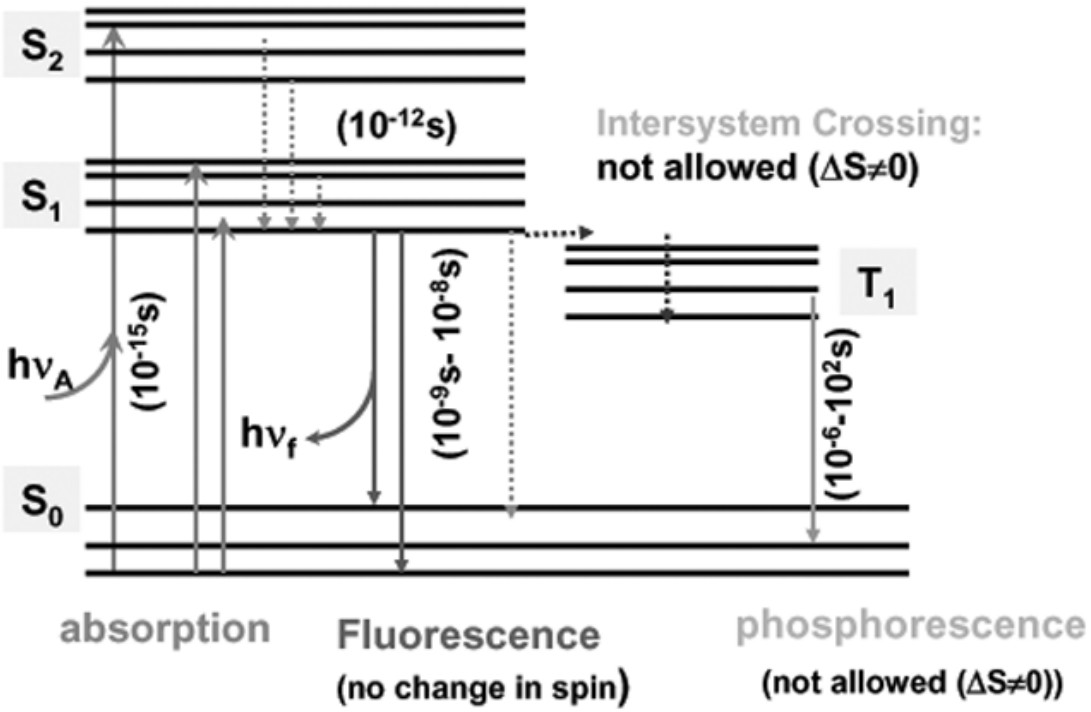

$$H_{ge} = \langle \psi_g | e\mathbf{D}.\mathbf{E} | \psi_e \rangle$$

$$\hbar\omega = E_e - E_g$$

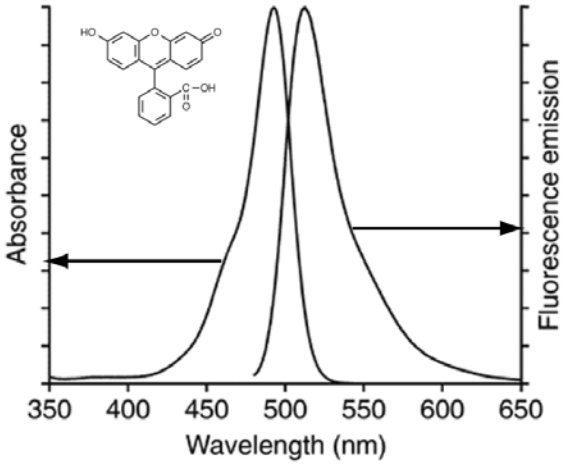

Absorption and emission spectrum of fluorescein dye

(Courtesy Professor Marcia Levitus)

Single molecule fluorescence

- Increases with E (use of intense lasers ensures emission of billions of photons from a single molecule)
- Limit $1/t_F$ – 10^9 s^{-1}
- Required good dye chemistry

Beating Rayleigh Resolution with Color Separation

- 10nm
- The width of the point spread function is 0.25 um. One can locate the centroid with high precision if molecules are sufficiently far apart

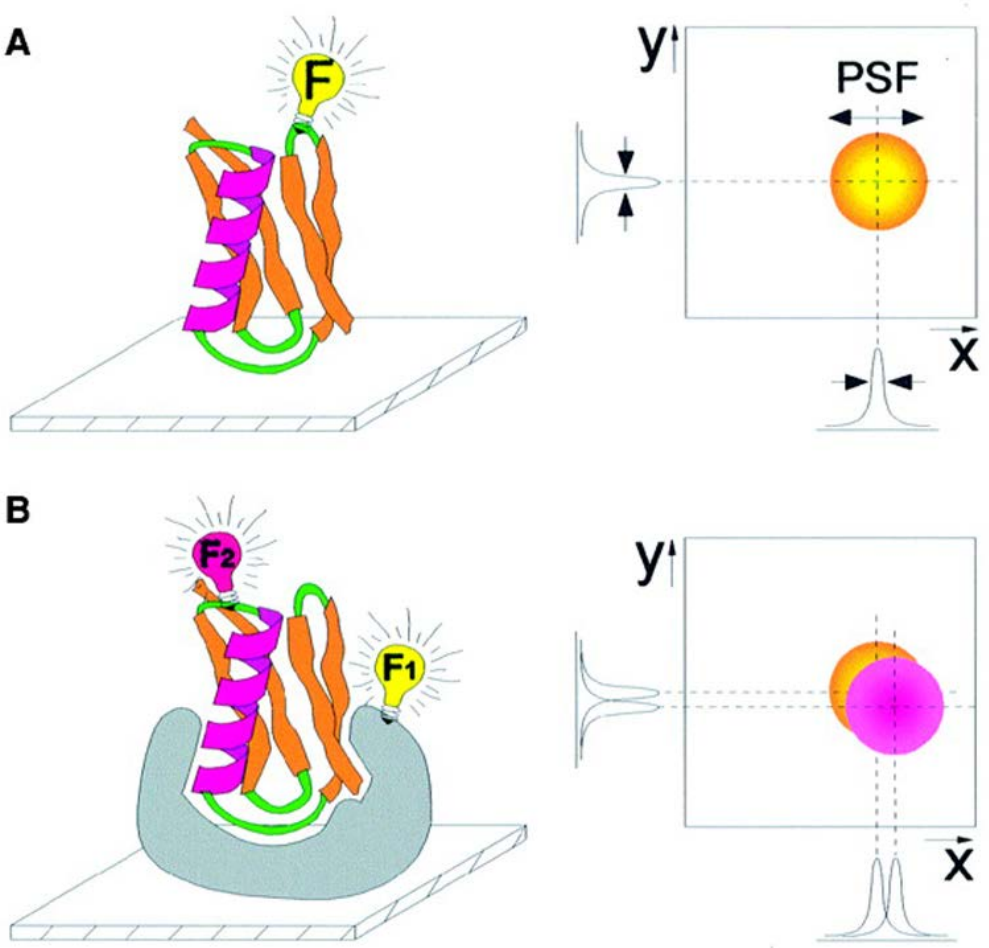

(Image public domain)

Single Particle Tracking

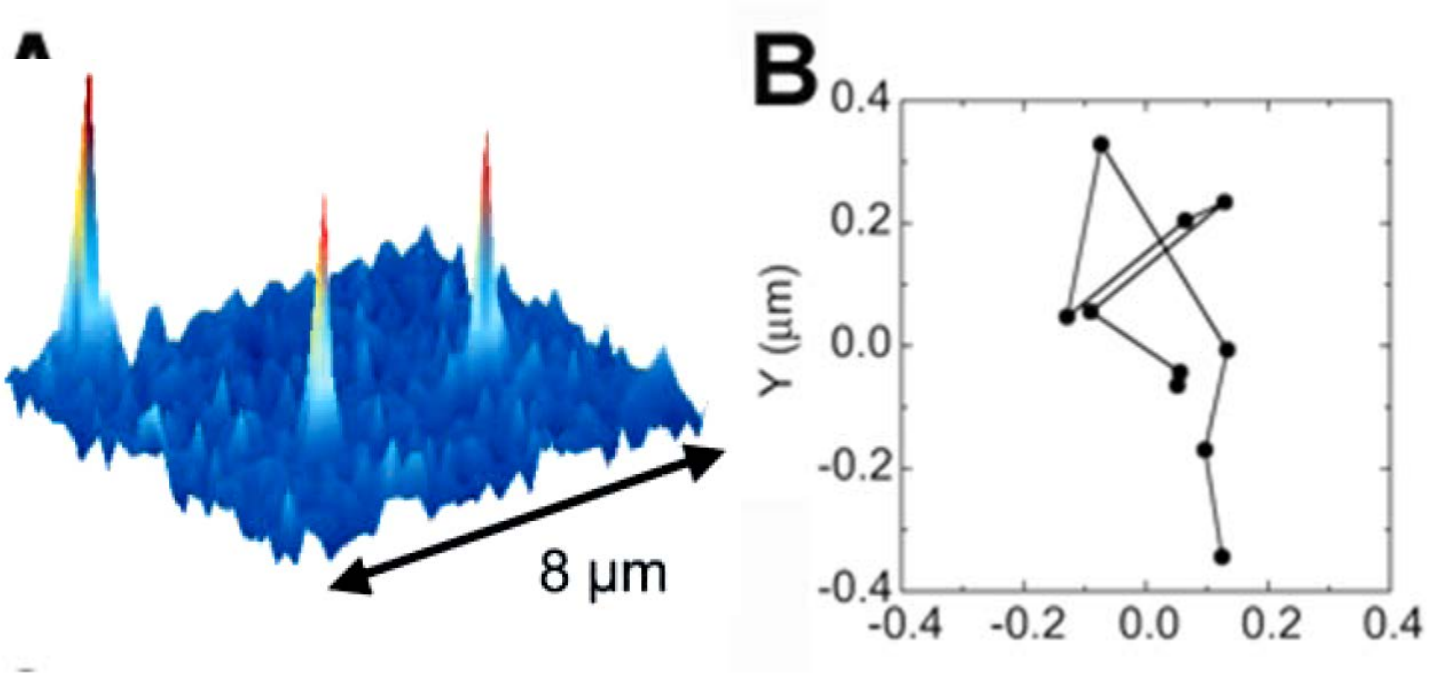

(Reproduced with permission. Journal of Cell Science, 2005, 118: 1799-1809 Single-molecule diffusion measurements of H-Ras at the plasma membrane of live cells reveal microfomain localization upon activation. Journal of Cell Science: jcs.biologists.org; doi: 10.1242/10.1242/jcs.02300)

Exposures are very long

Fluorescence resonant energy transfer (FRET)

Dipole-dipole mixing of states: $\mathbf{D}_1 \bullet \mathbf{D}_2$

FRET efficiency

$$E_{FRET} = \frac{1}{1+\left(\frac{d}{R_0}\right)^6}$$

d: is the distance between two molecules

$$R_0 = 9.78\times10^3\left[\kappa^2 n^{-4}\phi_D J(\lambda)\right]^{1/6}$$

2 to 8nm

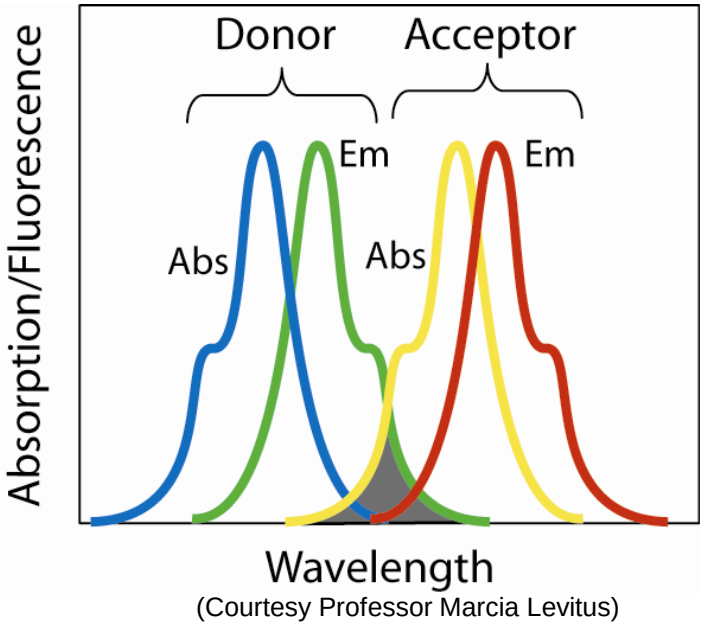

(Courtesy Professor Marcia Levitus)

FRET recording of DNA structural fluctuations

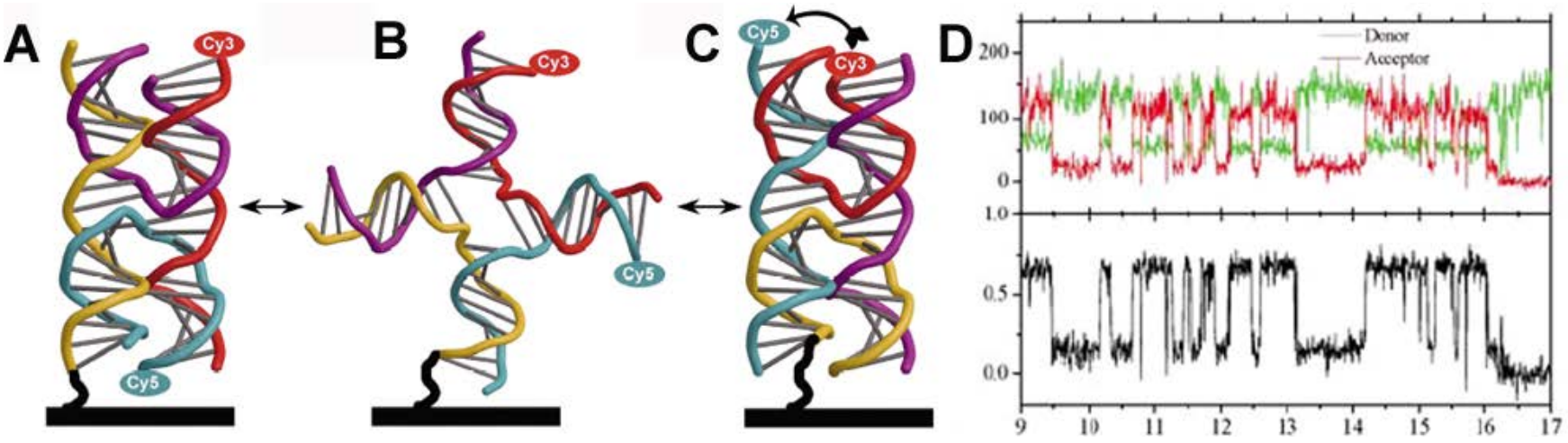

(Reprinted by permission from Macmillan Publishers Ltd:
Nature Structural & Molecular Biology, Watching flipping junctions, 2003)

(Reprinted by permission from Macmillan Publishers Ltd:
Nature Structural and Molecular Biology,
Structural dynamics of individual Holliday junctions, 2003)

DNA labeled with two different dyes that attached to different locations in the chain. The donor absorbs and emits in the green unless the acceptor is closed. In this case the emission is on the red.
Fret efficiency is shown in black. Units of time are seconds.

Time limit ca. 10 ms

Stimulated Emission Depletion Optical Microscopy

Used in biology – it is a far field fluorescence microscope capable to identify emission from non overlapping, dilute fluorophore. Uses scanning excitation illumination spot to excite a quantum dot. Then a second laser beam with a doughnut shape illumination is overlapped with the emitting fluorophore, de-exciting the fluorophore as shown in the figure. This is due to a phenomenon called STIMULATED EMISSION DEPLETION
8 nm spatial resolution has been reported with STED.

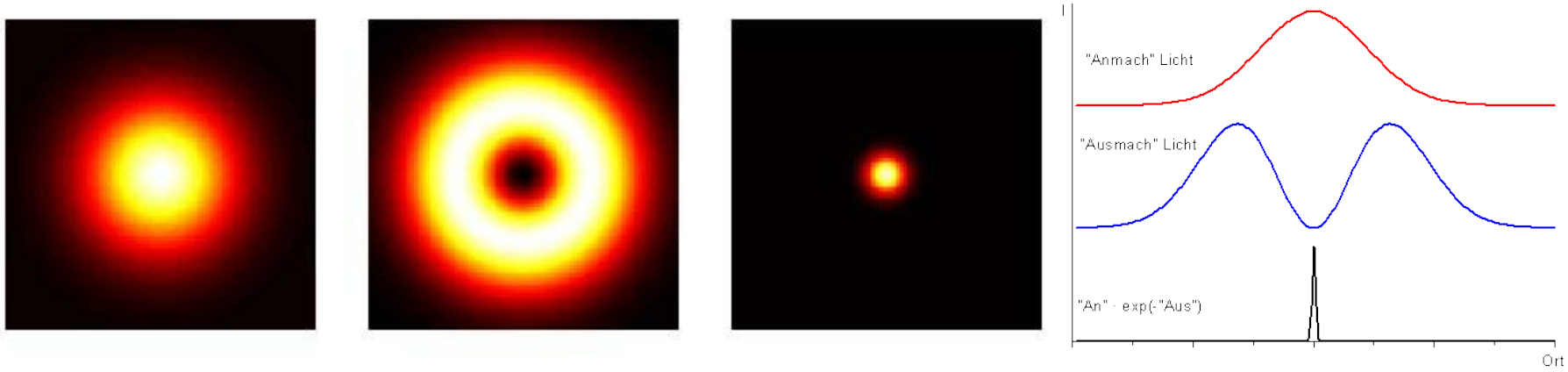

EXAMPLES OF STED

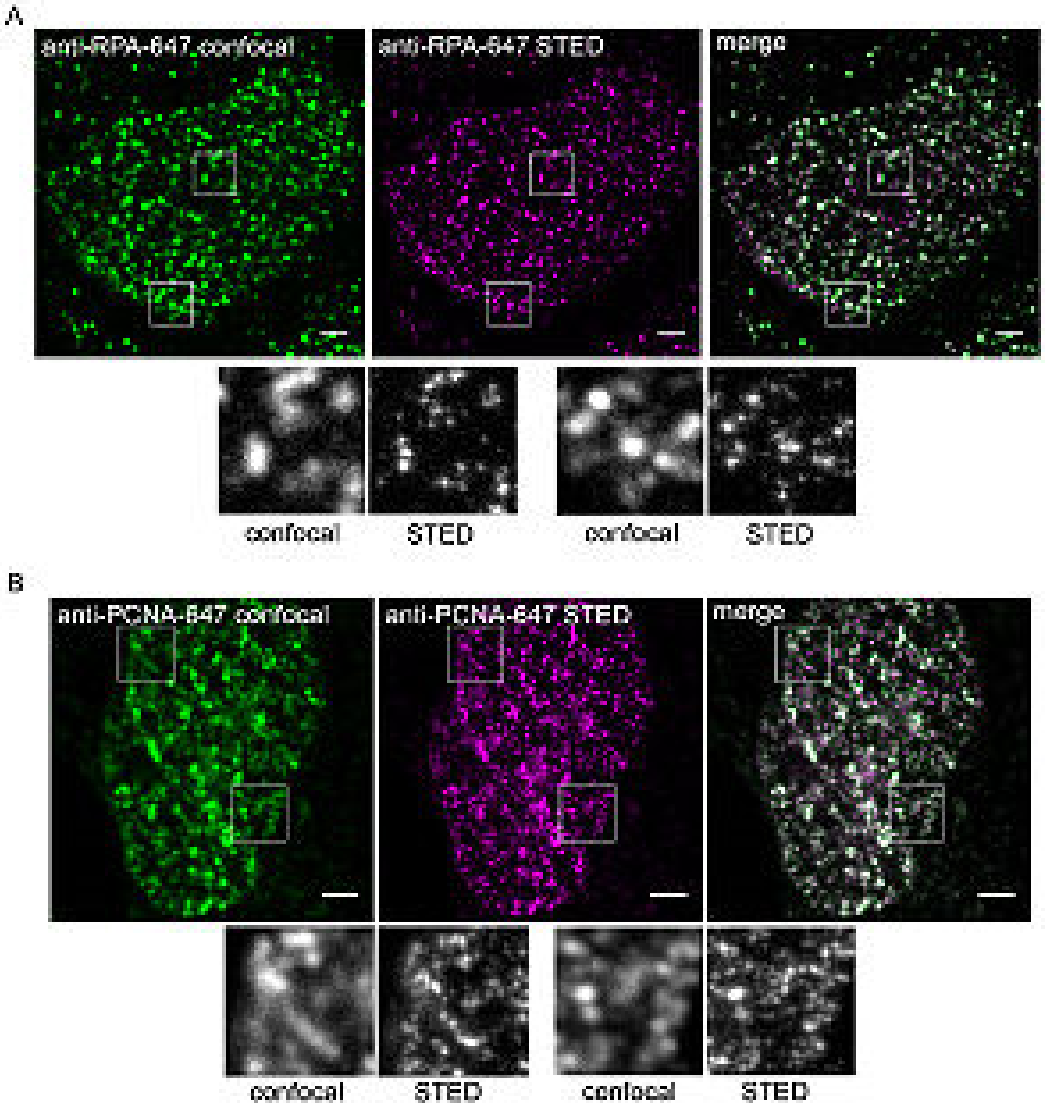

Comparison of confocal microscopy (green images, left) and STED microscopy (violet images, center). The images show DNA replication factories, protein complexes responsible for DNA replication in biological cells. Overlays of confocal and STED recordings (right) with enlargements (gray images) demonstrate the superior resolution of STED microscopy.

http://en.wikipedia.org/wiki/STED_microscopy

CARBON NANOTUBES

Carbon nanotubes are formed by a seamless bending of a graphene sheet

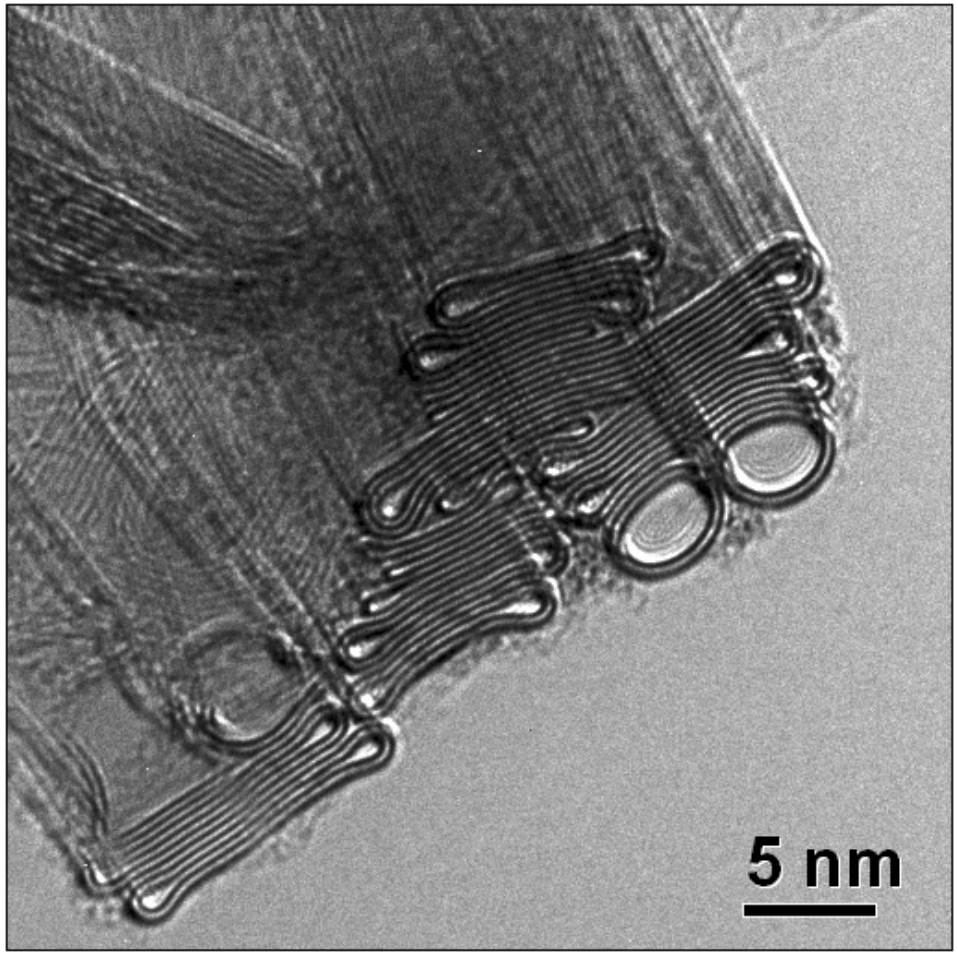

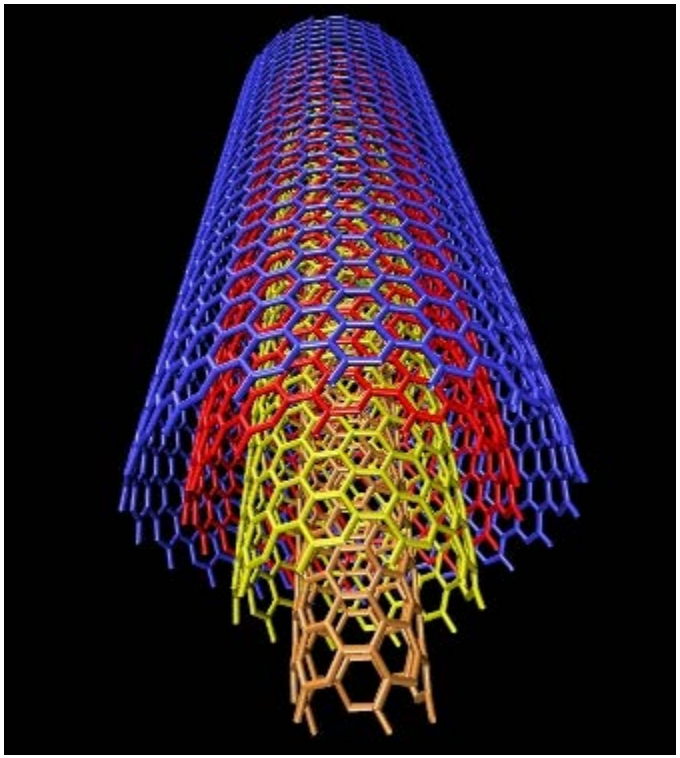

There are different types of CNT: single and multiwall.

In CNT each C atom is covalently bonded to its three neighbors and the fourth electron is smeared (sp^2 hybridization) over the entire structure. The bonding gives rise to three different structures: 'armchair', 'zigzag' and 'chiral'

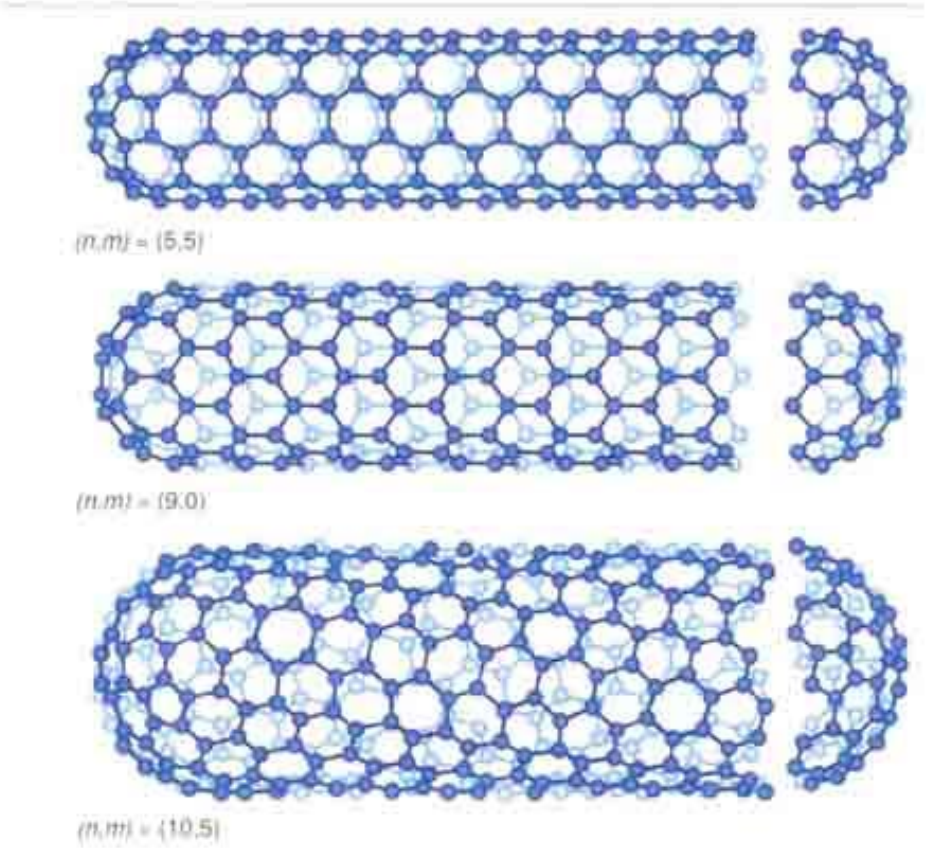

Armchair

Zigzag

Chiral

CARBON NANOTUBES

Each configuration is characterized by the vector (n,m) given in terms of vectors a1 and a2 where the magnitude of the vector is the circumference of the tube.

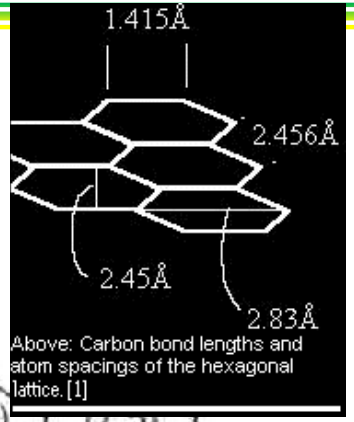

Above: Carbon bond lengths and atom spacings of the hexagonal lattice. [1]

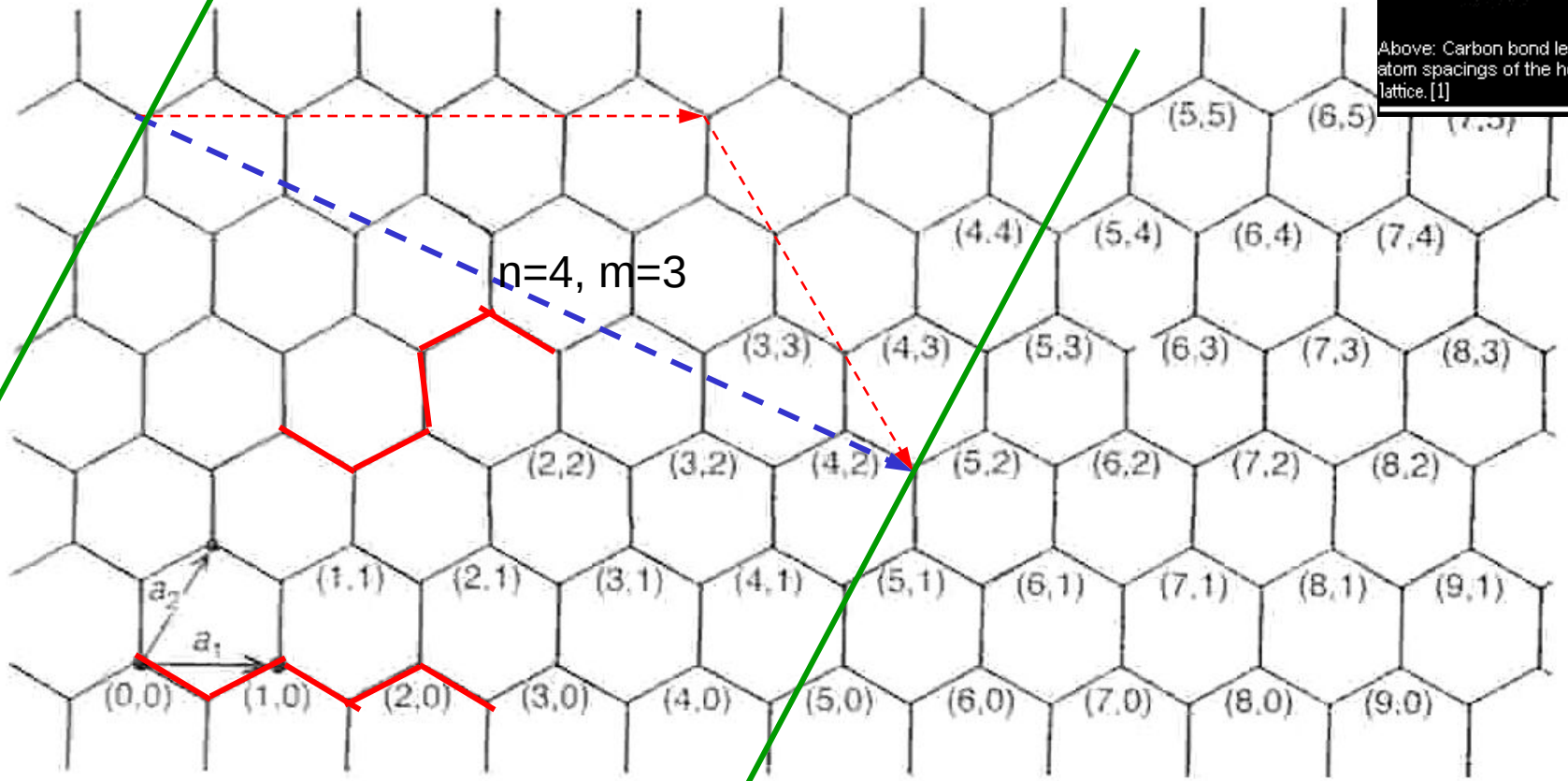

Movies of CNT - http://www.photon.t.u-tokyo.ac.jp/~maruyama/agallery/agallery.html

Synthesis of CNT

Arc discharge in an inert gas. Single wall (SNT) were grown in a Ar discharge where the anode is a graphite rod containing metal catalysts such as Fe, Co, and the cathode is pure graphite. For multiwall CNT (MWNT) a mixture of hydrogen and He or Ar is preferable.
Smallest CNT diameter: 0.3 nm (armchair configuration)
Longest SNT: 2 mm

Other methods:
Laser furnace method: SWNTs can be produced where diameter is controlled by furnace temperature and type of catalyst
Laser ablation
Chemical vapor deposition and plasma assisted CVD is used for growth of electronic CNT. Carbon species are decomposed from hydrocarbons dissolve in the metal nanoparticles present and after supersaturation precipitate in the form of fullereness dome extending into a CNT as shown in the figure.

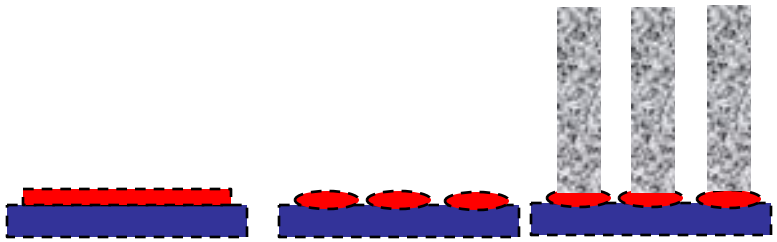

CNT can be semiconducting, insulators or metallic.
The semiconducting CNT can be doped with B (acceptor) or N (donor).
Most technologies require process control to realize: single wall, length, chirality, and electronic properties control.
There exist a number of post-synthesis control. Some applications also require tubes to be aligned.
Raman spectroscopy can be used to identify semiconducting from metal nanotubes.

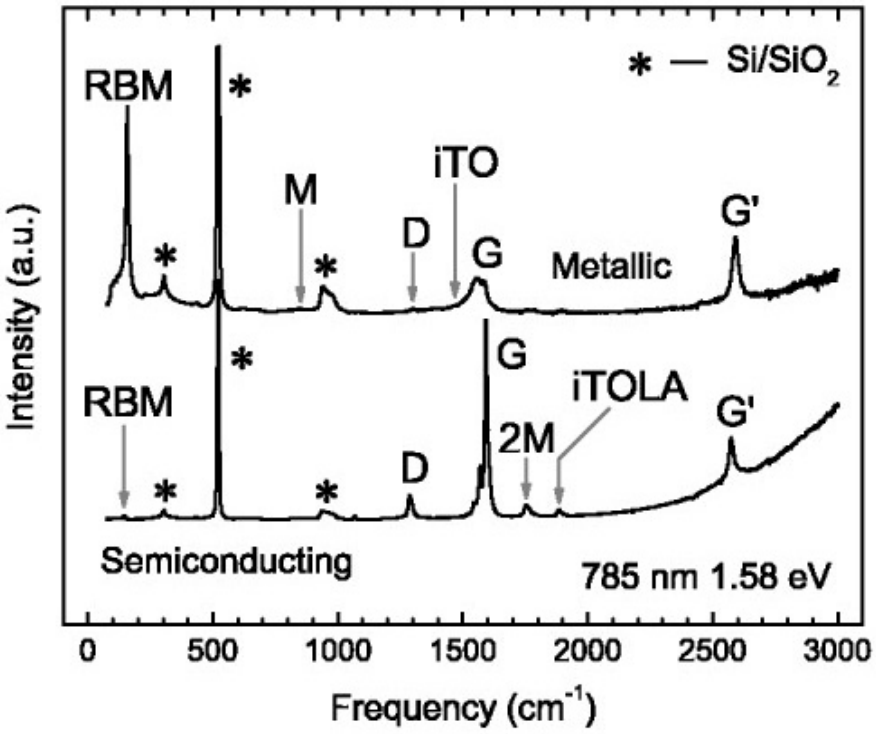

D and G ' bands for a metallic (top) and a semiconducting (bottom) SWNT at the single nanotube level using 785 nm (1.58 eV) laser excitation. First-order Raman spectra of the radial breathing mode (RBM), and G-band features, in addition to weak double resonance features associated with the M-band and the iTOLA second-order modes [8] (see the following sections) are shown. * denotes non-resonant Si Raman spectra from the Si/SiO2 substrate, which are used for calibration purposes [9].

New J. Phys. **5** (2003) 157

Electronic Properties

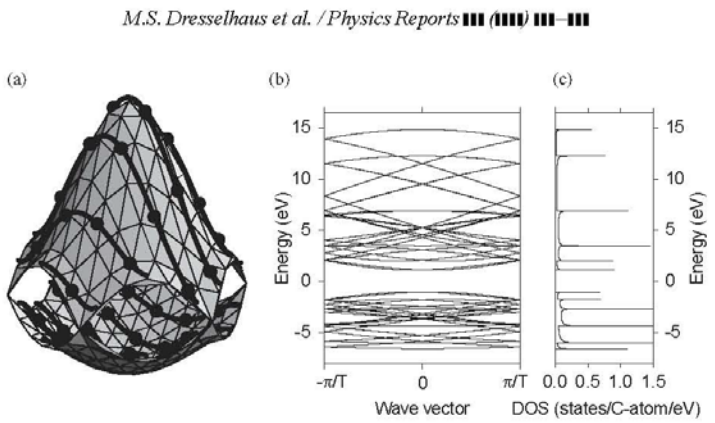

Fig. 3. (a) The calculated constant energy contours for the conduction and valence bands of a 2D graphene layer : Brillouin zone using the π-band nearest neighbor tight binding model [1]. The valence and conduction bands touc points. Solid curves show the cutting lines for the (4, 2) nanotube [8], as shown in Fig. 2(c), but translated to the firs zone of 2D graphite, the dark points indicating the connection points. (b) Electronic energy band diagram for the (4, 2 obtained by zone-folding from (a). (c) Density of electronic states for the band diagram shown in (b).

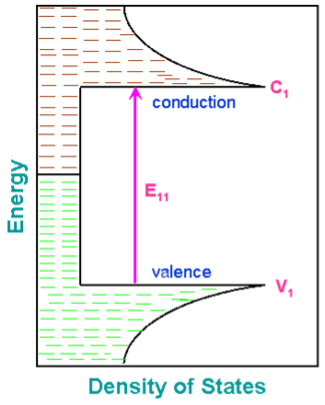

Metallic SWNT

$v_1 \rightarrow c_1$ corresponds to the "first van Hove" optical transition

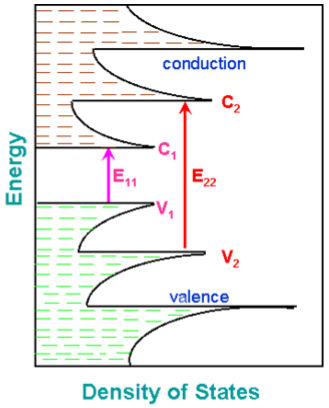

Semiconducting SWNT

$v_2 \rightarrow c_2$ corresponds to the "second van Hove" optical transition

Ultraclean CNTs are predicted metallic, but instead they show a gap. This is because for small diameter the Coulomb interaction among electrons overwhelms the total kinetic energy of the electron gas, thus behaving as what is known a Mott Insulator. Electronic properties are similar to graphene but show in addition the effect of electron confinement around the CNT circumference.

Electronic Properties

Mean free path of carriers in **metallic CNT**: several micrometers (much larger than in metals-40 nm). This results from confinement of carriers. In addition the absence of scattering at defects, low electron-phonon interaction allow CNT to sustain current densities as large as 10^{10} A/cm^2

Room temperature resistivity: 10^{-6} Ωcm (much better than Cu)
Thermal conductivity: 6000 W/(Km)
Piezoelectric strain: 0.11% at 1 V

Semiconducting CNT:
Bandgap=0.9eV/d_t where d_t is the tube diameter
Direct gap
Wannier like excitons identified
Photoluminescence is very inefficient, due to quenching by sidewall chemisorption of oxygen
Semiconducting CNT have been used to demonstrate Field effect transistors

CARBON NANOTUBES

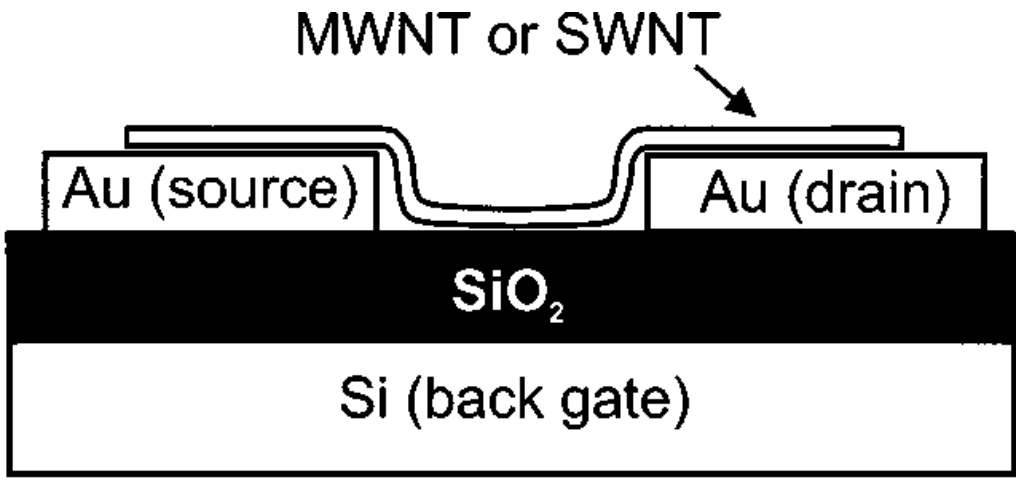

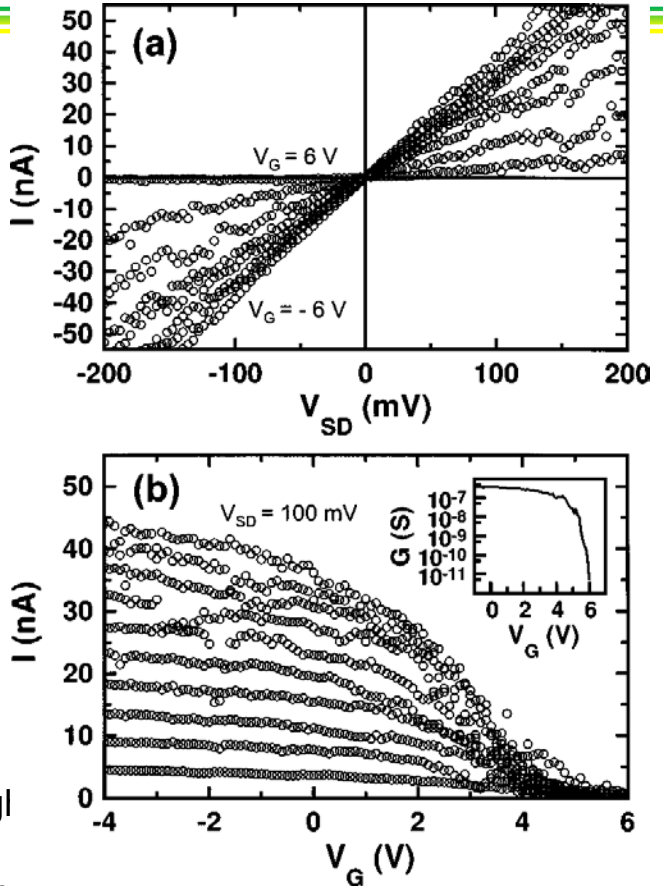

Single- and multi-wall carbon nanotube field-effect transistors
APL –vol 73, 2447, 1998 (No.cites 1521)

R. Martel, T. Schmidt, H. R. Shea, T. Hertel, and Ph. Avourisa)
IBM Research Division, T. J. Watson Research Center, Yorktown Heigl

~Received 1 July 1998; accepted for publication 24 August 1998

We fabricated field-effect transistors based on individual single- and multi-wall carbon nanotubes and analyzed their performance. Transport through the nanotubes is dominated by holes and, at room temperature, it appears to be diffusive rather than ballistic. By varying the gate voltage, we successfully modulated the conductance of a single-wall device by more than 5 orders of magnitude. Multi-wall nanotubes show typically no gate effect, but structural deformations—in our case a collapsed tube—can make them operate as field-effect transistors.

dI/dVg= 12 μA/V at Vg= 0.4 V

This translates to a transconductance per unit width of 3mS/ μm

MECHANICAL PROPERTIES

Young Modulus: 3.7 10^{12} Pa – (5x that of carbon fibers)
This property makes CNT desirable for lightweight composite materials. Due to their high elasticity and strength, CNT can be bent or twisted reversibly.

Material	Young's modulus (TPa)	Tensile strength (GPa)	Elongation at break (%)
SWNT	~1 (from 1 to 5)	13–53[E]	16
Armchair SWNT	0.94[T]	126.2[T]	23.1
Zigzag SWNT	0.94[T]	94.5[T]	15.6–17.5
Chiral SWNT	0.92		
MWNT	0.27[E][17]–0.8[E][24]–0.95[E][17]	11[E][17]–63[E][17]–150[E][24]	
Stainless steel	0.186[E][25]–0.214[E][26]	0.38[E][25]–1.55[E][26]	15–50
Kevlar–29&149	0.06[E][27]–0.18[E][27]	3.6[E][27]–3.8[E][27]	~2

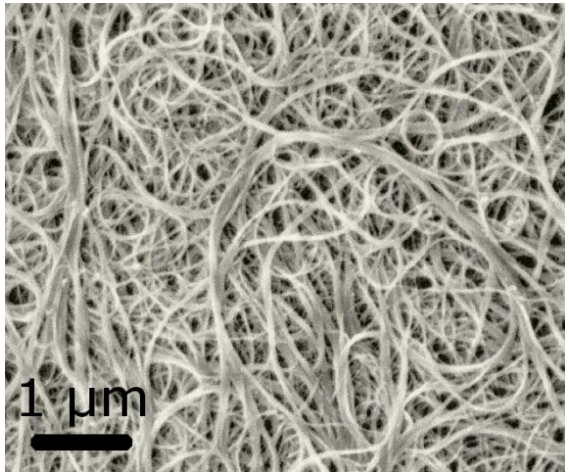

CNT bundles

THERMAL PROPERTIES

MWNT have been found stable to 3200 K – better than diamond and graphite
Thermal conductivity: 3500 W/(m-K) – along axis (much better than metal) –
Radial Thermal conductivity is 1-2 W/(m-K)

OPTICAL PROPERTIES

Sharp transitions identify quality of nanotubes.

Interaction among nanotubes broadens transitions.

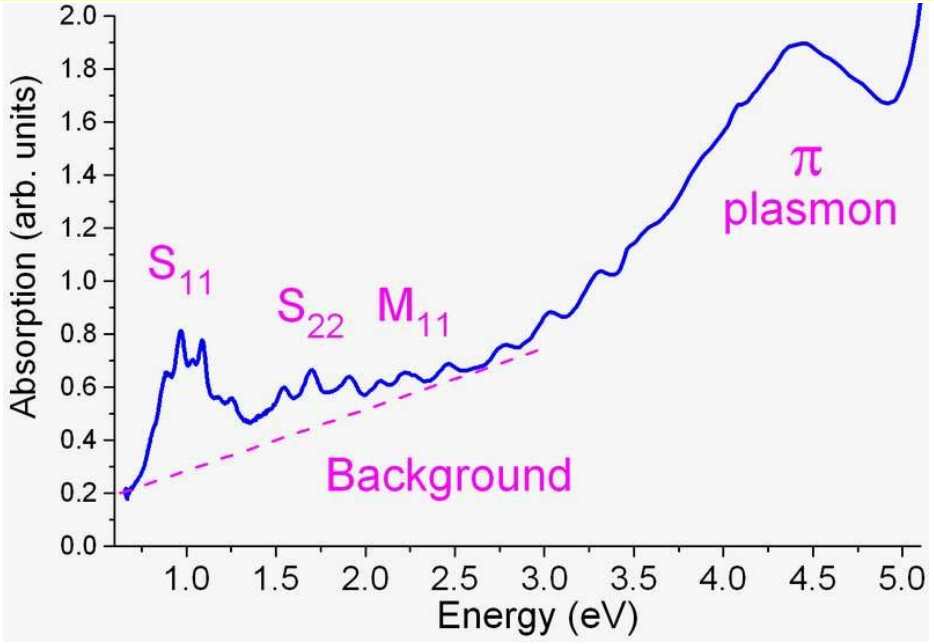

CNT are almost perfect black bodies – with emissivity close to 1

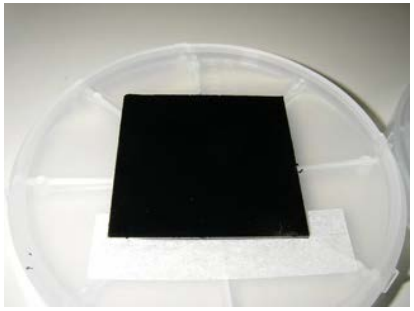

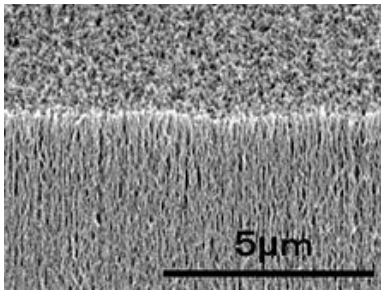

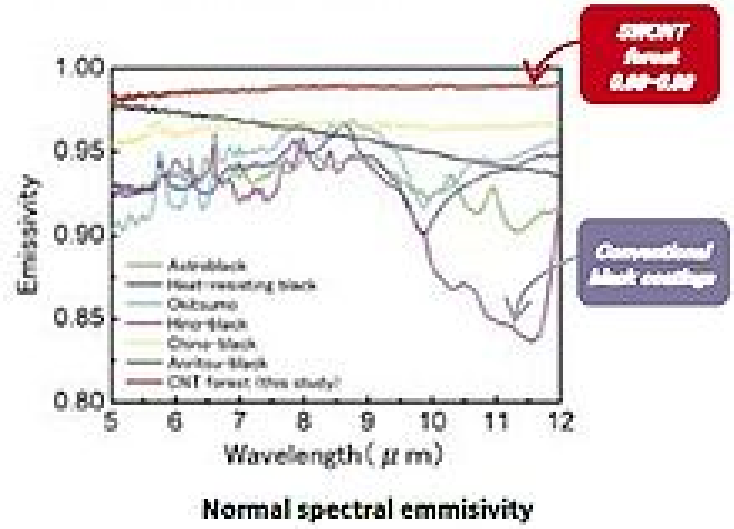

APPLICATIONS
Structural

Textiles—CNT can make waterproof and/or tear-resistant fabrics
Body armor—MIT is working on combat jackets that use CNT fibers to stop bullets and to monitor the condition of the wearer.[1] Cambridge University developed the fibres and licensed a company to make them.[2]
Concrete—CNT in concrete increase its tensile strength, and halt crack propagation.[3]
Polyethylene—Adding CNT to polyethylene can increase the polymer's elastic modulus by 30%.
Sports equipment—Stronger and lighter tennis rackets, bicycle parts, golf balls, golf clubs, and baseball bats.
Space elevator—CNT are under investigation as possible components of the tether up which a space elevator can climb. This requires tensile strengths of more than about 70 GPa.
synthetic muscles: Due to their high contraction/extension ratio given an electric current, CNTs are ideal for synthetic muscle.[4]
High tensile strength fibers—Fibers produced with polyvinyl alcohol required 600 J/g to break.[5] In comparison, the bullet-resistant fiber Kevlar fails at 27–33 J/g.
Bridges—CNT may be able to replace steel in suspension and other bridges.
Flywheels—The high strength/weight ratio enables very high rotational speeds.
Fire protection—Thin layers of buckypaper can significantly improve fire resistance due to the efficient reflection of heat by the dense, compact layer of CNT or carbon fibers.[6]

http://en.wikipedia.org/wiki/Potential_applications_of_carbon_nanotubes

APPLICATIONS - Electromagnetics

Artificial muscles—CNT's have sufficient contractility to make them candidates to replace muscle tissue.[7]
Buckypaper—Thin nanotube sheets are 250 times stronger than steel and 10 times lighter and could be used as a heat sink for chipboards, a backlight for LCD screens or as a faraday cage to protect electrical devices/aeroplanes.
Chemical nanowires—CNTs can be used to produce nanowires of other elements/molecules, such as gold or zinc oxide. These nanowires in turn can be used to cast nanotubes of other chemicals, such as gallium nitride. These can have very different properties from CNTs—for example, gallium nitride nanotubes are hydrophilic, while CNTs are hydrophobic, giving them possible uses in organic chemistry.
Conductive films—Drawing transparent high strength swathes of SWNT is a functional production technique[8] and is in use at Canatu [9] of Helsinki, Finland, Eikos Inc of Franklin, Massachusetts and Unidym Inc.[10] of Silicon Valley are developing transparent, electrically conductive CNT films and NanoBuds to replace indium tin oxide (ITO) in LCDs, touch screens, and photovoltaic devices. Nanotube films show promise for use in displays for computers, cell phones, Personal digital assistants, and automated teller machines.
Electric motor brushes—Conductive CNTs are used in brushes for commercial electric motors. They replace traditional carbon black, which is mostly impure spherical carbon fullerenes. The nanotubes improve electrical and thermal conductivity because they stretch through the plastic matrix of the brush. This permits the carbon filler to be reduced from 30% down to 3.6%, so that more matrix is present in the brush. Nanotube composite motor brushes are better-lubricated (from the matrix), cooler-running (both from better lubrication and superior thermal conductivity), less brittle (more matrix, and fiber reinforcement), stronger and more accurately moldable (more matrix). Since brushes are a critical failure point in electric motors, and also don't need much material, they became economical before almost any other application.
Light bulb filament: alternative to tungsten filaments in incandescent lamps.
Magnets—Multi-walled nanotubes (MWNT coated with magnetite can generate strong magnetic fields.
Optical ignition—A layer of 29% iron enriched single-walled nanotubes (SWNT) is placed on top of a layer of explosive material such as PETN, and can be ignited with a regular camera flash.[11]
Solar cells—GE's CNT diode exploits a photovoltaic effect. Nanotubes can replace ITO in some solar cells to act as a transparent conductive film in solar cells to allow light to pass to the active layers and generate photocurrent.
Superconductor—Nanotubes have been shown to be superconducting at low temperatures.[12]
Ultracapacitors—MIT is researching the use of nanotubes bound to the charge plates of capacitors in order to dramatically increase the surface area and therefore energy storage ability.[13]
Displays—CNTs can be used as extremely fine electron guns, which could be used as miniature cathode ray tubes in thin high-brightness, low-energy, low-weight displays. This type of display would consist of a group of many tiny CRTs, each providing the electrons to hit the phosphor of one pixel, instead of having one giant CRT whose electrons are aimed using electric and magnetic fields. These displays are known as field emission displays (FEDs).
Transistor—CNT transistors have been developed at Delft, IBM, and NEC.
Electromagnetic antenna—CNTs can act as antennas for radios and other electromagnetic devices.[14]

CARBON NANOTUBES – APPLICATIONS

Electroacoustic

* Loudspeaker—In November, 2008 Tsinghua-Foxconn Nanotechnology Research Centre in Beijing announced that it had created loudspeakers from sheets of parallel CNT, generating sound similar to how lightning produces thunder. Near-term commercial uses include replacing piezoelectric speakers in greeting cards.[15]

Chemical

* Air pollution filter—CNT membranes can filter carbon dioxide from power plant emissions.
* Biotech container—CNT can be filled with biological molecules, aiding biotechnology.
* Hydrogen storage—CNT have the potential to store between 4.2 and 65% hydrogen by weight. If they can be mass produced economically, 13.2 litres (2.9 imp gal; 3.5 US gal) of CNT could contain the same amount of energy as a 50 litres (11 imp gal; 13 US gal) gasoline tank. See Hydrogen Economy.[citation needed]
* Water filter—CNT membranes can aid in filtration. This can purportedly reduce desalination costs by 75%. The tubes are so thin that small particles (like water molecules) can pass through them, while blocking larger particles (such as the chloride ions in salt).

Mechanical

This section does not cite any references or sources.
Please help improve this article by adding citations to reliable sources. Unsourced material may be challenged and removed. (November 2008)

* Oscillator—Oscillators based on CNT have achieved higher speeds than other technologies (> 50 GHz).
* Nanotube membrane—Liquid flows up to five orders of magnitude faster than predicted by classical fluid dynamics.
* Slick surface—Some CNT-based fabrics have shown lower friction than Teflon.
* Waterproof—Some CNT-fabrics are waterproof.
* Carbon nanotube actuators—
* Infrared detector—The reflectivity of the buckypaper produced with "super-growth" chemical vapor deposition method is 0.03 or less, potentially enabling performance gains for pyroelectric infrared detector.[16][17]

This article needs attention from an expert on the subject. See the talk page for details. Consider associating this request with a WikiProject.

* Radiometric standard—As a standard of the black.
* Thermal radiation—For thermal emission in space such as space satellites.
* stealth—Absorbance is high in wide ranges from FUV to FIR.

GRAPHENE

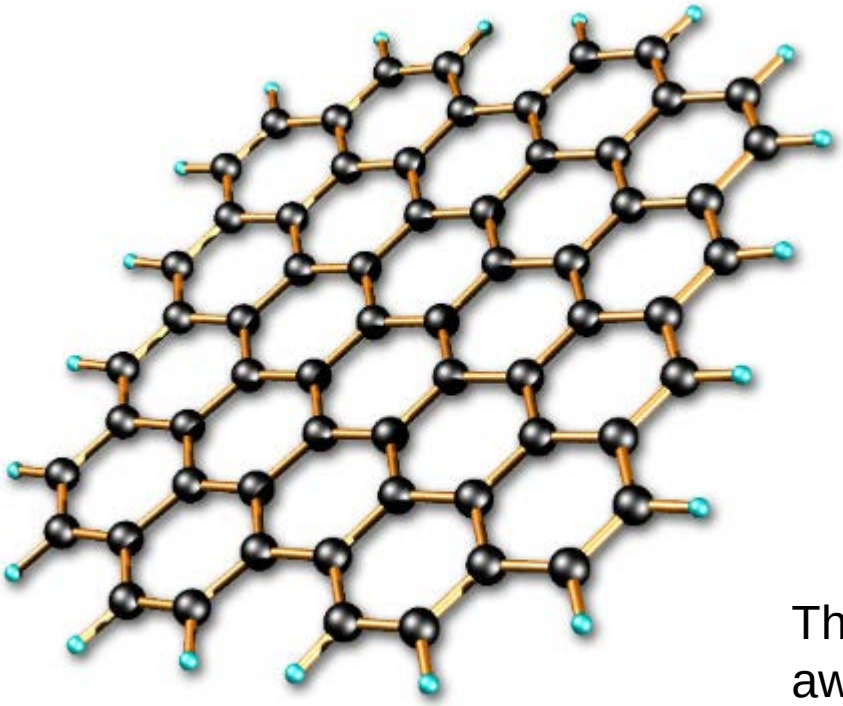

Sp^2 bonded C

The theory behind the substance graphene was first explored by theoretical physicist Philip Wallace in 1947

Graphene sheets demonstrated in 2004. Graphene the thinnest possible material that is feasible, but it's also about 200 times stronger than steel and conducts electricity better than any material known to man—at room temperature.

The Nobel Prize in Physics for 2010 was awarded to Andre Geim and Konstantin Novoselov "for groundbreaking experiments regarding the two-dimensional material graphene"

http://bigthink.com/ideas/24381

Electronic properties

Graphene is a semimetal or zero gap semiconductor. E-k relationship has zeros on the six corners of BZ.
E-k relationship is linear – thus electrons and holes have zero effective mass.
Thus, electrons and holes behave like relativistic particles that satisfy Dirac equation for spin ½.
Electron and holes have same effective mass

Calculation band structure
http://en.wikipedia.org/wiki/File:Cnt_zz_v3.gif

Electron mobility: 15,000 $cm^2V^{-1}s^{-1}$ have been measured - .
Mobility is nearly independent of temperature – indicating that defect scattering is only mechanism controlling mobility
Resistivity: 10^{-6} Ωcm^{-1}

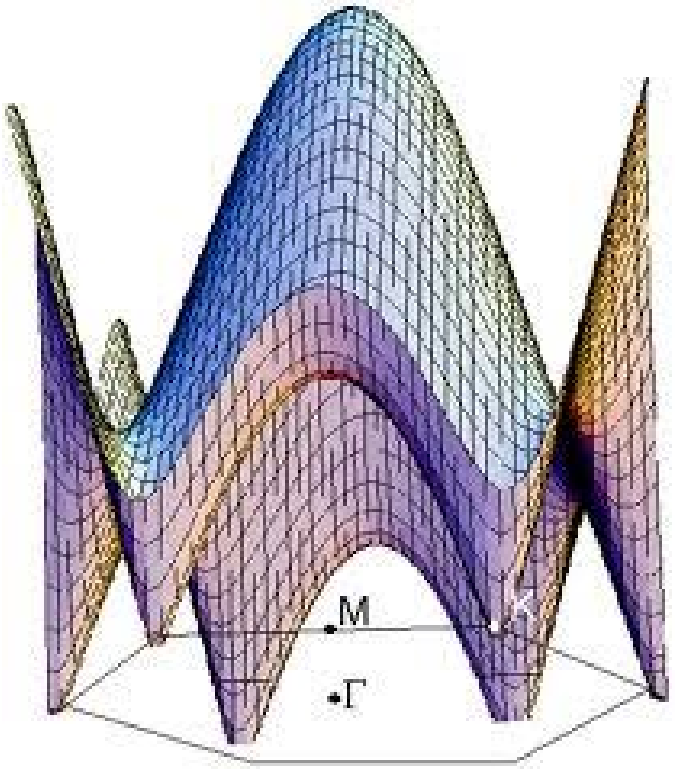

Graphene valence band

Optical properties:
Absorbs 2.3% of white light
Bandgap can be changed from 0 to 0.5 eV with applied voltage. This effect was used to demonstrate FET in a dual sheet of graphene. (http://en.wikipedia.org/wiki/Field-effect_transistor)

Graphene can be made an insulator by hydrogenation – i.e attaching hydrogen atoms. This modification is reversible.

THERMAL PROPERTIES
Thermal conductivity: $(4.84\pm0.44) \times 10^3$ to $(5.30\pm0.48) \times 10^3$ $Wm^{-1}K^{-1}$

THERMAL PROPERTIES
Breaking strength; 200x that of steel
Bulk Strenght: 130 Gpa
Young Modulus: 0.5 Tpa
These properties make Graphene very strong and rigid. Potential for use in NEMS